POLO-LIKE KINASE 1 AS A PROGNOSTIC AND THERAPEUTIC TARGET IN HIGH-GRADE BRAIN TUMORS

by

Joanna Catherine Caprio Triscott

BSc Honors Molecular Genetics, The University of Alberta, 2010

A THESIS SUBMITTED IN PARTIAL FULFILLMENT OF
THE REQUIREMENTS FOR THE DEGREE OF

DOCTOR OF PHILOSOPHY

in

THE FACULTY OF GRADUATE AND POSTDOCTORAL STUDIES
(Experimental Medicine)

THE UNIVERSITY OF BRITISH COLUMBIA
(Vancouver)

August 2015

ABSTRACT

High-grade brain tumors have some of the highest rates of cancer-related death. Occurring predominately in adults, patients with glioblastoma (GBM) are not expected to survive longer than two years. Similarly, medulloblastoma (MB) is the most commonly occurring malignant brain tumor in children and, although these cases have a much better probability of survival, the severe impact of high-intensity treatment often causes long-term negative side effects. Unfortunately, high-grade brain tumors are frequently resistant to standard treatments like temozolomide (TMZ). Further, the development of new drugs is hindered by the blood-brain barrier and the astronomical cost of drug discovery and clinical evaluation. The immediate need for new treatment options encouraged our approach of querying compounds that have previously been tested in clinical trials. Herein, we found that TMZ resistant GBM cells express high levels of the mitotic kinase, Polo-Like Kinase 1 (PLK1) and that TMZ resistance can be overcome using PLK1 kinase inhibitors, such as BI-2536. An assessment of off-patent drugs revealed that the anti-alcoholism treatment, disulfiram (DSF), also had efficacy in eliminating PLK1-high cells and this work proposes DSF can be repurposed for cancer treatment. The importance of PLK1 was further investigated in a retrospective study of MB patient samples that were assessed with the NanoString nCounter system. Cases with high PLK1 expression were more likely to relapse and had worse overall survival. This work suggests that stratification of these high-risk cases can identify patients that may benefit from PLK1 inhibitors, which cause G2/M arrest and apoptosis. Notably, both DSF and BI-2536 treatment had no negative growth effects on normal brain cells. Finally, translationally controlled tumor protein (TCTP) is a substrate of PLK1 that is used as a marker of kinase activity. An exploration of the clinical and mechanistic impact of TCTP demonstrated a striking association with the sonic hedgehog (SHH) MB subtype, as well, as establishing its role in cancer cell proliferation. In conclusion, the studies outlined in this thesis encourage the investigation of PLK1 as a therapeutic target in high-grade brain tumors and emphasizes the potential benefit of fighting cancer with repurposed drugs.

PREFACE

Chapter 2: Repurposing Disulfiram as an alternative therapeutic against TMZ resistant GBM.

Joanna Triscott conceived the project and performed all experiments involving disulfiram, was responsible for primary GBM cell extraction and testing, and generated all supplementary Figures. JT was responsible for data analysis in all Figures except those generated by Cathy Lee, and prepared the manuscript.

Contributions of co-authors:

- Cathy Lee contributed to a number of cell-based growth and neurosphere assays in Figure 2.7C-D, Figure 2.8C-D, Figure 2.9D, and Figure 2.10.
- Kaiji Hu provided plating scanning and data analysis of cell growth assays using the high-content screening Cellomics instrument.
- Abbas Fotovati, contributed immunohistochemical staining data show in Figure 2.11A.
- Mary Rose Pambid and Rachel Berns assisted in performing replicate western blot experiments from Figure 2.7A-B and 2.8A-B.
- Ester Kong, Eric Toyota, and Stephen Yip generated MGMT data for Figure 2.4A.
- Brian Toyota and Margaret Luk contributed to the collection of primary tumor samples.
- Richard E. Kast assisted in the conception of the project.
- Sandra E. Dunn provided supervision of the project and contributed to manuscript design and editing.

Collection and testing of primary human brain tumor samples was performed under approval of the UBC Human Ethics committee (certificate H08-02838).

A version of this chapter has been published as a research article and in a concise review paper. Figure 2.5 and Figure 2.12 contain data not included in published material.

Triscott J, Lee C, Hu K, Fotovati A, Berns R, Pambid M, Luk M, Kast RE, Kong E, Toyota E, Yip S, Toyota B and Dunn SE. Disulfiram, a drug widely used to control alcoholism, suppresses self-renewal of glioblastoma and overrides resistance to temozolomide. *Oncotarget* (2012).

****Triscott J**, Pambid MR, and Dunn SE. Bullseye: Targeting cancer stem cells to improve the treatment of glioma by repurposing Disulfiram. *Stem Cells* (2015).

** Text elements of this published review paper were also incorporated into Chapters 1 and 5.

Chapter 3: Targeting PLK1 in pediatric medulloblastoma.

Joanna Triscott designed and conceived all clinical and gene expression data in this chapter. JT is responsible for ~70% of the Figures/Tables in the manuscript as well contributed to *in vitro* immunofluorescence experiments, TCTP immunoblotting, MED8A assays, and BT025 primary cell experiments. As well, involved in manuscript preparation and revision.

Contributions of co-authors:

- Cathy Lee contributed to the conception of the study and involved in the manuscript preparation and editing. CL performed a number of key *in vitro* experiments in Figures 3.7B, 3.7E, 3.9B-E (excluding TCTP and PARP blotting), 3.10B, 3.10D, 3.12D, and 3.13.
- Rachel Berns assisted in various *in vitro* experiments in the study.
- Colleen Foster and Katrina O'Halloran were involved in the collection and organization of clinical data.
- Branavan Manoranjan and Chitra Venugopal are members of Sheila K. Singh's group (McMaster University, Hamilton, ON) that performed the *in vivo* experiment. SKS also provided medulloblastoma cell lines for this study.
- Mary Rose Pambid contributed to drug screens in Figure 3.4A and Figure 3.13.
- Abbas Fotovati provided images in Figure 3.14B.
- Cynthia Hawkins, Vijay Ramaswamy, Eric Bouffet, and Michael D. Taylor provided the RNA and clinical information for the validation patient cohort (The Hospital for Sick Children, Toronto, ON).
- Paul Northcott assisted in subtype assignment of the discovery cohort Table 3.2.
- Ash Singhal, Juliette Hukin, and Rod Rassekh provided primary brain tumor samples and clinical data for the discovery cohort (BC Children's Hospital, Vancouver, BC).
- Christopher Dunham is the neuropathologist involved in identifying all tumor specimens involved in the study, interpretation of Figure 3.14B, and manuscript editing. CD is considered a senior author on this project.
- Sandra E. Dunn provided supervision of the project and contributed to manuscript design and editing.

Collection and testing of primary human brain tumor samples was performed under approval of the UBC Human Ethics committee (certificates H09-02812, and H11-03397).

A version of this chapter has been published.
Triscott J, Lee C, Foster C, Manoranjam B, Pambid MR, Berns R, Fotovati A, Venugopal C, O'Halloran K, Narendran A, Hawkins C, Ramaswamy V, Bouffet E, Taylor MD, Singhal A, Hukin J, Rassekh R, Yip S, Northcott P, Singh S, Dunham C, and Dunn SE. Personalizing the Treatment of Pediatric Medulloblastoma: Polo-like Kinase 1 as a Molecular Target in High-Risk Children. *Cancer Research* (2013).

Chapter 4: The role of PLK1 kinase substrate TCTP in medulloblastoma.

Joanna Triscott conceived the project and performed all the experiments except Figures 4.3A and 4.11B. JT is responsible for data analysis and composition of all Figures and Tables.

Contributions of co-authors:

- Marcus Green contributed to optimization experiments with TCTP targeted reagents and performed the western blot in Figure 4.11B.
- Ash Singhal, Juliette Hukin, and Rod Rassekh provided primary brain tumor samples and clinical data for the discovery cohort (BC Children's Hospital, Vancouver, BC).
- Christopher Dunham is the neuropathologist involved in identifying all tumor specimens in the study, and interpretation of Figure 4.3A. CD is a senior author on this project.
- Colleen Foster was involved in the collection and organization of clinical data. As well, conducted the p53 IHC staining and scoring for figure 4.3A.
- Donna Johnston and Jean Michaud provided the FFPE tissue for the validation patient cohort (Children's Hospital of Eastern Ontario, Ottawa, ON)
- Sandra E. Dunn, provided supervision of the project and contributed to text editing.

Collection and testing of primary human brain tumor samples was performed under approval of the UBC Human Ethics committee (certificates H09-02812, and H11-03397).
A version of this chapter is currently being prepared as a manuscript and is a work in progress.

Appendix B Technical Report: Development of a brain tumor xenograft model through using bioluminescent and fluorescent markers for monitoring progression.

Joanna Triscott conceived the project and conducted all outlined procedures. Surgical procedures were conducted in partnership with the below co-authors. JT is responsible for all data analysis, animal monitoring, and generation of Figures.

Contributions of co-authors:

- Abbas Fotovati, worked directly alongside JT in all animal surgery and imaging procedures. AF majorly contributed to mouse tissue preservation and processing.
- Branavan Manoranjan, Chitra Venugopal, and Sheila K. Singh generated the original surgical protocol our methods were modeled from, and assisted with troubleshooting.
- Shelly McErlane and Kris Andrews provided hands-on animal training.
- Sandra E. Dunn, provided supervision and financial grant support for this project.

Animal work was performed under approval of the UBC Animal Care Committee (certificate A13-0192). Content of this appendix is currently being prepared as a technical report.

TABLE OF CONTENTS

LIST OF TABLES

LIST OF FIGURES

LIST OF ABBREVIATIONS

ABC	ATP binding cassette
ALA	5-aminoevulinic acid
ALDH	Aldehyde dehydrogenase
ANOVA	Analysis of variance
APC	Adenomatous polyposis coli
APC/C	Anaphase-promoting complex/cyclosome
ATCC	American type culture collection
ATM	Ataxia telangiectasia mutated
ATR	Ataxia telangiectasia and Rad3-related protein
AuHCR	Autologous hematopoietic cell rescue
BBB	Blood-brain barrier
BCCH	British Columbia Children's Hospital
BER	Base excision repair
BMI1	BMI1 polycomb ring finger oncogene
BMP	Bone morphogenic protein
CB	Normal cerebellum
CD133	Prominin 1
CD15	Stage-specific embryonic antigen 1
CDK	Cyclin-dependent kinase
CHEO	Children's Hospital of Eastern Ontario
CI	Confidence interval
CMB	Classic medulloblastoma
CNS	Central nervous system
CSC	Cancer stem cell-like
CSF	Cerebrospinal fluid
CT	Computed tomography
CTNNB1	Catenin (cadherin-associated protein), beta 1
DAPI	4', 6-diamidino-2-phenylindole
DEAB	N,N-diethylaminobenzaldehyde
DESI	Desorption electrospray ionization
DIPG	Diffuse intrinsic pontine glioma
DKK1	Dickkopf WNT signalling pathway inhibitor 1
DMSO	Dimethyl sulfoxide
DN	Desmoplastic/nodular
DNA	Deoxyribonucleic acid
DNMT1	DNA methyltransferase 1
DREAM	Dimerization partner, RB-like, E2F and multi-vulval class B complex
dsDNA	Double-stranded DNA
DSF	Disulfiram

DSH	Dishevelled
ECT2	Epithelial cell transforming 2
EGF	Epidermal growth factor
EGFR	Epidermal growth factor receptor
EGFRvIII	Epidermal growth factor receptor variant III
EGL	External granular layer
EMI1	Early mitotic inhibitor 1
FFPE	Formalin-fixed paraffin embedded
FGF	Fibroblast growth factor
FGS	ALA-fluorescence-guided
FISH	Fluorescence in situ hybridization
FZD	Frizzled
G-CIMP	Glioma-CpG island methylator phenotype
GBM	Glioblastoma
GEM	Genetically engineered mouse
GFAP	Glial fibrillary acidic protein
GLI	GLI family zinc finger
GLUT1	Glucose transporter 1
GNP	Granule neuron precursor
GSK3	Glycogen synthase kinase 3
Gy	Gray; unit of radiation dose
H3K27	Histone H3 lysine 27
HCl	Hydrochloric acid
hNSC	Human neural stem cells
HR	Hazard ratio
i17q	Isochromosome 17q
IDH1	Isocitrate dehydrogenase 1 (NADP+), soluble
IDH2	Isocitrate dehydrogenase 2 (NADP+), mitochondrial
IDL	Inter-domain linker
IGL	Internal granule layer
IHC	Immunohistochemistry
INCENP	Inner centromere protein
KCNA1	Potassium voltage-gated channel subfamily A member 1
KD	Kinase domain
KDM	Lysine-specific demethylase
Ki67	Marker of proliferation Ki67
LCA	Large-cell/anaplastic
LITT	Laser interstitial thermal therapy
MB	Medulloblastoma
MBEN	Medulloblastoma with extensive nodularity
MCT1	Monocarboxylate transporter 1

MDM2	MDM2-proto-oncogene, E3 ubiquitin protein ligase
MGMT	O-6-methylguanine methyltransferase
miRNA	MicroRNA
MITC	5-(3-methyltriazen-1-yl) imidazole-4-carboxamide
MLH1	MutL homolog 1
MMR	Mismatch repair pathway
MPF	M-phase-promoting factor
MRI	Magnetic resonance imaging
mRNA	Messenger RNA
MYC	V-myc avian myelocytomatosis viral oncogene homolog
MYCN	V-myc avian myelocytomatosis viral oncogene neuroblastoma derived Homolog
Mypt1	Protein phosphatase 1
NFkB	Nuclear factor kappa-light-chain-enhancer of activated B cells
NLP	Ninein-like protein
NPR3	Natriuretic peptide receptor 3
OTX	Orthodenticle Homeobox 2
PAM	Prediction analysis for microarrays
PARP	Poly (ADP-ribose) polymerase
PBD	Polo-box domain
PC	Polo-cap
PCM	Pericentriolar material
PDGFR	Platelet-derived growth factor receptor
PI3K/AKT	Phosphoinositide 3-kinase/protein kinase B
PKA	Protein kinase A
PLK1	Polo-like Kinase 1
PMS2	PMS2 postmeiotic segregation increased 2 (S. cerevisiae)
PNET	Primitive neuroectodermal tumor
PTCH1	Patched
PTEN	Phosphatase and tensin homolog
Ras/ERK	Ras/ extracellular-signal-regulated kinase
RB	Retinoblastoma gene
RNA	Ribonucleic acid
RT-PCR	Real-time polymerase chain reaction
RTK	Receptor tyrosine kinase
SAC	Spindle assembly checkpoint
SB	Sleeping beauty transposon
SFRP1	Secreted frizzled-related protein 1
SHH	Sonic hedgehog
siRNA	Small interfering RNA
SLK	STE20-like kinase
SMO	Smoothened

SOX2	SRY (Sex Determining Region Y)-Box 2
ssDNA	Single-stranded DNA
SUFU	Suppressor of fused homolog
SVZ	Subventricular zone
TCGA	The Cancer Genome Atlas
TCTP	Translationally controlled tumor protein
TMZ	Temozolomide
TP53	Tumor protein p53
VEGFR	Vascular endothelial growth factor receptor
VZ	Ventricular zone
WHO	World Health Organization
WNT	Wingless

ACKNOWLEDGEMENTS

I would like to take this opportunity to thank the many individuals and groups that have made this project possible. Thank you to my committee: Drs. Stephen Yip, Catherine Pallen, and Blair Leavitt. As well, I am also grateful to Dr. Vincent Duronio for his very generous support and guidance.

I was very fortunate to be involved in a project that allowed me to collaborate with world-class researchers and clinicians. Thank you to the labs of Drs. Michael Taylor and Sheila Singh. Specifically, Branavan Manoranjan, Chitra Venugopal, Vijay Ramaswamy, and Paul Northcott. Locally at BC Children's Hospital and Vancouver General Hospital, I am grateful to Drs. Brain Toyota, Ash Singhal, Juliette Hukin, and Rod Rassekh. As well, to others who are not listed but have contributed to the acquisition of study materials from other institutes. Furthermore, I would like to emphasis my appreciation for the work of Dr. Christopher Dunham. It has been an absolute privilege to learn from and collaborate with you.

None of this would have been possible without financial support. I would like to acknowledge Hannah's Heroes Foundation, the Child & Family Research Institute, the Michael Cuccione Foundation, Mitacs, Summits of Hope, Canucks for Kids, and Brain Care BC. This includes the multitude of donors who have contributed their resources in support of these foundations over the years. Thank you for your generosity.

Extreme gratitude is due to the members of my research team. Thank you to Aarthi, Anna, Alastair, Barbara, Brenda, James, Jennifer, Kaiji, Kristen, Marcus, Mary and Rachel. I would especially like to highlight my appreciation for my collaboration with Drs. Abbas Fotovati and Cathy Lee. Most importantly, thank you to the Captain Janeway reincarnate, Dr. Sandra Dunn. Words fail to do justice to the valuable mentorship and empowerment you have instilled in me. To all of you, I am very proud of the work we have accomplished.

Finally, to my parents, this would not have been possible without your encouragement.

DEDICATION

This work is dedicated to Hannah's Heroes Foundation. As well, to the patients and their families that contributed clinical materials for brain tumor research.

CHAPTER 1: INTRODUCTION

1.1 High-grade brain tumors

A brain tumor is a mass of abnormal cells that occurs in brain tissue. Brain and central nervous system (CNS) tumors are the most common neoplasms for ages 0-19 years (5.42 per 100 000), and the seventh most common in adults (27.86 per 100 000) (Ostrom et al., 2014). There are over 120 varieties of brain tumor that may be either benign or malignant. Tumors may be considered primary, meaning the brain is their anatomical origin, or secondary where tumorigenesis is a result of progression or metastasis of other cancer types. While relatively rare, the mortality rate of brain tumors is high compared to other cancers due to limitations of current treatment options and the nature of the disease. This is especially true for high-grade tumors, which are malignant, rapidly growing and invasive. High-grade primary brain tumors are classified as World Health Organization (WHO) grade IV tumors that are highly mitotic with microvascular proliferation and/or necrosis (Louis et al., 2007). Glioblastoma (GBM) is the most commonly occurring malignant brain tumor in adults, while medulloblastoma (MB) has the highest frequency in pediatric cases; therefore, we focused our efforts towards these incredibly aggressive cancer models.

1.1.1 Challenges

The treatment of brain tumors relative to other cancer types has unique obstacles. Tumor formation in non-essential organs can be resolved with surgical removal of the tumor and extra surrounding tissue. For example, total mastectomy for breast cancer or radical prostatectomy for prostate cancer. Unfortunately, removal of extra brain tissue is not an option due to its essential biological role for survival and cognitive function. Adding to this, details of human neurobiology still remains relatively unmapped in function and mechanism (Thompson et al., 2014). This emphasizes the dire need for brain tumor-specific studies. There are key challenges in brain tumor biology that cause many promising cancer treatments to be ineffective.

1.1.1.1 Detection

The intracranial detection of tumors is a major barrier to providing timely treatment to patients. Usually, the first indication of disease is the presentation of neurological symptoms such as headache, vomiting, or seizures. An estimated 50-70% of pediatric patients report severe symptoms within 12 weeks of presentation, however, on average this timeframe is longer in adults as headaches may be ignored or misattributed as common migraines (Park et al., 1983). The rigid bone of the surrounding skull creates the need for advanced imaging to make a diagnosis, and detection is usually accomplished with magnetic resonance imaging (MRI).

1.1.1.2 Blood-brain barrier

The ability of chemotherapeutic drugs to access the tumor site is crucial for them to elicit an anti-cancer effect. A specialized blood-brain barrier (BBB) of capillary endothelial cells complicates drug delivery to the brain and CNS. The BBB is selectively permeable and tightly controls the transport of molecules either entering or leaving the neurological system. Fewer than 10% of therapeutic agents for neurological diseases proceed to clinical trials because of poor brain penetration (Pangalos et al., 2007). Over 98% of small-molecule inhibitors also fail to cross the BBB making the development of new drugs exceptionally difficult (Gabathuler, 2010).

The BBB is composed of luminal and abluminal plasma membranes of capillary endothelial cells that are firmly attached to each other with tight-junctions (Janzer and Raff, 1987). Generally, free diffusion across the BBB is limited to small (<400Da) lipid-soluble molecules preventing most drugs from entry (Oldendorf, 1974). The BBB blocks substances circulating in the bloodstream while facilitating entry and secretion of other specific molecules (Quan and Banks, 2007). These regulatory actions are carried out through the use of multiple active transport complexes. For example, small molecule transport from the bloodstream to the brain may use carrier-mediated transporters such as glucose carrier (GLUT1), or monocarboxylic acid carrier (MCT1) (Morgello et al., 1995; Takanaga et al., 1995). Small molecules leaving the brain may do so via active efflux transporters such as the ATP-binding cassette (ABC) protein family (Begley, 2004). Receptor-mediated transporters are used for larger molecules, such as transferrin or insulin, to gain entry. These transporters have become a major focus in drug delivery research (Coloma et al., 2000; Fishman et al., 1987). Agarwal and colleagues used a

GBM xenograft model to demonstrate that ABC transporters were responsible for the efflux of the cancer drug erlotinib, and that transporter inhibition could be used to increase drug delivery to tumor tissue (Agarwal et al., 2013). Another drug design strategy is to make compounds more lipid- soluble by encapsulating them with lipoproteins; however, once compounds cross the BBB they need to diffuse in an aqueous environment to reach the target tissue. As a result, highly hydrophilic substances are frequently sequestered in the capillary bed (Greig et al., 1995). By increasing access of anti-cancer compounds to the tumor site, the overall dose administered to the patient could be decreased thereby reducing the negative impact of treatment.

1.1.1.3 Radiation

Radiotherapy is a fundamental strategy in most aggressive cancer treatment protocols. It uses high energy X-ray, gamma ray or charged particles to target rapidly dividing cancer cells by damaging DNA. Radiation also increases the cellular concentration of free-radicals, which can also result in DNA damage and the initiation of apoptosis (Diehn et al., 2009; Lawrence et al., 2008). While many studies demonstrate the anti-cancer benefit of treating brain tumor patients with radiation, it can cause severe damage to normal non-tumor tissue. Patients treated with whole brain radiation may experience loss of cognitive function, hearing loss, seizures, and speech problems. The sequelae from radiation can have a dramatic impact on quality of life, especially for pediatric cases whose neurological systems are still undergoing development (Kulkarni et al., 2013; Ris et al., 2014). In addition, patients who have already been treated with radiation and received a maximum safe lifetime dose may not be able to receive additional treatment if a brain tumor regrows. It is paramount that new therapeutic agents are developed that can effectively eliminate brain tumor cells and decrease the use of radiation in treatment protocols.

1.1.2 Glioblastoma (GBM)

Malignant gliomas represent the most frequently occurring primary malignant brain tumors in adults. Patients with GBM have an extremely dismal prognosis. Nearly all GBM tumors are expected to regrow following treatment, and fewer than 5% of patients survive five years following diagnosis (Ostrom et al., 2014). GBM is arguably the most tragic and

devastating form of cancer; however, there has been very little advancement to treatment. Due to its heterogeneous and diffuse nature researchers hope to identify useful molecular targets to better manage this disease.

1.1.2.1 GBM clinical attributes

GBM is the most frequently occurring malignant brain tumor. Between 8 000 and 10 000 new cases of GBM are diagnosed annually in the USA. As well, approximately 45.6% of malignant brain tumors, and 15.7% of all brain and CNS tumors are diagnosed as GBM (Ostrom et al., 2014). GBM occurs more commonly in adults and has a median age of diagnosis of 64 years. Malignant gliomas account for 11.7% of brain and CNS tumors in children (0-19 years), and there are unique challenges associated with treating younger patients (Jansen et al., 2012; Ostrom et al., 2014). Of note, the incidence of GBM is reported to be skewed with a preponderance of 1.6 males to every 1 female diagnosed. As well, a significant variability of incidence based on geographic region has also been reported (Ostrom et al., 2014). The causes of these differences in incidence remain to be determined, and no single underlying origin can be attributed to GBM formation. In this regard, provocative evidence suggesting environmental risk factors such as ionizing radiation may play a role (Fisher et al., 2007). Similarly, occupational risk factors, electromagnetic fields and foods containing N-nitroso compounds have also been considered for having a role in GBM incidence; however, the significance of these factors still requires robust evidence (Fisher et al., 2007; Preston-Martin et al., 1982). Regardless, astrocytic tumors like GBM are ranked as the third leading cause of cancer-related death in middle-aged men, and the fourth leading cause in young women between the ages of 15-34 (Prados et al., 1998; Stiles and Rowitch, 2008).

GBM is classified by the WHO as a grade IV astrocytoma that usually occurs supratentorially in the cerebral hemispheres of the brain. Histologically, GBM has dense cellularity, nuclear pleomorphism, and mitotic figures. Microvascular proliferation and pseudopalisading necrosis are considered hallmarks of GBM by pathologists (Louis et al., 2007; Wen and Kesari, 2008). Some less common histological variants of GBM include gliosarcomas, giant-cell glioblastoma, small-cell glioblastoma, and glioblastoma with oligodendroglial features. While the small-cell variant is thought to be associated with epidermal growth factor receptor

(*EGFR*) gene amplification, oligodendroglial features are reported to have a more favorable prognosis (Louis et al., 2007). Additionally, an index of cell proliferation is commonly measured for GBM using Ki67 staining (Raghavan et al., 1990). GBM is an especially aggressive cancer, the characterization of which has begun to evolve beyond histological prognostication towards molecular characterization.

At the time of diagnosis patients with GBM usually present with one or more generalized or focal neurological symptoms including headaches, seizures, confusion, dizziness, memory loss, or even personality change. An increase in intracranial pressure due to tumor growth or obstruction of normal flow of cerebral spinal fluid (CSF) is responsible for most symptoms at diagnosis (Cha, 2006; Wen and Kesari, 2008). Diagnosis of GBM utilizes MRI, or computed tomography (CT) to image the brain and look for a heterogeneous mass with surrounding edema (abnormal swelling). Other forms of imaging can also be used in order to determine surgical margins and degree of tumor infiltration into normal tissue. These may include perfusion imaging, dynamic contrast-enhanced MRI, proton magnetic resonance spectrometry and positron-emission tomography (Cha, 2006; Chen, 2007; Giovannini et al., 2015; Wen and Kesari, 2008; Young, 2007). These techniques are also used post-operatively to monitor response to treatment.

1.1.2.2 Current treatment and temozolomide (TMZ) resistance

The location and infiltrative nature of GBM has made it one of the most challenging forms of cancer to treat. Quite often, by the time GBM is detected, it has progressed beyond what may be currently curable. Patients newly diagnosed with GBM are treated with the standard regime of maximal safe surgical resection, followed by radiation, in combination with chemotherapy.

Surgery

The goal of a surgical operation is to remove as much tumor tissue as safely possible. Unlike other tumor types, GBM is very infiltrative and spreads into surrounding tissues to a much greater extent than is usually feasible to remove (Barker et al., 1998). Biopsy of GBM is generally not done unless MRI detection determines the tumor location to be inoperable. This is

regrettably the case in most diffuse intrinsic pontine glioma (DIPG) patients as tumors form along the brain stem (Hargrave et al., 2006; Jansen et al., 2012). A number of technological advancements have improved surgical techniques such as: intraoperative MRI mapping, MRI-guided neuronavigation, and fluorescence-guided surgery. Further improvements to these technologies are encouraged as they have facilitated slight improvements to survival (Stummer et al., 2006; Wirtz et al., 2000). Interestingly, Santagata and colleagues (2014) demonstrate the use of new surgical technologies that permit rapid molecular characterization at the time of surgery. They examined the use of desorption electrospray ionization (DESI) mass spectrometry to analyze the metabolites present in tumor tissue. This can be used to detect residue tumor characteristics intraoperatively as opposed to days later through pathology analysis (Santagata et al., 2014). For example, the immediate detection of isocitrate dehydrogenase 1 and 2 (*IDH1/IDH2)* mutation can aid in decision making to either extend resection or hold back. Even more recently, laser interstitial thermal therapy (LITT) has been tested in Phase I clinical trials with recurrent GBM. Under the commercial name of Neuroblate (Monteris Medical Inc.), this technology uses a robotic heat laser to eliminate tumor cells. MRI detection guides surgeons in real-time and requires minimal probe insertion in a 4.3 mm skull opening (Sloan et al., 2013). Maximal safe resection has been used by oncologists for hundreds of years and still remains an important method for brain tumor treatment today.

Radiotherapy

Radiotherapy has been one of the only treatments to consistently delay progression of GBM. Standard treatment regimens will deliver 60 Gy of partial-field external-beam radiation in 2.0 Gy fractions, five days per week. A reduced radiation dose of 40 Gy in 15 fractions of 3 weeks, or a radiation-sparing protocol, may be given to elderly patients (>70 years) due to poor tolerance (Glantz et al., 2003; Roa et al., 2004). Radiation protocols have been reported to increase average patient survival from 3-4 months to 7-12 months post diagnosis (Stupp et al., 2005). Although a modest improvement, 90% of GBM will re-grow at the original site and current radiation protocols are not curative (Hochberg and Pruitt, 1980). As a result, potential drug candidates that may enhance tumor sensitivity to radiotherapy are currently being

researched. These have included specific inhibitors (Kim et al., 2004; Stea et al., 2003), and chemotherapeutics (Prados et al., 2009; Stupp et al., 2005).

Chemotherapy

Surgery and radiation are not enough to prevent tumor growth and thus chemotherapy is also included in standard GBM treatment protocols. The use of temozolomide (TMZ) (Temodal®) has been established in the widely used Strupp protocol. This protocol includes concurrent chemotherapy and radiation followed by adjuvant chemotherapy using TMZ. It was first developed with a phase III clinical trial that tested the efficacy of radiation alone (60 Gy over 6 weeks) versus radiation with TMZ (concurrent and adjuvant). A dose of 75mg/m^2 body surface per day for 6 weeks is used during radiation, followed by 150-200mg/m^2/day for 6 cycles (Stupp et al., 2005). TMZ is a 'prodrug' that is incorporated in oncology protocols for its DNA alkylating mode of action. Following oral administration, TMZ is converted into its physiologically active form, 5-(3-methyltriazen-1-yl) imidazole-4-carboxamide (MITC). MITC then forms unstable methyldiazonium cations that facilitate the transfer of methyl groups to DNA. The methylation of the O^6 position of guanine is thought to be the most cytotoxic lesion caused by TMZ, and it promotes the formation of DNA adducts that result in cell apoptosis (Friedman et al., 2000; Pletsas et al., 2013). Unlike many chemotherapeutics, TMZ can cross the BBB (Baker et al., 1999; Ostermann et al., 2004). The addition of TMZ to treatment protocols increased the patient 2-year survival from only 10.4% to 26.5%; however, the median overall survival was only increased to 14.6 months from 12.1 months. Many GBM tumors demonstrate resistance to TMZ.

TMZ resistance

There are limited chemotherapeutic options for the treatment of GBM making TMZ resistance a major problem. The activity of the DNA repair enzyme, O^6-methylguanine methyltransferase (MGMT), is presently the most well-characterized marker of TMZ resistance in GBM. MGMT has the ability to remove the cytotoxic methyl groups placed on DNA by TMZ treatment and, as a result, prevent cell death (Donson et al., 2007; Gerstner et al., 2009; Hegi et al., 2005). In a study that coincided with the Strupp clinical trials, Hegi and colleagues

determined that GBM patients with MGMT promoter methylation had improved 2 year survival compare to unmethylated MGMT promoters (Hegi et al., 2005). Promoter methylation is an epigenetic modification that disallows the transcript expression of MGMT. Mutation or deletion of MGMT is not common (Esteller et al., 2000) and it is degraded by the proteasome after it has completed its function and cannot be recycled (Tubbs et al., 2007; Xu-Welliver and Pegg, 2002). The median survival for MGMT methylated patients is 21.7 months with a 46% survival after two years following radiation and TMZ protocols. However, MGMT unmethylated patients have only 12.7 month median survival with a 13.8% 2 year survival rate (Hegi et al., 2005; Stupp et al., 2005). MGMT promoter methylation does not correlate with GBM molecular subtype (Verhaak et al., 2010). Currently, MGMT methylation is the strongest predictor of outcome validated for GBM, but patient survival longer than 5 years is rare regardless of MGMT status (Donson et al., 2007; Wang et al., 2015).

DNA repair and apoptosis pathways have also been implicated in resistance to TMZ. When TMZ treatment causes the alkylation of DNA that cannot be reversed by MGMT, cells depend on alternative pathways to halt the cell cycle and direct the apoptotic cell fate. For example, the mismatch repair pathway (MMR) will initiate cell death if it comes in contact with adducts caused by TMZ. This pathway is responsible for sensing, and repairing, mispaired bases during DNA replication. It is capable of excising thymine, which mispairs with O^6-methyl-guanine, and will eventually initiate cell cycle arrest. The MMR is not able to repair the O^{6-} methyl-guanine modification, and this will result in apoptosis (Fu et al., 2012). Perturbation of MMR pathways in cancer cells can prevent detection of TMZ-induced aberrations and allow cells to continue replicating through treatment (Cahill et al., 2007; Friedman et al., 1998; Liu et al., 1996; Yip et al., 2009). For example, inactivation of MMR gene MSH6 has been observed in recurrent GBM and associated with more aggressive cell proliferation in the presence of TMZ (Cahill et al., 2007; Yang et al., 2005).

The base excision repair pathway (BER) is another DNA repair system that can influence sensitivity to TMZ. While downregulation of MMR pathway can lead to poor drug response, the upregulation of the BER pathway contributes to TMZ resistance. The BER pathway coordinates a number of DNA repair proteins to remove damaged or inappropriate DNA bases, for example TMZ alkylated nucleotides (i.e., N^7-methyl-guanine) (Trivedi et al., 2005; Zhang et al., 2010).

Poly (ADP-ribose) polymerase (PARP) acts within this pathway to sense single stranded DNA breaks, then further functions by modulating surrounding chromatin structures, and recruiting DNA repair machinery (Althaus et al., 1999; Malanga and Althaus, 2005). As a result, the BER pathway may facilitate repair of N^3 and N^7 guanine or adenine methylation caused by TMZ and avoid initiation of apoptosis (Horton and Wilson, 2007). Although O^6 methylation has a greater cytotoxic effect in cells, N^3 and N^7 alkylation does contribute to the cumulative DNA adducts that promote TMZ-induced cell death.

Resistance to TMZ is not restricted to DNA repair mechanisms. Key driver pathways have a role in promoting aggressive GBM proliferation and escape from normal regulatory checkpoints. These include: EGFR overexpression, p53, phosphatase and tensin homolog (PTEN) mutation, and, more recently, miRNA (Brown et al., 2008; Golding et al., 2009; Hirose et al., 2001; Mizoguchi et al., 2013; Neyns et al., 2009; Prados et al., 2009). For example, enhanced TMZ resistance may be observed in GBM cells with the downregulation of miR-130a and miR-145 (Chen et al., 2015; Yang et al., 2012), or upregulation of miR-10a*, miR-195, miR-455-3p or miR-21 (Shi et al., 2010; Ujifuku et al., 2010; Wong et al., 2012).

Other treatments

Treating patients with GBM often presents greater challenges than the tumor itself. Along with therapies directed at killing tumor cells, physicians may also prescribe corticosteroids (e.g. Dexamethasome) to alleviate the pressure caused by building edema in brain tissues. Anti-epileptic drugs may also be prescribed if patients experience seizures as a result of GBM or in the aftermath of treatment. In addition, psychiatric care is an overlooked aspect of GBM treatment and antidepressants have been used to support the emotional health of brain tumor patients (Litofsky et al., 2004). There is some controversy as to whether adding more drugs can affect the efficacy of anti-tumoral methods. A recent study suggests MGMT methylation status fails to accurately predict response to TMZ in patients treated with corticosteroids (Weiler et al., 2014). As well, anti-epileptic drugs, such as carbamazepine and phenytoin, have been shown to induce liver enzymes that can elevate the metabolism of some chemotherapeutic agents. The addition of these types of drugs to treatment is generally recommended on an individual basis (Guthrie and Eljamel, 2013; Pursche et al., 2008). Other complications that commonly require

additional treatment may include: cognitive dysfunction and venous thromboembolism (Wen et al., 2006). While the impact of GBM and its treatment is often severe, the reduction of long-term sequela has not been a major focus due to the unfortunate fact that most patients succumb to disease within months of diagnosis.

1.1.2.3 Molecular pathology and classification of GBM

Various molecular pathways have been linked to the initiation and progression of GBM. The identification of key drivers of disease has mainly been the result of cytogenetic, transcript, and mutation profiling. By deciphering recurrent traits of GBM, researchers have developed useful subgroup classification schemes and identified potential therapeutic options.

Major signaling pathways

Malignant transformation of normal cells is frequently caused by the deregulation of growth factor signaling or the accumulation of genetic abnormalities (Furnari et al., 2007; Ohgaki and Kleihues, 2007). There are two varieties of GBM that develop, either primary (de novo) or secondary. Primary GBM is more common and forms in older patients (>50 years). Recurrent traits of primary GBM may include: *EGFR* overexpression, *p16* and *PTEN* deletion (Costello et al., 1996; Ekstrand et al., 1991; Li et al., 1997; Smith et al., 2001). In contrast, secondary GBM occurs in younger patients and forms through the malignant transformation of a lower grade infiltrative glioma (i.e.,WHO II infiltrative astrocytoma or oligodendroglioma). These tumors are less common and are characterized by platelet-derived growth factor receptor (PDGFR) overexpression (10% of cases), *TP53*, and *IDH1/IDH2* mutations (Ohgaki et al., 2004; Watanabe et al., 1996; Yan et al., 2009). Secondary GBM usually have promoter methylation of MGMT and respond more favorably to treatment compared to *de novo* GBM (Nakamura et al., 2001). The presence of *IDH1* mutation in GBM defines a distinct subset of tumors with a unique epigenetic profile. These cases have been reported to have >60% two-year survival compared to <20% for GBM subsets with wild-type *IDH1* (Sturm et al., 2012). *IDH1* mutations almost exclusively affect amino acid residue 132 and alters the enzymatic role of IDH1 in metabolism. Isocitrate is converted to α-ketoglutarate through a reaction catalyzed by wild-type IDH1, but mutant *IDH1* instead produces 2-hydroxyglutarate, a novel onco-metabolite, and accumulation of

this molecule has been shown to have oncogenic effects. *IDH2* codes for a related enzyme that is mutated in secondary GBM at residue 172, which is analogous to *IDH1* amino acid 132 (Dang et al., 2009; Ward et al., 2010). Secondary GBM truly is a distinct subgroup of malignant gliomas with unique metabolic features.

Familial genetic diseases can predispose for GBM. For example, germline mutations in *TP53* associated with Li-Fraumeni Syndrome, or Turcot's Syndrome with mutations in *MLH1* or *PMS2* (Hamilton et al., 1995; Sadetzki et al., 2013). As well, brain tumors may often form in patients with type 1 or 2 neurofibromatosis caused by abnormal *NF1* and *NF2* genes (Huttner et al., 2010; Sadetzki et al., 2013). It is estimated that a minority of 5% of GBM have a familial source leaving the cause of gliomagenesis less straight-forward for the majority of patients. The most common defects associated with GBM include: aberrations in receptor tyrosine kinases (RTK), tumor suppressors, and cell survival pathways.

RTK signaling enables the activation of key proliferation and cell survival pathways such as Ras/ERK and PI3K/Akt. Perhaps the most prominent is abnormalities in EGFR that occur in 40-50% of patients (Heimberger et al., 2005). Mutations or amplifications result in the overexpression of EGFR signaling, often in a ligand-independent state. Approximately 50% of cases with aberrant EGFR carry an in-frame deletion of exons 2-7 that constitutively activates the receptor by removing its extracellular ligand-binding requirement (EGFRvIII; EGFR variant III) (Frederick et al., 2000; Wong et al., 1992). Inhibitors targeting EGFR and EGFRvIII have been tested in clinical trials with variable results (Neyns et al., 2009; Prados et al., 2009). Aside from EGFR, other RTKs contribute to the growth of GBM including vascular endothelial growth factor receptor (VEGFR) and platelet-derived growth factor receptor (PDGFR) pathways. VEGFR is an essential regulator of angiogenesis and creates blood vessel systems that provide for tumor tissues. The invasive nature of GBM has drawn a great deal of attention into VEGFR inhibitors as it is highly expressed in tumor tissue. Clinical trials with the FDA approved VEGFR inhibitor, Bevacizumab, show its well tolerated, but still incapable of preventing relapse (Friedman et al., 2009; Gilbert et al., 2014; Iwamoto et al., 2009).

Deactivation of tumor suppressors is another form of oncogenic lesion in GBM. Mutation in *TP53* -or amplification of its negative regulatory factor MDM2-proto-oncogene, E3 ubiquitin protein ligase (MDM2)- can disrupt the ability of cells to halt cell cycle and initiate apoptosis in

the event of dysregulated growth or drug treatment (Burton et al., 2002; Forbes et al., 2011). Further, PTEN is another tumor suppressor that is mutated in approximately 40% of primary GBM and even completely deleted in some lower grade gliomas (Kato et al., 2000; Ohgaki et al., 2004). This enzyme acts to negatively regulate the PI3K pathway and, as well, can block transcription of MDM2 (Mayo et al., 2002). Other pathways implicated in GBM include Notch (Purow et al., 2005; Ying et al., 2011), mTOR (Narita et al., 2002), and STAT3 (Kohsaka et al., 2012).

Aberrant microRNA (miRNA) signaling has also been shown to modulate GBM sensitivity to treatment. Both the up-regulation of tumor promoting miRNA (i.e., miR-21, miR-195, and miR-455-3p) and down-regulation of tumor suppressing miRNA (i.e., miR-145) occurs in GBM and may offer an alternative therapeutic target in future studies (Ujifuku et al., 2010; Yang et al., 2012).

Subgroups of GBM

For decades the only established predictor for patient outcome was tumor grade (Louis et al., 2007). While aberration to multiple signaling pathways can result in GBM formation, other molecular characteristics indicate the presence of distinct molecular subtypes. A number of large-scale microarray gene expression and DNA sequencing studies have been used to classify tumors with similar molecular characteristics, as well as identify genes that are associated with tumor progression and clinical outcome (Godard et al., 2003; van den Boom et al., 2003). One of the earliest gene expression studies used EGFR overexpression or upregulation of chromosome 12q13-15 as markers of distinct groups of GBM (Mischel et al., 2003). In subsequent work, Phillips and colleagues (2006) used two-way agglomerative clustering of microarray gene expression to identify three distinct groups of high-grade astrocytoma. The Phillips subgroups include: proneural (PN), proliferative, and mesenchymal. This study used a narrowed probe set for genes whose expression strongly correlated with survival, and suggests that different subclasses of GBM resemble the stages of neurogenesis. They found the PN subgroup had a more favorable outcome compared to proliferative or mesenchymal, and suggest that tumors often recur with mesenchymal characteristics (Phillips et al., 2006).

More recently, Verhaak and colleagues (2010) refined GBM molecular subtyping through analysis of data accessed from The Cancer Genome Atlas (TCGA) Research Network. They assessed gene expression, chromosomal copy number alterations, and gene mutation data in combination with clinical and morphological characteristics of approximately 433 primary tumors. This resulted in the identification of four subgroups: proneural, neural, classic, and mesenchymal (Verhaak et al., 2010).

Proneural Subtype. Enhanced PDGFRA signaling and mutations to *IDH1* and *TP53* are hallmarks of proneural tumors. This subgroup is enriched with cases of *PDGFRA* point mutations or amplification at its locus at chromosome 4q12. Genes involved in proneural and oligodendrocytic development signaling were elevated in the proneural gene signature (DLL3, NKX2-2, SOX2, ERBB3, and OLIG2) (Phillips et al., 2006). Approximately 54% and 30% of cases were mutated for *TP53* or *IDH1,* respectively. Three of four known secondary GBM samples were found in this group, which generally occurred in younger patients (frequently <40 years). Proneural classification carries a slightly better prognosis compared to other subgroups, but there was no significant benefit reported for treatment of these cases with higher intensity chemotherapy and radiation protocols (Verhaak et al., 2010).

Neural Subtype. The molecular profile of the neural subtype is enriched for neuronal lineage markers (NEFL, SYT1, GABRA1, and SLC12A5). This group did not have any trademark copy number or mutations. Interestingly, the genetic profile of neuronal tumors clustered similarly to two normal brain tissue samples that were included in the study dataset. Similar to the proneural subgroup intensified treatment protocols did not show significant benefit in survival of neural classified cases.

Classic Subtype. EGFR amplification and overexpression is most prominent in the classic subtype. Approximately 95% of tumors had *EGFR* amplification and 5 of 7 *EGFRvIII* cases included in the study cohort were classic. No cases of *TP53* or *IDH1* mutation were detected in this subgroup. Other studies have also reported that EGFR amplification and p53 mutation are mutually exclusive and do not occur in the same tumor (von Deimling et al., 1995; Watanabe et al., 1996). In addition, 93% of classic tumors had amplification of chromosome 7 and chromosome 10 deletion. Expression of nestin (NES), members of the *sonic hedgehog* (SHH; SMO, GAS1, and GLI2) and Notch (NOTCH3, JAG1, and LFNG) signaling pathways were also

indicative of the classic subtype. Survival analysis suggests these patients would significantly benefit from more intensive treatment regimes (Verhaak et al., 2010).

Mesenchymal Subtype. Abnormal *NF1* is a major distinguishing trait of mesenchymal tumors. As well, 38% of these tumors had deletions of 17q11.2, a region containing the *NF1* locus. This subtype expresses genes similar to those that mark microglial or Schwann-like cells. Expression of previously reported mesenchymal markers *CHI3L1* and *MET* were also detected (Phillips et al., 2006). As well, mesenchymal tumors had a greater proportion of necrosis. Necrosis is associated with an elevated inflammatory response and NF-kB signaling (TRADD, RELB, and TNFRSF1A). Finally, the mesenchymal subtype may benefit from more intensive radiation and chemotherapy.

Epigenetic profiling of GBM

Expanding on the original Phillips and Verhaak subtypes, researchers have further refined GBM subgroups with epigenetic profiling (Noushmehr et al., 2010; Sturm et al., 2012). The first DNA methylation array study examined promoter methylation in 272 GBM in the TCGA. Here researchers distinguished methylation profiling that they termed glioma-CpG island methylator phenotype (G-CIMP) that indicates a cancer-specific CpG island hypermethylation of a subset of genes in a small group of tumors (Noushmehr et al., 2010; Toyota et al., 2000). They found G-CIMP tumors associated with the proneural subgroup, with *IDH1* mutations, and had a significantly better clinical outcome than non-G-CIMP tumors.

Another study also used epigenetic profiling to further stratify GBM subgroups. Sturm and colleagues (2012) separated out 6 molecular groups of GBM by integrating gene expression, DNA methylation, and copy number changes. The groups still include distinct mesenchymal and classic categories, but have further categorized the proneural tumors into RTK1, IDH, K27 or G34 groups. The RTK1 group is distinguished by *PDGFRA* alterations, while mutant *IDH1* and G-CIMP profile hallmark the IDH group. K27 and G34 represent critical *H3F3A* mutations that affect histone H3.3, which is a key regulator of epigenetic gene controls and telomere length (Schwartzentruber et al. 2012). This study included both GBM and DIPG, and the K27 and G34 groups are composed mostly of pediatric cases (<21 years). *H3F3A K27* tumors have poor clinical outcome, while *H3F3A G34* cases have a more intermediate outcome (Sturm et al.

2012). Advancements in bioinformatic technologies allow us to map the complex cancer genome. Molecular subtyping of GBM provides cues to which patient may experience greater benefit from specific treatments, and which would not. With such few therapeutic options that influence GBM progression, classification is a step towards the identification of new targetable biomarkers.

1.1.2.4 Mouse models and cell of origin

Animal models of brain tumors have been developed for the purpose of understanding tumor development, and in order to preclinically test new drugs. The first glioma mouse models were generated using carcinogenic chemical induction. Exposure to methylcholanthrene or nitrosoureas resulted in the formation of brain tumors that histologically resembled some aspects of GBM while failing to fully encompass the genetic profile of the human disease (Barth, 1998; Seligman et al., 1939). This approach depends on the random chance of mutation and, although tumors are generated, chemical induction is inconsistent in location, tumor type, and rate of incidence (Barth, 1998; Schmidek et al., 1971). The most commonly used technique for GBM mouse modeling is xenograft transplantation (Shapiro et al., 1979). This involves the surgical implantation of human brain tumor cells either intracranially (orthotopic) or subcutaneously (heterotypic), into immunocompromised mice. Although some groups question how surgical implantation itself can affect the biology of xenograft tumor models (Stylli et al., 2000), malignancies that form frequently recapitulate the human tumor of origin from which the cells were collected (Horten et al., 1981). Most importantly, orthotopic xenografts are especially useful for assessing the efficacy of novel therapeutics in the ability to transverse the blood-brain barrier.

The development of genetically engineered mouse models (GEM) has accelerated the knowledge of signaling pathways that are essential for tumor formation and as well, have been an important tool for pinpointing GBM cells of origin. One of the first GEM brain tumor models involved the injection of the SV40 virus with a metallothionein fusion gene into eggs (Brinster et al., 1984; Stylli et al., 2015) . Since then more refined models that target molecular drivers of gliomagenesis have been used to produce human glioma characteristics. For example, loss of function p53 and RB models are common, as is deletion of NF-1, and inactivation of PTEN

(Huse and Holland, 2009; Reilly et al., 2000; Xiao et al., 2002; Zhu et al., 2005). Mouse models have also validated the importance of RTK signaling in glioma biology. The overexpression of EGFR signaling- either from gene amplification or EGFRvIII- is one of the most prominent GBM traits. Numerous mouse models have aided in the development of EGFR pathway inhibitors (Brown et al., 2008; Franceschi et al., 2007; Prados et al., 2009), as well, GEM overexpression of PDGFB has produced successful models of GBM (Fisher et al., 1999; Hambardzumyan et al., 2009; Uhrbom et al., 1998). Most importantly, GEMs have allowed researchers to target subpopulations of cells for specific oncogenic changes. Using adenoviral transduction methods, Llaguno and colleagues (2009) silenced *Nf1*, *Trp53*, and *Pten* with a Cre/lox system. They found that high-grade gliomas formed when this adeno-cre/lox construct was injected into the subventricular zone (SVZ); however, there was limited tumorigenesis when it was injected into the striatum or cerebral cortex (Alcantara Llaguno et al., 2009). This study highlights the importance of inactivation of tumor suppressors (i.e., p53, PTEN, NF1) in GBM formation; as well, suggests a requirement for this to happen in undifferentiated progenitor cells. Other groups also show the potential for progenitors to be the cell of origin. Chen and colleagues (2012) used nestin-ΔTK-IRES-GFP transgene expression to show that the hierarchies of GBM cells that regrow after TMZ treatment originate from a neural stem cell origin. These findings not only suggest progenitor cell of origin, but provides evidence that this subpopulation can repopulate the tumor following chemotherapy treatment (Chen et al., 2012). Alternatively, another study used retrovirus-mediated PDGFB expression (in combination with inactivated *Trp53* and/or $Cdkn2a^{INK4A/ARF}$) in Nestin+ progenitor cells to generate gliomas (Hambardzumyan et al., 2009). However, when this was done in mature GFAP+ glial, or committed oligodendroglial precursors, gliomas were also formed. These findings suggest that while neural stem cells may act as the cell of origin in the SVZ, gliomagenesis is not restricted to this subpopulation. Different cell types most likely have the ability to transform, but may also depend on the perturbation of different molecular pathways for this to occur. This further exemplifies the heterogeneity of GBM and emphasizes the need to design therapeutic approaches to address this variability.

1.1.3 Medulloblastoma (MB)

While brain tumors in adults can be devastating, the treatment of pediatric brain tumors like MB has added complexity. At present, brain tumors are responsible for the highest rate of cancer-related death in children. Improvement of treatment regimes have dramatically increased progression-free and overall survival rates; however, this has been at the cost of quality of life (Gatta et al., 2009). Standard radiotherapy and surgical procedures often result in sequelae that can impact neurological development and endocrine regulatory systems. There is a need for better therapeutics that can provide personalized targetable options in order to avoid negative treatment side effects in children.

1.1.3.1 MB clinical attributes

MB accounts for upwards of 20% of pediatric brain tumors (Crawford et al., 2007). 21% of MB occurs in infants with the peak incidence of approximately 44% MB of pediatric MB occurring between the ages of 4-9years (Kool et al., 2012; Tabori et al., 2006). Fewer than 12% of cases fall into the young adult age group (>16 years) with less than 1% of MB in older adult patients making it an especially rare occurrence (Kool et al., 2012; Roberts et al., 1991). The WHO lists MB as a Grade IV embryonal tumor that occurs infratentorially in the cerebellum or 4^{th} ventricle (Louis et al., 2007). Originally considered to be a primitive neuroectodermal tumor (PNET), MB was later found to be molecularly distinct from supratentorial PNETs. The term MB includes embryonal malignancy of the brain stem and posterior fossa (Pomeroy et al., 2002; Rorke, 1983). Symptoms that are commonly presented at time of diagnosis usually hint towards cerebellar dysfunction, involvements of the brainstem nuclei and tracts, or hydrocephalus, for example: vomiting, headache, macrocephalus, and ataxia. Elevated intracranial pressure can cause compression of the 4^{th} ventricle and dilatation of the 3^{rd} and the lateral ventricles due to hindered CSF flow, and is detectable with MRI. Diagnosis of infants is more difficult. The loss of developmental milestones and the "setting-sun" sign head tilt may be observed.

Traditional methods of tumor staging are used for clinical characterization of MB. A primary tumor (T) -stage (T1, T2, T3a, and T4) is determined depending on whether the tumor has reached a diameter of 3 cm and infiltrated surrounding tissues. This is paired with a metastasis (M) -stage value (M0, M1, M2, M3, and M4) that ranks the severity of tumor cell

spread in the CSF, ventricles, or subarachnoid space (Chang et al., 1969). Unlike solid tumors of other organs, the spread of brain tumors are generally contained in the CNS; however, aggressive infiltrative tumors can disseminate along the CSF. Metastatic disease has been reported in 30% of MB patients (Gerber et al., 2014).

On a microscopic level, the histopathological appearance of MB tissue is one of the current methods for risk stratification. There are four major histopathological categories of MB based on the extent of tissue nodularity, desmoplasia, anaplasia, and nuclear size (Eberhart et al., 2002). First, approximately 80% of MB have classic (CMB) histology that is distinguished by the appearance of uniform sheets of small round blue cell appearance with a high nuclear to cytoplasmic ratio (Provias and Becker, 1996). Secondly, desmoplastic/nodular (DN) histology is found in 15% of cases (Provias and Becker, 1996) and have a distinct pale nodular architecture with neuronal differentiation patterns. These cases stain for reticulin in dense intercellular networks of desmoplastic fibers that form between the nodules (McManamy et al., 2007; Northcott et al., 2012b). Third, MB with extensive nodularity (MBEN) is the least frequently occurring histological group. It has lobular architecture surrounded by zones that do not stain for reticulin. MBEN and DN are suggested to have a better prognosis than CMB (Garrè et al., 2009; McManamy et al., 2007). This is not the case for the fourth major histological classification, large-cell/ anaplastic (LCA) MB, which is regarded as a marker of high-risk disease (Eberhart et al., 2002). LCA is highly mitotic and characterized by pleomorphism, tumor cell 'wrapping', and large anaplastic nuclei (Northcott et al., 2012b).

1.1.3.2 Current treatment protocols

The overall survival rates for MB have improved remarkably over the last few decades (Gatta et al., 2009). This improvement can mostly be attributed to the adoption of intense, escalating radiation protocols (Carrie et al., 1999; Grabenbauer et al., 1996; Jakacki et al., 2012) along with better surgical maintenance of CSF and tumor resection. Unfortunately, there is often a trade-off between the benefit of high intensity, and invasive, techniques and the long-term quality of life of patients. To this point, long term side effects have a much greater impact on children compared to adults for two reasons, (1) they can disrupt key developmental stages, and (2) children generally have more remaining lifespan compared to adults that are considerably

older in age. As a result, it is necessary to create strategies to stratify risk in pediatric MB in order to de-escalate treatment intensity and decrease negative sequela. Current stratification used for clinical decision-making include: patient age, M-stage, extent of resection, and more recently histology (Pietsch et al., 2014). These criteria are used to dictate a specific approach to the treatment of MB using surgical resection, radiation, and chemotherapy.

Surgery

The medical term for surgical removal of tumors like MB is *posterior fossa craniotomy.* Craniotomy means, "*drilling bone out from the skull",* and the procedures are done by making an incision near the bottom of the skull in order to access the cerebellum. There are three main objectives when operating. The first objective is to establish an official diagnosis for tumor (Von Hoff and Rutkowski, 2012). Second, to restore normal CSF flow in the ventricles of the brain. Some of the major symptoms at diagnosis of MB are due to an increase in intracranial pressure from CSF blockages, also known as *hydrocephalus*. This can result from the tumor itself, or even infections following treatment. A ventriculoperitoneal shunt is used to relieve CSF pressure either at time of surgery-or in the days following- for a reported 50% of patients (Bartlett et al., 2013; Bhatia et al., 2009). The third goal of surgery is to resect as much tumor as possible without causing damage to the normal surrounding tissue. Remaining tumor tissue >1.5 cm^2 is considered a risk factor and patients with sub-total resection have significantly lower overall survival compared to gross total resection (Grill et al., 2005). Regardless, surgeons must determine a balance between achieving maximal resection and avoiding neurological damage. Negative sequela may be experienced immediately after surgery and include non-obstructive hydrocephalus, bleeding, neurocognitive impairment, and 'posterior fossa syndrome' (Korah et al., 2010). This outcome is worsened with the combination of radiation to the brain that has been associated with neuroendocrine defects such as hypothyroidism and delayed puberty (Frange et al., 2009).

Radiation and chemotherapy

The postoperative management of MB is approached differently between infants and older children, but the objective in all age groups is to promote patient survival while reducing

long-term side effects. To attempt to achieve this, clinical trials stratify children into high and standard-risk groups. Standard-risk cases are generally non-infant with no metastatic dissemination that may benefit from protocols with reduced radiation. For example, these cases have been shown to have equal survival benefit when a full dose of 36 Gy radiation to the posterior fossa was dropped to 23.4 Gy (Packer et al., 2006). Currently, there is an ongoing clinical trial testing if this radiation boost can be dropped to 18 Gy in order to further reduce neurological sequelae (NCT00085735). In addition, this trial is also testing whether the radiation of only the tumor bed is sufficient for standard-risk cases as opposed to the whole posterior fossa. Following surgery and radiation, standard-risk MB patients are usually treated with cocktails of chemotherapeutics, including: cisplatin, carboplatin, cyclophosphamide, and vincristine. (Packer et al., 2006). Chemotherapy is occasionally used immediately after surgery in hopes of delaying or completely avoiding radiation (Duffner et al., 1993).

The high-risk group of childhood MB generally either have >1.5 cm^2 residual tumor or metastatic dissemination located at the neuraxis. Recurrent cases of tumor relapse are also considered high-risk in older children and, unfortunately, have a lower than 10% salvage rate (Pizer et al., 2011; Warmuth-Metz et al., 2011). The therapy protocols for these cases are intended to benefit patient survival, and the reduction of negative side effects is a secondary consideration. The benefit of current protocols depend on using higher doses of radiation such as 36 to 39.6 Gy plus boosts to the posterior fossa and solid metastases (Jakacki et al., 2012). In addition, these high-risk cases are candidates for testing radio-sensitizing drugs and protocols involving hyperfractionation of high radiation doses (i.e., dividing the radiation into multiple doses per day) (Gandola et al., 2009; Pizer et al., 2011; Warmuth-Metz et al., 2011). Aside from radiotherapy, there are a number of clinical trials questioning if there may be any benefit provided for high-risk MB from a specific chemotherapy regimen (Chi et al., 2004; Dhall et al., 2008; Jakacki et al., 2012; Pizer et al., 2011; Warmuth-Metz et al., 2011). Unfortunately, any dose de-escalation for high-risk MB children will require the adoption of accurate prognostic markers to clinical practice.

Treatment protocols for infant and younger children aim to completely avoid the use of craniospinal radiation. An age cut off for the use of radiotherapy is <3 years in some institutions and <6 years in others. In cases with no metastasis, favorable results are achievable with surgery

and post-operative chemotherapy only (Dhall et al., 2008; Grill et al., 2005). One study that used three cycles of intravenous chemotherapy (cyclophosphamide, methotrexate, vincristine, etoposide, and carboplatin) and intraventricular methotrexate following surgery report a 77% 5-year survival rate. However, there was only a 38% 5-year survival for children with detectable metastases (Rutkowski et al., 2005). Further, a series of "Head Start" protocols have been tested in multiple institutions. Head Start I ran from 1991 to 1997 and was initially started as a chemotherapy-only treatment option for children <6 years old. It includes five cycles of a post-operative chemotherapy cocktail (vincristine, cisplatin, cyclophosphamide and etoposide) followed by myeloablative chemotherapy (carboplatin, thiotepa and etoposide) with autologous hematopoietic cell rescue (AuHCR) (Dhall et al., 2008). Head Start II ran from 1997 to 2003 and incorporated the addition of high doses of methotrexate into each cycle. Early reports from Head Start I/II show that patients benefitted from intensified induction chemotherapy in the absence of radiation (Fangusaro et al., 2008). Trials with Head Start III ran from 2003 to 2009 and are reported to have the best survival outcomes of children receiving a radiation-sparing chemotherapy protocol. This version incorporated oral TMZ and etoposide into alternating cycles of the chemotherapy cocktail used in Head Start II. Approximately 52% of patients <6 years avoided craniospinal radiation, and 2-year overall survival was 80% for M0 cases (Suneja, 2011). Although there was only a 54% 2-year overall survival for M1 cases, this is still a significant improvement from other radiation-sparing regimes (Rutkowski et al., 2005; Suneja, 2011).

There have been no MB clinical trials specifically for adults (>18 years) due to the low frequency of adult cases. As a result, the role of chemotherapy in adult MB is relatively unknown. One study tested the efficacy of treating adult (>20-years of age) MB with the pediatric HIT 2000 protocol (Friedrich et al., 2013; Warmuth-Metz et al., 2011). Approximately 70 patients were treated with 35.2 Gy craniospinal radiation with boosts to the posterior fossa, along with chemotherapy (lomustine, vincristine, and cisplatin). Of note, chemotherapy was found to be beneficial for M0 adult MB. As well, tumor location and histology was found to be influential risk factors for adult MB (Friedrich et al., 2013). More work needs to be done as a growing body of evidence suggests the biology of adult and pediatric MB are reasonably distinct (Northcott et al., 2011a; Remke et al., 2011b).

Along with clinical features, histological subtype has further stratified patient risk and been incorporated into treatment decision-making. Intensified adjuvant protocols for chemotherapy and radiation are warranted for non-infant patients with residual tumor, evidence of metastasis, or LCA histology (Rutkowski et al., 2010). These are characteristic of high-risk disease and represent fewer than 30% of non-infant children. For infants, the DN histology is considered a marker of better outcome compared to LCA or CMB, but again, this only encompasses a small subset of MB cases (Rutkowski et al., 2005; von Hoff et al., 2009). The majority of MB diagnosed has CMB histology assessed as standard-risk according to current clinical practice, but while some of these patients fail to respond to treatment, others have the ability achieve remission from surgery alone. As a result, there has been a paradigm shift in the MB field to emphasize the use of molecular markers and technologies to develop better tools for clinical prognostication. To do this, researchers look for molecular cues in systems that control brain development.

1.1.3.3 Hijacking cerebellar development

Tumor formation is often the result of aberrant signaling pathways that are normally essential for the growth and maintenance of specific tissues. As an embryonic tumor, strong evidence suggests that specific developmental pathways are responsible for MB formation. To strategically develop therapy and prognostic markers, an understanding of the fundamental biology of MB is necessary.

Cerebellum development

The cerebellum has a number of different precursor cell populations that are regulated by signaling pathways during development. There are two major embryonic germinal zones from which cerebellar cells develop. The first is the ventricular zone (VZ) that lines the roof of the fourth ventricle. It contains GABAergic precursor cells that will later form cell types such as Purkinje neurons, astrocytes, oligodendrocytes and Bergman glia (Eberhart, 2008). The second cerebellum germinal zone is the rhombic lip. This is the location of glutamatergic precursors that migrate to the nuclear transitory zone to form the deep nuclei. In addition, the rhombic lip produces granule neuron precursor (GNP) cells that proliferate transiently to form the external

granular layer (EGL). GNPs are considered lineage-committed and will differentiate into mature granule neurons that form an internal granule layer (IGL). As well, GNPs express high levels of the transcription factor *ATOH1* (*MATH1*), which is essential for EGL development and used as a marker for GNP cells. It has been suggested that another population of undifferentiated stem cells may exist within the white matter of the postnatal cerebellum. It is interesting to note that this population can generate astrocytes, neurons, and oligodendrocytes, but does not generate GNPs (Goldowitz and Hamre, 1998; Pei et al., 2012a; Wang and Zoghbi, 2001). As this variety of embryonic precursor cells develops into a postnatal cerebellum, there are key signaling pathways that control this process.

WNT signaling

The WNT pathway was originally discovered through the *wingless* phenotype of Drosophila melanogaster developmental studies. In humans, it has an important developmental role in the embryonic brain and neural stem cell signaling (Ciani and Salinas, 2005). Pei and colleagues (2012) have shown that WNT signaling promotes the proliferation of GABAergic neural stem cells located in the VZ. It is suggested that elevated WNT signaling not only drives proliferation but disrupts neural stem cell differentiation (Pei et al., 2012a). The activity of the WNT pathway depends on the cellular accumulation of free β–catenin (CTNNB1). Normally maintained at low levels, β–catenin is contained by an APC/AXIN/GSK3 multiprotein complex. GSK3 or another kinase, CK1α, will phosphorylate β–catenin and thereby target it for ubiquitination and proteolysis. The canonical pathway is activated when extracellular WNT ligands bind frizzled (FZD), a family of G-protein coupled transmembrane receptors. Activation of FZD sends a direct signal to the cytosolic protein disheveled (DSH) that causes a disruption of the inhibitory APC/AXIN/ β–catenin complex. This liberates β–catenin from targeted degradation and it increases cytosolic concentration. β–catenin will translocate to the nucleus where it interacts with TCF co-factor proteins to activate transcription of WNT pathway genes such as Cyclin D1 and c-MYC (Figure 1.1). Activation of WNT pathway transcript substrates affects proliferation, and cell fate determination (Zechner et al., 2003).

Familial activating mutations in the WNT pathway have been reported to cause MB. Specifically, Turcot's syndrome results from the mutation of the adenomatous polyposis coli

(*APC*) gene and predisposes for MB and GBM (Thompson et al., 2006). Modifications to APC affect its ability to complex with β–catenin thereby blocking regular β–catenin degradation programs. Somatic mutations can also occur in the gene that codes for β–catenin, *CTNNB1*. This mutation disrupts the negative regulatory systems that tightly control β–catenin resulting in accumulation in the nucleus (Eberhart et al., 2000; Zurawel et al., 1998).

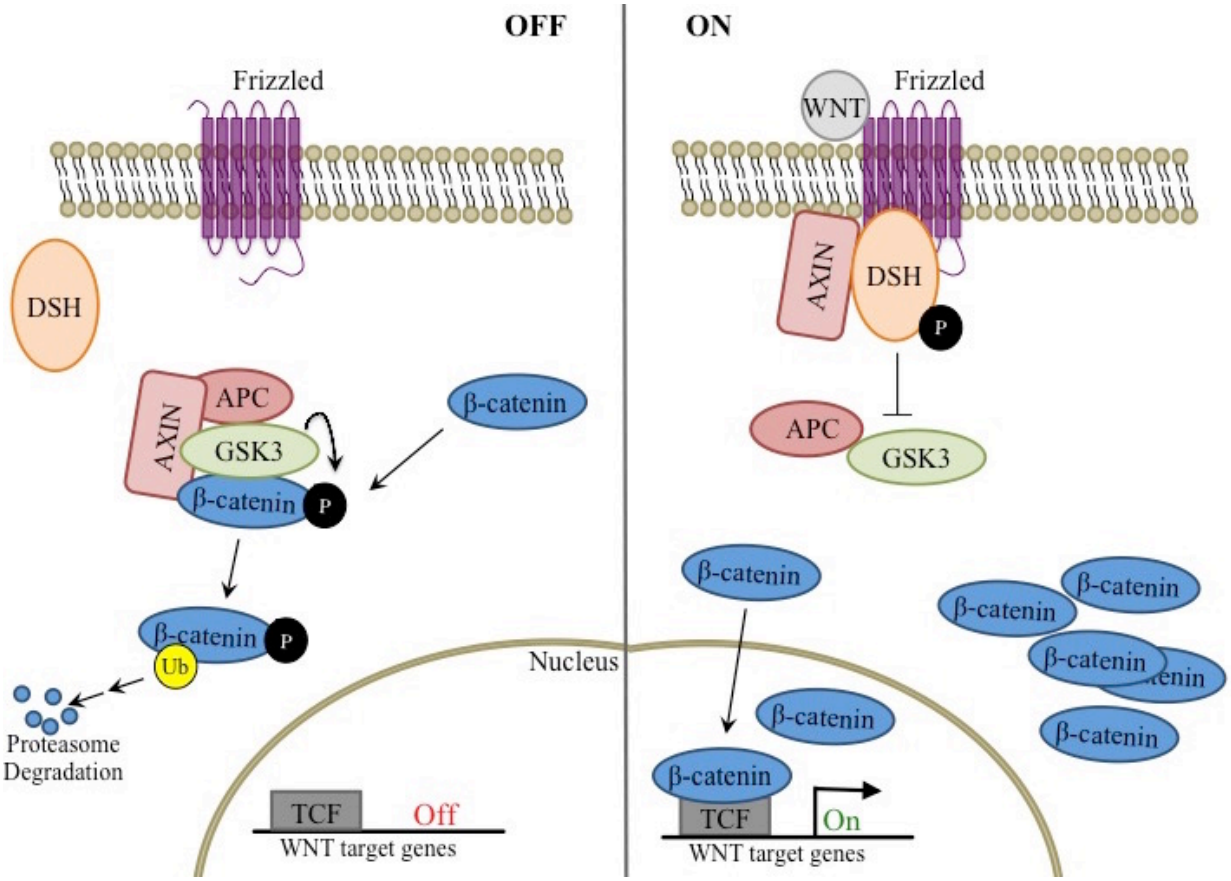

Figure 1.1 Summary graphic of canonical WNT signaling pathway.

Sonic Hedgehog (SHH) signaling

SHH is one of three human homologs of the *Drosophila melanogaster* Hedgehog (*Hh*) gene, and its expression is crucial to neural tube and brain development early in embryogenesis (Odent et al., 1999). GNPs- after migrating to the EGL- proliferate in response to SHH ligands that are secreted by Purkinje neurons. In the canonical pathway, SHH ligands bind the

transmembrane receptor patched (PTCH1) on the surface of GNPs. When not bound by SHH, PTCH1 represses the activity of another transmembrane protein, smoothened (SMO). Ligand binding results in the internalization of PTCH1 thereby releasing the inhibition of SMO that then recruits and binds other pathway components to the membrane. Within the cell, the proteins SUFU and Kif7 sequester a pool of microtubule-bound GLI transcription factors. PKA, CK21, and GSK3 are kinases that oppose the SHH pathway by phosphorylating GLI when sequestered; this causes GLI degradation (Ingham et al., 2011). Proteasome-dependent cleavage of GLI also result in the conversion of carboxy-terminus repressor GLI proteins that are able to translocate to the nucleus and block the transcription of SHH target genes (Ruiz i Altaba et al., 2002).When SMO is active, the repression of GLI is released, and it translocates to the nucleus. Nuclear GLI binds DNA to activate or repress specific genes such as *PTCH1*, *HHIP*, *MYCN*, *BMI1*, and *ATOH1* (Dahmane et al., 1997; Ruiz i Altaba et al., 2002) (Figure 1.2)

Mutations found in the gene coding for PTCH1 are responsible for causing Gorlin's Syndrome, a disease that increases susceptibility for MB (Cowan et al., 1997). This autosomal dominant disorder is also associated with mental defects. Other mutations affecting *SMO, SUFU,* and *GLI1/2* may cause constitutive activation of the SHH pathway, thereby promoting dysregulated proliferation in the GNP cell population that can result in MB tumor formation (Schüller et al., 2008; Taylor et al., 2002)**.** Along with embryonic development, the SHH pathway regulates neural stem cells in the adult brain; however, this regulation in non-GNPs is not as well characterized (Palma et al., 2005). Notably, crosstalk of the SHH pathway with other signaling networks - such as WNT, BMP, NOTCH and MYC - is in part responsible for controlling both normal and cancer cell development (Natarajan et al., 2013; Oliver et al., 2003; Pan et al., 2006; Rios et al., 2004).

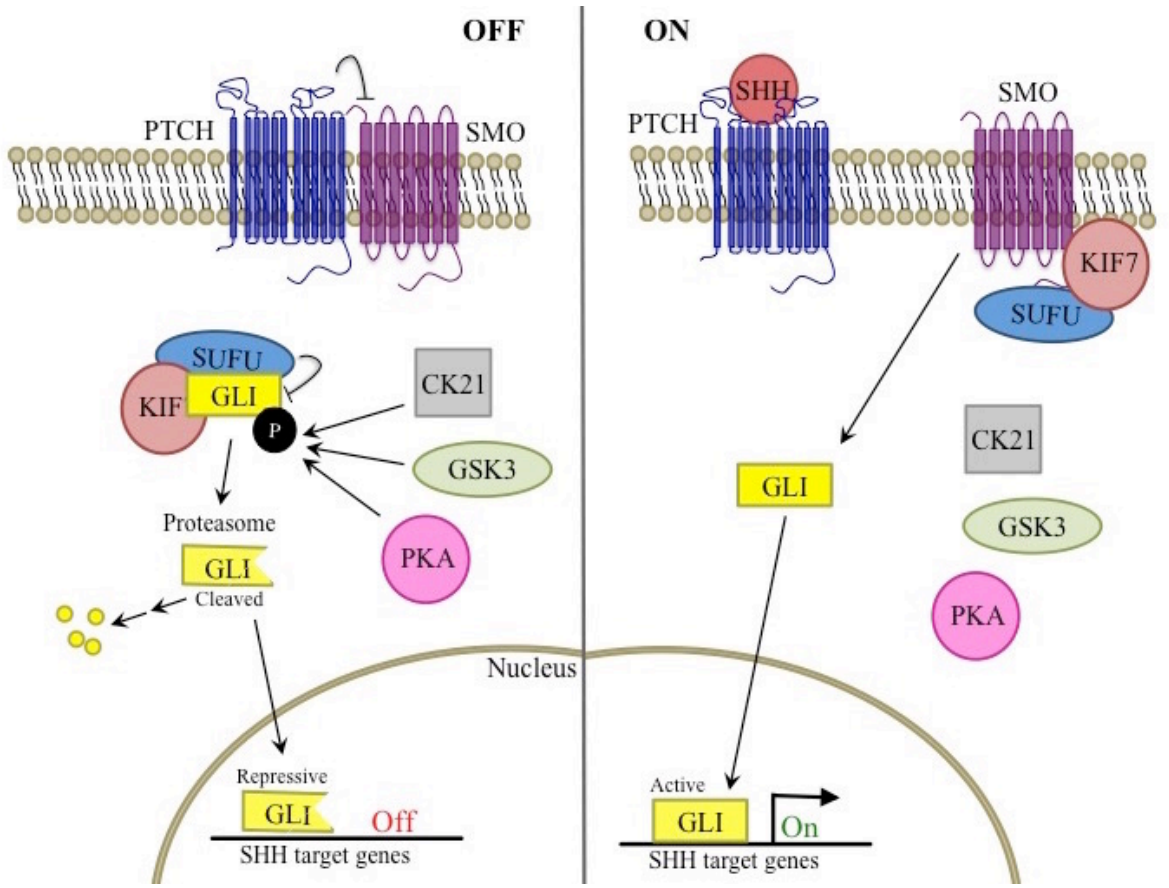

Figure 1.2 Summary graphic of SHH canonical signaling pathway.

BMP signaling

Members of the bone morphogenic protein (BMP) family are thought to be responsible for providing the initiatory signal for granule cell specification of precursors in the rhombic lip. BMPs - specifically BMP6, BMP7, and GDF7- are produced by cells in the dorsal midline (Alder et al., 1999). This pathway stimulates GNPs to begin to differentiate into mature granule neurons that eventually form the IGL. BMP2 signaling is reported to suppress the proliferative response of GNPs to SHH to cause cell cycle exit (Angley et al., 2003; Rios et al., 2004; Zhao et al., 2008). Alder and colleagues demonstrated that treating neural cells with BMPs and transplanting them into the postnatal mouse cerebellum causes the differentiation of mature granule neurons in the EGL (Alder et al., 1999). As a negative regulator of SHH-driven cell proliferation in the cerebellum, BMP signaling is highlighted as an influential regulation pathway in MB (Fogarty et al., 2005; Merve et al., 2014).

NOTCH signaling

The proliferation and differentiation of GNPs are also coordinated by the NOTCH pathway (Yoon and Gaiano, 2005). This pathway is characteristically involved with cell-cell communication, and its canonical pathway includes juxtacrine binding of membrane-bound ligand receptors (Natarajan et al., 2013). The transmembrane receptor, Notch2, binds a membrane-bond ligand (i.e., JAG1/2 or DLL family) from another cell to activate cleavage of its intracellular domain, NICD, which then translocates to the nucleus to activate transcript of genes like p21, MYC and the HES family. There are multiple proteins that modulate this pathway (Solecki et al., 2001; Yoon and Gaiano, 2005). *NOTCH2* signaling is down-regulated as GNPs exit the cell cycle. The NOTCH pathway reportedly inhibits differentiation and promotes proliferation, which has implications for sustaining oncogenesis if dysregulated (Solecki et al., 2001). Hallahan and colleagues have shown that *NOTCH2* and *HES5* pathway members are elevated in MB compared to normal cerebellum; as well, they have been linked to SHH signaling using *in vivo* models of MB (Hallahan et al., 2004). An understanding of the biology of development is an asset in decoding the biology of cancer.

1.1.3.4 Molecular classification of MB

The classification of molecularly distinct subgroups within single cancer types has become common in oncology. Genomic technologies and advanced biostatistics have identified four subgroups of MB based on patient demographics, clinical outcomes, somatic genetic events and gene expression (Taylor et al., 2012). Establishment of these subgroups has resulted from over a decade of research depicting the influence of specific cell signaling pathways and identifying chromosomal abnormalities**.** The initial attempts to deduce the clear number of subgroups by different research groups had variable results mainly due to variation in patient cohorts (Cho et al., 2011; Kool et al., 2008; Northcott et al., 2011b; Thompson et al., 2006). Cooperation within the research community resulted in the acceptance of four main subgroups at a consensus meeting held in 2010 (Taylor et al., 2012). These include: WNT, SHH, Group 3, and Group 4.

WNT subtype

The WNT subtype of MB is the most established but occurs in fewer than 10% of cases (Northcott et al., 2012a). These cases are generally older children and lack leptomeningeal dissemination. Over 90% of individuals with WNT MB have long-term survival, and this subtype is considered a good prognosis. Ellison and colleagues report that death that do occur in the WNT subgroup are usually due to complications of treatment or formation of a secondary neoplasm (Ellison et al., 2011). Interestingly, LCA histology has been reported in a few rare WNT cases and is considered to have a good prognosis (Ellison et al., 2005), however, the vast majority of WNT MB have CMB histology. Traditional clinical stratification methods are useless in identifying these cases without additional markers.

As the name suggests, tumors in the WNT subgroup are recognized for a hyper- activation of the WNT, or β–catenin, signaling pathway. Familial activating mutations in the WNT pathway have been reported to cause MB. Specifically, Turcot's syndrome results from the mutation of the *APC* gene and predisposes for MB and GBM (Thompson et al., 2006). Modifications to APC affect its ability to complex with β–catenin thereby blocking regular β–catenin degradation programs. As a result of the loss of negative β–catenin regulation, it continues to translocate to the nucleus and activate the WNT signaling transcriptome. Somatic mutations can also occur in *CTNNB1*, and this mutation disrupts the negative regulatory systems that tightly control β–catenin resulting in accumulation in the nucleus.

Monosomy of chromosome 6 is the main cytogenetic characteristic of the WNT subtype (Ellison et al., 2011), and more recently elevated expression of CD15 (stage-specific embryonic antigen 1/SSEA-1/FUT4) (Manoranjan et al., 2013). Mutations in SMARCA4, CREBBP, DDX3X, and PIK3CA have also been found in WNT subgroup tumors (Robinson et al., 2012). In addition, immunohistochemical staining for high nuclear β–catenin or DKK1 positivity are useful tools for identifying WNT cases that has already been adopted by some pathologists (Ellison et al., 2005; Northcott et al., 2011b).

Sonic hedgehog (SHH) subtype

Between 20-25% of MB are classified in the SHH subtype (Northcott et al., 2012a). This group was originally considered to have an intermediate prognosis, and more recent findings

suggest there may exist further subcategories of SHH MB that accounts for its clinical heterogeneity (Kool et al., 2008; Pietsch et al., 2014). Between 15-20% of cases diagnosed present metastatic disease and there is an interesting bimodal distribution in patient age. (Northcott et al., 2012c, 2011b). Compared to other subtypes, there is a higher frequency in patients younger than 3 (infant) and older than 16. Clear differences in molecular and clinical attributes of pediatric and adult SHH MB have previously been reported (Northcott et al., 2011a). Histologically there is an enrichment of DN cases in the SHH subtype, however, while nearly all DN tumors are SHH, SHH tumors can also have CMB, LCA, and MBEN histology (Ellison et al., 2011). To add further complexity, having DN histology is suggested to be a good marker of prognosis for younger children, but a poor prognostic marker for adult cases (Northcott et al., 2011a).

The SHH subtype is another group identified based on the dysregulation of a previously studied signaling pathway. Compared to other MB subtypes, the highest rates of single gene mutations occur in the SHH subtype (Northcott et al., 2012c). Somatic mutations in *PTCH1*, *SUFU*, and *SMO,* as well as amplifications of *GLI1* and *GLI2,* have been found in MB (Kool et al., 2014; Parsons et al., 2011; Pugh et al., 2012; Taylor et al., 2002). There is also a number of SHH cases that have MYCN amplification. Both Group 4 and SHH groups can have MYCN overexpression whereas Group 3 MB are known for overexpression of a relative protein, c-MYC (Kool et al., 2008; Northcott et al., 2011b). SHH-driven MB also has identifying chromosomal aberrations, for example, the deletion of 10q, 14q, or 17q, and gain of 3p or 3q. Interestingly, *PTCH1* is located at 9q22, and the loss of 9q has also been reported in a small number of tumors. (Northcott et al., 2012c). Northcott and colleagues proposed the use of secreted frizzled-related protein 1 (SFRP1) protein to identify SHH cases, however, immunohistochemical detection of SHH has been less reliable than gene expression based methods (Northcott et al., 2011b).

Group 3 subtype

Group 3 MB are considered to have the worst prognosis of the four subtypes. This group is diagnosed in ~27% of MB and is associated with the highest rates of metastatic disease that are reported to be between 40-45% of patients (Kool et al., 2012; Taylor et al., 2012). The gender distribution is skewed with a 2:1 male to female cases and Group 3 occurs almost exclusively in

pediatric cases. Originally no adult Group 3 MB were reported (Remke et al., 2011b), but larger meta-analysis suggest they account for 6% of this group (Kool et al., 2012). This discrepancy can most likely be attributed to the difference in age cut-off used in these studies, as the classification of young adults (16-21) can be variable. Regardless, Group 3 MB is especially aggressive with an overall survival of only 33% adult, 39% infant, and 50% childhood cases. Agreeing with these survival trends, LCA histology occurs more frequently in Group 3 MB. CMB histology also occurs in Group 3 whereas DN and MBEN are absent from this subtype (Kool et al., 2012; Northcott et al., 2012a, 2011b).

Unlike WNT and SHH subtypes, Group 3 and Group 4 have more similar genetic profiles that rely on gene expression-based diagnosis. A single signaling pathway has not yet been identified as being responsible for Group 3 oncogenesis; however, there is precedence for overexpression of genes associated with retinal development. Orthodenticle Homeobox 2 (*OTX2)* is one such gene that is amplified in 7.7% of Group 3 MB (Adamson et al., 2009; Bai et al., 2010; Northcott et al., 2012c). The most highly associated genomic aberration is *MYC* amplification (16.7%), which was determined to occur mutually exclusive to *OTX2*. *MYC* over-expression is a candidate driver of this subtype and a marker of poor prognosis (Delmore et al., 2011; Northcott et al., 2012c, 2011b). It has also been suggested that Group 3 can be stratified into two subsets, Group 3α, which has amplified *MYC* and poor prognosis, and Group 3β, which does not have the amplification and experiences an intermediate prognosis (Cho et al., 2011). Although fluorescence in situ hybridization (FISH) detection of MYC is a commonly used in laboratories, there are limitations to sensitivity using this assay (Pfister et al., 2009). Similarly, natriuretic peptide receptor 3 (NPR3) has been developed as an immunohistochemical marker for the diagnosis of Group 3 MB, but its detection lacks the sensitivity required for robust clinical use (Min et al., 2013; Northcott et al., 2011b).

More recently, mutations affecting epigenetic regulatory proteins were discovered in Group 3 MB. For example, *SMARCA4*, *KMT2D*, and *CHD7* encode for proteins that remodel chromatin, as well as mutations affecting genes in the lysine-specific demethylase (KDM) family (Jones et al., 2013, 2012; Northcott et al., 2012a). More work is currently underway to decipher which important downstream systems are modified by these epigenetic signaling mutations. Single gene mutations are more common in SHH subgroup and are found in less than half Group

3 MB where chromosomal alterations are more prevalent. A gain of chromosome 1q, 7, 17q, and 18, as well as loss of 10q, 16q, and 17q have all been reported (Northcott et al., 2012c; Pfister et al., 2009). Researchers are now beginning to pinpoint functional reasons as to why such chromosomal alterations drive MB progression. In a recent publication, somatic genomic rearrangements were found to increase the expression of *GFI1* and *GFI1B* in one-third of Group 3 MB. It is suggested that rearrangements of chromosomal DNA modifies the proximity of enhancer regions to the promoters of these oncogenes thereby elevating expression within the cell (Northcott et al., 2014). Under this premise, the downregulation of genes as a result of chromosomal rearrangements is also a consideration that requires further investigation.

Group 4 subtype

The final and most common occurring MB subgroup is Group 4. Just over 35% of MB are classified as Group 4 and between 35-40% of these cases are metastatic at the time of diagnosis (Kool et al., 2012; Northcott et al., 2012a). The highest disproportion in gender distribution is within this group, as there are 3 boys diagnosed for every 1 girl (Kool et al., 2012; Northcott et al., 2012a). Taylor and colleagues (2011) describe Group 4 as being "prototypical MB" in clinical appearance, however, at this point it can only be identified using transcriptional profiling. Between 40-45% Group 4 MB occur in the childhood age bracket, with 25% in adult and considered rare in infants. Group 4 has an intermediate prognosis for childhood cases but is a marker of poor outcome for adults. Infants with Group 4 MB have the worst outcome relative to other age groups (Kool et al., 2012; Remke et al., 2011a; Shih et al., 2014). Histologically, the majority of Group 4 patients have CMB with a few cases of LCA. DN has been reported in Group 4, but it has been suggested that this may have been due to a categorization error (Gajjar and Robinson, 2014; Kool et al., 2012). Further, LCA and Group 4 tumors with metastasis are considered high risk and show about 60% 5-year survival. Standard risk Group 4 cases with no metastasis and gross total resection have >80% 5-year survival with current treatment strategies. (Kool et al., 2012; Shih et al., 2014; Taylor et al., 2012). Recent studies using cytogenetic markers demonstrate a low-risk population of Group 4 based on chromosome 11 loss or 17 gain. Both low and standard risk Group 4 individuals have the potential to do well with current treatment strategies (Shih et al., 2014).

Although Group 4 occur frequently, there is least known about the molecular pathology of this subgroup. There are no known syndromes that predispose for Group 4 MB, and it was originally identified based on the bioinformatic clustering of cases that overexpress neuronal differentiation and glutamatergic genes (Kool et al., 2008; Northcott et al., 2011b). Aside from gene expression, the use of potassium voltage-gated channel subfamily A member 1 (KCNA1) has been proposed as an immunohistochemistry (IHC) marker of Group 4, however, validation studies found it to be detectable in all four subgroups making it ineffective for classification (Min et al., 2013; Northcott et al., 2011b). The most common aberration in Group 4 is an isochromosome 17q (i17q), which is found in 66% of cases. This aberration occurs when an additional q-arm is used to replace a lost p-arm of chromosome 17 (Kool et al., 2012; Northcott et al., 2012a; Robinson et al., 2012). Although never seen in WNT or SHH tumors, i17q is present in both Group 3 and Group 4 MB. Of note, i17q is a marker of poor prognosis in Group 3 where it is found in 26% of cases, but has no prognostic influence in Group 4 relative to balanced karyotype patients (Shih et al., 2014). Other rearrangements that have been found in Group 4 include gains in chromosome 7, 17q, 18q, and loss in 11p, 8, and X. Approximately 80% of Group 4 female patients have a complete loss of X chromosome (Kool et al., 2008; Northcott et al., 2011b; Taylor et al., 2011).

One of the initial challenges is finding characteristics that differentiate Group 4 from Group 3 tumors. For example, *MYCN* and *CDK6* are amplified in approximately 6% and 5% of Group 4 MB, respectively, but rarely found in Group 3 (Cho et al., 2011; Northcott et al., 2011b). *SNCATP,* a gene implicated in Parkinson disease, is also amplified in around 10% of Group 4 tumors. The mechanistic importance of this modification in MB is still to be determined (Northcott et al., 2012a, 2012c). Other genes that are mutated in Group 4 include *KDM6A* (12%), *MLL3* (5%), *ZMYM3* (5%), and *CBFA2T2* (3%) (Cho et al., 2011; Northcott et al., 2012c; Robinson et al., 2012). Like Group 3 MB, amplification of OTX2, overexpression of GFI1, and mutations in the KDM protein family are routinely found. However, unlike Group 3, there is a greater proportion of amplified MYCN than MYC in Group 4 (Gajjar and Robinson, 2014; Jones et al., 2012; Northcott et al., 2012c).

1.1.3.5 Mouse models and cell of origin

WNT. Gibson and colleagues (2010) developed the first WNT specific animal model. This was achieved through the induction of *CTNNB1* activating mutations in progenitor cells of the lower rhombic lip and embryonic dorsal brainstem. Herein the first evidence of a different cell of origin between subtypes was established (Gibson et al., 2010). The progenitor cell populations driven by WNT signaling appear to differ in location and activity compared to SHH-driven progenitors. This same group later improved their first WNT model, which had 15% penetrance, to add a $PIK3CA^{E545K}$ mutant allele. This mutant had been identified in human WNT tumors, and its addition increased the WNT mouse model to 100% penetrance (Robinson et al., 2012). In support of the first model, an independent group found that the Gibson and colleagues (2010) mouse model accurately resembled human tumors using gene expression profiling (Pöschl et al., 2014). The creation of animal models that truly replicate the characteristics of WNT tumors is essential for creating better methods to safely eliminate tumor growth in children.

SHH. Mouse models of the SHH subgroup of MB have fueled much of the information known about MB. There are more models of SHH than any of the other subtypes, and they are mostly derived through the modification of various components of the SHH pathway. For example, the first models were generated using germline deletion of one *Ptch1* allele ($Ptch1^{+/-}$) (Goodrich et al., 1997; Wetmore et al., 2000). Similarly, another group has developed a transgenic mouse model using *Smoothened* (*Smo*) mutations (Hallahan et al., 2004; Hatton et al., 2008). These animal studies have revealed the cell of origin for SHH MB through the promotion of tumorigenesis with deletion of *Ptch1* specifically in committed cerebellar GNPs (Schüller et al., 2008; Yang et al., 2008). More recently, genomic studies have enhanced the $Ptch^{+/-}$ penetrance with the addition of the *Sleeping Beauty* (SB) transposon system to study metastatic dissemination and screen for gene candidates responsible for driving tumorigenesis (Dupuy et al., 2005; Genovesi et al., 2013; Wu et al., 2012). The development of animal models of the SHH has been a valuable tool for understanding this MB subtype.

Group 3. Less is known about the molecular drivers of Group 3 making the generation of animal models more difficult compared to the WNT or SHH subtypes. In the same journal issue, two groups are credited with developing the first animal models of Group 3 using orthotopic

transplantation of murine neural progenitor cells. Pei and colleagues (2012) did so using orthotopic transplantation of cerebellar stems cells, which were modified to overexpress *Myc* (*MYC*) along with mutant *Trp53* (p53). The tumors that developed resembled LCA histology including cell wrapping morphology and a gene expression profile that differed from SHH based mouse models (Pei et al., 2012b). Kawauchi and colleagues (2012) also developed a *Myc* based mouse model in combination with a loss of *Trp53* in GNPs. This group used the neuronal lineage marker, *Atoh1*, to sort for GNPs, but its expression disappeared in the transformation of the tumor cells. The *Myc*-induced tumors were distinct from WNT or SHH models (Kawauchi et al., 2012). Herein, the Group 3 mouse models from both studies demonstrate that this subtype may develop from neural stem cells or de-differentiated cells as a result of MYC-dependent transformation. The aforementioned mouse models were examined for similarity to human Group 3 tumors. Although initially distinct from WNT and SHH murine models using a 50-100 gene panel, neither model matched the profile of Group 3 patient tumors; instead they were found to be most similar to SHH (Pöschl et al., 2014). The authors suggest this may be attributable to the use of loss of function p53 in the Group 3 models because this aberration is more commonly found in SHH patients. It is also valuable to note that only a portion of human Group 3 MB have MYC amplification, and more work needs to be done to establish models for other subsets of Group 3. Finally, a third research group used a patient-derived metastatic Group 3 sample to derive the cell line HD-MB03. They suggest that orthotopic transplantation of HD-MB03 into mice produced tumors reflecting the original patient tumor (Milde et al., 2012). Although patient sample xenograft may not truly reflect the developmental biology of tumor development, this approach provides useful preclinical models for therapeutic testing.

Group 4. At this point in time, there are no animal models that accurately reflect Group 4 MB. This may be attributed to the current lack of understanding of the exact molecular mechanisms that drive this subgroup. Of note, the use of MYCN amplified mouse models have been suggested to partially reflect the small subset of MYCN amplified Group 4 MB (Eberhart, 2012; Swartling et al., 2010). As more is learned about the molecular basis of MB subgroups, greater opportunities for prognostication and therapy development have become apparent.

	WNT	SHH	Group 3	Group 4
Proportion of cases:	~10%	20-25%	25-30%	35-40%
Common age groups:	Children, few adults	Adults and infants, some children	Young children, some infants	Mostly children, few infants and adults
Gender ratio (F/M):	1:1	1:1.5	1:2	1:3
Prognosis:	Good	Intermediate to Poor	Poor	Intermediate
Proposed cell of origin:	Lower rhombic lip and dorsal brainstem progenitor cells	- Neural stem cells from SVZ -GNPs from EGL	-Neural stem cells -GNPs from EGL	Unknown
Signaling Expression:	WNT pathway	SHH pathway	-MYC signature -Retinal genes	Neuronal genes
Histology:	Mostly Classic	DN, Classic, LCA, MBEN	Classic, LCA	Classic, LCA
Cytogenetics	Monosomy 6	3q+, 9q-, 10q-	i17q, 1q+, 7+, 10q-, 16q-, 17q-	i17q, X-, 11p-, 7+, 18q+
Examples of altered genes:	*CTNNB1, APC, SMARCA4, CREBBP, DDX3X, PIK3CA*	*PTCH1, SMO, SUFU, TP53, MYCN, GLI2*	*MYC, OTX2, SMARCA4, KMT2D, CHD7*	*MYCN, CDK6. SNCATP, KDM6A, MLL3, ZMYM3, CBFA2T2*

Adapted from (Northcott et al., 2012a, 2012b; Taylor et al., 2011)

Table 1.1 General summary of features of MB molecular subtypes.

1.1.3.6 Additional drivers of MB

Since the identification of the four MB subgroups, further large-scale, whole genome studies have uncovered more information that will undoubtedly refine our perception of this disease (Jones et al., 2012; Pugh et al., 2012; Robinson et al., 2012). The pathogenesis of a portion of tumors can be attributed to disruption of established development signaling pathways (i.e., WNT or SHH), however, these cases are considered a minority and the exact mechanism behind the majority of tumors is relatively unknown. One hypothesis is that the answer lies in posttranslational regulation of gene expression and not solely dependent on the direct aberration of canonical pathway components.

Epigenetic regulators

The role of epigenetic regulation of the oncogenome has gained a great deal of momentum in MB research. Whole-genome sequencing revealed that many of the most frequently mutated genes in MB coded for proteins with epigenetic activity. For example, mutations in *SMARCA4* and *KMT2D* are recurrently detected and not limited to specific subgroups (Pugh et al., 2012; Robinson et al., 2012). These genes are involved in chromatin remodeling. Simply, this can either increase or restrict access of transcriptional machinery to specific gene promoters. Other epigenetic factors make up the list of most frequently mutated in WNT (i.e., *CREBBP, SMARCA4, KMT2D),* SHH (i.e., *BCOR, KMT2D)*, Group 3 (i.e., *CHD7, SMARCA4, KMT2D, KDM family*), and Group 4 (i.e., *CHD7, KMT2D, KMT2C, KDM6A)* (Northcott et al., 2012a; Pugh et al., 2012; Robinson et al., 2012). Additionally, truncating mutations in *MLL2 and MLL3* also occur in a subgroup independent manner and have a significant impact on regulation of histone H3 methylation that is indicative of patient outcome (Dubuc et al., 2012).

Epigenetic factors also have influential roles within specific subtypes. BMI1 is involved in neural stem cell self-renewal and acts as a regulator in an epigenetic polycomb complex (Leung et al., 2004). Expression of *BM1I* has been linked to the SHH subtype, and there is a suggested regulatory feedback loop between BMI1 and SHH ligand in MB tumor initiating cells (Wang et al., 2011). As well, amplifications of the transcript factor OTX2 are reported in Group 3 and Group 4 MB. Bunt and colleagues suggest OTX2 activity may cause the upregulation of the epigenetic complex genes *SUZ12, EZH2,* and *EED* (Bunt et al., 2013; Jones et al., 2012). Experimentally silencing OTX2 caused a reduction in polycomb remodeler expression with a coinciding increase of demethylase activity. As a result this produced a decrease in histone H3 lysine 27 (H3K27) methylation, which is a key epigenetic modification suggested to allow gene expression that promotes stem cell-like properties (Bunt et al., 2013). Disruption of epigenetic regulation is a unifying theme across MB subtypes; however, the downstream consequence to transcription still remains unclear.

TP53

Another important driver of MB that is not restricted to a subgroup identifying signaling pathway is *TP53. TP53* mutations are some of the most frequently reported in cancer. This gene

codes for p53, which is considered the "guardian of the genome" and has roles in controlling apoptosis, DNA repair, growth arrest, and stress response (Brosh and Rotter, 2009; Muller and Vousden, 2013; Strano et al., 2007). Li-Fraumeni syndrome is a familial disease caused by the heritable *TP53* mutations that predispose children to MB (Malkin et al., 1990). These cases normally present with LCA histology, MYCN amplification and assign to the SHH subgroup (Kool et al., 2014). Sporadic mutations of *TP53* occurs in 16% WNT and 21% SHH MB tumors (Zhukova et al., 2013). *TP53* mutations are essentially absent from Group 3, and are rare in Group 4. Patients positive for *TP53* mutation have a dramatically worse prognostic outcome (Northcott et al., 2012a; N. Zhukova et al., 2013). Although molecularly important, the exact genesis of *TP53* mutation in MB remains to be determined. Rausch and colleagues (2012) propose an interesting concept that links *TP53* mutations in MB to catastrophic DNA rearrangements. Specifically, they suggest that a process called chromothripsis causes a single event of dramatic chromosomal "shattering" that can result in gene mutations and copy number changes, and that this may be a driver of *TP53* mutations in SHH MB (Rausch et al., 2012). It has become clear that the pathogenesis of MB extends beyond canonical signaling pathways; therefore, our approach to treating cancer must do so as well.

1.2 Modern approaches to therapy development

The body of knowledge on high-grade brain tumor biology has vastly expanded. Work to improve the precision of surgical resection, as well, the implementation of novel biotechnologies, has resulted in a better understanding of the molecular characteristics of tumors. Further, the discovery of cancer stem cell-like (CSC) populations has offered some explanation into the complexity of recurrent disease. Researchers are now searching for clinically approved drugs that can be repurposed for the elimination of therapy-resistant tumor subpopulations.

1.2.1 Surgical advancements

Some of the recent advances in malignant brain tumor treatment strategies have aimed to improve the accuracy and precision of surgical techniques. In one German study, the use of ALA-Fluorescence-guided (FGS) surgery in combination with chemotherapy has increased the

percentage of complete resections from 27.2% to 48.4% and the mean overall survival from 16.6 to 20.1 months (Slotty et al., 2013). Similarly, 3D ultrasound technology has also made modest improvements to the surgical removal of GBM. Another European study reports a mean overall survival increase from 9.6 to 11.9 months since incorporating 3D ultrasound visualization into surgical practice (Sæther et al., 2012). Additional technologies have also been used to attempt to circumvent drug delivery limitations created by the BBB. The implantation of biodegradable carmustine- releasing wafers (Gliadel® wafer) into the peritumoral tissue following surgery has been explored. This approach would ideally increase the direct infusion of chemotherapy to the surgical cavity while reducing systemic toxicity to the patient, but early trials with this technique have mixed reviews. Some studies report slight improvements to survival, but carmustine wafers have also been shown to cause complications such as intracranial infection, hydrocephalus, and ventricular defects (Perry et al., 2007; Westphal et al., 2003). While innovative methods to enhance surgical resection and drug delivery are being developed, the issue remains that there is limited to no progress in the hunt for drug therapies to overcome drug resistance and some of these being developed have limited efficacy.

1.2.2 NanoString gene expression technology

Bioinformatic technologies have taken the center stage of experimental and future clinical diagnostics. Genetic tests using cytogenetics, gene sequencing, RNA transcript expression profiling, and more recently, DNA methylation arrays, are molecular platforms that provide integral information about the specific characteristics of neoplasms. The amalgamation of the aforementioned methodologies have been used to establish molecular subtypes of multiple cancer types, including GBM and MB (Cho et al., 2011; Jones et al., 2012; Kool et al., 2012; Northcott et al., 2011b; Phillips et al., 2006; Sturm et al., 2012; Verhaak et al., 2010). Specifically, the use of mRNA gene expression has triggered the implementation of molecular profiling into patient stratification. The next major step is the translation of genetic-based technologies out of research laboratories and into functional clinical diagnostic use.

Quantitative real-time polymerase chain reaction (RT-PCR) and RNA microarrays are established tools for measuring transcript levels in biological samples to make up gene expression profiles. While both methods have been instrumental in retrospective studies, they

lack the sensitivity and reproducibility required for prospective clinical use. For instance, microarrays have the ability to compare gene expression of hundreds of targets, but requires lots of high-quality RNA, is expensive, and produces variable data. RT-PCR is a great deal more sensitive than microarrays but is only capable of measuring a single gene target per reaction. As well, RT-PCR depends on a reverse transcriptase enzymatic reaction that demands the use of high-quality input material. The ideal gene profiling system should be able to accurately measure multiple targets in a quick, reproducible manner with limited biological samples of clinical relevance.

The NanoString nCounter system is a relatively recent technology for the ultra sensitive, multiplexed measurement of nucleic acid targets. This system detects individual mRNA transcripts and uses molecular barcodes with an automated digital read out (Geiss et al., 2008). This is done through the hybridization of two sequence-specific probes (35-50bp) per gene of interest. First, the "capture probe" that has a complementary sequence to the target mRNA and is linked to a biotin tag. Second, the "reporter probe", which also has complementary target gene sequence, but is also linked to a color-coded detection tag. The detection tag is composed of a single-stranded DNA backbone that is annealed to RNA segments with specific fluorophores. There are seven fluorophore-coupled segments per gene forming a specific color bar code that is unique to a specific gene target. The nCounter system is capable of detecting approximately 800 targets in a single 100 ng total RNA sample. A hybridization reaction of sample RNA, capture and reporter probes are mixed and allowed to form triplexes. Following this the complexes are fixed to a streptavidin-coated surface in the presence of an electric field. The biotin from the capture probe has an extremely high affinity for this surface, and the field orientates the complexes so they can be easily counted. A digital analyzer then uses the fluorescent signals from the reporter probe to quantify the desired gene targets. The nCounter system is more sensitive than standard Affymetrix U133 microarrays and equally as sensitive as RT-PCR. Additionally, this system requires only a fraction of the amount of RNA as other methods and does not depend on enzymatic reaction (Geiss et al., 2008). This is a huge benefit for clinical samples that are often limited in quality and quantity.

Tumor tissue is preserved in formalin-fixed paraffin-embedded (FFPE) blocks as standard practice by pathologists. The use of IHC protein stains on FFPE tissue has been

attempted for brain tumor subtype classification, however, there remains too much lot-to-lot variation in detection materials as well differences in pathologist interpretation (Goschzik et al., 2014; Northcott et al., 2011b). Fortunately, the NanoString nCounter system can reliably detect transcript expression in highly fragmented RNA that can be extracted from FFPE. It has demonstrated additional efficacy using RNA from flash frozen tissue and crude tissue lysates (Malkov et al., 2009). One study used this technology to profile malignant hematologic disease and found the NanoString mRNA expression of important surface markers correlated to levels of antigen detection using flow cytometry. This suggests the nCounter platform has the potential to replace a number of subjective and labor intensive methods used by technicians (Fernandez et al., 2012).

Most importantly, Northcott and colleagues (2012d) have created a NanoString based molecular subtyping method for MB. A 25-gene minimal marker signature can be used to determine subtype using low quantities of RNA from extracted from FFPE. In an early study researchers were able to assign either WNT, SHH, Group 3, or Group 4 classification to 88% of clinical FFPE samples assessed with 100% accuracy (Northcott et al., 2012d). The reason some samples could not be subtyped is attributed to the age and degradation of archived FFPE tumor tissue. NanoString nCounter technology offers an opportunity to predict MB tumor subtype that may be instrumental in providing accurate patient stratification and dictate effective treatment protocols.

1.2.3 Cancer stem cells

The complexity of malignant brain tumors is not restricted to intertumor diversity, but intratumoral heterogeneity. For example, the presence of undifferentiated subpopulations in adult and infant tissues that are responsible for tissue maintenance and development. Neural stem cells were first identified in mouse models, which led to the discovery and isolation of human neural stem cell populations (Reynolds and Weiss, 1992; Roy et al., 2000). Understanding the characteristics of stem cell populations is of upmost importance for cancer research due to the discovery of CSCs. CSCs are a small subset of cells that are capable of unlimited self-renewal, can undergo differentiation, and are tumor-initiating when transplanted orthotopically (Figure 1.3A). The general premise of the “cancer stem cell hypothesis” is that not all cells have equal

ability to proliferate and maintain tumorigenesis. While the bulk of the tumor is made up of differentiated cells, the CSC population can continually self-renew and asymmetrically divide to generate tumor mass. It is hypothesized that cancer treatments fail to prevent tumor relapse as they target the tumor bulk and not CSCs (Tan et al., 2006; Vescovi et al., 2006).

Singh and colleagues were the first to isolate and characterize brain tumor CSCs from both GBM and MB (Singh et al., 2003). *In vitro*, brain CSCs are grown and propagated in selective neurosphere culture conditions that are non-adherent, and in serum-free medium supplemented with epidermal growth factor (EGF) and fibroblast growth factor (FGF). A neurosphere is a "ball of cells" generated from the self-renewal and proliferation of viable CSCs. Some semi-differentiated progenitor cells can also generate neurospheres, but the true test of CSC function is whether the cell population can sustain neurosphere growth following multiple serial passages (Singec et al., 2006). Extraction of primary brain tumor neurospheres is a valuable practice because primary neurospheres will often more closely retain the characteristics of the neoplasm of origin when compared to cell lines that are propagated adherently in serum (Lee et al., 2006).

Prominin 1 (CD133) is a cell surface glycoprotein suggested to be a marker of multipotent stem cells in the brain and other tissues (Galli et al., 2004; Singh et al., 2003). CD133-positivity correlates with the CSC population and is enriched for in the SVZ leading to the question of whether these cells are the cells of origin for malignant glioma. When sorted using flow cytometry and orthotopically transplanted into immunocompromised mice, CD133-negative cells require $>10^5$ cells for tumor initiation whereas the CD133-positive population could generate tumors with as few as 100 cells (Singh et al., 2004). GBM having >2% CD133-positive cells or high ki67 staining are considered to have a poor prognosis (Pallini et al., 2008).

CD15 is another proposed marker of brain tumor CSCs (Read et al., 2009; Son et al., 2009). Sorting for CD15-positive cells enriches for tumor initiation and proliferation; however, there is a lack evidence of multi-lineage differentiation. As well, CD15-positive MB cells do not consistently form self-renewing neurospheres and are expressed in lineage-committed GNP cells (Read et al., 2009).

Aldehyde dehydrogenase (ALDH) is a family of metabolic enzymes that catalyze the oxidation of aldehydes, which are toxic products of alcohol metabolism (Lipsky et al., 2001). A

relationship between high ALDH activity and stem cell behavior prompted the use of an ALDH based fluorescence assay, Aldefluor®, to identify undifferentiated populations both within cancer and normal tissues (Corti et al., 2006; Deleyrolle et al., 2011; Rasper et al., 2010). In cancer studies, high ALDH expressing cells have been associated with enhanced xenograft tumor formation in mice and chemotherapeutic resistance (Choi et al., 2014b; Schäfer et al., 2012)

An exact marker for, and the origin of CSCs remains a controversial topic. The overlap between developmental pathways and drivers of tumorigenesis causes one to postulate how traits within lineage hierarchies influence brain tumor formation. Experimental evidence supports the idea that glioma CSCs could arise from abnormal stem cells that gain oncogenic traits, and also supports the possibility that they could form due to the activation of stem cell genes in more restricted progenitors (Alcantara Llaguno et al., 2009; Hambardzumyan et al., 2009; Read et al., 2009). While it was initially thought that CD133-negative cells represented a non-tumor initiating population, it was later shown that they can generate tumors that also contain CD133-positive cells (Wang et al., 2008). This plasticity may suggest that CD133 is not a reliable marker of CSCs; in addition, CD133 is also expressed by endothelial cells that may contaminate the sorting of GBM cells, skewing experimental results. Differing traits between CD133-positive and CD133-negative cells might even represent CSCs from distinct cells of origin. Gene expression profiles suggest CD133-positive cells resemble a proneural glioma signature while CD133-negative correlates with a mesenchymal signature (Lottaz et al., 2010).

Regardless of markers, resistance to chemotherapy and radiation regimes is the most important characteristic of CSCs. While treatments often are successful in killing off the tumor bulk, CSCs have unique properties that allow them to continue to proliferate and self-renew thereby regrowing the neoplasm (Figure 1.3B) (Diehn et al., 2009; G. Liu et al., 2006; Stiles and Rowitch, 2008). Radioresistance can result from the activation of DNA damage response pathways (Bao et al., 2006; Hambardzumyan et al., 2008). As well, CSC populations have been shown to elevate expression of anti-apoptotic and drug resistance proteins such as MGMT. This increase results in heightened resistance to chemotherapies, namely carboplatin, etoposide, paclitaxel and TMZ (G. Liu et al., 2006). It is absolutely critical that new therapies be developed to eliminate the tumor bulk, while also targeting CSC subpopulations, in order to prevent relapse of high-grade brain tumors.

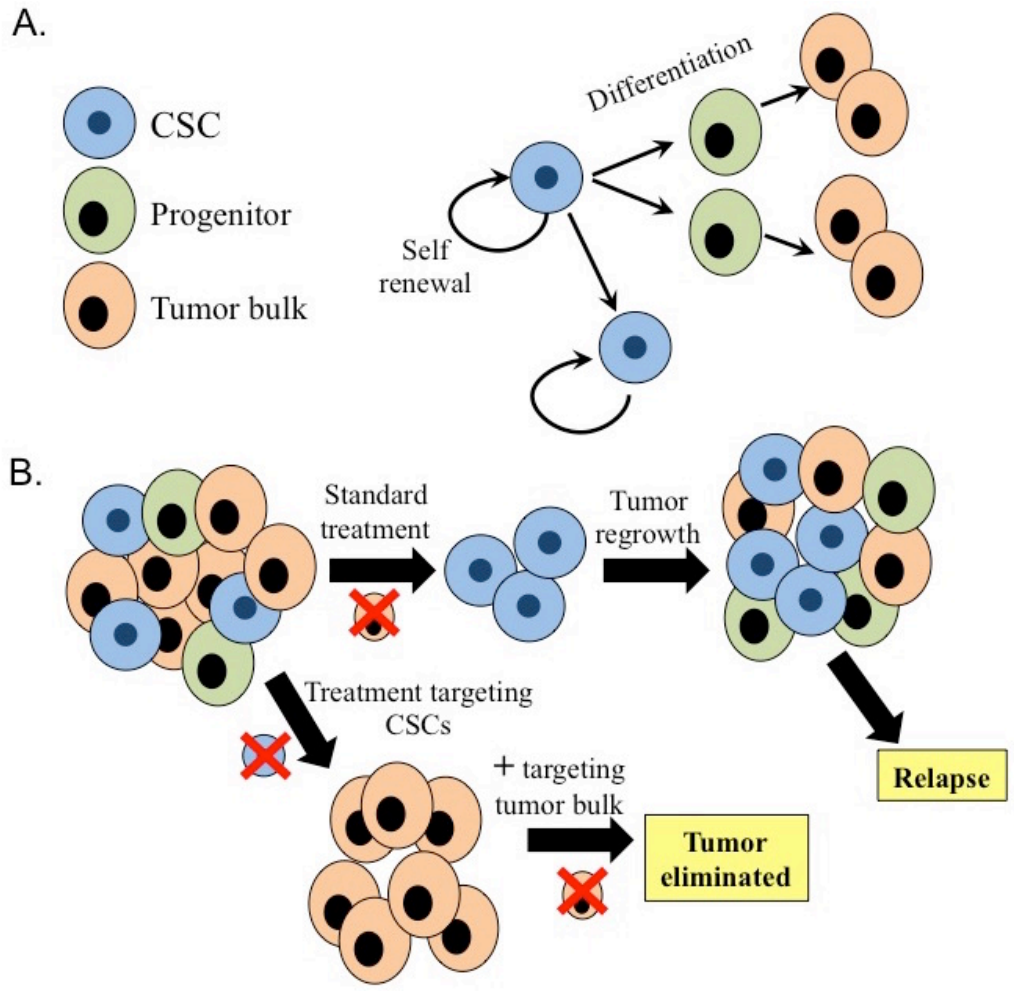

Figure 1.3 Summary graphic of the cancer stem cell hypothesis.

(A) Cancer stem-like cells (CSCs) have the ability to self renew, and differentiate into tumor bulk to re-establish tumor formation upon relapse. **(B)** Standard treatments that fail to target CSCs result in tumor regrowth, whereas elimination of CSCs in combination with therapies that target the growth of more differentiated cells may prevent tumor relapse.

1.2.4 Repurposing off-patent drugs

One of the biggest problems in advancing the treatment of brain tumors is the time and resources required to develop new therapeutics. It is estimated to take 15 years and somewhere between $500 million and $2 billion in preclinical and clinical testing to bring a single drug to market (Chong and Sullivan, 2007; Karamehic et al., 2013). All new drugs need to be rigorously evaluated for safety, and phase I clinical trials alone typically take two years and over $17 million to complete (DiMasi et al., 2003). According to one health report, only 1 in 1000

compounds in preclinical testing will proceed to clinical trials. From those, 1 in 5 will be approved for use in humans, and only 2 in 10 of those drugs approved will generate sustainable revenue to recoup development costs (Karamehic et al., 2013). As a result, the pharmaceutical industry often delegates its resources toward developing therapeutics for larger target populations and not towards less common diseases. This is especially true for pediatric cancers, which are often highly complex, and childhood specific clinical trials are exceptionally rare (Milne and Bruss, 2008).

There are nearly 10 000 drugs known to modern clinical medicine, and the full multitude of functions for the majority of these compounds is still to be determined. Currently, only 1 in 10 drugs tested clinically is covered by exclusivity patents, which leaves a plethora of drugs that could potentially be repurposed in an affordable manner. By repurposing off-patent drugs for cancer treatment, the overall cost of drug development could be cut by at least 40% due to previously conducted safety trials (Chong and Sullivan, 2007). TMZ has been the primary chemotherapeutic used to treat GBM for over a decade; this is despite the fact that most patients develop resistance to it (Stupp et al., 2005). Approximately $15 000 over an average of 5.1 months is the cost of treating a malignant glioma patient with TMZ. This consumes an estimated 61% of the total cost of patient care, and TMZ does not come close to ranking as one of the pricier cancer drugs (Meropol and Schulman, 2007; Wasserfallen et al., 2005). There is a vast amount of un-mined potential in repurposing off-patent drugs that could potentially revolutionize the treatment of high-grade brain tumors.

1.2.4.1 Repurposing disulfiram (DSF)

Disulfiram (DSF), also known as Antabuse®, is used for treatment of substance abuse and in addiction studies (Hald and Jacobsen, 1948; Suh et al., 2006). Initially, the compound had been used in the process of rubber manufacturing. In 1937, it was discovered that factory workers, who were regularly exposed to DSF, would experience flu-like symptoms when they ingested alcohol (Suh et al., 2006). The first clinical trials for the use of DSF as an anti-alcoholic treatment began in 1948, and it has been used in patients for over 60 years (Hald and Jacobsen, 1948). With the more recent discovery of a stem cell population in cancer, scientists are once again finding new purposes for DSF.

DSF is most widely known as an inhibitor of ALDH. A relationship between high ALDH activity and stem cell behavior prompted the use of an ALDH based fluorescence assay. ALDH enzyme activity is thought to be involved in cell detoxification and Aldefluor® active cells have been associated with resistance to cisplatin, docetaxel, and doxorubicin (Jiang et al., 2009). The drug cyclophosphamide is a fundamental chemotherapeutic in many pediatric brain tumor treatment protocols. High levels of ALDH have been directly shown to intervene with cyclophosphamide metabolism and decomposition making this a potential mechanism for chemotherapeutic resistance (Hipkens et al., 1981; Sládek et al., 2002). The ALDH1a1 isoform was previously thought to have the strongest association with the CSC phenotype; however, Marcato et al. (2011) suggest expression of ALDH1a3 to have greater CSC correlation and prognostic importance compared to ALDH1a1 in breast cancer (Marcato et al., 2011). With a family of 19 total ALDH isoforms, it is difficult to pinpoint complete functional independence due to redundancy in activity.

DSF was identified in several studies as an agent that inhibits CSCs for cancers of the breast, ovary, pancreas, lung and blood (Hothi et al. 2012; Iljin et al. 2009; Mimeault and Batra 2008). It could, therefore, have great promise in brain tumor treatment particularly given that it not only kills CSCs but seems to do so by targeting multiple pathways operative in these refractory cells.

1.3 Polo-like Kinase 1 (PLK1) a potential target of high-grade brain tumors

Uncontrolled proliferation is a hallmark of cancer, and targeting drivers of the cell cycle could prevent tumorigenesis. Polo-like Kinase 1 (PLK1) is a serine/threonine kinase that promotes cell cycle progression and is often used as a marker of proliferation (Yuan et al., 1997). Overexpression of PLK1 is common in aggressive forms of cancer (Harris et al., 2012; Takahashi et al., 2003; Takaoka et al., 2014; Wolf et al., 1997). It enables cells to override regulatory checkpoints that can promote genomic instability and cell transformation (Smith et al., 1997; Smits et al., 2000). A small interfering RNA library screen by our group identified PLK1 as a promising target for rhabdomyosarcoma, a common pediatric soft-tissue tumor (Hu et al., 2009). As well, multiple studies report that PLK1 is an extremely attractive target for eliminating

CSCs across different types of tumors (Francescangeli et al., 2012; Grinshtein et al., 2011; Harris et al., 2012). Further, specific small molecule inhibitors against PLK1 are already available and being tested in various clinical trials. Therefore, we question whether PLK1 could be a valuable target for the treatment of high-grade brain tumors.

1.3.1 PLK1 structure

The PLK protein family was discovered in *Drosophila melanogaster,* and alteration of the *polo* gene caused defects in mitosis and meiosis. Evolutionarily, PLK1 is the original ancestral family member with at least three duplication events producing paralogs, PLK2, 3, 4, and 5 (Carvalho-Santos et al., 2010; Kothe et al., 2007). PLK1 is highly conserved in organisms that use centrioles in mitosis and is not present in most plant species (Karpov et al., 2010). Other PLK family members have been implicated in roles in centriole duplication (PLK2 and 4), regulation in checkpoint transition, and cytokinesis (PLK3). PLK5 lacks a functional kinase domain and little is known about its cellular function (reviewed in Zitouni et al. 2014).

PLK1 is a 603 amino acid kinase composed of a polo-box domain (PBD), an inter-domain linker (IDL) region, and a serine/threonine kinase domain (KD). The C-terminal PBD is made up of two smaller polo-box structures (PB1 and PB2) separated by a loop switch region and preceded by the Polo-Cap (PC). This region functions primarily to mediate protein interactions, localization, and regulate the activity of N-terminal KD (Elia et al., 2003a, 2003b; Lee et al., 1998). An IDL connects the PBD and KD. This region also participates in regulation of the KD and contains a D-box motif at PLK1Arg337 that is used to target PLK1 for degradation (Lindon, 2004; Xu et al., 2013). Finally, the KD contains regulatory T-loop, and an ATP-binding site for the transfer of phosphate groups to substrates (Figure 1.4) (Macůrek et al., 2008).

The KD is activated through phosphorylation of it T-loop site at Thr210 and a Ser137 hinge activation in the ATP-binding pocket. When these sites are not phosphorylated the PBD has the ability to directly bind and inhibit the KD through bending of the flexible IDL (Y.-J. Jang et al., 2002; van de Weerdt et al., 2005). Displacement of the PBD from the KD increases PLK1 kinase activity. This occurs as a result of activation phosphorylations on the KD or through phosphopeptide binding of the PBD to target proteins (Elia et al., 2003a; Y.-J. Jang et al., 2002).

The PBD is not regulated through direct phosphorylation, but the affinity of the PBD for binding phosphosubstrates can be modified by ubiquitination (Beck et al., 2013). Kachaner and colleagues recently uncovered the crystal structure of the KD and PBD inhibitory complex and discovered that the stability of this interaction is dependent on the binding of another protein, Map205 (Kachaner et al., 2014). Various cell cycle proteins interact and modify the PBD, IDL and KD of PLK1 in order to regulate the various roles of PLK1 throughout mitosis.

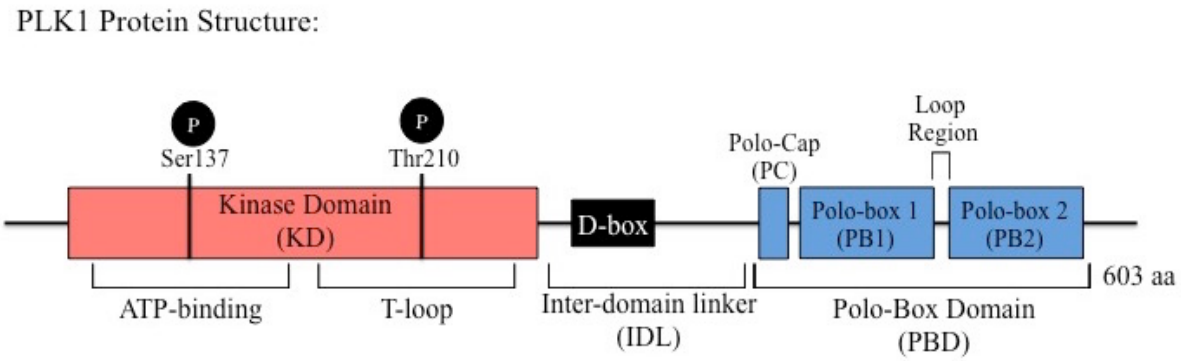

Figure 1.4 Summary graphic of the protein structure of PLK1.

1.3.2 PLK1 regulation

The activation of PLK1 activity needs to be tightly regulated both temporally and spatially for the dynamic execution of cell division. Expression of PLK1 is low during interphase then is up-regulated during S-phase. Levels of PLK1 mRNA and protein peak during the G2/M transition in mitosis and decline following anaphase (Uchiumi et al., 1997; Winkles and Alberts, 2005). Rb and E2F protein families can repress transcription of *PLK1* during interphase while various activators of transcription increase *PLK1* production during mitosis. FOXM1 and B-myb are transcription factors reported to up-regulate PLK1, which occurs following cyclin-dependent kinase (CDK) inactivation of the transcriptionally repressive DREAM complex (Down et al., 2012; Pilkinton et al., 2007; Sadasivam et al., 2012; Wen et al., 2008).

Once expressed, the timely localization of PLK1 during various stages of mitosis is key in dictating its function. There are low levels of PLK1 located in the cytoplasm and associated

with microtubules or centrosomes during interphase. Once mitosis is initiated, a high level of PLK1 is associated with microtubules at the centrosomes, and kinetochores, as well as being highly concentrated at the central spindle and midbody during anaphase (Lee et al., 1998; Seong, 2002). PLK1 accumulates in both the nucleus and cytoplasm. The KD contains a nuclear localization sequence (residues 134-146) that aids PLK1 in accessing the nucleus before breakdown of the nuclear envelope (Taniguchi et al., 2002); however, the PBD has a greater role in localization through binding of various phosphopeptides. Of note, PBD has a higher affinity for substrates that have already been 'primed' through phosphorylation by either PLK1 itself or another cell cycle kinase such as CDK1. This is an example of a mechanism used for signal amplification as the higher the cellular concentration of phosphorylated PLK1 substrates, the greater the affinity of the PLK PBD to bind them. This results in the release of the PBD intramolecular binding of the KD and enhances kinase activity (Elia et al., 2003a, 2003b; Y.-J. Jang et al., 2002; McInnes et al., 2012). Localization of PLK1 to the kinetochores and the central spindle is achieved through PBD interaction with P-INCENP, which is primed by CDK1 (Goto et al., 2006). In addition, ubiquitination can modify the attachment of phosphosubstrates to the PBD causing PLK1 to separate from binding partners and leave kinetochores as a means of progressing out of metaphase (Beck et al., 2013).

The activation and deactivation of PLK1 serine/threonine kinase activity is a critical regulatory control that can be manipulated in a short timeframe. Kinase activity mirrors the cyclic changes of PLK1 expression that increase in the G2/M transition and is highest during mitosis (Figure 1.5A). Activity is increased when the PBD is bound to phosphoproteins and releases the KD to become available to other factors. Similarly, activation occurs in part from other kinases that phosphorylate Ser137 and Thr210 in the KD. The phosphorylation of Ser137- by an unknown kinase- helps control PLK1 function later at the spindle checkpoint (Y. J. Jang et al., 2002; van de Weerdt et al., 2005; Xu et al., 2013). Aurora A and its cofactor, Bora, are responsible for phosphorylating Thr210 in G2 phase (Macůrek et al., 2008; Seki et al., 2008). Evidence also suggests protein kinase A (PKA) and STE20-like kinase (SLK) may also phosphorylate Thr210 (Ellinger-Ziegelbauer et al., 2000; Kelm, 2002). Activation of PLK1 can also be indirectly affected through upregulation of its inhibitors or downregulation of its activators (i.e., Aurora A). Constitutive activation of PLK1 kinase activity have been shown to

produce defects in mitotic and cytokinetic events (Kong et al., 2014; Lindon, 2004). Therefore, regulatory factors like myosin phosphatase 1 (Mypt1) can dephosphorylate the Thr210 activation residue. Mypt1 is first primed by CDK1 then directly binds the PLK1 PBD and removes the phosphosite from the KD (Yamashiro et al., 2008).

Final downregulation of PLK1 occurs in anaphase as cells exit from mitosis. PLK1 normally has a short half-life and is targeted for degradation via the ubiquitination dependent proteasome pathway. Protein phosphatase CDC14B activates the anaphase-promoting complex (APC/C) that then ubiquitinates PLK1 at the D-box motif located in the IDL (Figure 1.5B). Polyubiquitination targets PLK1 for proteolysis by the proteasome and protein levels drop until the next round of mitosis (Bassermann et al., 2008; Lindon, 2004).

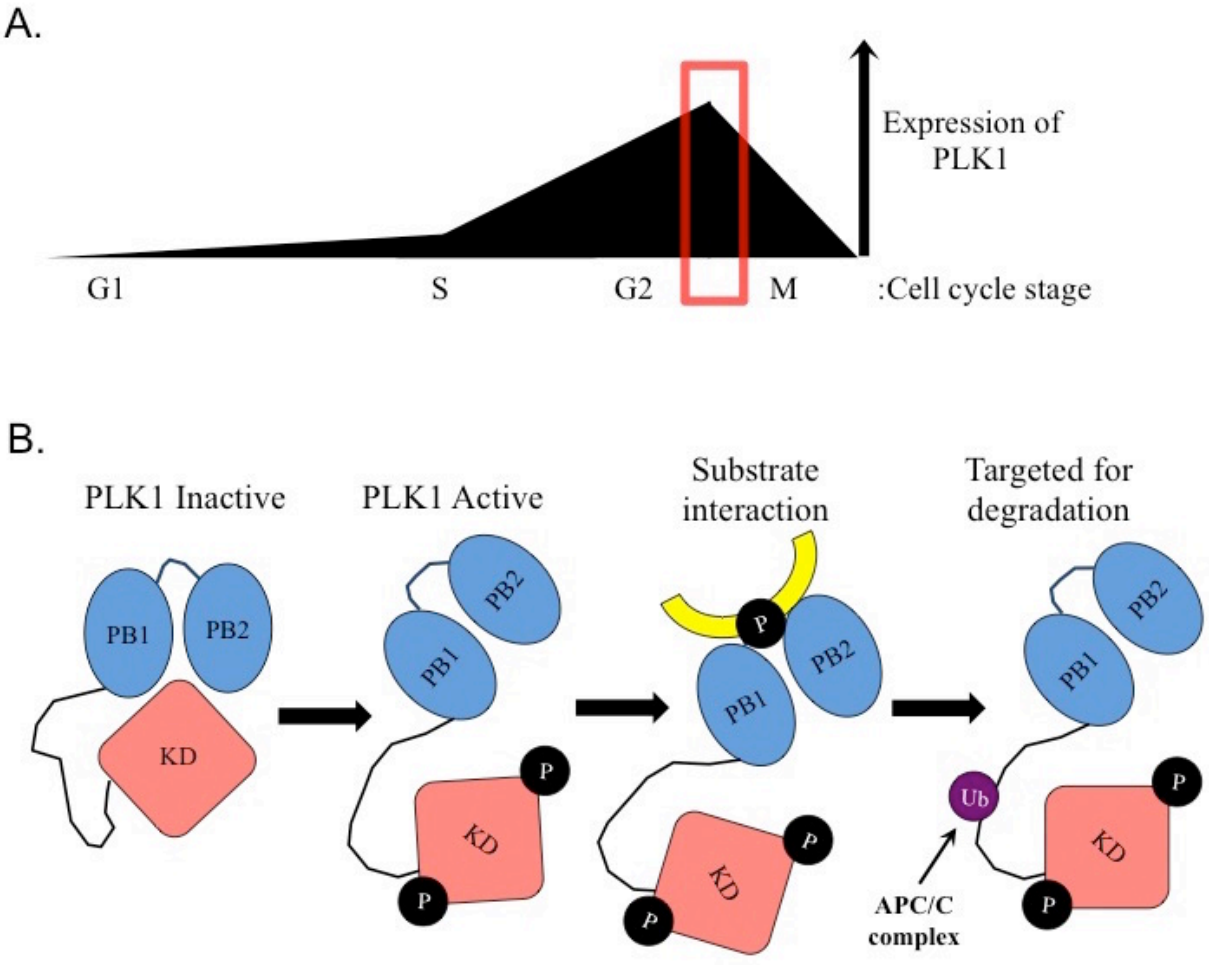

Figure 1.5 Summary graphic of PLK1 expression and activation.

(A) PLK1 expression and kinase activity begins to activate in S phase, and peaks in mitosis before being down-regulated at the end of cell division. **(B)** The secondary structure of PLK1 enables intramolecular regulation. In the absence of activating phosphorylation the polo-box domains (PB1 and PB2) domains inhibit the kinase domain (KD). Following phospho-activation by other mitotic kinases, a steric change in morphology allows access of the PB domains to phoshosubstrates. The anaphase-promoting complex (APC/C) ubiquinates the D-box in the inter-domain linker (IDL) region to target PLK1 for proteasomal degradation at the end of mitosis.

1.3.3 PLK1 function

PLK1 is a driver of cell cycle that functions at various points of mitosis. In mammalian systems, PLK1 is essential for embryonic development and knockout mouse models do not survive past the 8-cell stage of growth (Lu et al., 2008). PLK1 acts as a molecular hub that both receives and transmits mitotic signals at specific times and locations that are essential for the coordination of mitosis (Archambault et al., 2015). Work in both *Drosophila* and mammalian models have implicated PLK1 involvement in mitotic entry, G2/M transition, centrosome coordination, spindle assembly, chromosome segregation, and cytokinesis (Figure 1.6).

Mitotic entry. At the end of the G2 growth phase, cells must initiate the appropriate signaling program in order to commit to entering mitosis and commit to duplication. CDK1 and cyclin B complex together to form the M-phase-promoting factor (MPF) that is kept inactive through inhibitory CDK1 phosphorylation by mitotic kinases, Wee1 and MYT1 (McGowan and Russell, 1995; Mueller et al., 1995). Activation of the MPF causes the onset of mitosis and synchronizes its progression by phosphorylating specific targets. The MPF can become active when phosphatases, such as CDC25C, remove the inhibitory phosphorylation. CDC25C is a phospho-substrate of PLK1, and when PLK1 becomes active in late G2 it activates CDC25C, which allows activation of the MPF (Roshak et al., 2000; Toyoshima-Morimoto, 2002). In addition, PLK1 can phosphorylate Wee1 and MYT1 directly. This increases the affinity for SCF/beta-TrCP E3 ubiquitin ligase and results in the targeting of Wee1 for degradation (Nakajima et al., 2003; Watanabe et al., 2004). PLK1 has also been shown to directly phosphorylate cyclin B when located at the centrosome. This results in the activation of cyclin B and it then translocates to the nucleus (Jackman et al., 2003; Toyoshima-Morimoto et al., 2001).

PLK1 kinase activity effectively promotes the initiation of the mitotic "start" program while also removing the mitotic "breaks".

G2/M checkpoint. The transition to mitosis involves the initiation of M-phase signaling programs, but also requires approval to continue through the G2 DNA damage checkpoint. Duplication of the genome occurs during S-phase and DNA damage sensing pathways will halt cell cycle progression if an error in replication is detected. For example, the ATM and ATR kinase programs are initiated in the presence of single-stranded (ssDNA) and double-stranded DNA (dsDNA) breaks, respectively. ATM phosphorylates CHK2 that can then inhibit CDC25C, PLK1, and promote p53 activity. Similarly, ATR targets CHK1 that also inhibits CDC25C, but promotes the activity of Wee1 and p53. The MPF is indirectly inactivated by p53 and a cell cycle arrest occurs until DNA damage is repaired (Krause et al., 2000; Zitouni et al., 2014). DNA damage stops cell cycle progression and causes the inhibition of PLK1. Experiments testing expression of a constitutively active PLK1 mutant show it can overcome DNA damage arrest (Smits et al., 2000). PLK1 can directly deactivate CHK2, as well, PLK1 has been shown to bind to p53 and interfere with its pro-apoptotic function (Ando et al., 2004; van Vugt et al., 2010). As well, PLK1 phosphorylates the ATR and CHK1 stimulatory protein Claspin and targets it for degradation (Mamely et al., 2006). Similarly, the PLK1 substrate, RAD51, is a DNA repair protein that can inactivate CHK2 and CHK1, inhibit Wee1 and Claspin, and promote dissociation of repair factors from DNA (Limbo et al., 2011; Yata et al., 2012). PLK1 also inhibits breast cancer susceptibility protein BRCA2, which is important for dsDNA break repair (Lin et al., 2003; Takaoka et al., 2014). When PLK1 is active, it allows G2/M transition by blocking factors that have roles in preventing mitotic progression.

Centrosome coordination. PLK1 is involved in promoting the maturation of the major microtubule organizing organelle called the centrosome. Centrosomes are made up of centrioles and function in the construction of the mitotic spindle by recruiting microtubule nucleating and regulatory factors. They are duplicated during interphase, mature during G2, and separate to daughter cells during mitosis. Maturation involves the accumulation of γ-tubulin attachments and pericentriolar material (PCM) around the centrioles. PLK1 facilitates the attraction of γ-tubulin recruiting and organizing PCM proteins such as CEP192, pericentrin, NEK9, NEDD1, and Aurora A (Haren et al., 2009; Lane and Nigg, 1996; Sdelci et al., 2012). Inhibition of PLK1

results in the formation of a monopolar spindle with poor microtubule organization and reduced γ-tubulin levels (Lane and Nigg, 1996; Lénárt et al., 2007; Santamaria et al., 2007). Ninein-like protein (NLP) is another centrosome-associated protein that is phosphorylated by PLK1 in the reorganization of the microtubule scaffold (Casenghi et al., 2005, 2003; Rapley et al., 2005).

In prometaphase, the mature centrosomes separate to the plasma membrane on opposite ends of the cell. PLK1 coordinates this disjunction in two steps. First, it phosphorylates Ser/Thr protein kinase 3 (STK3) that relieves the inhibition of NEK2A from protein phosphatase 1γ (PP1γ). As a result, NEK2A phosphorylates two proteins that link centrosomes, CEP250, and rootelin and initiates separation (Mardin et al., 2011, 2010). Additionally, PLK1 phosphorylates NEK family proteins that signal along with kinesin-related motor protein, EG5 to localize it to the centrosome. Mitotic kinases and motor proteins coordinate the separation of the centrosomes (Smith et al., 2011; Tsou et al., 2009).

Spindle assembly. The mitotic spindle is an apparatus of microtubules that connect centrosomes to chromosomes- via kinetochore attachment- that is used to divide cellular material during mitosis. PLK1 functions to regulate the spindle assembly checkpoint (SAC), which is responsible for ensuring that chromosomes are properly aligned and connected to the microtubule-kinetochore network (van de Weerdt et al., 2005). Kinetochore-microtubule attachments are bi-directionally oriented and require high tension. Low tension and unattached kinetochore detection results in checkpoint activation and cell cycle arrest (Nicklas and Ward, 1994; Stern and Murray, 2001). The stable association of PLK1 and α, β, and γ- tubulin facilitates its role in spindle assembly. Linker proteins like translationally controlled tumor protein (TCTP) are responsible for complexing PLK1 to the cytoskeleton and other cell cycle proteins. TCTPSer46 is a target residue that is exclusive to PLK1 and is phosphorylated at the metaphase-anaphase transition to dissociate TCTP from microtubules and destabilize the mitotic spindle (Figure 1.7) (Gachet et al., 1999; Yarm, 2002). TCTP has also been associated with tumorigenesis and DNA damage response pathways (Amson et al., 2011; Tuynder et al., 2004), but whether PLK1 phosphorylation of Ser46 affects these roles is currently undetermined. PLK1 also contributes to the recruitment of important kinetochore proteins such as Aurora B, survivin, INCENP, and borealin that aid in the detachment of incorrect microtubules. Activation of PLK1 occurs when it binds to INCENP and is phosphorylated by Aurora B at the centromere, and

similarly kinetochore-microtubule attachment is stabilized (Carmena et al., 2012; Chu et al., 2011; D. Liu et al., 2012).

Chromosome segregation. Sister chromatids are separated and pulled to opposite poles of the dividing cell during anaphase. Cohesin protein complexes hold chromatids tightly together as they are appropriately attached and aligned to the mitotic spindle. PLK1 affects the removal of cohesin in two ways. First, in prophase PLK1 is recruited to the chromosome arms where it docks with Sororin that enables it to directly phosphorylate subunit SA2 of cohesin to cause the removal of the complex (Zhang et al., 2011). Some cohesin remains through to metaphase. Next, during metaphase, PLK1 phosphorylates early mitotic inhibitor 1 (EMI1) to target it for degradation, which results in activation of the APC/C complex. Separase is a protease that is activated when APC/C-CDC20 targets its inhibitor, securin, for degradation. This causes the final cleavage of cohesin and the separation of sister chromatids (Hansen et al., 2004; Moshe et al., 2004). Of note, experiments in PLK1 depleted cells show that APC/C activation and substrate degradation still take place suggesting this may be a redundant function that does not depend solely on PLK1 (Kraft et al., 2003; van Vugt et al., 2004). Finally, before sister chromatids are separated PLK1 is ubiquitinated at Lys492 by CUL-KLHL22 to reduce its affinity for kinetochores and cause its release (Beck et al., 2013).

Cytokinesis. Cytokinesis involves the rearrangement of the cytoplasmic membrane and cytoskeleton. Initially, a midbody is formed that develops into a cleavage furrow and leads to the abscission of two daughter cells. During anaphase, PLK1 relocates from the centrosome to kinetochores at the spindle midzone. The purpose of this is suggested to allow PLK1 to serve as a platform for the recruitment of signaling factors to control cytokinesis. For example, microtubule interaction stimulates PLK1 to phosphorylate targets like PRC1, which prevents premature formation of the midzone (Hu et al., 2012; Neef et al., 2007). Also at the midzone, PLK1 phosphorylates components like MKLP1 and HsCyk-4. This promotes the recruitment of epithelial cell transforming 2 (ECT2), which is a RHO guanine nucleotide exchange factor. ECT2 activates RHOA GTPase that drive the formation of the cleavage furrow and contractile ring (Petronczki et al., 2008, 2007). In addition, phosphorylation of CEP55 by PLK1 prevents its localization to the central spindle and it interaction with MLKP1. When PLK1 is removed from the kinetochores and subsequently degraded it allows CEP55 recruitment to the midbody where

it promotes abscission (Bastos and Barr, 2010). The role of PLK1 in cytokinesis may not be completely essential. PLK1 depletion in cells activates cell cycle arrest; however, Van Vugt and colleagues (2004) demonstrate that simultaneous depletion of important checkpoint factors can result in the induction of early stages of cytokinesis.

PLK1 has many roles in the coordination of mitosis. Studies in model organisms have uncovered additional functions, such as: promoting Golgi fragmentation (Sütterlin et al., 2001), DNA replication (Mandal and Strebhardt, 2013), meiosis (Jordan et al., 2012), and asymmetrical cell division (Wang et al., 2007). Understanding the cellular functions of PLK1 provides clues into which processes cancer cells are heavily dependent.

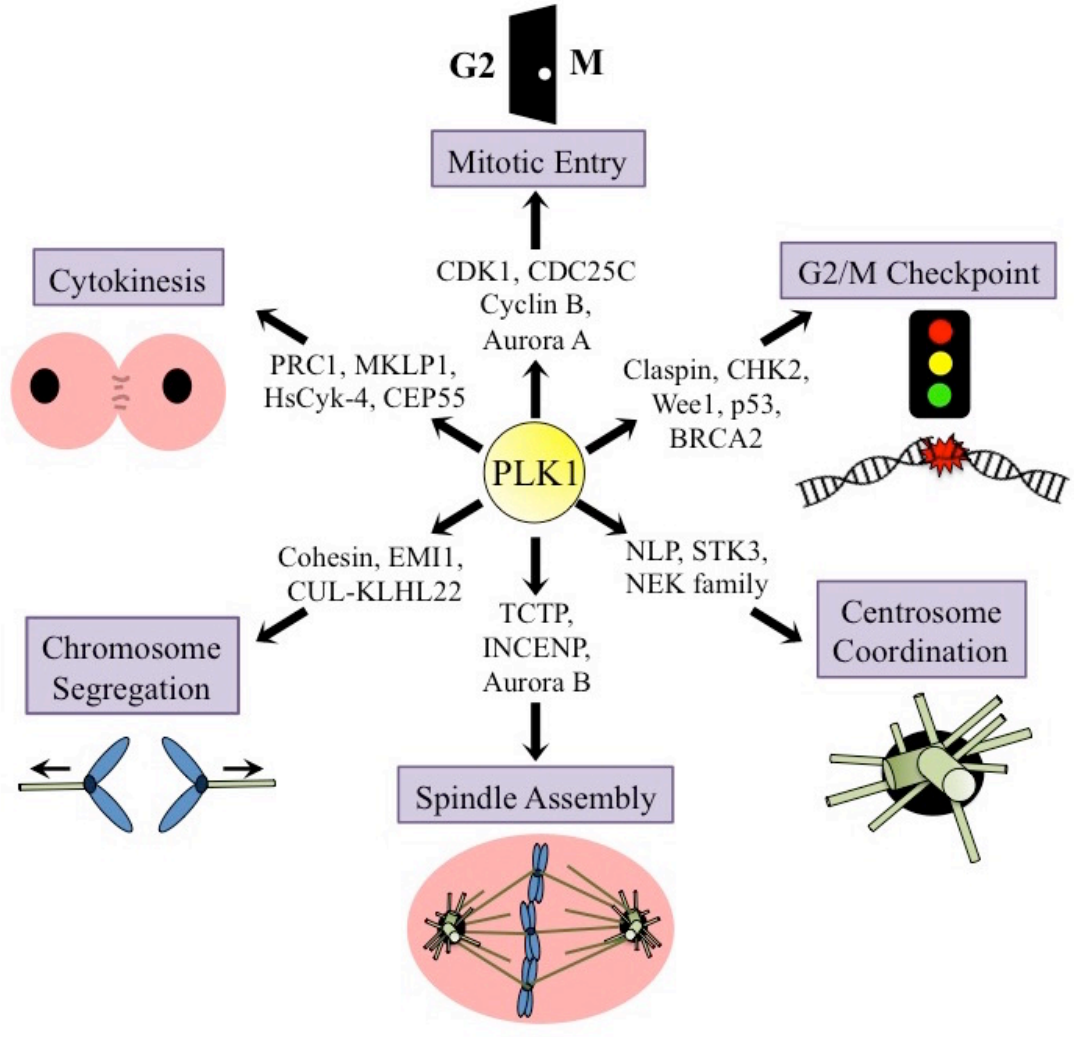

Figure 1.6 Summary graphic of the substrates and functions of PLK1 in regulation of the cell cycle.

1.3.4 PLK1 inhibitors

Presently, there are three main strategies to target PLK1 with novel inhibitors that are at various stages of clinical development. Some of the more notable inhibitors include BI-2536 (Boehringer Ingelheim), BI-6727 (Boehringer Ingelheim), GSK461364A (GlaxoSmithKline), TAK-960 (Takeda Pharmaceuticals), and NMS-1286937 (aka NMS-P937; Nerviano Medical Sciences).

1.3.4.1 Targeting ATP binding site

The first compounds designed to target PLK1 were designed as ATP-competitive inhibitors that block the activity of the PLK1 kinase domain. For example, BI-2536 is a dihydropteridinone derivative with nanomolar potency against PLK1 (IC_{50}=0.83nM), but it also inhibits PLK2 and PLK3 isoforms at higher concentrations (Steegmaier et al., 2007). BI-6727 is a second-generation small molecule with structural similarities to BI-2536. Interestingly, preclinical studies involving combinational therapy have demonstrated multidrug resistance enhanced by CSC drivers such as ABC transport proteins may be overridden with the use of BI-6727 (To et al., 2013).

GSK461364 is another ATP-competitive inhibitor that is reported to inhibit the catalytic activity of PLK1 over 100 fold more than other isoforms and related kinases. This imidazotriazine derivative reduces tumor formation *in vivo* and has been used to enhance GBM cell radiosensitivity *in vitro* (Gilmartin et al., 2009; Tandle et al., 2013). Interestingly, GSK461364 has substantial uptake to the brain using animals models and has been used to study the potential of targeting PLK1 to prevent breast to brain metastasis (Qian et al., 2011).

A final ATP-competitive inhibitor is NSM-1286937. One of the advantages of this compound is that it has been formulated for oral availability as opposed to intravenous injection. When compared to BI-2536 or BI-6727, NMS-1286937 is highly specific to PLK1 relative to other isoforms, however, it still shows off target effects on other proteins such as MELK, FLT3 and CD2 (Valsasina et al., 2012). The highly conserved nature of many human Ser/Thr kinase domains has initiated studies into alternative structural features of PLK1 that might offer greater target specificity.

1.3.4.2 Targeting Polo-box domain

A second approach to PLK1 drug design is the development of PBD targeting inhibitors. The PBD uses selective protein-protein interactions for subcellular localization of PLK1 and to target substrates to the kinase domain. Structural differences in the PBD composition of the different PLK isoforms can be exploited for the development of greater isoform specificity for PLK1. Screens of small molecule libraries have identified a handful of nonpeptidic compounds that interact with the PBD in a way that reduces downstream Plk1 function, notably: purpurogallin, poloxin, and thymoquinone. As well, work with synthetic phosphopeptides designed from structural mimics of PLK1 substrate CDC25C have developed this approach and molded further drug design (McInnes et al., 2012). Preliminary testing of PBD targeted inhibitors demonstrates great promise in various cancer models, but these compounds have yet to be tested in clinical trials.

1.3.4.3 Targeting PLK1 expression with siRNA

The third method to target PLK1 in cancer involves RNA-based gene inhibition technology. TKM-080301 (Tekmira Pharmaceuticals) is an interfering RNA formulation encapsulated by lipid nanoparticles that are designed to reduce *PLK1* specific transcript expression. Initial *in vivo* experiments demonstrated PLK1 silencing for up to 10 days following administration with low myelosuppression, which is a limitation of many PLK1 kinase inhibitors (Semple et al., 2011).

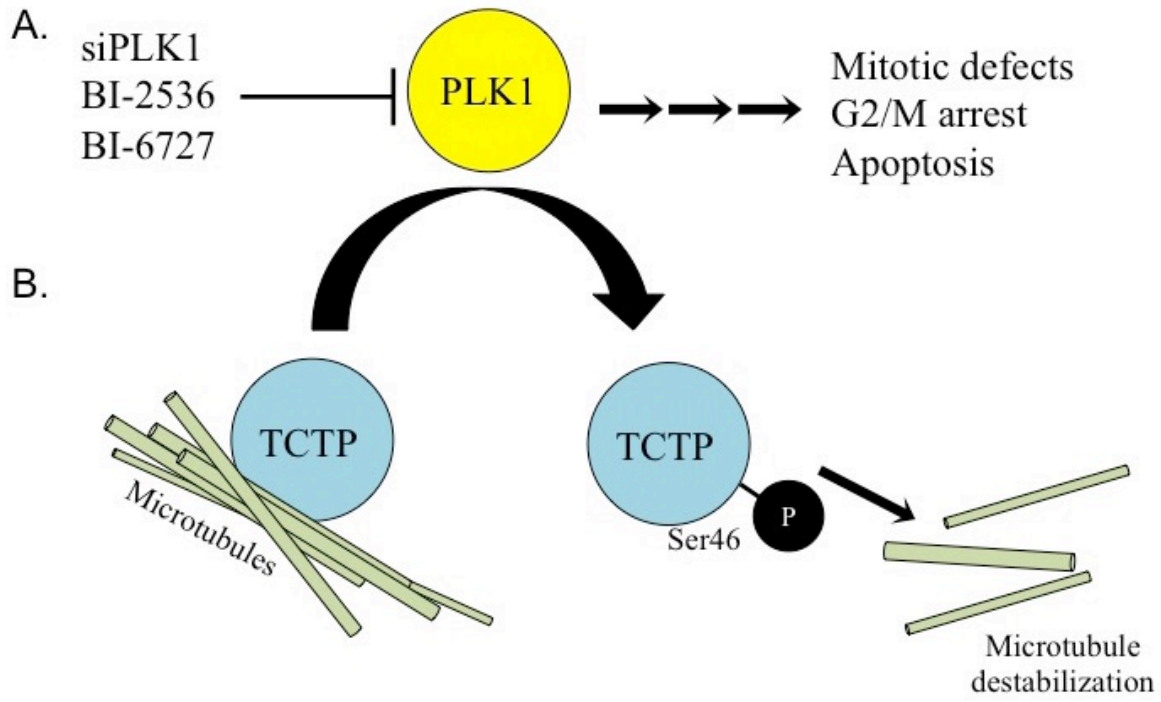

Figure 1.7 Inhibition of PLK1 prevents phosphorylation of substrates and has implications to mitosis. **(A)** Specific inhibitors can be used to block PLK1 kinase activity and result in mitotic defects due to the number of regulatory functions of PLK1. **(B)** The substrate TCTP is phosphorylated by PLK1, which results in abrogated affinity to bind microtubules. Inhibition of PLK1 directly correlates to reduced levels of P-TCTP^{Ser46}.

1.4 Hypothesis & aims

There are limited options available for the treatment of high-grade brain tumors, and those currently available are often associated with long-term sequelae. The overarching objective of this research is to identify key molecular drivers of aggressive GBM and MB that can be safely targeted in patients. It is known that (1) PLK1 is a mitotic kinase that is overexpressed in a variety of cancers (Holtrich et al., 1994; Smith et al., 1997), and (2) through phosphorylation of a variety of substrates PLK1 influences cancer cell proliferation and survival pathways (Smits et al., 2000; Yarm, 2002). Based on this, *the hypothesis tested in this research is whether PLK1 expression is associated with highly aggressive disease and if its activity can be targeted to overcome drug-resistant tumor growth*.

To test this, I cultured primary GBM cells derived from patient tumors and measured levels of PLK1 following standard of care TMZ treatment. The efficacy of targeting PLK1 in TMZ resistant cells was assessed, as well as the potential of an off-patent drug, DSF. Therefore, I show that elevated PLK1 expression may be associated with resistance to TMZ and discovered the potential for DSF in overcoming TMZ-resistant GBM growth (chapter 2). Further investigation suggested PLK1 might be an important target in pediatric brain tumors. Thus I further examined its role in MB. Highly sensitive gene expression profiling of MB patient cohorts was used to correlate PLK1 expression with clinical outcome. As well, the potential to target PLK1-high cases with PLK1 specific inhibitors was addressed (chapter 3). Finally, I characterized the importance of the PLK1 downstream substrate, TCTP, to better understand why PLK1-high MB is especially aggressive. TCTP expression in clinical patient samples was evaluated, and siRNA inhibition of TCTP was used to assess its oncogenic role in SHH MB cell lines. Targeting the PLK1-TCTP axis could influence cell cycle checkpoint activation to improve the clinical efficacy of cancer treatments (chapter 4).

CHAPTER 2: REPURPOSING DISULFIRAM AS AN ALTERNATIVE THERAPEUTIC AGAINST TMZ RESISTANT GBM

2.1 Overview

Resistance to the chemotherapeutic temozolomide (TMZ) is one of the greatest problems in the current treatment of glioblastoma (GBM). Even in cases lacking markers of resistance, such as O^6-methylguanine methyltransferase (MGMT) expression, TMZ treatment fails to prevent tumor recurrence for most patients. In the present study, we address the anti-cancer potential of disulfiram (DSF), an off-patent drug that has been routinely used to control alcoholism for the past six decades. Monolayer cell growth assays were conducted to test the influence of DSF and TMZ on GBM proliferation. As well, neurosphere self-renewal assays were used to assess whether DSF could be used to target undifferentiated tumor cell populations. Detailed investigation found the expression of the oncogenic cell cycle kinase, polo-like kinase 1 (PLK1), was reduced with DSF treatment but up-regulated in drug resistant GBM treated with TMZ. Further experimentation revealed PLK1 inhibition with siRNA or small molecules blocks the growth of TMZ resistant GBM cells *in vitro*. Consequently, freshly isolated primary GBM patient samples were found to express high levels of PLK1 and be especially sensitive to DSF. Our studies encourage DSF being repurposed for the treatment of refractory GBM.

2.2 Introduction

Glioblastoma (GBM) is considered the most aggressive variety of brain tumor that unfortunately has limited treatment options. Surgical resection and radiation is often ineffective due to the location and infiltrative nature of GBM, therefore, recurrence is extremely common. The median expected survival of patients with GBM is only 14 months regardless of aggressive treatment protocols (Rock et al., 2012). Current treatment for GBM involves a regime of the chemotherapeutic temozolomide (TMZ) in combination with radiation, however resistance to TMZ is common in GBM. TMZ is an alkylating agent and tumors expressing O6-methylguanine methyltransferase (MGMT) have the ability to overcome its anti-proliferative effect by enzymatically removing the methyl groups added to DNA by TMZ (Gerstner et al., 2009; Hegi

et al., 2005). Even MGMT silenced cases acquire TMZ resistance, which further complicates treatment of GBM (Blough et al., 2010). Mutations in mismatch repair genes have been shown to be generated following long-term exposure to TMZ and exemplify an additional route of treatment resistance (Yip et al., 2009). There are limited options available to overcome GBM growth and recurrence.

The major issue in treating GBM is the re-growth of the tumor following resection and treatment. A growing number of genetic based GBM studies suggest there are key drivers of the disease, specifically cell cycle regulatory factors that correlate with patient survival (Duncan et al., 2010; Hulleman and Helin, 2005; Smits et al., 2010). The heterogeneous nature of GBM is also considered a major obstacle in therapeutic development. Studies using animal models show that a mixture of cells with different properties within GBM contributes to treatment resistance (Dell'Albani, 2008; Galli et al., 2004; Molofsky et al., 2003; Muñoz and Guha, 2011; Park and Rich, 2009; Singh et al., 2004). The majority of cancer treatments target the proliferative capacity of tumor cells, however, the ability of more undifferentiated populations of GBM cells to self-renew is often unaffected by chemotherapy (Eramo et al., 2006; Weber et al., 2011). Self-renewal is a process that allows the indefinite perpetuation of cells that are uncommitted to terminal tissue-specific lineages and is controlled by cell cycle pathways (Kenney and Rowitch, 2000; Kippin et al., 2005; Molofsky et al., 2003; Morrison et al., 1999). By using culture conditions that enrich for these self-renewal abilities, a number of groups have successfully isolated and characterized the undifferentiated cell population in GBM that retain properties of the primary tumor (Galli et al., 2004; Pandita et al., 2004; Piccirillo et al., 2006; Singh et al., 2004; Wakimoto et al., 2009). Propagation and *in vitro* experiments with brain tumor cell self-renewal is done using neurosphere tissue culture methodology (Deleyrolle and Reynolds, 2009; Reynolds and Weiss, 1992; Singh et al., 2004). Using these growth conditions cells can be serial passaged to continually form new spheroid clusters as they self-renew. There must be alternative methods developed that target both the proliferation and self-renewal of cancer cells as the heterogeneity of GBM may be responsible for evading current treatment protocols resulting in relapse (Park and Rich, 2009).

Polo-like kinase 1 (PLK1) is a serine/threonine kinase that is influential in many essential cell cycle functions. These include mitotic entry, centrosome maturation, cell cycle progression

and cytokinesis (Arnaud et al., 1998; Golsteyn et al., 1995; Lane and Nigg, 1996; Mundt et al., 1997; van Vugt et al., 2004). Our group has previously shown that PLK1 is highly over-expressed in cancer compared to normal tissue and is a promising therapeutic target for brain tumors (Hu et al., 2009; Lee et al., 2012b). Specifically, a high level of PLK1 expression in GBM is associated with a worse overall survival. We have demonstrated that PLK1 is essential for sustaining the growth of neurospheres and PLK1 inhibition can delay tumor growth using an orthotopic brain tumor model (Lee et al., 2012b). Although chemical inhibitors of PLK1 are being developed for clinical use (Garuti et al., 2012; Wäsch et al., 2010), the long expensive pipeline of drug development prompts the question of whether there are off-patent drugs with undiscovered anti-cancer potential that are already clinically approved.

Disulfiram (DSF) is an off-patent small molecule that has been safely used for the treatment of alcohol abuse for over sixty years. This compound is an inhibitor of the aldehyde dehydrogenase (ALDH) enzyme family, which is involved in the metabolism of alcohol, and has been used as a marker for self-renewing tumor cell populations (Lipsky et al., 2001; Rasper et al., 2010). Although best characterized for its activity against ALDH, DSF is not specific or exclusive to these enzymes and there are a number of reports that have uncovered alternative effects of DSF on cell activity (Musacchio et al., 1966; O'Brien et al., 2012). Initially we identified DSF in a screen for drugs that inhibit tumor-initiating cells using the Prestwick Library (unpublished data). In a position article by Kast et al (2009), DSF was discussed for the treatment of GBM (Kast and Belda-Iniesta, 2009); therefore, we questioned whether DSF would target drug resistant cells. DSF is an attractive compound for the treatment of brain tumors because it is a small molecule with the potential to cross the blood-brain barrier (Eneanya et al., 1981; Maj et al., 1970; Oskarsson, 1984). This study provides *in vitro* evidence promoting DSF as an effective treatment for GBM and suggests it could augment cytotoxicity of the currently used chemotherapeutic, TMZ. The data presented here proposes a new use for the clinically safe compound, DSF, as a treatment for cancer.

2.3 Results

2.3.1 DSF inhibits GBM self renewal and proliferation

To examine the efficacy of current standard-of-care TMZ and DSF, proliferation and self-renewal was examined in GBM cell lines. The proliferation of pediatric GBM SF188 cells is unaffected by TMZ tested at 5-15μM concentrations, which are physiologically achievable (Figure 2.1). SF188 cells are classified as TMZ resistant with a suggested IC50 of 500μM (Gao et al., 2009). These cells are sensitive to DSF with a concentration of 500nM being sufficient to suppress monolayer growth by ~100% over 72 hours (Figure 2.2A). Neurosphere self-renewal of SF188 cells is completely inhibited with similar DSF concentrations (Figure 2.2B). The primary adult GBM cells, BT074, are also refractory to TMZ (Kanai et al., 2012; Pandita et al., 2004) but demonstrate sensitivity to DSF in neurosphere self-renewal assays (Figure 2.2C). Likewise, the self-renewal of GBM4 primary cells is also inhibited with DSF treatment (Figure 2.2D). Microscope images exemplifying the impact of DSF on BT74 and GBM4 neurosphere formation is illustrated in Figures 2.2E-F. Next we questioned whether the combination of DSF and TMZ has an additive cytotoxic effect. When used as single agents, low doses of DSF (50nM) or 10μM TMZ had no anti-proliferative effect, however proliferation and self-renewal was reduced by ~50% with combination treatment (Figure 2.3A-C).

Based on our observations in established GBM cell lines, we next looked to expand our findings with primary tumor samples. Primary GBM cells were freshly isolated from two adult patient samples that are denoted aBT001 and aBT003. GBM with mutations in *IDH1* or *IDH2* genes are reported to have aberrant metabolic remodeling that influences tumor survival pathways in response to therapy and hypoxia (Sanson et al., 2009; Wolf et al., 2010). *IDH1* and *IDH2* sequencing of aBT001 and aBT003 tumor samples was negative for mutation (data not shown). In addition, both cases had unmethylated *MGMT* promoters, which suggests they may be less susceptible to TMZ (Figure 2.4A). As expected, monolayer growth of aBT001 was not affected by TMZ (Figure 2.4B), however, 500nM DSF inhibited proliferation by 87% after 72 hour (Figure 2.4C). aBT003 primary cells also demonstrated resistance to TMZ in neurosphere assays (Figure 2.4D). Conversely, DSF blocked aBT003 cell self-renewal capacity by 95-98% (Figure 2.4D-E). Cells from a third adult GBM primary isolate, aBT015, were also found to be resistant to TMZ but sensitive to DSF in neurosphere assay (Figure 2.5). *IDH1/2* mutation and

MGMT promoter methylation status is presently unknown for aBT015. While DSF inhibits growth of GBM cells, it is important to note that concentrations up to10μM DSF had no anti-proliferative effect on normal human astrocytes (Figure 2.6). These *in vitro* data suggest that DSF may have anti-tumorigenic potential for targeting TMZ resistant GBM.

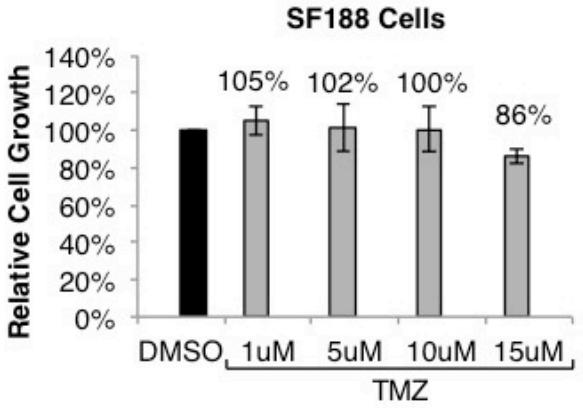

Figure 2.1 SF188 cells are resistant to TMZ.

SF188 cells demonstrate drug resistance when treated with concentrations of 1-15μM TMZ for 72 hour and assessed for monolayer growth. Treatments were plated in triplicate and the experiment performed thrice.

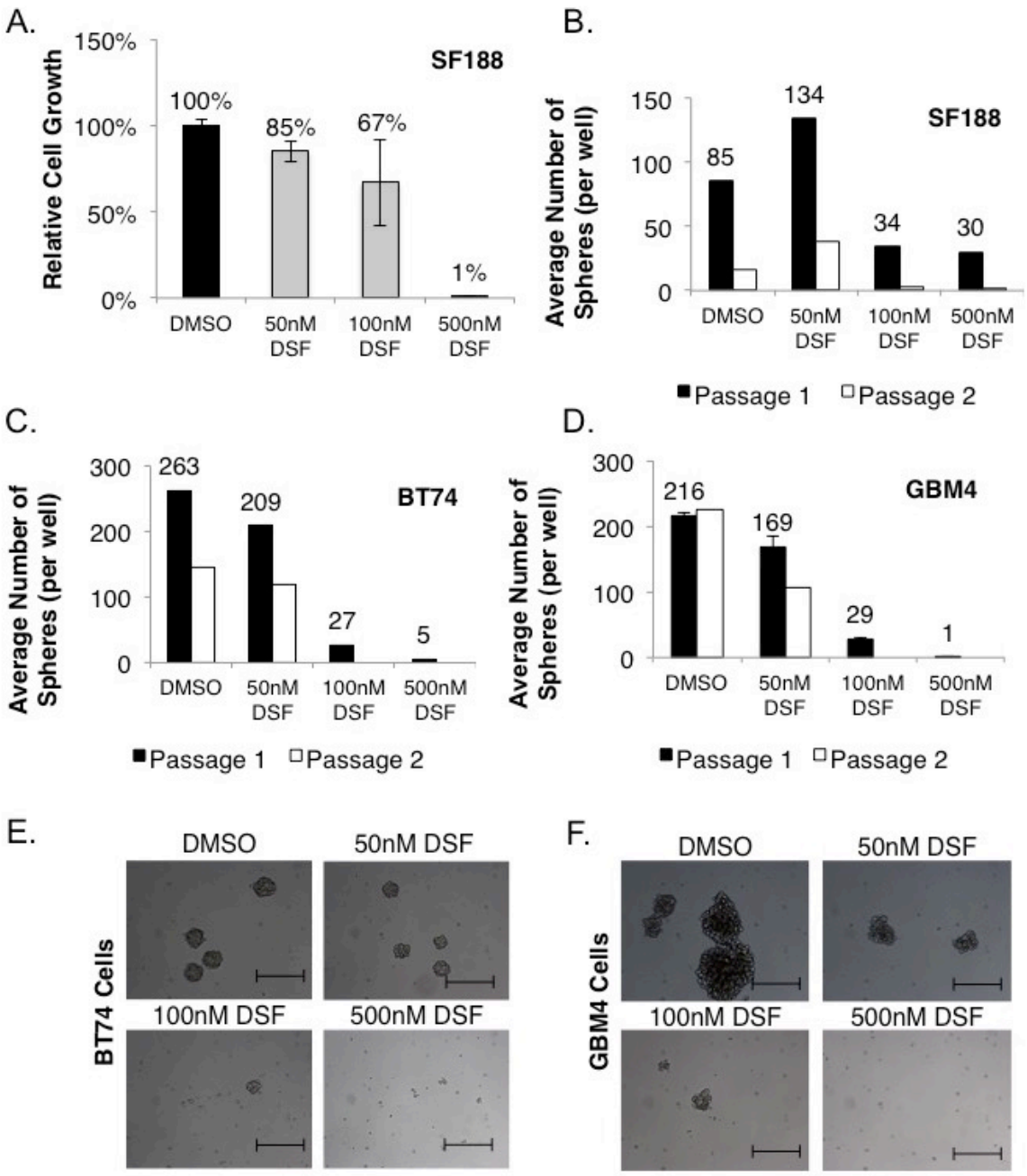

Figure 2.2 DSF inhibits GBM cell growth and self-renewal.

(A) SF188 monolayer cell proliferation following 72 hours 50, 100 and 500nM DSF treatment. 7-day neurosphere assay with serial passaging that tests the effect of 50, 100 and 500 nM DSF on self-renewal of **(B)** SF188, **(C)** BT74, and **(D)** GBM4 cells. Representative images from neurosphere microscopy demonstrate effect of DSF treatment on **(E)** BT74 and **(F)** GBM4 neurosphere growth. Scale bar= 200μm.

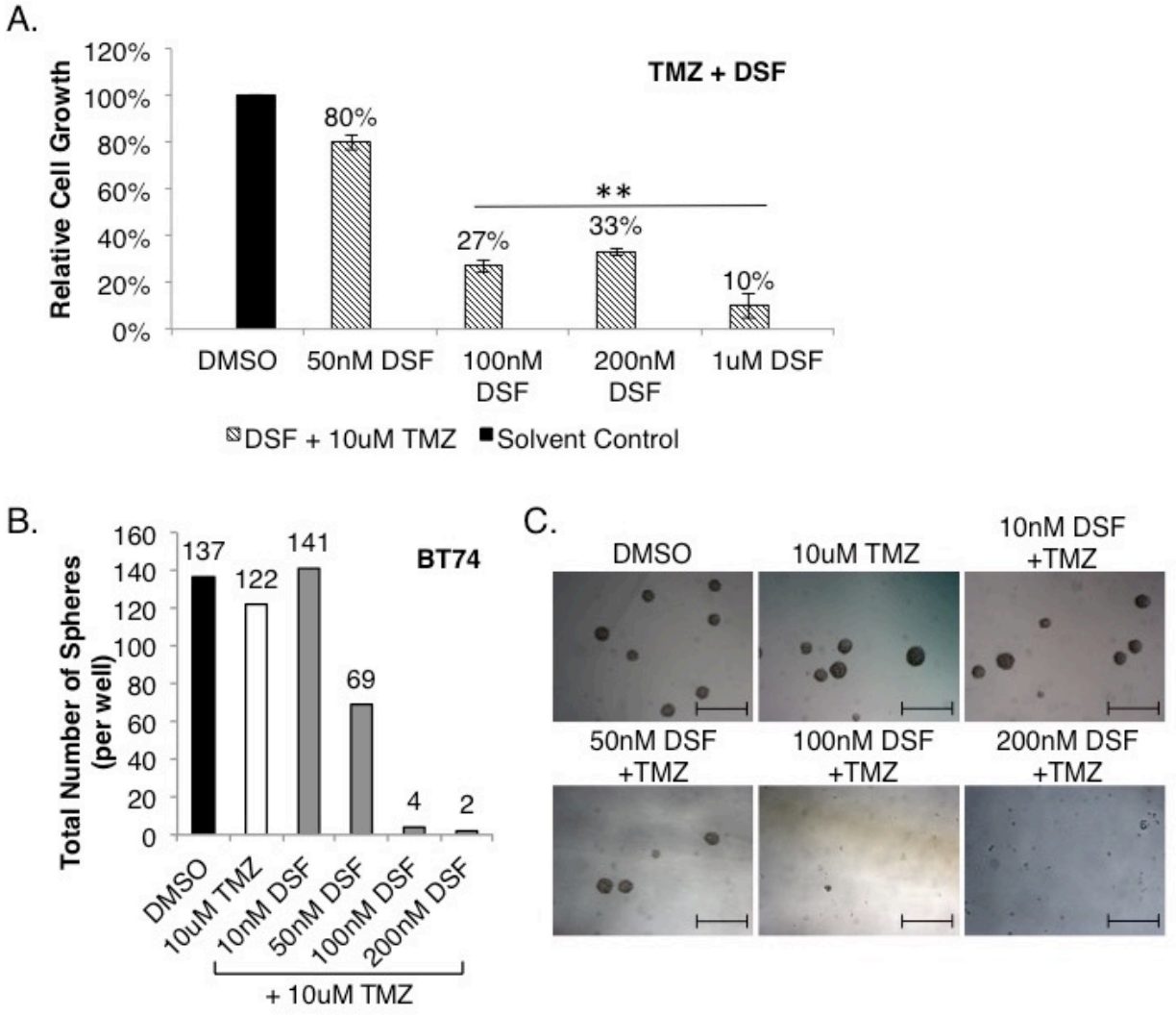

Figure 2.3 Combination treatment with DSF augments TMZ cytotoxicity.

(A) SF188 cells treated with 50nM-1μM DSF, in combination with 10μM TMZ, in a monolayer growth assay over 72 hours. Cells were plated in triplicate and growth calculated relative to DMSO control treatment [**p< 0.005, T-test]. **(B)** BT74 neurosphere assay testing 10μM TMZ and in combination with 10-200nM DSF. BT74 spheres >30μM were counted following 5-6 days of non-adherent growth, then chemically dissociated to serial passage and grown for an additional 5-6 days. Data in A and B represents a single experiment. **(C)** Morphology of BT74 spheres are shown following 6 days of drug treatment. Scale bar = 200 μm.

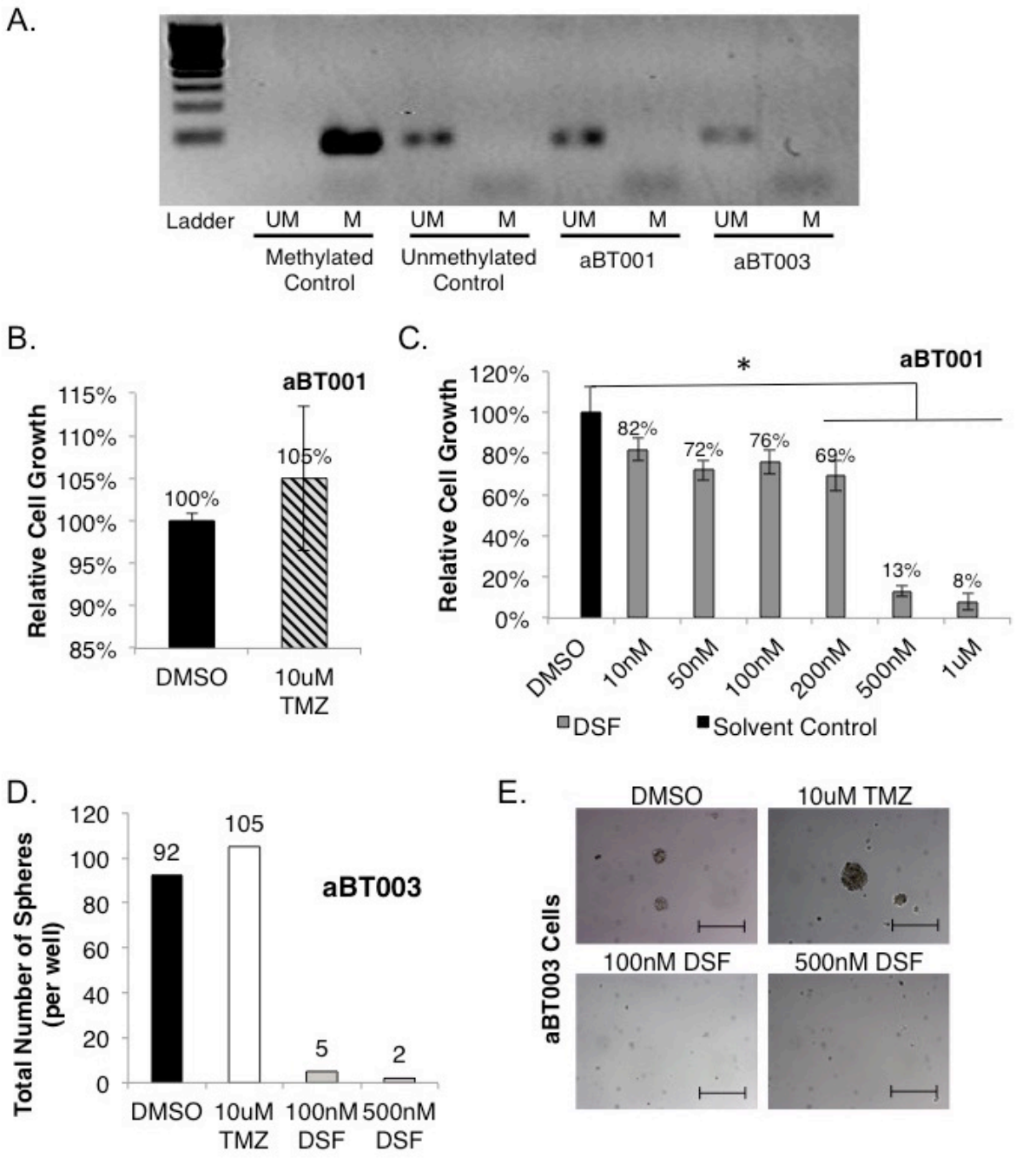

Figure 2.4 Primary isolated GBM cells demonstrate sensitivity to DSF yet resistance to TMZ.
aBT001 and aBT003 primary GBM cells were isolated from adult patients. **(A)** DNA extracted from these cases was assessed for MGMT promoter methylation via PCR reaction. An unmethylated MGMT promoter suggests the protein is expressed in the cases (M= methylated, UM= unmethylated). **(B-C)** Monolayer growth of aBT001 was unaffected by TMZ, but DSF suppressed growth by as much as 92% in 72 hour with a single treatment. **(D-E)** aBT003 neurosphere growth was unaffected by TMZ, however DSF treatment reduced self-renewal by 95-98% with a single treatment. Scale bar = 200μm.

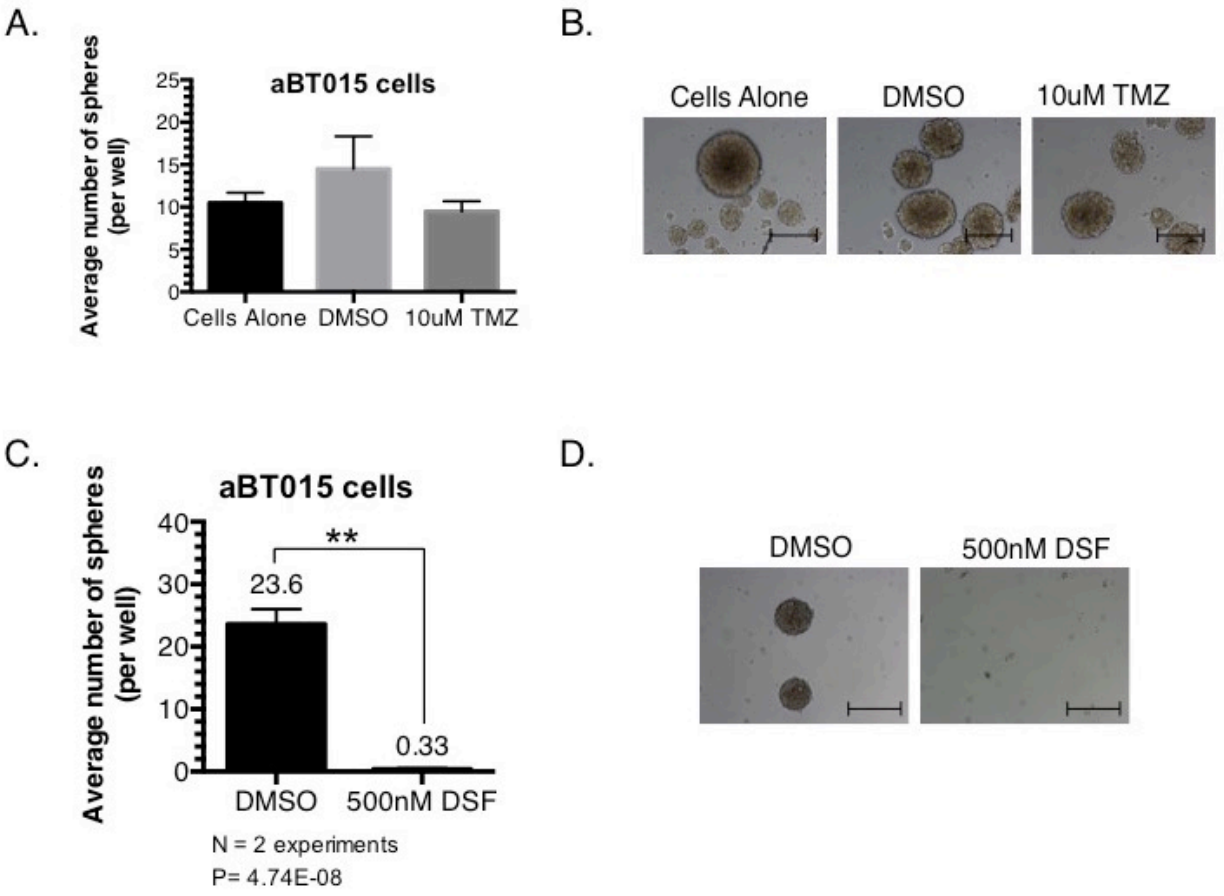

Figure 2.5 aBT015 primary adult GBM cells are resistant to TMZ but sensitive to DSF.

aBT015 primary GBM cells were isolated from an adult patient. **(A)** Self-renewal was unaffected by TMZ in a 7-day neurosphere assay using a 24-well plate format. Data represents a single experiment and **(B)** sphere morphology is represented. Scale bar = 200μm. **(C)** aBT015 self-renewal was abolished with 500nM DSF treatment in neurosphere assay also using a 24-well plate format. Data from two experiments represented and **(D)** sphere morphology is represented. Scale bar = 200μm.

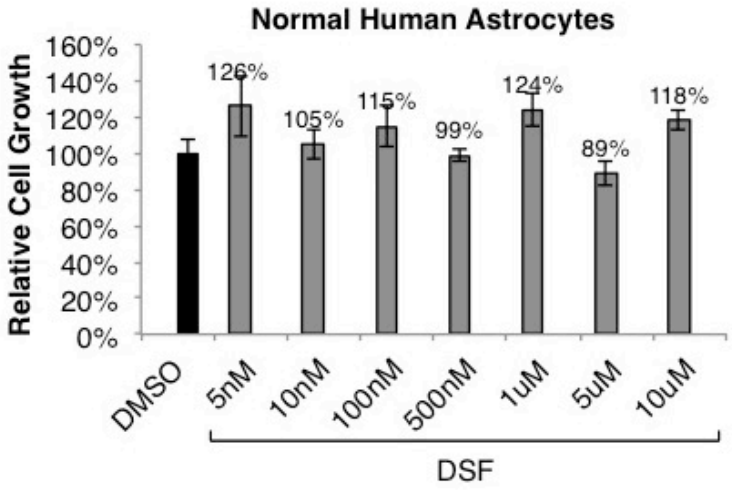

Figure 2.6 High doses of DSF do not affect proliferation of normal human astrocytes.

Normal human astrocyte cells show no reduction in proliferation when treated with concentrations of 5nM-10μM DSF for 72 hours and assessed for monolayer growth. Treatments were plated in triplicate and the experiment performed thrice.

2.3.2 DSF treated GBM cells decrease expression of PLK1

With such a drastic impact on cancer cell growth and self-renewal, we next investigated whether DSF treatment impacts important signaling pathways. Our group recently reported that highly aggressive GBM express PLK1 and have an oncogenic addiction that promotes cancer cell survival (Lee et al., 2012b). Whether PLK1 has a role in overcoming TMZ resistance in GBM still has not been addressed, therefore, we questioned whether the dramatic anti-growth effect of DSF has an impact on PLK1. Interestingly, PLK1 expression was reduced following 24 hour DSF treatment at both 500nM (Figure 2.7A) and 250nM concentrations (Figure 2.7B). Inhibiting PLK1 expression with siRNA prevented cell growth (Figure 2.7C). This result was also observed when cells were treated in combination with various concentrations of TMZ. Whereas high doses of TMZ failed to induce apoptosis in SF188 cells, the combination with siPLK1 produced strong detection of PARP and Caspase 3 cleavage by western blot (Figure 2.7D).

These results were confirmed in a second cell line. U251 cells treated for 24 hour had reduced PLK1 expression at 500nM (Figure 2.8A) and 250nM (Figure 2.8B) concentrations of DSF. Inhibiting PLK1 with siRNA or the small molecule BI-2536 blocked U251 cell proliferation. Like SF188, this U251 anti-growth effect also occurred with the combination of PLK1 inhibition and TMZ (Figure 2.8C-D). Finally, U251 cells treated with DSF were suppressed in growth ~81% at 200nM and ~100% at 500nM doses (Figure 2.8E). In summary these data suggest PLK1 expression is reduced with DSF treatment and inhibition of PLK1 has an anti-proliferative effect in TMZ resistant cells.

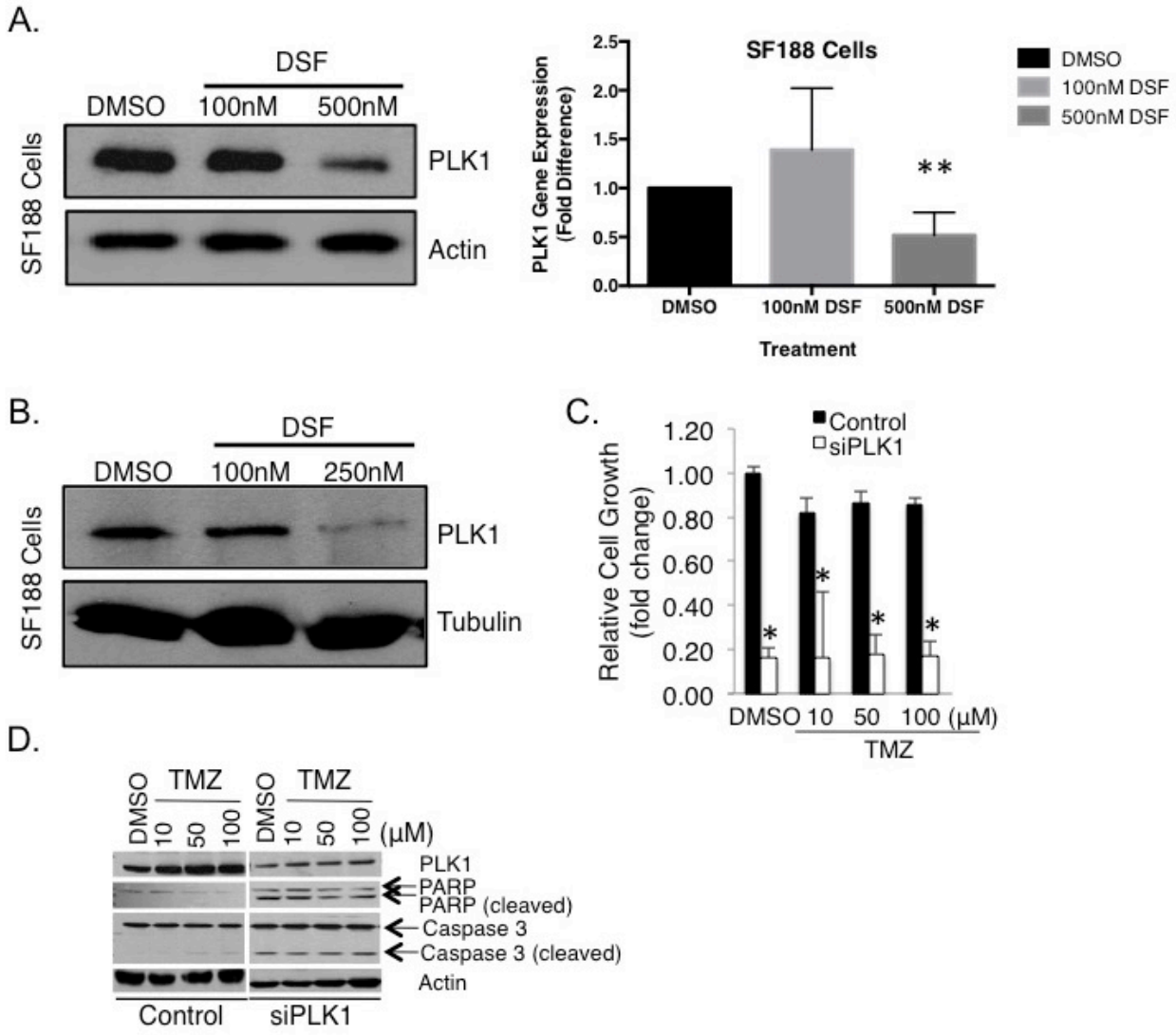

Figure 2.7 PLK1 expression is reduced in pediatric GBM SF188 cells treated with DSF.

(A-B) SF188 protein and RNA was extracted following a 24 hour treatment with DSF or DMSO solvent control. Levels of PLK1 assessed using immunoblotting and qRT-PCR. Inhibition of PLK1 expression with siRNA **(C)** reduces SF188 monolayer cell growth and **(D)** induces apoptosis, either alone, or in combination with TMZ. Cleavage of PARP and caspase 3 was used to detect apoptosis by immunoblotting and a scramble RNA oligo was used as a siRNA transfection control.

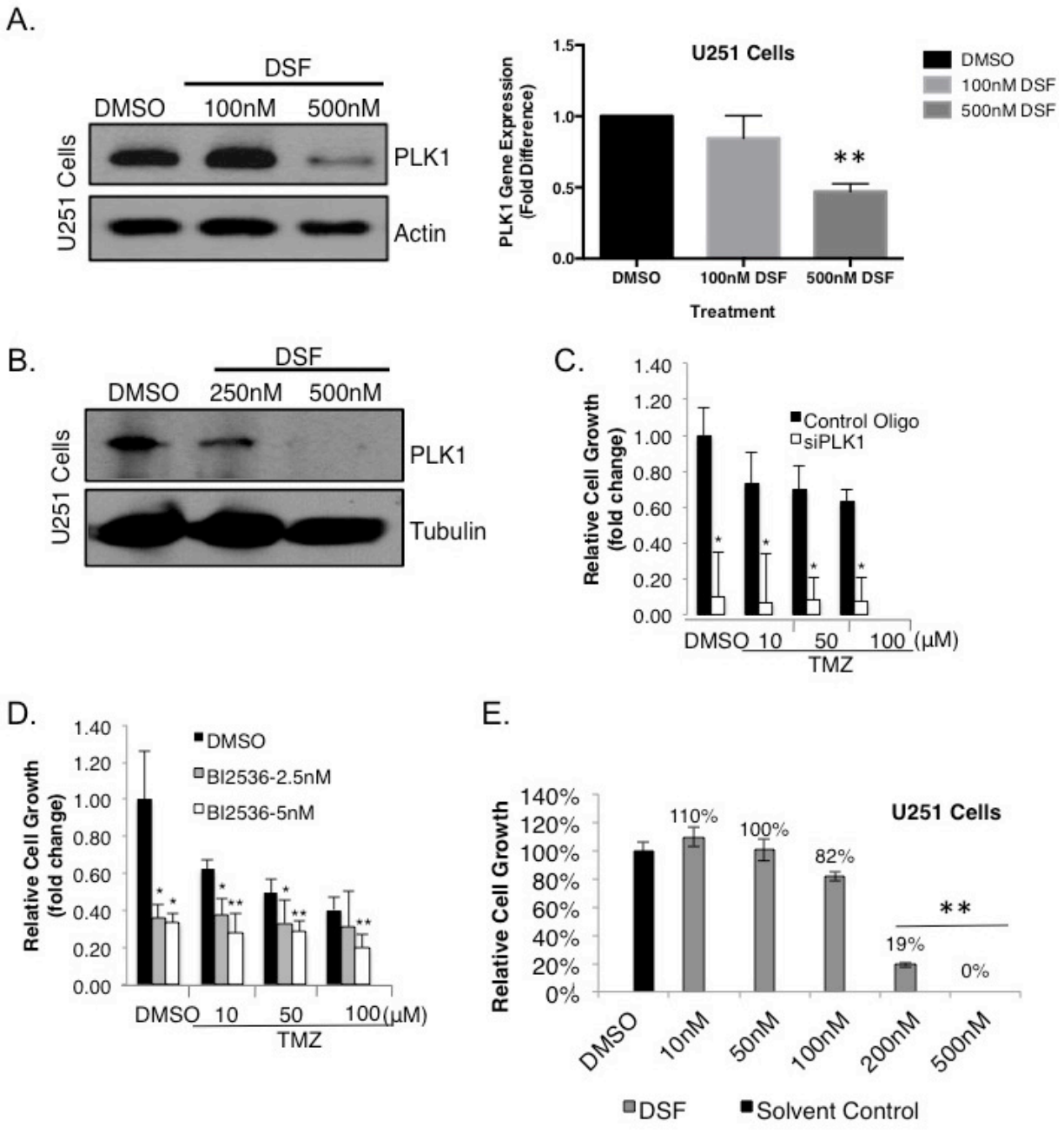

Figure 2.8 PLK1 expression is reduced in adult GBM U251 cells treated with DSF.

(A-B) U251 protein and RNA was extracted following a 24 hour treatment with DSF or DMSO solvent control. Levels of PLK1 assessed using immunoblotting and qRT-PCR. **(B)** Inhibition of PLK1 expression with siRNA reduces U251 monolayer cell growth either alone, or in combination with TMZ. A scramble RNA oligo was used as a siRNA transfection control. **(C)** BI-2536 PLK1 kinase inhibitor also reduces U251 monolayer growth alone, and in combination with TMZ. **(D)** Likewise, DSF treatment prevented U251 growth relative to DMSO solvent control treated cells in a dose-dependent manner.

2.3.3 Efficacy of PLK1 inhibition in overcoming TMZ resistance

We have previously published results showing SF188, BT74, BT241 and GBM4 cells have between 203-470 fold transcript overexpression of *PLK1* compared to normal human astrocytes (Lee et al., 2012b). In the present study, we found the TMZ resistant SF188 cells have approximately double the detected *PLK1* transcript compared to the partially TMZ sensitive U251 cells (Figure 2.9A). Interestingly, while U251 cells are reported to be sensitive to TMZ there was always ~30% of cells that remained viable following TMZ treatment. For example, after treating U251 cells with TMZ for 7 days approximately 71.5% of cells had died off leaving behind a residual population (Figure 2.9B). This cell population was harvested and evaluated for PLK1 using western blot in order to study the impact of PLK1 expression in TMZ drug resistance. It was discovered that PLK1 protein expression was much higher in the residual population compared to the untreated and DMSO solvent controls (Figure 2.9C). Considering these results we next inquired whether the residual TMZ resistant population could be targeted with the PLK1 inhibitor, BI-2536. The U251 7 day experiment was repeated which left a residual population of TMZ resistant cells. TMZ was removed, and the residual cells were then exposed to a single dose of BI-2536 ranging between 5-100nM. The TMZ resistant population was extremely sensitive to growth inhibition with BI-2536 treatment (Figure 2.9D). Nearly 90% of cells from the TMZ residual population underwent cell death following treatment with 10nM BI-2536. These findings suggest that PLK1 may be a potential driver of TMZ resistance that can be overcome with therapeutic intervention.

Adult GBM BT74 cells have previously been reported to be resistant to TMZ (Kanai et al., 2012). The efficacy of BI-2536 against these cells was tested using neurosphere self-renewal assays with serial passaging. While TMZ treatment had no effect, BI-2536 eliminated the neurosphere growth of BT74 cells (Figure 2.10A-B). Similarly, the adult GBM BT241 cells also demonstrated sensitivity to PLK1 inhibition but resistance to TMZ (Figure 2.10C-D). There was no additional benefit from combining BI-2536 and TMZ in either BT74 or BT241 tests (Figure 2.10A-D). Cumulatively, these data indicate the use of PLK1 inhibition may be integral in targeting GBM with TMZ resistant characteristics.

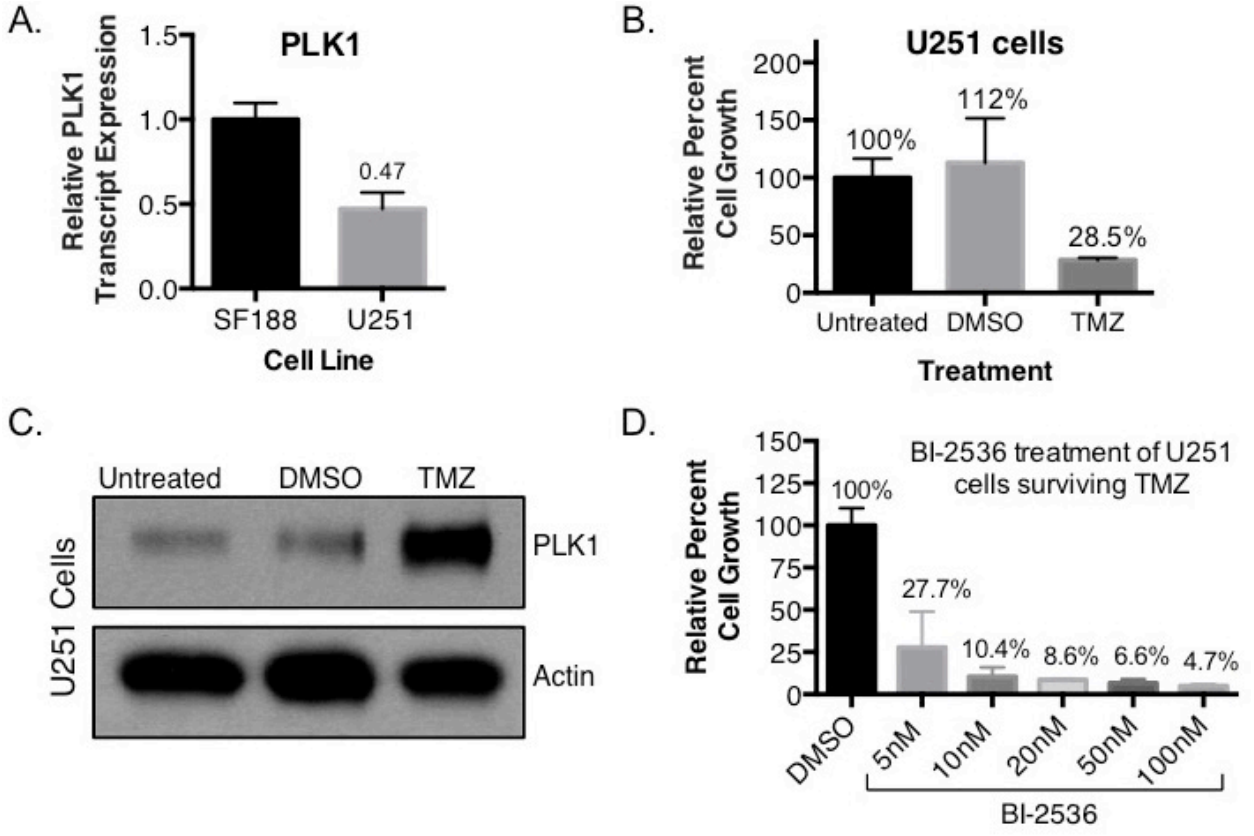

Figure 2.9 Targeting PLK1 inhibits growth of TMZ resistant cells.

(A) U251 cells have lower *PLK1* transcript expression compared to the TMZ resistant SF188 cells by qRT-PCR. **(B)** Growth assay showing partial TMZ sensitivity following a long-term 7-day treatment of U251 cells with TMZ. Cells were treated with 10μM TMZ every 48 hour. **(C)** Immunoblot demonstrating an increase of PLK1 protein levels in TMZ treated U251 cells compared to untreated and DMSO controls after 24 hours. Actin is used as a loading control. **(D)** Residual U251 cells that survived long-term 10μM TMZ treatment were re-plated and treated with BI-2536 for a 5 day growth assay.

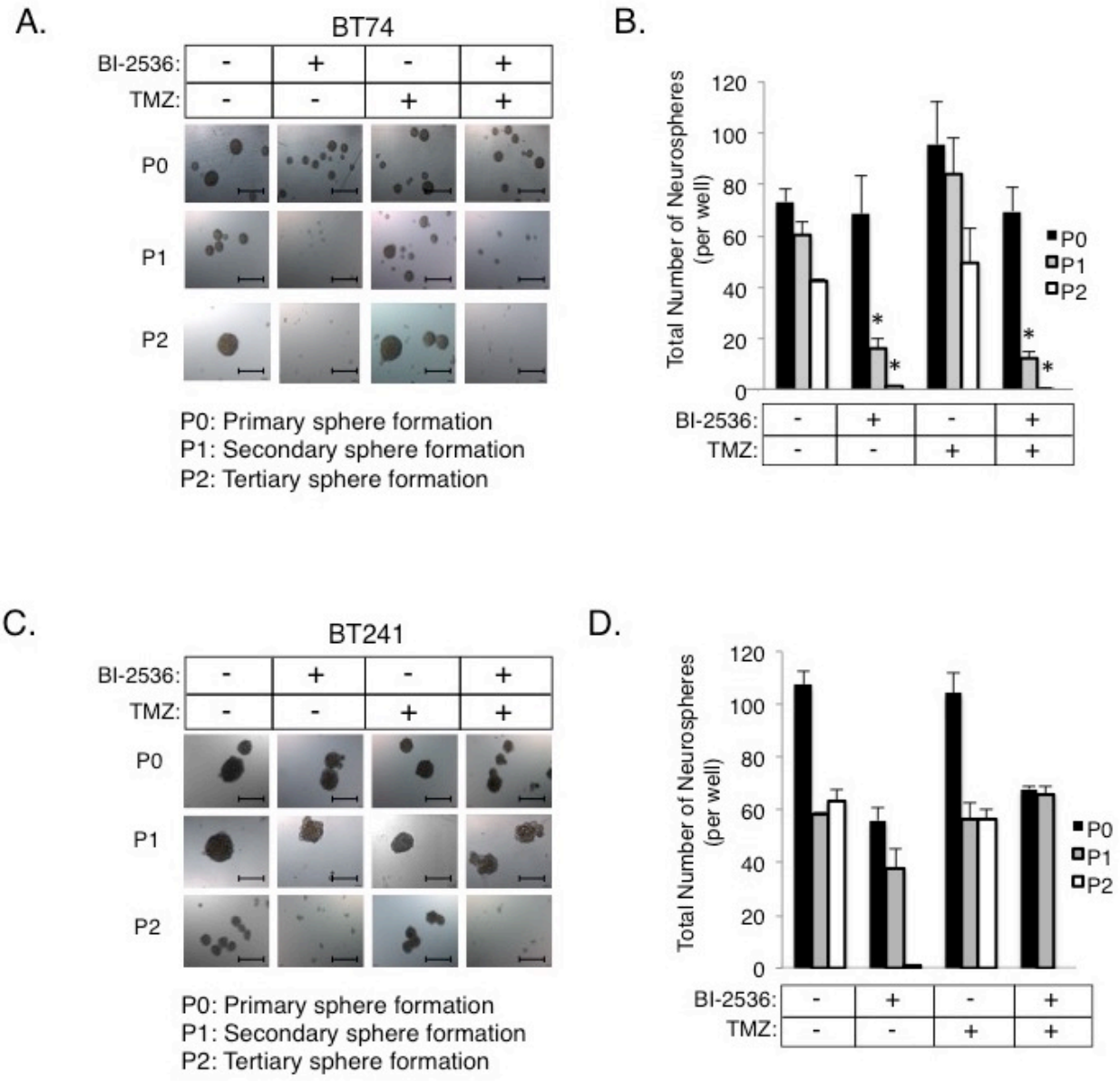

Figure 2.10 PLK1 inhibitors can be used to overcome TMZ resistance.

(A-B) Neurosphere growth with serial passaging demonstrates TMZ resistant BT74 cells are sensitive to reduced self-renewal with treatment of 10nM BI-2536. **(C-D)** BT241 cells are another example of TMZ resistant cells that show sensitivity to PLK1 inhibition. Both BT74 and BT241 cells are maintained as primary isolates and cultured only in neurosphere conditions. The combination of TMZ and BI-2536 did not enhance efficacy of BI-2536 administered alone. Scale bar = 500μM.

2.3.4 Patient derived GBM samples that express high levels of PLK1 demonstrate sensitivity to PLK1 inhibitors

As previously mentioned aBT001 and aBT003 were freshly isolated from adult GBM patients. Cells extracted from both these cases were sensitive to DSF, therefore we addressed whether they also expressed PLK1. Tissue sections from these cases were stained using immunohistochemical detection and PLK1 protein was found to be highly abundant (Figure 2.11A). Given that PLK1 was highly expressed, aBT001 cells were treated for 72 hours with BI-2536 in a monolayer growth assay 25nM of BI-2536 inhibited aBT001 cell proliferation by up to 80% and induced apoptosis (Figure 2.11B-C).

Recently, PLK1 overexpression has also been reported in pediatric medulloblastoma, which is another highly aggressive brain tumor (Harris et al, 2012). As a final test we examined if PLK1 inhibition had efficacy against the extremely proliferative MED8A medulloblastoma cell line. Indeed various concentrations of BI-2536 reduced monolayer cell growth >95%. Even greater of note, treatment of this medulloblastoma cell line with DSF completely eliminated viable cells in most replicate experiments (Figure 2.12). In conclusion, high levels of PLK1 are detectable in aggressive brain tumors and compounds such as BI-2536 or DSF are promising options for enhancing current treatments.

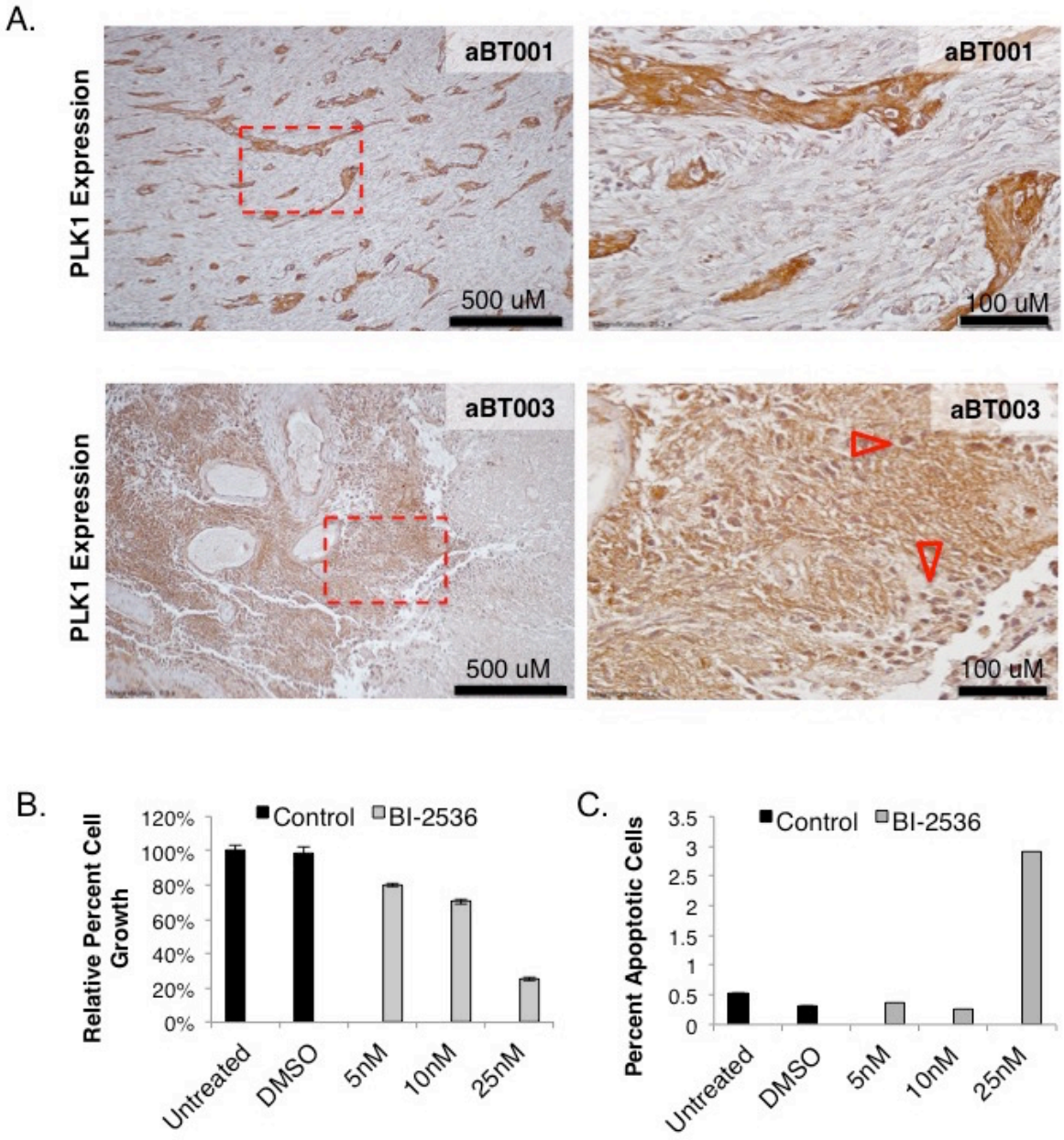

Figure 2.11 aBT001 and aBT003 patient tissue express high levels of PLK1.

(A) aBT001 and aBT003 GBM patient tissue was assessed for PLK1 levels using immunohistochemical detection. High levels of PLK1 are detected in both cases. **(B-C)** BI-2536 PLK1 inhibition suppresses the growth of aBT001 in monolayer and induces apoptotic cell death.

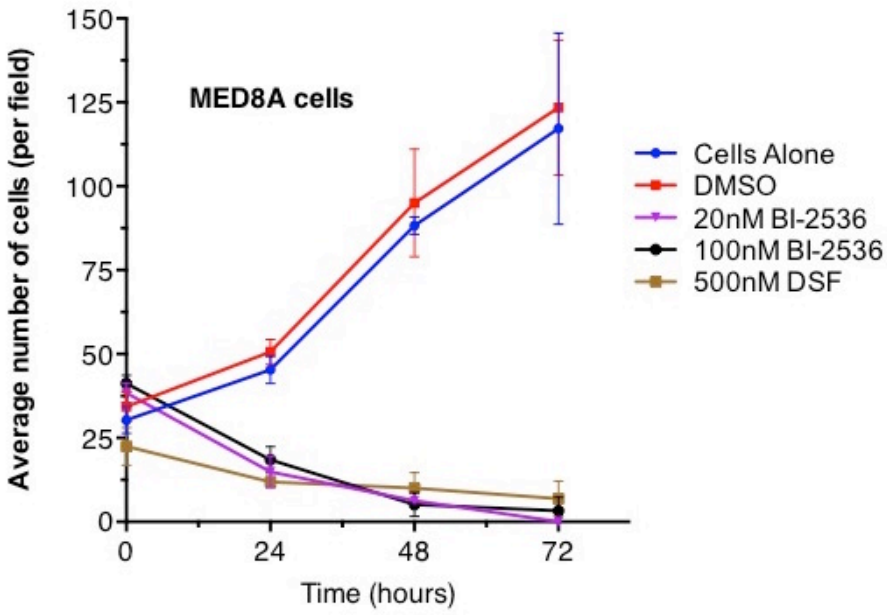

Figure 2.12 BI-2536 and DSF treatment blocks growth of MED8A medulloblastoma cells.
Pediatric medulloblastoma MED8A cell line assessed for monolayer cell proliferation following single treatment of BI-2536 (20 or 100nM) and 500nM DSF. DMSO is used as a solvent control for both compounds. BI-2536 efficacy on MED8A has been tested in three experiments, however data presented here are representative of a single experiment.

2.4 Discussion

There are several characteristics of GBM that hinder therapeutic development. These include a heterogeneous morphology, a delicate location, and the problem of TMZ resistance. For some patients, TMZ treatment induces a response that may initially reduce tumor growth, but relapse eventually occurs for most cases. The long-term survival rate for GBM patients treated with TMZ is extremely low and this harsh chemotherapeutic is ineffective at targeting the cancer cell self-renewal that may cause tumor regrowth (Burkhardt et al., 2011; Gao et al., 2009; Rock et al., 2012). In the present study we demonstrate that DSF has efficacy against GBM *in vitro* by completely suppressing cell growth. Adding to this, we observe the same degree of inhibition in self-renewal assays. Concentrations as low as 100nM DSF were sufficient to eliminate monolayer proliferation and similarly inhibit self-renewal using neurosphere assays. Perhaps most importantly, DSF was highly effective against GBM cells that are refractory to TMZ.

One of our most striking observations was that DSF was effective against GBM models where cells have developed TMZ resistance. In this study we found the important cell cycle kinase, PLK1, is down-regulated following treatment of cell lines with DSF. We also show that TMZ treatment increased expression of PLK1 protein and speculate this phenomenon may have a role in the aggressive nature of recurrent GBM. It is interesting to note that TMZ resistant SF188 cells have approximately double the *PLK1* transcript expression when compared to the U251 cells, which are partially TMZ sensitive. This collection of evidence suggests that DSF has great potential for the treatment of aggressive brain tumors.

Several other studies have used DSF in combination with standard cancer chemotherapy agents, such as: paclitaxel (Yip et al., 2011), gemcitabine (Guo et al., 2010), docetaxel (Budman and Calabro, 2002), cyclophosphamide (Magni et al., 1996), and 5-fluorouracil (Wang et al., 2003). We found the combination of DSF and TMZ treatment was helpful in some instances but not others. While monolayer proliferation assays did not show drastic changes with the drug combination, some cytotoxic augmentation was observed in GBM cells tested in neurosphere self-renewal assays. These data agrees with a breast cancer study that examines DSF toxicity to cancer stem cells *in vitro* (Yip et al., 2011). Similarly, we show enhanced cytotoxicity to TMZ and investigate the use of DSF to target self-renewing primary cells that may be responsible for driving recurrence.

DSF is also being evaluated in other cancer types including metastatic melanoma, prostate cancer, and another phase II/II trial assessing its use in combination with cisplatin for treating metastatic small cell lung carcinoma (ClinicalTrials.gov Identifier NCT00312819). Verma and colleagues have also examined the use of DSF in combination with cisplatin with hopes to decrease nephrotoxicity in a randomized study of cisplatin sensitive malignancies (Verma et al., 1990). They report that combining DSF with cisplatin did not reduce toxicity, however, there was a markedly high patient dropout rate that made data analysis inconsistent between groups. This study also used concentrations of 2000mg/m^2 oral DSF, which far exceed the minimal concentrations required to elicit a response as suggested by our *in vitro* data. The treatment of alcoholism with DSF only requires 250mg/day and this leads us to speculate that the unnecessarily high dose may have created issues in the Verma et al study (Suh et al., 2006; Verma et al., 1990). Final results of the ongoing GBM clinical trials will not be available for at least another three years. We believe DSF will have great benefit if used to treat primary tumors for a number of reasons. Not only is DSF inexpensive and easily administered, it has the capability to cross the blood-brain barrier, which is a major limitation in brain tumor therapeutic design (Faiman et al., 1980; Maj et al., 1970; Oskarsson, 1984).

In the context of this study, the exact mechanism of action of DSF was somewhat elusive for us. However, DSF could be a powerful therapeutic given that it has been reported to target multiple pathways that are operative in cancer. Other researchers speculate the metal chelating properties of DSF metabolites may be responsible for inducing apoptosis. For example, cell death may be a result of redox induced oxidative stress (Cen et al., 2002), proteasome inhibition (Chen et al., 2006), or modulation of the NFkB pathway (Nogueira et al., 2011; Yip et al., 2011). When considering mechanisms proposed by these studies it is important to note they were conducted using the combination of DSF with metal ion additives (eg. $CuCl_2$). In contrast, we demonstrate exceptional activity of DSF in the absence of metal supplementation and therefore question an alternative mechanism of action of DSF on cancer cells.

Initially we suspected DSF targeted cancer cells through inhibition of ALDH (Lipsky et al., 2001); however, we found this was not entirely the case. Greater concentrations of DSF are required to inhibit cell proliferation than those needed to block ALDH activity in GBM cells. Adding to this, the inhibition of ALDH activity with DEAB, an ALDH pan inhibitor, failed to

suppress growth to the degree of DSF. Loss of ALDH did not induce dramatic cell death in GBM cells even when *ALDH1A1* and *ALDH1A3* isoforms were individually silenced with siRNA (data not shown). These studies redirected our focus toward a pathway that does cause considerable cell death and to this end we address a possible link to PLK1. GBM cells are dependent upon PLK1 and inhibiting expression of this kinase suppresses growth of GBM cells nearly 100% and this is associated with cell death (Lee et al., 2012b). Serendipitously we noted that DSF treatment reduced PLK1 expression in both SF188 and U251 cells. The influence of DSF on the PLK1 pathway would have significant implications given that PLK1 is central to the growth of many varieties of cancer (Harris et al., 2012; Lee et al., 2012b; McInnes and Wyatt, 2011; C. Zhang et al., 2012). This opens up several new lines of investigation given that this is the first demonstration of an off-patent drug that inhibits PLK1 expression.

Here we demonstrate the efficacy of DSF in suppressing refractory GBM growth and self-renewal at low concentrations. DSF is safe and has been approved for clinical use for decades; therefore, DSF has excellent potential to be repurposed for the treatment of GBM.

2.5 Experimental procedures

Cell culture

The American Tissue Culture Collection (ATCC) supplied pediatric GBM SF188 (TMZ resistant), adult GBM U251 (partial TMZ sensitivity), and normal human astrocyte cells. GBM4 and BT74 GBM cells are well-established GBM models that were obtained from Dr. Hiro Wakimoto at Massachusetts General Hospital, Boston (Kast and Belda-Iniesta, 2009; Pandita et al., 2004; Wakimoto et al., 2011, 2009). BT241 is another primary isolate model that was isolated from a patient with GBM, and obtained from Dr. Sheila Singh at McMaster University, Hamilton (Singh et al., 2004; Venugopal et al., 2012). GBM4, BT74 and BT241 cells have all been previously characterized both *in vitro* and *in vivo* using xenograft experiments (Pandita et al., 2004; Piccirillo and Vescovi, 2007; Singh et al., 2004; Venugopal et al., 2012; Wakimoto et al., 2009). Primary patient isolated cells, aBT001, aBT003 and aBT015, were isolated using methods previously described (Fotovati et al., 2011; Piccirillo and Vescovi, 2007). All primary samples were acquired in accordance with the guidelines of the Institutional Review Board, and

along with patient consent. SF188, U251, and aBT001 cells were grown in monolayer using Minimum Essential Medium/Earle's Balanced Salt Solutions (MEM/EBSS) (Hyclone, Logan UT, USA) and Dulbecco's Modified Eagle Medium (DMEM)/High Glucose (Hyclone), respectively, supplemented with 10% fetal bovine serum (FBS). BT74, aBT003, aBT015 and sphere assays were grown non-adherently using NeuralBasal medium with Neurocult supplement and growth factors, EGF (20ng/ml), bFGF (20ng/mL) and heparin (2mg/mL). Normal human astrocytes were grown in Astrocyte medium (ScienCell cat. #1801) on adherent plates coated with poly-L-lysine (ScienCell cat. #0413).

Drug treatment and proliferation assay

Proliferation assays were conducted by plating 1000 cells/well in 96-well plates with a range of concentrations of TMZ or DSF. All treatments were done in triplicate, and plates incubated at 37°C in a 5% CO_2 incubator. After 72 hours, cells are fixed with 2% paraformaldehyde in 100µl PBS, and stained with Hoechst 33342 dye (2µg/ml) at room temperature for 30 minutes before a wash with 100µl PBS. Plate analysis and image capture was done using an ArrayScan VTI Reader (Thermal Fisher) (Hu et al., 2009). Dimethyl sulfoxide (DMSO) was used to reconstitute TMZ and DSF and also was used as a solvent control at equivalent proportions to the concentration of DMSO in drug treatments. Ethanol was used as a control for DEAB. Solvent controls were used below 1/1000 dilution in cell medium.

For analysis of effect of BI-2536 on U251 TMZ resistant cells, U251 cells were treated with 10µM of TMZ (or DMSO) every 2 days for a total of 7 days. The cells were harvested for protein extraction and immunoblotting was done to examine PLK1 expression. The cells were then re-plated and treated with increasing concentrations of BI-2536 (5-100nM) for 5 days before the cells were stained with Hoechst dye and quantified on Cellomics. The effect of PLK1 inhibition was investigated using siRNA or BI-2536 as previously described (Lee et al., 2012b).

Neurosphere assay

Self-renewal in BT74, GBM4 and SF188 cells was examined using a neurosphere suspension assay (Note: BT74 and GBM4 cells are always maintained as spheres as were the primary isolates described below). Approximately 10 000 cells/well were plated into a low

adherent 6 well dish using neurobasal medium supplemented with human recombinant EGF (20 ng/ml), human recombinant bFGF (20ng/ml) and heparin (2µg/ml) [Stem Cell Technologies]. Primary samples were obtained from adult patients under informed consent according to the BC Cancer Agency guidelines. Tumor cells were isolated as previously described by us (Lee et al., 2012b). Neurospheres were grown for 5-6 days following plating. Spheres >30µm were counted and photographed using an Axiovert 40CFL microscope and AxioCam MRc camera. NeuroCult Chemical Dissociation kit (Stem Cell Technologies, cat. #05707) was used to passage cells, which are counted and replated as single cells. All drug treatments of TMZ and DSF were done at the time of plating, and repeated during serial passaging.

PLK1 regulation and expression

SF188 or U251 cells were treated with DSF (100-500 nM) for 24 hours, proteins were harvested and levels of PLK1 were evaluated by immunoblotting. RNA for gene expression analysis was isolated using Qiagen RNeasy Mini Kit (cat. #74106). Transcript expression was determined using qRT-PCR with PLK1 Assay on Demand (Applied Biosystems, cat. #4331182). *PLK1* expression was silenced using siRNA as previously described (Lee et al., 2012b). Tumor cell growth following siPLK1 transfection was evaluated compared to scramble control RNA in SF188 cells. PLK1 was also inhibited with BI-2536 and growth was assessed in SF188, BT74, and BT241 all of which are TMZ resistant.

Immunohistochemisty

Primary adult GBM cases (aBT001 and aBT003) were formalin-fixed, paraffin embedded, sectioned and immunostained for PLK1. PLK1 protein expression was evaluated using LSBio antibody (diluted 1:200, PLK1 rabbit anti-Human polyclonal Antibody LS-B4225-LSBio LifeSpan Bioscience, Seattle, WA). The secondary antibody was universal detection kit from DAKO LSAB2 System-HRP (DAKO, Carpinteria, CA). MGMT status of these tumors was determined by methylation specific PCR as previously described (Gerstner et al., 2009).

Statistical analysis

Experimental data were collected from multiple experiments and reported as the treatment mean ± standard error. Significance was calculated using the Student's T-test, where *$p<0.05$, and **$p<0.01$.

CHAPTER 3: TARGETING POLO-LIKE KINASE 1 (PLK1) IN PEDIATRIC MEDULLOBLASTOMA

3.1 Overview

Advances in molecular subtype classification of medulloblastoma (MB) have provided insight into the complex heterogeneity of this primarily pediatric brain tumor. Here, we validate the use of subtyping methodology and further investigate new therapeutic targets for poor prognosis cases, namely SHH and Group 3 MB. Using a drug screen of compounds currently in clinical trials we identified PLK1 as an oncogenic driver of MB that can be inhibited with the small molecule BI-2536. As well, we measured *PLK1* transcript expression in two independent patient cohorts and found its overexpression correlated significantly with poor prognosis across all subtypes of MB. While *PLK1* is high in MB, this was not the case in normal tissues and treatment of non-malignant cells with BI-2536 had no negative effect on cell survival. Primary patient-derived cell culture was used to discover a relationship between BI-2536 sensitivity and the gene expression of *PLK1*. As well, an *in vivo* xenograft demonstrated a survival advantage for BI-2536 treated animals that were comparable to a model of standard-of care chemotherapy.

3.2 Introduction

Medulloblastoma (MB) is the most frequently occurring malignant pediatric brain tumor. A regime of surgical resection, radiation and aggressive chemotherapy is the current treatment approach for MB; however, the success of these strategies may vary on a case-by case basis. For example, the location may restrict the degree of maximal safe resection of the tumor. As well, whole brain and spinal radiation is generally advised against for children under the age of 3 years. Over the past few decades the patient survival rate for standard-risk disease has improved from 5% to >70% due to medical advances (Sirachainan et al., 2011; Taillandier et al., 2011), however, the five-year survival rate for high-risk MB remains dismal (16-70%) (Sirachainan et al., 2011). Unfortunately, almost all survivors will inevitably suffer from long-term adverse sequelae. These undesirable side-effects are attributed to the impact that invasive surgery, radiation, and toxic chemotherapy has on the developing brain (Mabbott et al., 2005). Therefore,

it is imperative to develop novel therapeutics that could reduce sequelae while improving the cure rate of high-risk brain tumors.

MB can be divided into four different molecular subtypes: WNT, Sonic Hedgehog (SHH), Group 3 and Group 4. These subtypes were originally described based on differences in gene expression using cDNA microarrays (Northcott et al., 2011a) which were subsequently substantiated by immunohistochemistry (IHC) (Ellison et al., 2011; Northcott et al., 2011a). Microarrays are problematic because they require fresh snap-frozen tissues whereas IHC is hindered by the subjectivity of scoring and differential staining across laboratories. Recently, mRNA based assays have been developed using the Nanostring nCounter system to avoid some of the problems associated with prior methods of classification (Northcott et al., 2012d). Advantages of NanoString are: 1) multiple genes are used to distinguish MB subtypes, 2) it is highly quantitative, and 3) it does not require an amplification step allowing for low abundance genes to be detected from formalin-fixed paraffin embedded (FFPE) tissues.

The MB subtypes differ not only in genetic signatures but also in response to clinical therapy (Kool et al., 2012). In studies of MB where adult and pediatric patients were evaluated collectively, the WNT molecular subtype was associated with the best prognosis while the Group 3 tumors fair the poorest. The SHH and Group 4 tumors correlate with intermediate outcomes in studies that captured adult and pediatric patients (Northcott et al., 2011b). However it is not known whether the risk associated with each subtype holds true when the cohort(s) is solely comprised of pediatric patients.

Extensive insights into the biology of the SHH pathway have spearheaded significant progress into the development of related targeted therapies, notably to Smoothened (SMO) for which there are several open clinical trials (Lauth et al., 2007). There are already reports of acquired resistance due to point mutations in *SMO* (Yauch et al., 2009), amplification in *GLI2* (Dijkgraaf et al., 2011) and signaling through the PI3K pathway (Buonamici et al., 2010). It is therefore possible that other signal transduction pathways may provide alternative approaches to the management of MB. The identification of targeted therapies for Group 3 and Group 4 tumors also remain a challenge. We provide clinical and pre-clinical evidence suggesting that Polo-Like Kinase 1 (PLK1) is a provocative molecular target for pediatric MB with prognostic importance.

3.3 Results

3.3.1 Molecular subtype classification of pediatric MB correlates with clinical outcome.

Northcott and (2011b) report MB to be comprised of 4 distinct subgroups that can be identified by measuring differences in patterns of gene expression. One of our objectives is to improve methods of prognostication for childhood brain tumors; therefore, we addressed whether these subtypes can be validated as an informative tool for predicting patient outcome. Archived FFPE tissues from 72 pediatric MB cases treated at BC Children's Hospital (Vancouver, BC) between 1986 and 2012 were obtained. Table 3.1 provides a summary of general clinical information from these cases denoted the "discovery" cohort. NanoString based gene expression data was acquired to assign subtype classification to these cases using PAM class predication statistical method (Table 3.2). Based on these subtype classifications, patients with SHH and Group 3 tumors had greater chance of relapse (Figure 3.1A) and death (Figure 3.1B). Relative to SHH and Group 3 cases, children with WNT or Group 3 subtypes experienced fewer cases of relapse and longer overall survival (Figure 3.1A-B). Patient tumors from which tissue specimens were collected for primary cell culture are indicated (Figure 3.1C). The subtype dependent survival trend was also observed in a separate "validation" cohort that comprised of 61 cases of pediatric MB treated at The Hospital for Sick Children (Toronto, ON) (Figure 3.2A-B). Table 3.3 demonstrates available clinical information for these cases, which were also assessed for molecular subtype (Table 3.4). In combination with survival data, heatmaps of the discovery and validation cohort illustrates MB subtype distribution using Northcott and colleagues (2012d) gene list for molecular classification (Figure 3.1C and Figure 3.2C).

The poor outcome of SHH cases prompted us to address whether novel compounds that are currently being tested in adult clinical trials might benefit these children. To do this, we included MB cell lines (ONS76, UW228, UW228, and Daoy) into our NanoString subtyping analysis to incorporate them as tools for *in vitro* drug screening. Each of the cell lines clustered most similarly to the SHH patient subgroup following both hierarchical clustering (Figure 3.1C and Figure 3.2C) and PCA analysis (Figure 3.3). This cluster similarity was further suggested using PAM (PAM-SHH=1.0^{E}+00) and subsequently verified again using the validation cohort as the data training set (data not shown) (Northcott et al., 2012d; Tibshirani et al., 2002). These data suggest the molecular signature of our cell line models resemble the SHH MB subtype.

Characteristic:			WNT	SHH	Group 3	Group 4
	Total Number of Patients Between 1986-2012:	72	9 (13%)	19 (26%)	18 (25%)	26 (36%)
	Excluded from Survival Analysis*:	9**	1	4	2	2
	Number of Patients:	63	8 (13%)	15 (24%)	16 (25%)	24 (38%)
Age						
	<3 years	14 (22%)	0 (0%)	8 (53%)	6 (37%)	0 (0%)
	Between 3 to 8 years	30 (48%)	2 (25%)	6 (40%)	7 (44%)	15 (62%)
	Between 8 to 12 years	10 (16%)	2 (25%)	0 (0%)	3 (19%)	5 (21%)
	12-18 years	9 (14%)	4 (50%)	1 (7%)	0 (0%)	4 (17%)
	Average (years)	6.6	11.3	4.3	4.7	7.9
	Range (years)	1.31 to 16.8	6.1 to 14.8	1.31 to 16.8	1.5 to 10.2	3.8 to 15.4
Sex						
	Female	25 (40%)	7 (88%)	8 (53%)	7 (44%)	3 (12%)
	Male	38 (60%)	1 (12%)	7 (47%)	9 (56%)	21 (88%)
Metastasis						
	M0	30 (48%)	4 (50%)	8 (53%)	6 (37%)	12 (50%)
	M1	14 (22%)	1 (12%)	3 (20%)	5 (32%)	5 (21%)
	M2	3 (5%)	0 (0%)	1 (7%)	1 (6%)	1 (4%)
	M3	10 (16%)	1 (12%)	1 (7%)	3 (19%)	5 (21%)
	Unknown	6 (9%)	2 (25%)	2 (13%)	1 (6%)	1 (4%)
Extent of Resection						
	Gross Total Resection	47 (75%)	6 (75%)	14 (93%)	10 (63%)	17 (70%)
	Subtotal or less	14 (22%)	2 (25%)	1 (7%)	4 (25%)	7 (30%)
	Unknown	2 (3%)	0 (0%)	0 (0%)	2 (12%)	0 (0%)
Treatment						
	Chemotherapy Only	13 (21%)	0 (0%)	7 (47%)	3 (19%)	3 (13%)
	Radiation Only	4 (6%)	3 (38%)	0 (0%)	0 (0%)	1 (4%)
	Both Chemo and Radiation	44 (70%)	5 (62%)	7 (47%)	12 (75%)	20 (83%)
	No Treatment or Incomplete	2 (3%)	0 (0%)	1 (7%)	1 (6%)	0 (0%)

*9 Patients were excluded from survival analysis due to inhomogeneity of treatment regime
Note: of 75 original blocks with follow up 3 were not a MB sample and therefore excluded

Table 3.1 Summary of the pediatric MB patients included in the discovery cohort

Sample Labels	Cultured Labels	Predicted Class	WNT	SHH	Group 3	Group 4
DUNN-101A		SHH	1.0E-09	1.0E+00	4.2E-07	3.7E-07
DUNN-102A	BTX001	SHH	5.3E-07	1.0E+00	6.2E-06	4.9E-06
DUNN-107A		Group4	4.7E-07	7.2E-06	2.4E-01	7.6E-01
DUNN-109A		Group3	2.1E-05	1.2E-04	9.9E-01	8.9E-03
DUNN-113A		Group4	2.9E-04	1.2E-03	2.3E-02	9.8E-01
DUNN-114A		Group4	1.1E-07	1.8E-05	8.5E-03	9.9E-01
DUNN-115A		SHH	4.0E-08	1.0E+00	9.0E-06	3.3E-06
DUNN-117A		Group3	1.5E-07	8.1E-07	8.6E-01	1.4E-01
DUNN-118A		Group4	3.3E-06	1.0E-05	9.2E-02	9.1E-01
DUNN-120A		Group4	5.2E-04	1.7E-03	1.1E-02	9.9E-01
DUNN-121A		Group3	6.6E-08	3.9E-05	1.0E+00	2.1E-03
DUNN-122A		Group3	3.0E-05	6.8E-06	9.9E-01	5.7E-03
DUNN-123A		Group4	4.6E-08	4.7E-06	5.0E-02	9.5E-01
DUNN-124A		SHH	4.3E-10	1.0E+00	6.7E-07	3.3E-07
DUNN-125A		Group4	3.8E-07	4.0E-05	5.4E-03	9.9E-01
DUNN-126A		Group4	4.5E-05	1.5E-03	6.1E-02	9.4E-01
DUNN-127A		Group3	2.2E-05	3.1E-04	9.8E-01	1.8E-02
DUNN-130A		Group3	4.0E-05	3.3E-04	7.9E-01	2.1E-01
DUNN-131A		Group4	1.3E-07	2.3E-04	1.7E-01	8.3E-01
DUNN-132A		Group4	4.8E-08	1.5E-05	8.7E-04	1.0E+00
DUNN-133A		Group3	1.1E-04	2.4E-05	9.9E-01	1.1E-02
DUNN-135A		Group3	2.8E-03	1.9E-04	9.4E-01	5.8E-02
DUNN-138A		SHH	2.9E-08	1.0E+00	3.3E-06	3.2E-06
DUNN-139A		WNT	1.0E+00	8.9E-06	3.5E-05	3.9E-06
DUNN-140A		Group4	4.6E-05	5.4E-05	4.8E-01	5.2E-01
DUNN-142A		WNT	1.0E+00	2.5E-07	9.8E-07	2.3E-07
DUNN-143A		Group4	9.6E-09	1.8E-05	1.9E-03	1.0E+00
DUNN-145A		Group4	7.5E-04	3.1E-04	1.4E-01	8.6E-01
DUNN-146A		SHH	1.8E-05	6.1E-01	3.5E-01	3.5E-02
DUNN-147A		Group3	5.5E-05	1.7E-04	1.0E+00	2.4E-03
DUNN-149A		WNT	1.0E+00	4.9E-05	5.0E-05	2.1E-04
DUNN-150A		Group3	6.2E-06	5.4E-05	5.3E-01	4.7E-01
DUNN-151A		Group4	5.6E-08	3.9E-05	2.0E-03	1.0E+00
DUNN-152A		Group4	2.8E-03	4.2E-04	8.7E-02	9.1E-01
DUNN-153A		Group4	4.1E-06	1.3E-04	1.4E-02	9.9E-01
DUNN-154A		Group4	3.4E-06	2.5E-05	1.0E-01	9.0E-01
DUNN-155A		Group3	8.6E-07	1.2E-06	9.9E-01	1.0E-02
DUNN-156A		Group4	2.5E-03	8.0E-04	9.4E-02	9.0E-01
DUNN-157A		SHH	1.1E-07	1.0E+00	8.0E-06	8.6E-06
DUNN-184A		WNT	1.0E+00	2.2E-09	8.9E-13	2.2E-11
DUNN-185A	BT007	SHH	2.3E-14	1.0E+00	7.2E-09	7.3E-08
DUNN-186A	BT006	SHH	1.4E-12	1.0E+00	3.6E-07	8.3E-06
DUNN-104A		Group4	1.8E-15	3.0E-11	2.6E-05	1.0E+00
DUNN-105A		Group4	6.8E-11	1.2E-06	5.5E-02	9.4E-01
DUNN-106A		SHH	1.7E-14	1.0E+00	5.2E-08	1.6E-05
DUNN-108A		Group4	5.3E-12	2.8E-08	2.1E-03	1.0E+00
DUNN-109A		Group3	2.3E-08	1.0E-07	1.0E+00	4.8E-04
DUNN-110A		SHH	6.8E-13	1.0E+00	3.6E-07	1.2E-06
DUNN-112A		SHH	4.8E-09	1.0E+00	1.6E-05	8.5E-04
DUNN-136A		Group4	5.2E-09	5.3E-06	4.9E-02	9.5E-01
DUNN-158A		Group4	6.8E-14	1.3E-09	1.9E-04	1.0E+00
DUNN-159A		Group4	1.1E-14	6.1E-11	2.5E-03	1.0E+00
DUNN-160A		Group3	1.9E-12	1.6E-10	1.0E+00	2.6E-04
DUNN-161A		SHH	3.1E-12	1.0E+00	1.2E-08	3.2E-08
DUNN-162A		Group3	7.8E-12	1.0E-10	8.8E-01	1.2E-01
DUNN-163A		Group3	2.5E-10	7.3E-09	1.0E+00	2.2E-03
DUNN-164A		WNT	1.0E+00	1.1E-10	2.1E-09	5.2E-11
DUNN-165A		Group4	7.0E-13	1.8E-09	7.9E-02	9.2E-01
DUNN-166A		WNT	1.0E+00	5.0E-12	3.2E-11	1.2E-11
DUNN-167A		SHH	2.5E-02	9.7E-01	9.7E-04	4.3E-03
DUNN-168A		SHH	2.8E-14	1.0E+00	1.4E-07	6.2E-06
DUNN-169A		Group3	3.2E-13	1.6E-11	1.0E+00	1.4E-03
DUNN-170A		SHH	5.5E-10	1.0E+00	8.5E-07	1.6E-05
DUNN-171A		SHH	3.0E-15	1.0E+00	2.7E-09	9.9E-08
DUNN-173A		Group3	5.0E-10	1.9E-08	9.9E-01	1.0E-02
DUNN-174A		Group3	3.2E-11	1.1E-09	1.0E+00	8.0E-04
DUNN-175A		WNT	1.0E+00	1.8E-10	2.8E-09	6.6E-11
DUNN-178A		WNT	1.0E+00	2.6E-11	3.9E-09	5.7E-10
DUNN-179A		WNT	1.0E+00	1.0E-07	3.1E-10	1.3E-09
DUNN-180A		SHH	7.8E-15	1.0E+00	1.0E-10	2.8E-09
DUNN-181A		SHH	9.4E-14	1.0E+00	1.6E-10	4.3E-08
DUNN-182A		Group4	3.8E-12	1.7E-07	2.2E-04	1.0E+00
	BT014	Group4	2.7E-8	3.4E-7	5.2E-3	9.9E-01
	BT025	Group4	2.6E-08	2.5E-06	2.4E-03	1.0E+00
	Daoy	SHH	1.2E-05	1.0E+00	1.4E-05	6.4E-05
	ONS76	SHH	1.1E-08	1.0E+00	1.0E-04	2.7E-04
	UW228	SHH	2.3E-08	1.0E+00	1.5E-04	5.0E-04
	UW426	SHH	3.7E-09	1.0E+00	2.4E-05	2.1E-05

Table 3.2 PAM class prediction validation for MB subgroup assignment of discovery cohort and cultured cells.

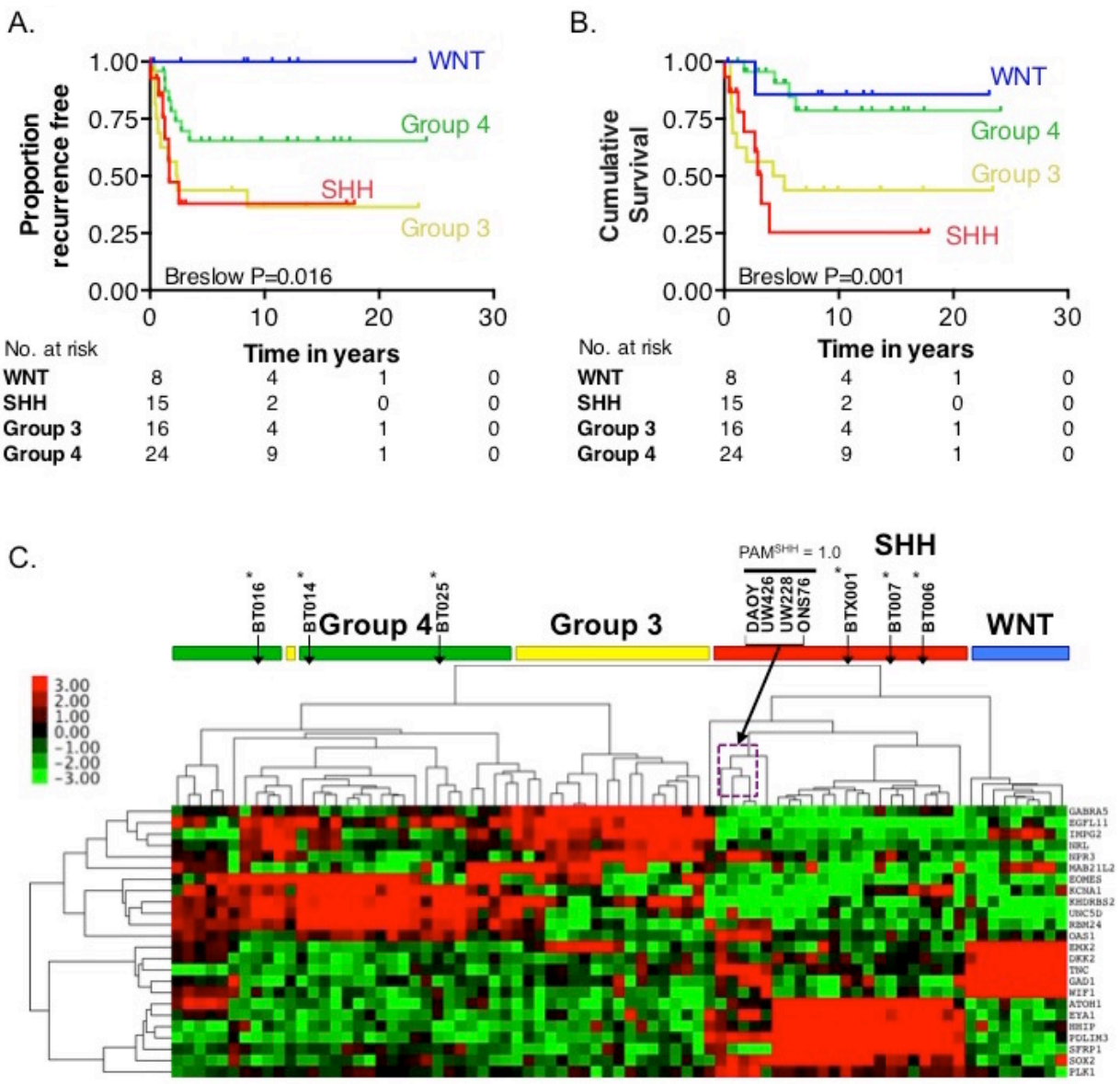

Figure 3.1 Molecular subtyping using gene expression dictates patient outcome and classifies medulloblastoma cell lines.

Patients classified as SHH MB subtype had the **(A)** highest rates of relapse and **(B)** worst chance of overall survival. **(C)** The patient cohort and four MB cells lines were subtyped into different subtypes based on gene expression and are represented using a heatmap (red, high expression; green, low expression). Cell lines ONS76, UW228, UW426, and Daoy were all statistically classified as SHH (PAM= 1.0^{E}+00). The asterisk (*) denotes patients from which the indicated primary cell cultures were established.

Characteristic:			WNT	SHH	Group 3	Group 4
	Total Number of Patients:	61	10 (16%)	16 (26%)	12 (20%)	23 (38%)
	Excluded from Survival Analysis*:	4	0	2	1	1
	Number of Patients:	57	10 (17%)	14 (25%)	11 (19%)	22 (39%)
Age						
	<3 years	11 (19%)	0 (0%)	6 (43%)	5 (45%)	0 (0%)
	Between 3 to 8 years	22 (39%)	3 (30%)	4 (29%)	3 (27%)	12 (54%)
	Between 8 to 12 years	16 (28%)	4 (40%)	2 (14%)	3 (27%)	7 (32%)
	12-18 years	8 (14%)	3 (30%)	2 (14%)	0 (0%)	3 (14%)
	Average (years)	7.2	9.6	5.4	5.0	8.4
	Range (years)	0.56 to 15.3	6.5 to 14.5	0.56 to 15.3	1.2 to 11.5	3.3 to 14.7
Treatment						
	Chemotherapy Only	12 (21%)	0 (0%)	6 (43%)	6 (55%)	0 (0%)
	Radiation Only	3 (5%)	1 (10%)	2 (14%)	0 (0%)	0 (0%)
	Both Chemo and Radiation	38 (67%)	7 (70%)	4 (29%)	5 (45%)	22 (100%)
	No Treatment or Incomplete	4 (7%)	2 (20%)	2 (14%)	0 (0%)	0 (0%)

*4 Patients were excluded from survival analysis due to inhomogeneity of treatment regime
Note: only 55/57 patients with survival outcomes had information on disease progression

Table 3.3 Summary of pediatric MB patients included in the validation cohort.

Sample Labels	Predicited Class	Class determined using BC Children's Training Set	WNT	SHH	Group3	Group4
MDTP1	Group4	Group4	9.89122E-09	2.41245E-07	0.01768734	0.982312409
MDTP12	Group4	Group4	1.09175E-06	7.92025E-05	0.037494784	0.962424922
MDTP13	SHH	SHH	6.39859E-08	0.999998483	4.84143E-07	9.69352E-07
MDTP14	SHH	SHH	5.9823E-05	0.997664881	0.000110842	0.002164455
MDTP16	Group4	Group4	4.07007E-08	1.44381E-06	0.049793432	0.950205084
MDTP17	WNT	WNT	0.999999997	9.50351E-10	1.36797E-09	2.23574E-10
MDTP18	Group3	Group3	4.0599E-06	2.88566E-05	0.985653353	0.01431373
MDTP19	WNT	WNT	0.999830602	7.92495E-05	8.14377E-05	8.71035E-06
MDTP20	Group3	Group3	0.001710482	0.460669399	0.47750042	0.066119699
MDTP23*	SHH	Group3	3.67579E-08	2.29665E-07	0.997970604	0.002029129
MDTP24	WNT	WNT	0.999999947	2.15315E-08	2.83077E-08	2.9531E-09
MDTP25	Group4	Group4	1.02363E-07	3.18434E-06	0.03763668	0.962360034
MDTP26	SHH	SHH	0.000540047	0.999276779	0.000102669	8.05054E-05
MDTP27	SHH	SHH	1.17106E-09	0.999999898	9.09833E-09	9.17498E-08
MDTP29	Group4	Group4	2.33529E-08	2.3282E-06	0.117858682	0.882138967
MDTP30	SHH	SHH	0.000920354	0.969499568	0.0059016	0.023678478
MDTP31	WNT	WNT	0.999999681	2.76395E-07	1.78896E-08	2.51734E-08
MDTP33	Group3	Group3	0.46151477	0.001043836	0.526893331	0.010548063
MDTP34	SHH	SHH	2.39643E-08	0.999996472	3.4002E-07	3.16405E-06
MDTP35	WNT	WNT	0.999961722	3.09955E-05	6.60996E-06	6.72564E-07
MDTP38	Group4	Group4	1.91879E-05	9.33544E-05	0.224767345	0.775120113
MDTP4	Group4	Group4	0.000101322	0.00013383	0.099065122	0.900699726
MDTP40	Group3	Group3	0.00011406	1.82831E-05	0.940544136	0.059323521
MDTP41	Group4	Group4	1.87867E-05	3.52935E-05	0.012754892	0.987191028
MDTP42	Group4	Group4	1.414E-05	0.000409733	0.006059541	0.993516586
MDTP44	SHH	SHH	5.82563E-05	0.99692063	0.000586179	0.002434934
MDTP45	SHH	SHH	5.73317E-05	0.999095394	0.000177121	0.000670154
MDTP46	WNT	WNT	0.631128392	0.01173149	0.130339635	0.226800484
MDTP47	Group3	Group3	0.000471717	4.30393E-05	0.874682586	0.124802658
MDTP5	WNT	WNT	0.999999718	3.32738E-08	2.12276E-07	3.6429E-08
MDTP50	Group4	Group4	8.20736E-05	5.53256E-05	0.153619798	0.846242803
MDTP51	SHH	SHH	0.030760456	0.796377504	0.072801576	0.100060464
MDTP55	SHH	SHH	7.08755E-07	0.999977851	3.46519E-06	1.79747E-05
MDTP56	Group3	Group3	0.006517638	0.027080571	0.498819186	0.467582605
MDTP57	Group4	Group4	0.000229699	0.000217733	0.134769932	0.864782635
MDTP6	Group4	Group4	3.32881E-05	0.000129889	0.050620764	0.949216058
MDTP63	SHH	SHH	8.24977E-08	0.999972264	3.23927E-06	2.44146E-05
MDTP64	Group4	Group4	1.47373E-07	6.03725E-06	0.08878266	0.911211156
MDTP66	Group4	Group4	1.84591E-05	0.00032924	0.093167545	0.906484755
MDTP67	Group4	Group4	2.0219E-08	4.09328E-07	0.014629122	0.985370449
MDTP69	WNT	WNT	0.999970517	6.20826E-06	1.97487E-05	3.52639E-06
MDTP7	Group3	Group3	1.53908E-06	2.32543E-06	0.994073947	0.005922189
MDTP70	Group3	Group3	7.05811E-06	1.21378E-05	0.817776241	0.182204564
MDTP72	Group4	Group4	1.32145E-05	0.000206255	0.022396472	0.977384058
MDTP73	Group3	Group3	4.13272E-06	1.26526E-05	0.902103292	0.097879923
MDTP74	SHH	SHH	0.001990139	0.975095671	0.006843241	0.016070949
MDTP75	Group4	Group4	3.52016E-09	1.61833E-06	0.000981582	0.999016796
MDTP76	Group3	Group3	0.001478502	0.000156232	0.700286469	0.298078797
MDTP77	WNT	WNT	0.997759653	0.000153756	0.001601526	0.000485066
MDTP78	Group4	Group4	1.83428E-06	1.48388E-05	0.012424433	0.987558894
MDTP8	Group4	Group4	6.62862E-05	0.000126182	0.003260733	0.996546799
MDTP81	Group4	Group4	6.55924E-07	5.17251E-06	0.002744848	0.997249324
MDTP82	SHH	SHH	2.03148E-05	0.995862498	0.00032353	0.003793658
MDTP83	Group4	Group4	3.89563E-07	9.68474E-06	0.002154549	0.997835377
MDTP84	Group4	Group4	4.05763E-05	0.000384784	0.235891962	0.763682678
MDTP88	WNT	WNT	0.999909244	1.41797E-05	7.0077E-05	6.49967E-06
MDTP89	SHH	SHH	9.33727E-06	0.999846138	6.27931E-05	8.17317E-05
MDTP9	Group4	Group4	9.43797E-08	2.01323E-05	0.004487636	0.995492137
MDTP90	SHH	SHH	5.41827E-07	0.999806277	4.41331E-05	0.000149048
MDTP91	SHH	SHH	1.23668E-05	0.993213466	0.000301811	0.006472356
MDTP92	Group4	Group4	0.000110324	0.000558898	0.090853583	0.908477195
MDTP93	Group3	Group3	7.0151E-06	6.22458E-05	0.988068964	0.011861775

Table 3.4 PAM class prediction validation for MB subgroup assignment of validation cohort.

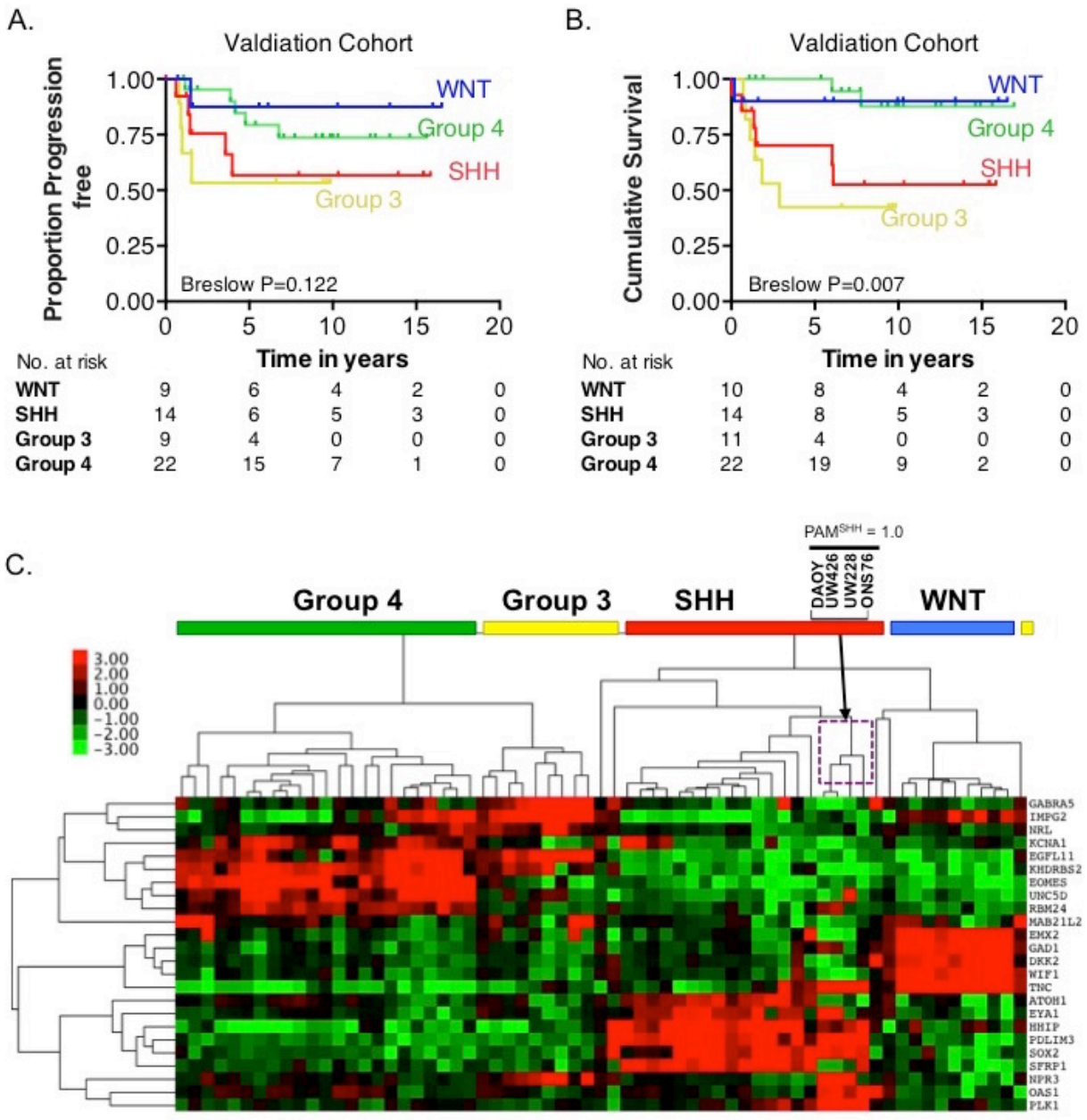

Figure 3.2 MB patient survival in the validation cohort is stratified by molecular subtype.

Subtype affiliation was assessed for **(A)** progression-free survival (n=54, Breslow P=0.122) and **(B)** overall survival (n=57, Breslow P=0.007) in the validation cohort. SHH and Group 3 MB did not statistically vary in outcome. **(C)** Patients as well as four MB cell lines were classified in subtypes based on gene expression and represented using a heatmap (red, high expression; green, low expression). Cell lines (ONS76, UW228, UW426, DAOY) were all statistically classified as SHH (PAM= 1.0^{E}+00).

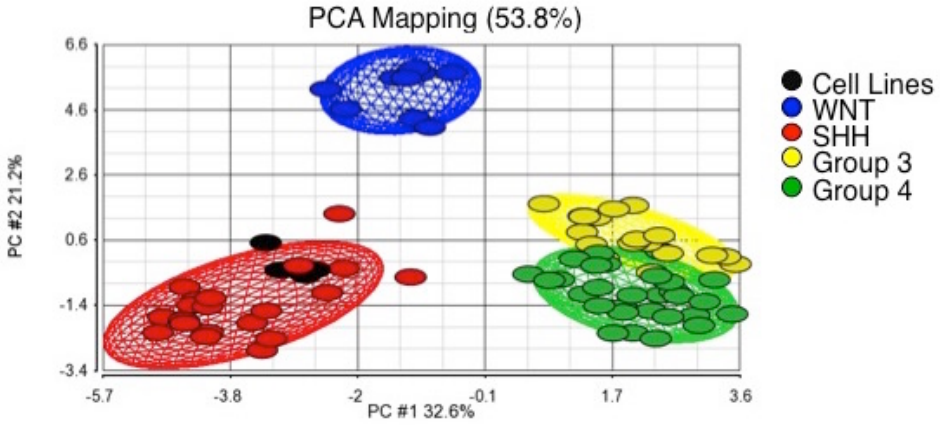

Figure 3.3 Principal component analysis comparison between MB patients and cell line gene expression. Principal component analysis (PAM) uses dimensionality reduction of the 22 subtyping genes (Northcott et al., 2012d) to show association of cell lines with the MB subtypes. Circles represent individual patients (WNT, blue; SHH, red; Group 3, yellow; Group 4, green). The black circles represent cell lines propagated as neurospheres (Daoy, ONS76, UW228, and UW426).

3.3.2 PLK1 is a promising drug target and prognostic marker.

There is a dire need to develop better targets of prognostication for high-risk MB patients that can be linked to individualized treatment options. To begin investigating potential targets the Daoy cell line was used to screen 129 drugs from a library of compounds that are nearly all involved in clinical trials. From this library, compounds of interest met a specific set of criteria: (i) ≥70% proliferation inhibition, (ii) activity at 1nM that is enhanced at 10nM, (iii) potential to cross the blood-brain barrier, (iv) currently in clinical trials, and (v) novelty. A shortlist of 11 compounds was found to match these requirements, but literature reviews further eliminated some candidates due to reported clinical trial toxicity or previous studies. Of the most promising drugs, a selection of three PLK1 inhibitors (BI-2536, BI-6727, and GSK461364) inhibited MB cell growth ~90%, therefore, we chose to pursue PLK1 as a novel target in MB (Figure 3.4A).

To further investigate its importance, transcript levels of *PLK1* were measured in MB patients using the nCounter system. *PLK1* expression was overexpressed in the majority of MB samples when compared to normal cerebellum ($P<0.001$; Figure 3.4B-C). Additionally, there was an equivalent level of *PLK1* expression across the four MB subtypes (Figure 3.4D). The expression of *PLK1* was then evaluated in relation to MB survival outcomes for both the discovery and validation cohort. Elevated transcript expression of *PLK1* was associated with higher rates of relapse and poor overall survival in a Kaplan-Meier univariate analysis (Figure (Figure 3.5A-B). Of note, cases included in the discovery and validation cohorts had similar overall survival outcomes and level of *PLK1* transcript (Figure 3.5C).

Other clinical factors that could influence disease progression were examined in relation of *PLK1* expression using multivariate survival analysis. Independent variables that significantly influence the survival of discovery cohort patients include: presence of metastasis (HR, 3.920; 95% CI, 1.083–14.198), having a SHH medulloblastoma (HR, 9.982; 95% CI, 1.587–62.765), a Group 3 medulloblastoma (HR, 8.874; 95% CI, 1.778–44.283), and expression of PLK1 (HR, 7.286; 95% CI, 1.469–36.142) (Table 3.5). Likewise, having SHH MB, Group 3 MB, or high expression of PLK1 were also significant indicators of outcome in the validation cohort (Table 3.6). It has been reported that younger patients often do poorly as protocols for children < 3 years avoid radiotherapy (Fouladi et al., 2005). Therefore, we questioned whether patients not receiving radiotherapy had even worse outcome. Age and radiotherapy therapy were

significantly associated with univariate survival analysis, but were not independent prognostic markers in the multivariate analysis. Finally, clinical characteristics such as sex, extent of resection, and chemotherapy were not significant variables associated with survival (Table 3.5). The molecular characterization of MB subtype and *PLK1* expression offers a powerful means for patient outcome stratification.

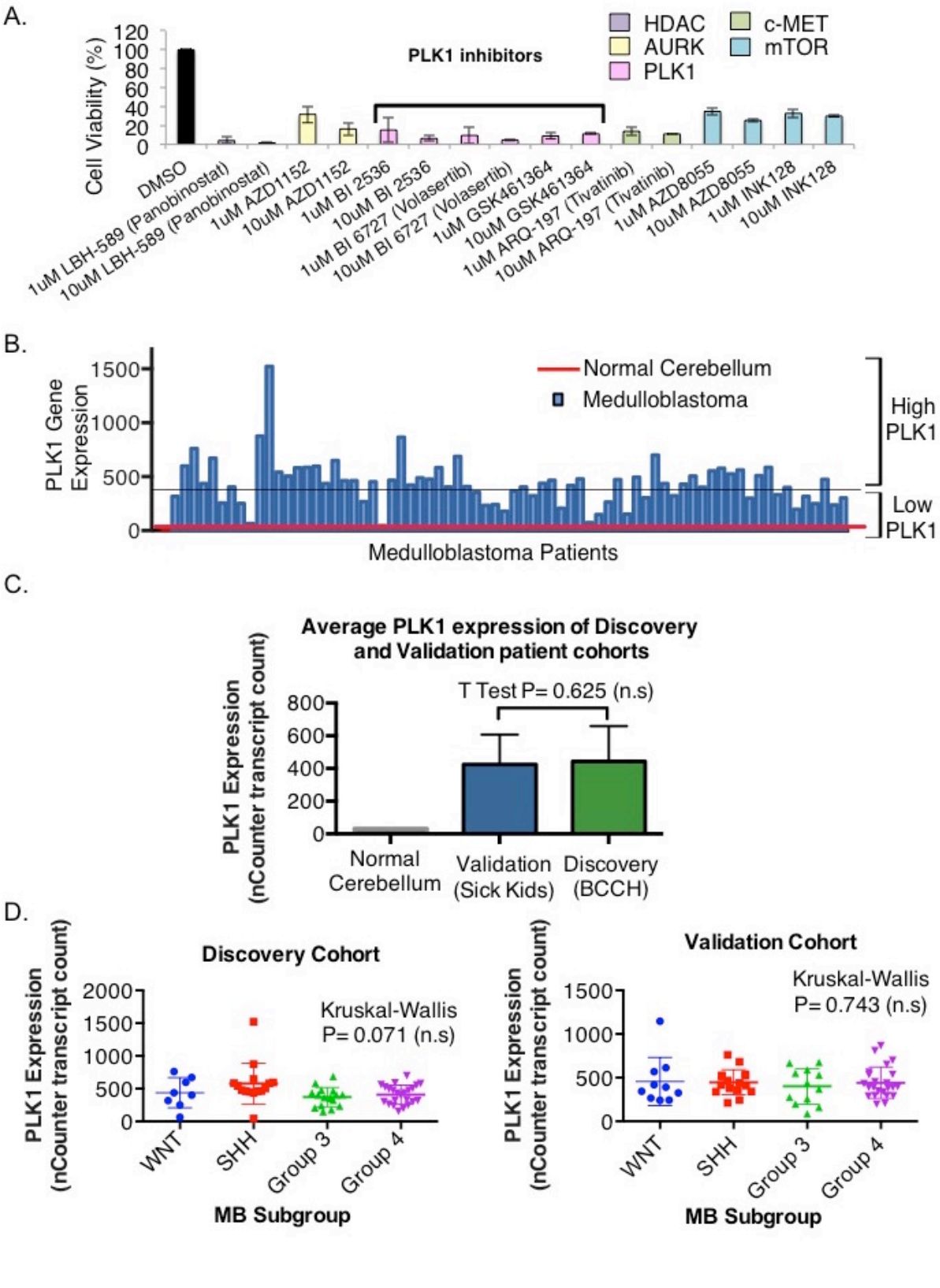
A.
Cell Viability (%)
120
100
80
60
40
20
0
PLK1 inhibitors
HDAC
AURK
PLK1
c-MET
mTOR
DMSO
1uM LBH-589 (Panobinostat)
10uM LBH-589 (Panobinostat)
1uM AZD1152
10uM AZD1152
1uM BI 2536
10uM BI 2536
1uM BI 6727 (Volasertib)
10uM BI 6727 (Volasertib)
1uM GSK461364
10uM GSK461364
1uM ARQ-197 (Tivatinib)
10uM ARQ-197 (Tivatinib)
1uM AZD8055
10uM AZD8055
1uM INK128
10uM INK128
B.
PLK1 Gene Expression
1500
1000
500
0
Normal Cerebellum
Medulloblastoma
High PLK1
Low PLK1
Medulloblastoma Patients
C.
Average PLK1 expression of Discovery and Validation patient cohorts
PLK1 Expression (nCounter transcript count)
T Test P= 0.625 (n.s)
800
600
400
200
0
Normal Cerebellum
Validation (Sick Kids)
Discovery (BCCH)
D.
Discovery Cohort
PLK1 Expression (nCounter transcript count)
2000
1500
1000
500
0
Kruskal-Wallis P= 0.071 (n.s)
WNT
SHH
Group 3
Group 4
MB Subgroup
Validation Cohort
PLK1 Expression (nCounter transcript count)
1500
1000
500
0
Kruskal-Wallis P= 0.743 (n.s)
WNT
SHH
Group 3
Group 4
MB Subgroup

Figure 3.4 *PLK1* is expressed in pediatric MB and can be targeted with kinase inhibitors.
(A) A library of small molecule inhibitors was screened in a 72 hour Daoy cell growth assay. **(B)** NanoString nCounter analysis of 72 patient samples (blue bars) shows *PLK1* mRNA is overexpressed in MB relative to normal cerebellum (red line) and indicates cut off between high and low expressers. **(C)** The average of all MB patient samples were significantly higher then the normal cerebellum and found at similar levels between discovery (n=63) and validation cohorts (n=58) (T-test, P=0.625). **(D)** The Grubb's test was used to remove single outliers from both data sets. *PLK1* was invariably expressed across all four MB subgroups in both the discovery cohort (Kruskal-Wallis, P=0.071) and Validation cohort (Kruskal-Wallis, P=0.743).

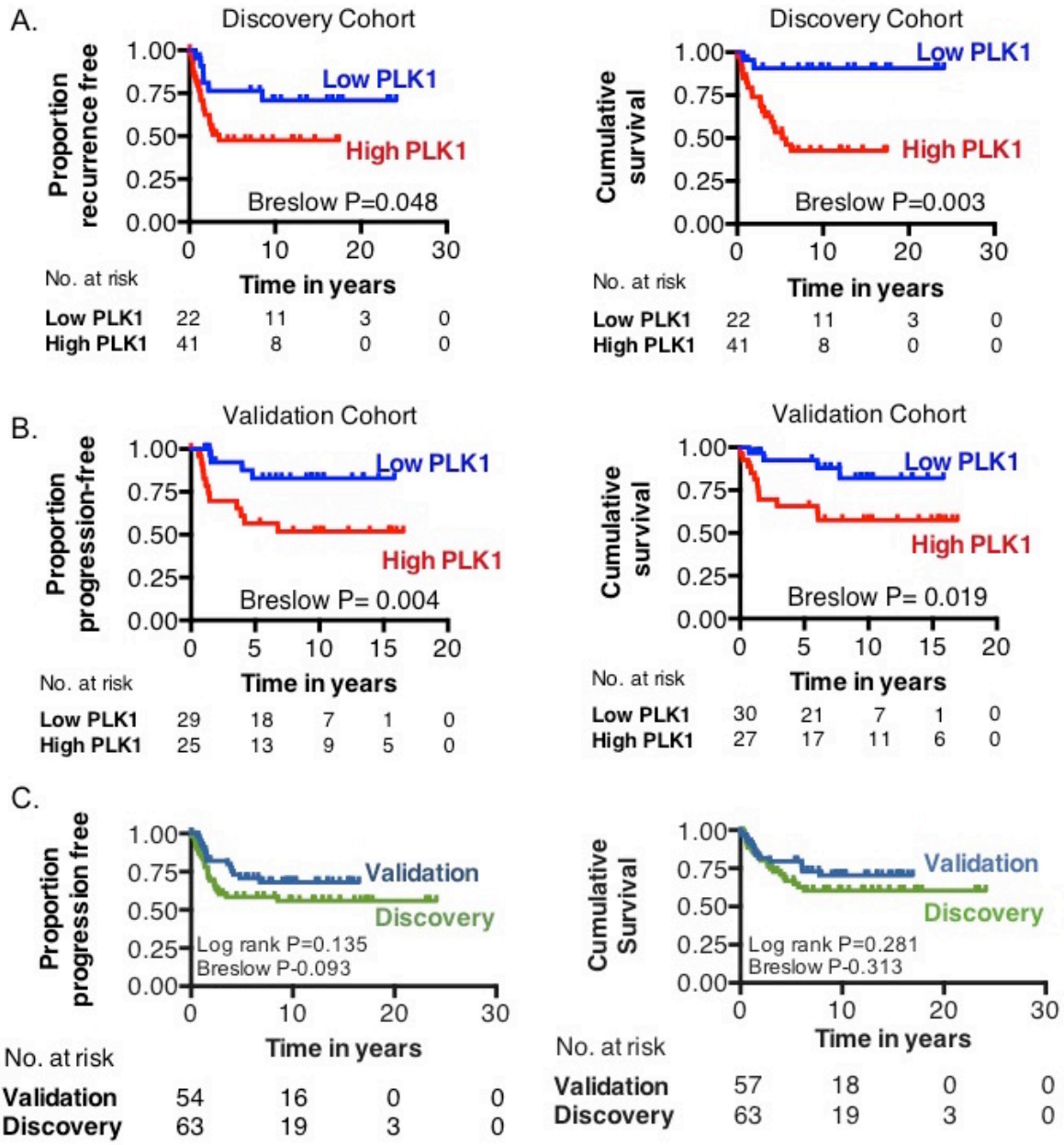

Figure 3.5 *PLK1* transcript expression correlates with poor patient survival.

Using NanoString nCounter analysis, **(A)** high *PLK1* mRNA expression predicts probability of patient relapse (n=63, P=0.048) and poor overall survival (n=63, P=0.003), and is **(B)** validated in a second independent cohort from Toronto, ON (Progression-free survival, n=55, P=0.004; Overall Survival, n=58, P=0.019).

(C) Progression or relapse free survival (Log rank P=0.135, Breslow P=0.093) and overall survival (Log rank P=0.281, Breslow P=0.313) between cohorts.

Variable	No.	Log-Rank test (p value)	No. (n=56)	Hazard ratio (95% confidence interval)	Cox regression analysis (p value)
Age					
< 3 years	14	0.108 (n.s)	11	0.886 (0.231 to 3.390)	0.859 (n.s)
≥ 3 years	49		45		
Sex					
Male	38	0.324 (n.s)	34	0.862 (0.267 to 2.786)	0.804(n.s)
Female	25		22		
Metastasis					
Present	27	0.026	25	3.920 (1.083 to 14.198)	**0.037**
Not Present	30		31		
Extent of Resection					
Gross Total Resection	47	0.663 (n.s)	44	1.187 (0.285 to 4.946)	0.814 (n.s)
Subtotal Resection or less	14		12		
Radiation					
Yes	48	0.102 (n.s)	42	1.688 (0.420 to 6.785)	0.461 (n.s)
No	15		14		
Chemotherapy					
Yes	57	0.938 (n.s)	52	3.708 (0.317 to 43.421)	0.296 (n.s)
No	6		4		
SHH Subtype					
SHH	15	0.007	14	9.982 (1.587 to 62.765)	**0.014**
Non SHH	48		42		
Group 3 Subtype					
Group 3	16	0.046	13	8.874 (1.778 to 44.283)	**0.008**
Non Group 3	47		43		
PLK1 Transcript					
High	41	0.001	36	7.286 (1.469 to 36.142)	**0.015**
Low	22		20		

n.s = not significant

Table 3.5 Univariate and multivariate analyses of clinical, pathological and biological endpoints of the Discovery cohort.

Variable	No. (n=58)	Log-Rank test (p value)	No. (n=57)*	Hazard ratio (95% confidence interval)	Cox regression analysis (p value)
Age					
< 3 years	11	0.150 (n.s)	11	0.294 (0.038 to 2.245)	0.238 (n.s)
≥ 3 years	46		45		
Radiation					
Yes	42	0.037	41	1.945 (0.306 to 12.360)	0.481 (n.s)
No	15		15		
Chemotherapy					
Yes	50	0.635 (n.s)	50	0.283 (0.035 to 2.292)	0.237 (n.s)
No	6		6		
SHH Subtype					
SHH	14	0.099 (n.s)	14	7.504 (1.316 to 42.783)	**0.023**
Non SHH	43		42		
Group 3 Subtype					
Group 3	11	0.010	11	9.710 (1.947 to 48.435)	**0.006**
Non Group 3	46		45		
PLK1 Transcript					
High	27	0.025	26	4.162 (1.156 to 14.987)	**0.029**
Low	30		30		

* 1 patient excluded from multivariate analysis due to incomplete outcomes information
n.s = not significant

Table 3.6 Validation cohort univariate and multivariate analyses of clinical, pathological and biological endpoints.

3.3.3 Abundance of *PLK1* transcript dictates efficacy of PLK1 kinase inhibitor treatment for primary patient isolates.

With the discovery that PLK1 is a marker of patient outcome we next questioned whether targeting it in primary MB cells is an effective means of treatment. Primary patient-derived MB cells were extracted from fresh surgical specimens and grown as neurospheres (BTX001, BT014, BT016, and BT025). To ensure the clinical translatability of our *in vitro* findings we sought to verify that the procedure of primary cell culture produced neurospheres reflects the biology of the original tumor. NanoString gene expression was used to compare RNA extracted from cultured neurospheres with RNA from matched tumor of origin FFPE sections. This is exemplified for BTX001, BT016, and BT025 (Figure 3.6). The cultured primary cells retained subtype and PLK1 expression patterns of the original tumors.

The mRNA expression of *PLK1* was 6.35 fold higher in BTX001 compared to normal cerebellum (CB) and 2.95 fold higher than hNSC *PLK1* expression using qRT-PCR (Figure 3.7A) and BI-2536 hindered BTX001 self-renewal upon serial passaging (Figure 3.7B). In contrast, BT014 and BT025 cells were derived from Group 4 tumors that expressed lower levels of *PLK1* and they were not responsive to BI-2536 (Figure 3.7A-D). In addition, BI-2536 was screened against hNSCs as an *in vitro* test for safety that produced negligible growth effects (Figure 3.7E). Finally, the expression of *PLK1* mRNA in other primary MB specimens (BTX001, BT006, BT007, and BT274) was comparable to Daoy cells, and higher than normal human astrocytes, which is another predominant type of brain cell (Figure 3.8). PLK1 inhibitors may offer a safe therapeutic option for cases of MB that overexpression *PLK1*.

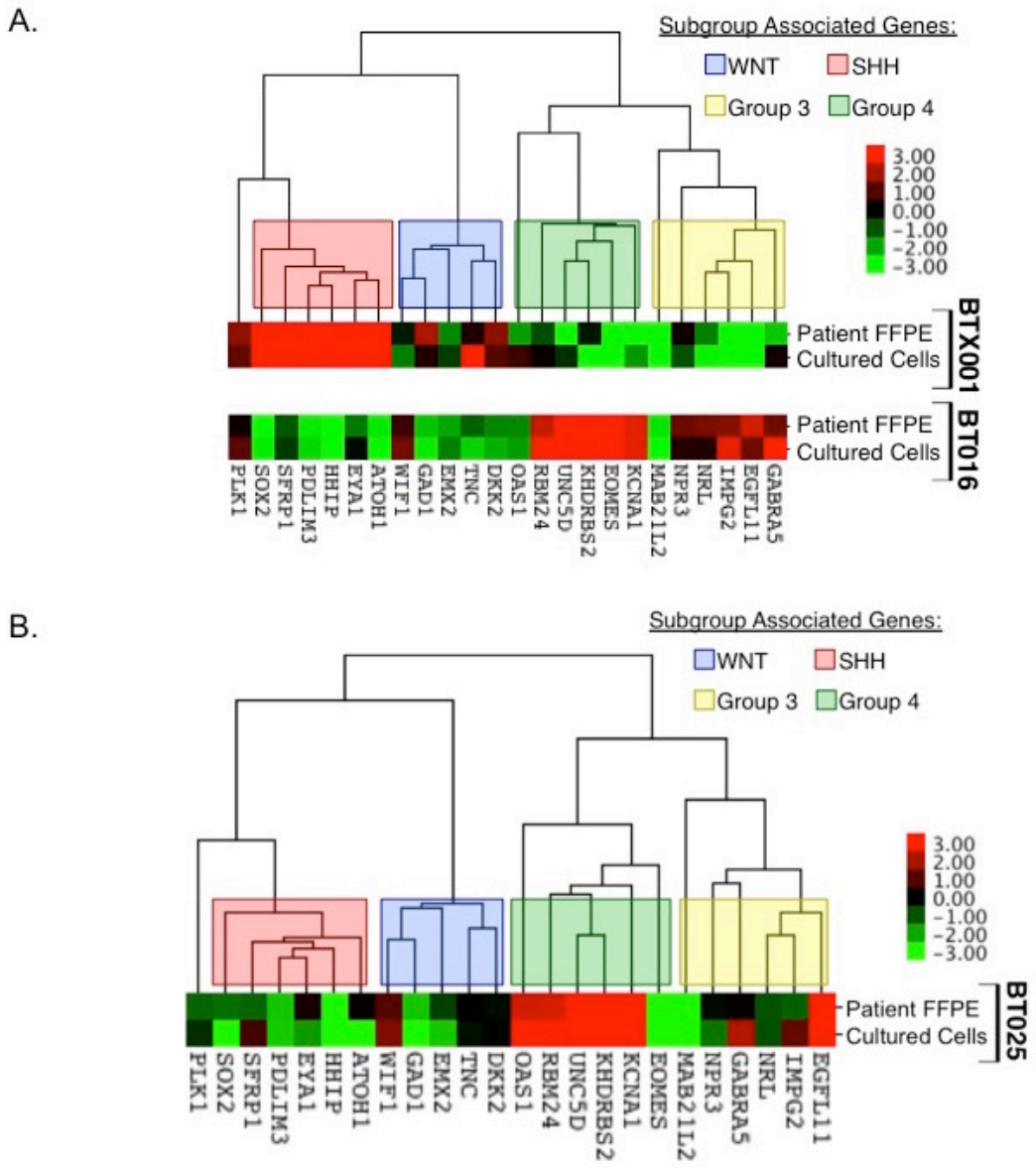

Figure 3.6 Primary culture MB cells retain gene expression signature of tumor of origin.

(A-B) NanoString analysis of mRNA from primary cells and FFPE tissue from origin patient tumors demonstrates primary cultured MB cells retain gene expression of the tumor of origin. BTX001 is high *PLK1* SHH MB, and BT016 and BT025 are low *PLK1* Group 4 MB.

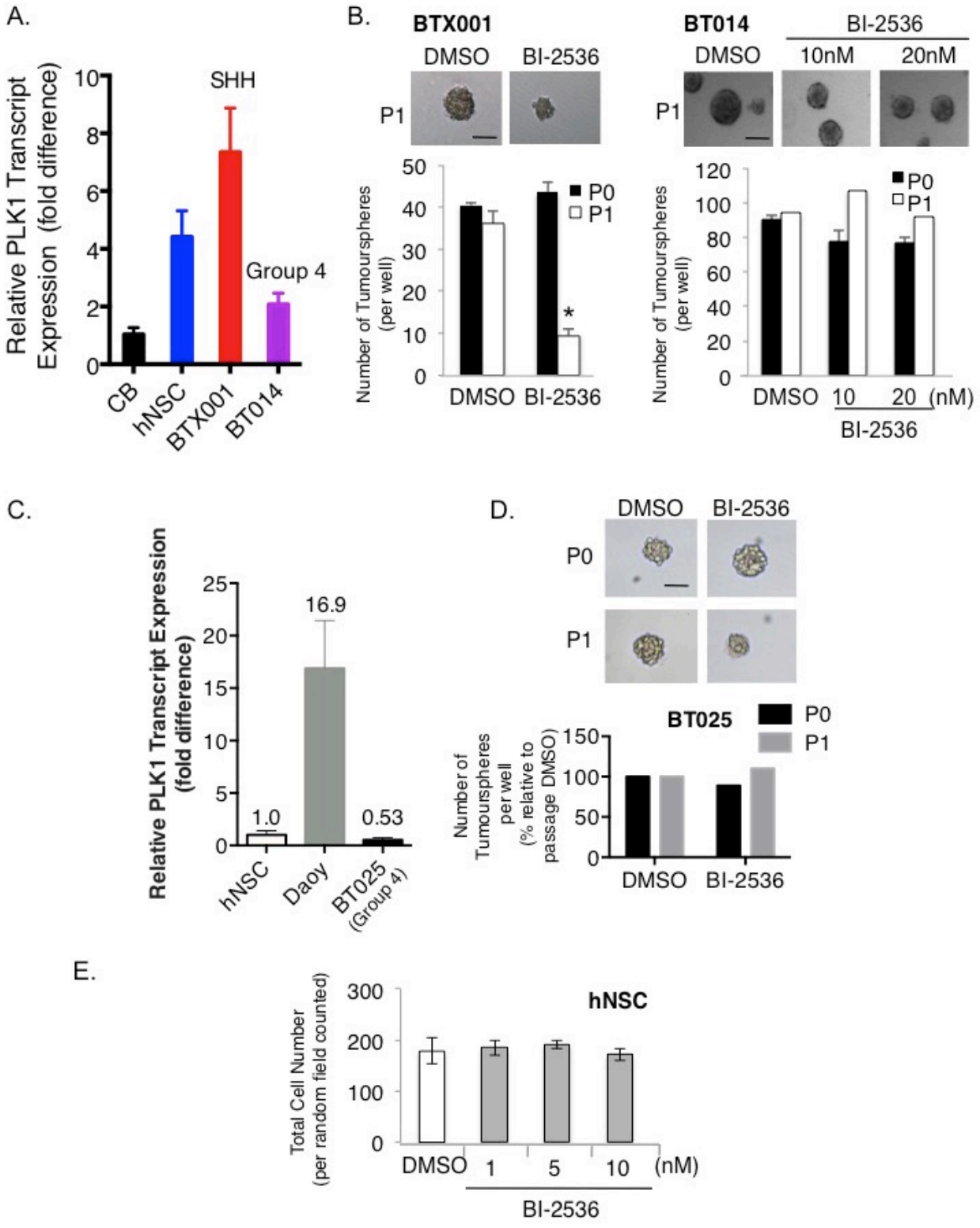

Figure 3.7 *PLK1* expression is required for MB primary cell sensitivity to BI-2536.

(A) *PLK1* transcript expression in cerebellum tissue (CB), human neural stem cells (hNSC), patient-derived MB samples BTX001, and BT014. **(B)** 10nM BI-2536 inhibited self-renewal of BTX001 over 6 days (*, P<0.05; scale bar, 140μm). BT014 cells were not responsive to 10nM BI-2536 over 6 days (scale bar, 140μm). **(C)** qRT-PCR analysis of PLK1 mRNA confirms low expression in BT025 relative to hNSC and Daoy. **(D)** BT025 were not responsive to 10nM BI-2536 following 6 day treatment exposure (scale bar, 140μm). **(E)** hNSCs were treated with 1, 5, and 10nM BI-2536 for 72 hours and stained with Hoechst.

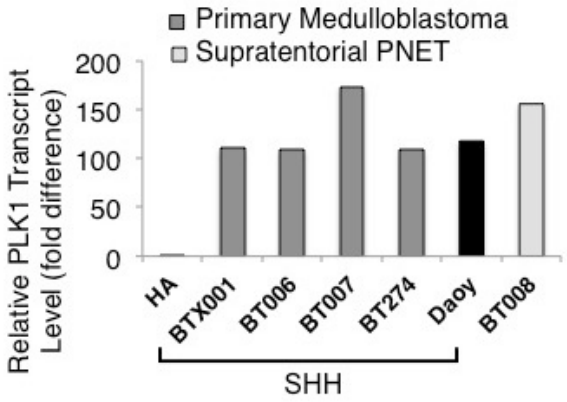

Figure 3.8 *PLK1* expression in a panel of primary brain tumor samples

PLK1 mRNA levels measured by qRT-PCR of freshly isolated patient-derived MB samples (BTX001, BT006, BT007, BT008, BT274) relative to normal human astrocytes (HA).

3.3.4 PLK1 inhibition reduces growth and causes cell death *in vitro.*

To decipher why PLK1 is an important target in MB we examined the mechanistic consequences of its inhibition *in vitro*. The Daoy cell line was used for this purpose because it expresses PLK1 at a similar level to that of poor prognosis MB patients (Figure 3.9A). Knocking down PLK1 with siRNA for 72 hours suppressed Daoy cell growth by approximately 90% (Figure 3.9B). Downregulation of PLK1 protein expression was confirmed using immunoblot. In conjunction, there was also an 80% decrease in the phosphorylation of translationally controlled tumor protein (TCTP), which is a direct substrate of PLK1 and an established marker of PLK1-specific kinase activity (Figure 3.9B) (Cucchi et al., 2010; Yarm, 2002). Treatment with BI-2536 also suppressed phosphorylation of TCTP along with an additional PLK1 substrate, CDC25C. Cell proliferation was reduced with an IC90 of 5nM BI-2536 after a single treatment over 72 hours (Figure 3.9C). Likewise, *PLK1* expression was measured in two additional cell lines, ONS76 and UW426, which were equally sensitive to BI-2536 (Figure 3.9A, D-E). A single 24-hour treatment of Daoy cells with BI-2536 caused a G2/M cell cycle arrest. This was demonstrated using flow cytometry and quantification of the percentage of phosphorylated histone H3 (Figure 3.10A-B). Similarly, immunofluorescent staining showed compromised cell division in the BI-2536 treatment group. PLK1 inhibition resulted in irregular centrosome duplication and separation with many cells appearing polynucleated relative to control treatments (Figure 3.10C and Figure 3.11). Both siPLK1 and BI-2536 treatment induced apoptosis after 48 hours (Figure 3.9C and 3.10D).

Although our focus has mainly pertained to SHH MB, our clinical PLK1 data suggest it could be equally as important in other high-risk classifications of MB. The MED8A cell line has previously been reported to originate from a Group 3 MB (Langdon et al., 2006) that expresses high levels of PLK1 similar to that of the Daoy cell line (Figure 3.12A). BI-2536 inhibited MED8A growth in a dose and time dependent manner (Figure 3.12B). As well, doses of 5 and 10nM BI-2536 abolished MED8A neurosphere self-renewal (Figure 3.12C). This effect on self-renewal was also observed with Daoy cells (Figure 3.12D).

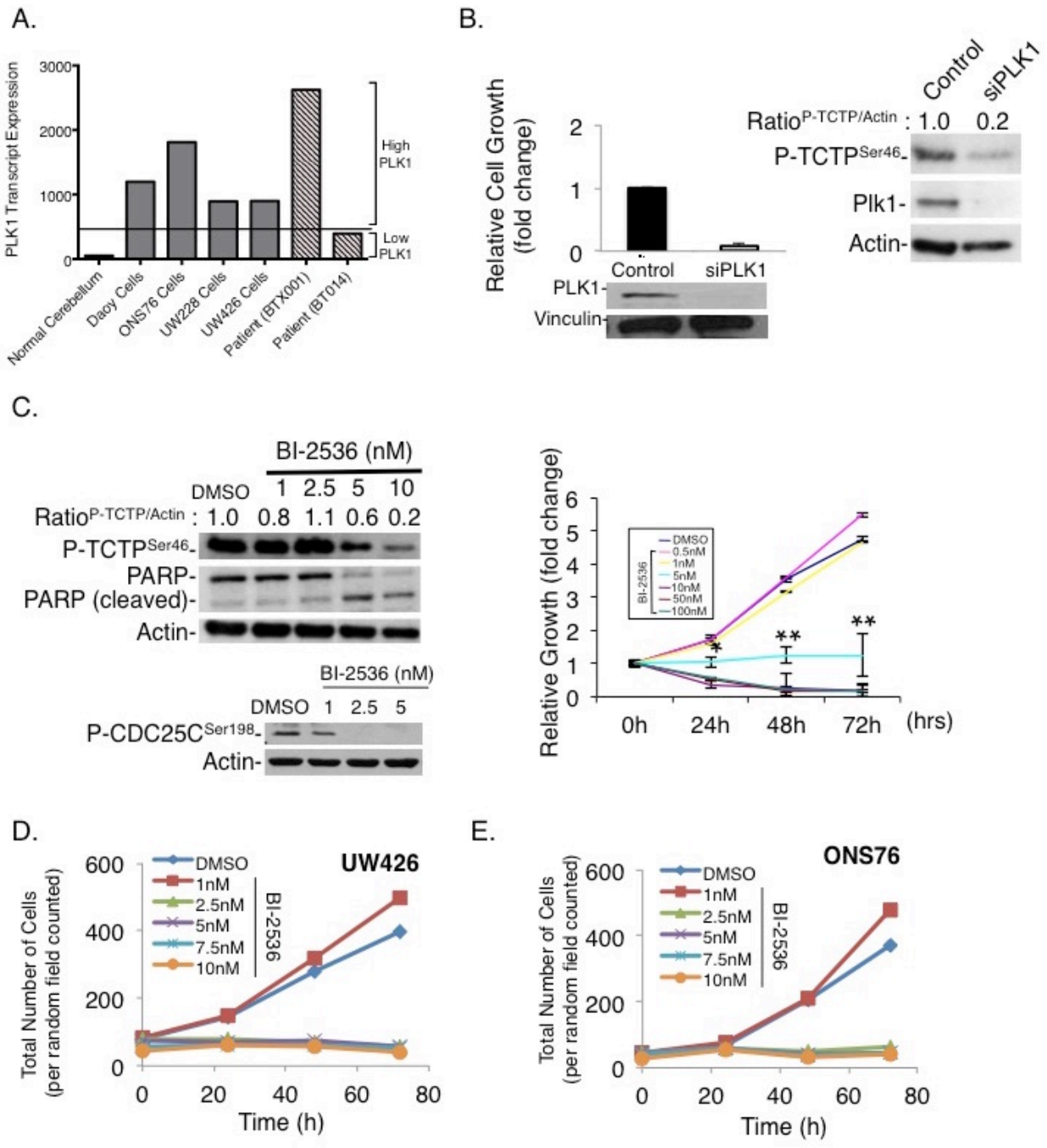

Figure 3.9 MB cell lines expression *PLK1* experience reduced proliferation with PLK1 inhibition.

(A) *PLK1* transcript levels were measured in normal cerebellum, MB cell lines, and patient samples corresponding to culture samples BTX001 and BT014 using NanoString nCounter analysis. **(B)** Daoy cells treated with 5nM PLK1 siRNA for 72 hours and knockdown was confirmed by immunoblotting (bottom). Cell growth was assessed using Hoechst staining (top). Immunoblotting for PLK1 substrate P-TCTP^{Ser46}, following PLK1 siRNA knockdown.

Densiometric quantification normalized to actin housekeeper. **(C)** P-TCTP^{Ser46}, PARP cleavage, and P-CDC25CSer198 in Daoy cells treated with dimethyl sulfoxide (DMSO), 1, 2.5, 5, or 10nM BI-2536 for 48 hours. Daoy cells treated with 0.5-100nM BI-2536 for 24, 48 for 72 hours then growth was assessed by Hoechst staining. **(D)** UW426 and **(E)** ONS76 cells were sensitive to BI-2536 as it inhibited growth in a time and dose dependent manner over 72 hours. Data represents three independent experiments.

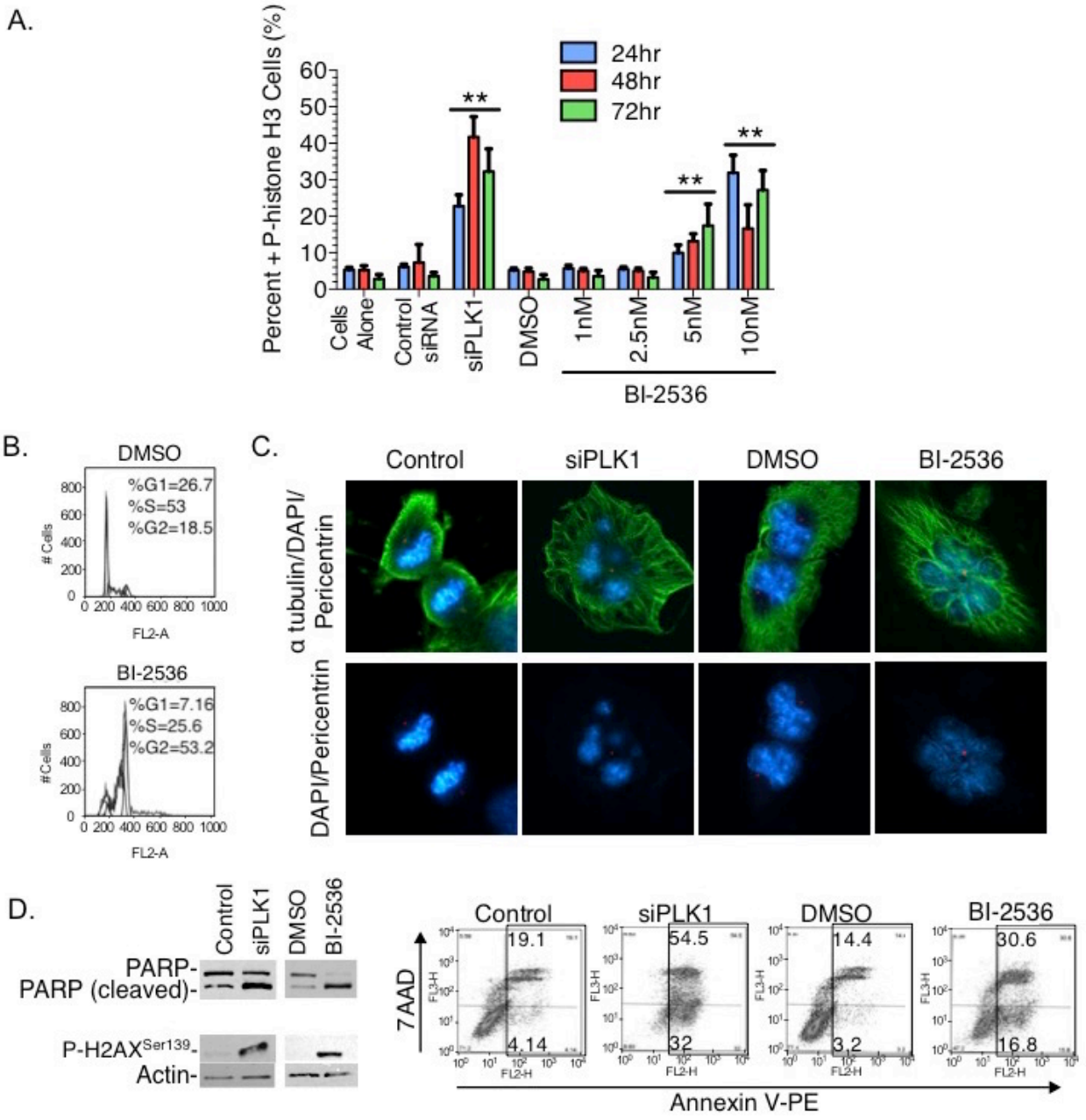

Figure 3.10 PLK1 inhibition causes G2/M arrest and induces apoptosis.

(**A**) The percent of Daoy cells positive for Ser10 phosphorylated histone H3 was measured using high content screening over a 72 hour timecourse to examine cell cycle G2/M arrest. **(B)** Daoy cells treated with 5nM BI-2536 for 24 hours were subjected to flow cytometry with propidium iodide for analysis of cell cycle profile. **(C)** PLK1 was inhibited in Daoy cells using siPLK1 or 10nM BI-2536 for 24 hours then stained for alpha-tubulin (green), pericentrin (red), and 4', 6-diamidino-2-phenylindole (DAPI) nuclear staining (blue). **(D)** Apoptosis was measured by PARP cleavage and P-H2AX^{Ser139} immunoblotting, or by Annexin V-PE/7AAD staining in Daoy cells treated with 5nM BI-2536 for 48 hours.

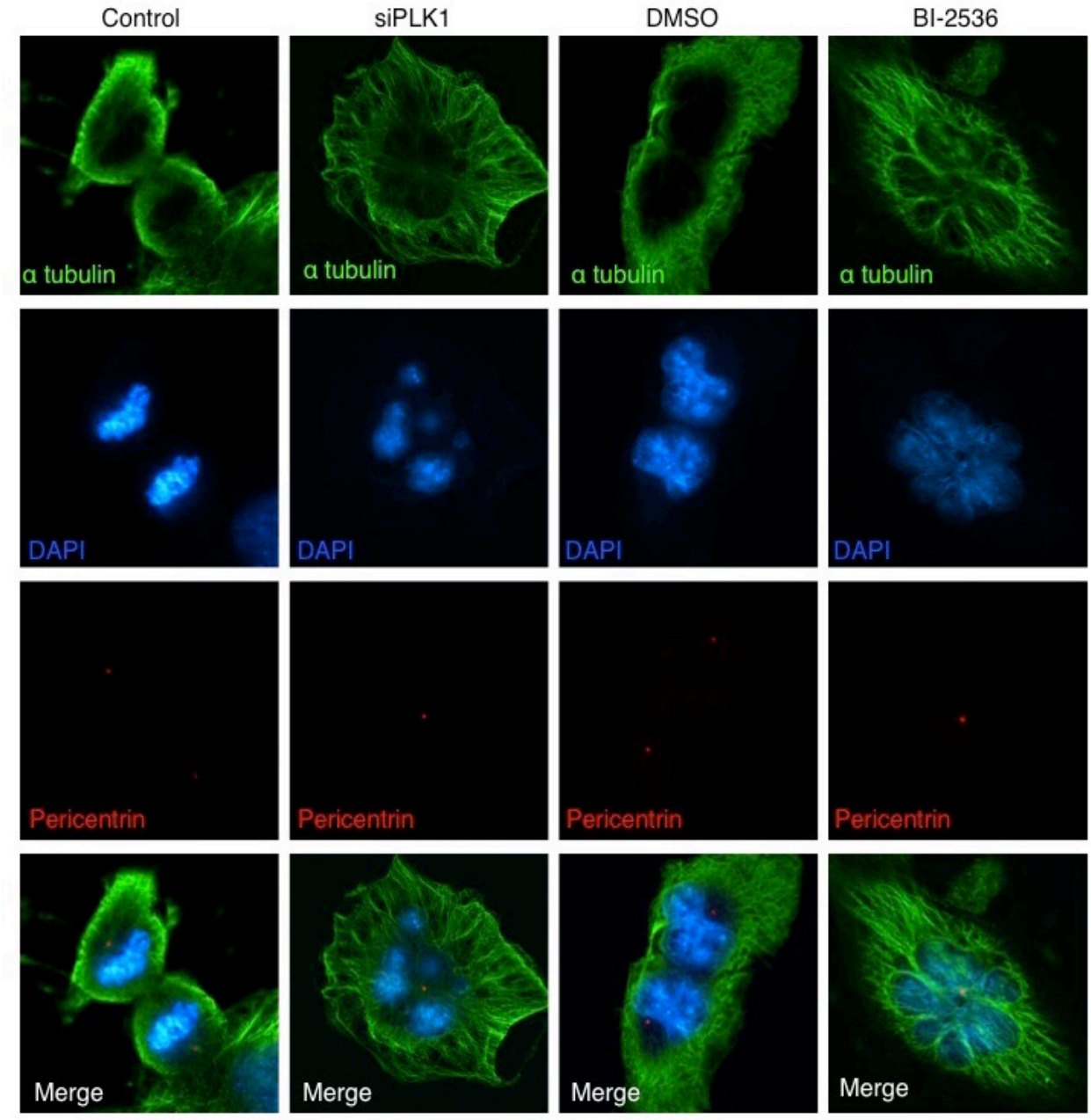

Figure 3.11 PLK1 inhibition disrupts normal mitotic replication in MB cells.

Daoy cells were treated with PLK1 siRNA and 10nM BI-2536 for 24 hours then fluorescently stained for alpha-tubulin (green), pericentrin (red) and 4', 6-diamidino-2-phenylindole (DAPI) nuclear staining (blue).

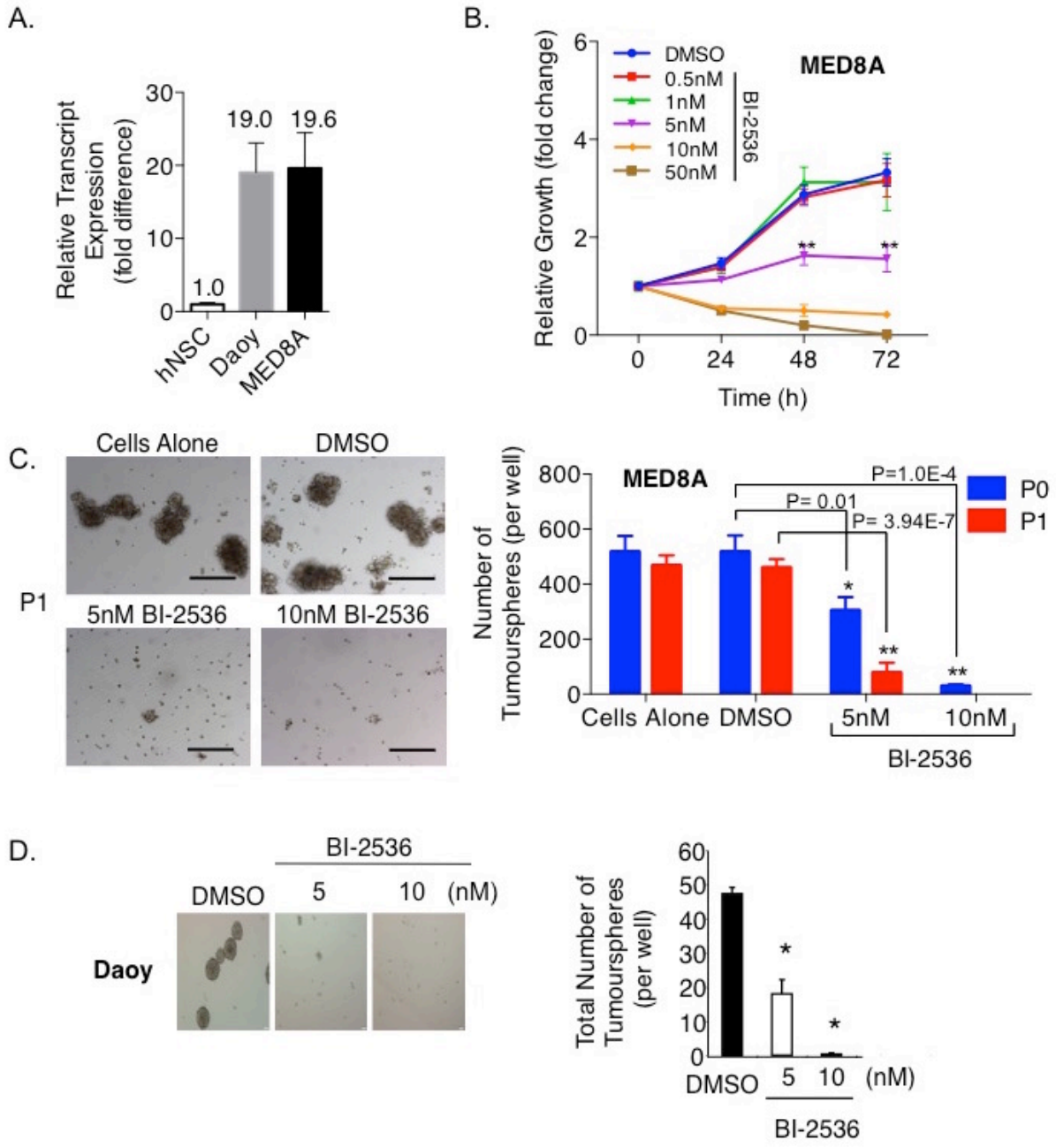

Figure 3.12 MED8A cells express high levels of *PLK1* and are sensitive to BI-2536.

(A) Relative *PLK1* expression of hNSC, Daoy and MED8A cells measured using qRT-PCR. **(B)** MED8A cells were treated with 0.5, 1, 5, 10 and 50nM BI-2536 over a 72 hour timecourse experiment and assessed for cell growth using Hoescht staining. **(C)** Neurosphere self-renewal growth of MED8A was tested with 5 and 10nM BI-2536 over serial passages of 6 days. Microscopy images are representative of P1 serial passage (scale bar, 200μm). **(D)** Daoy cells were propagated as neurospheres and treated with 5 and 10nM BI-2536. Ability of cells to self-renew was inhibited after 6 days exposure. Data represented in (A) is of a single experiment done in triplicate, while (B-D) represent the combined data of three independent experiments.

3.3.5 PLK1 inhibitors are as effective as standard chemotherapy as *in vivo*.

Current drug treatment protocols for pediatric MB include a cocktail of chemotherapeutic agents that have associated sequelae (Korah et al., 2010; Pasquali et al., 2012; Sands et al., 2011; Vieira et al., 2014). To this point we next aimed to determine how BI-2536 treatment compared to standard-of care chemotherapeutics. Daoy, ONS76 and UW426 MB cell lines were found to respond to treatment of common chemotherapeutic agents (vincristine, cisplatin, and etoposide) *in vitro* (Figure 3.13). Next we expanded our study to compare the efficacy of BI-2536 with conventional chemotherapy using an animal model. The BI-2536 treatment group showed delayed MB tumor growth and this was similar to the group treated with a standard-of care chemotherapy protocol (Figure 3.14A).

With hopes of extrapolating our *in vivo* experiment to suggest possible benefit for patients treated with PLK1 inhibitors, we proceeded to characterize our xenograft tissues. The histomorphology of the Daoy NOD-CB17-SCID xenografts was similar to large cell anaplastic (LCA) MB (Figure 3.14B). This observation is consistent with another group that similarly injected Daoy cells intracranially into Rag2 immunodeficient mice (Shu et al., 2006). LCA histology is an indication of poor survival in both SHH and Group 3 MB (Northcott et al., 2011b; Taylor et al., 2011). Finally, the gene expression profile of the Daoy xenograft was compared with a MB patient cohort and was found to cluster most similarly with the SHH patient subtype (Figure 3.14C). There was also consistent expression of the stem cell gene, *SOX2*, and the transcription factor, *GLI2*, which are both involved in SHH signaling (Ahlfeld et al., 2013). Taken together, BI-2536 is a promising chemotherapy alternative that may greatly benefit the treatment of the most aggressive type of MB.

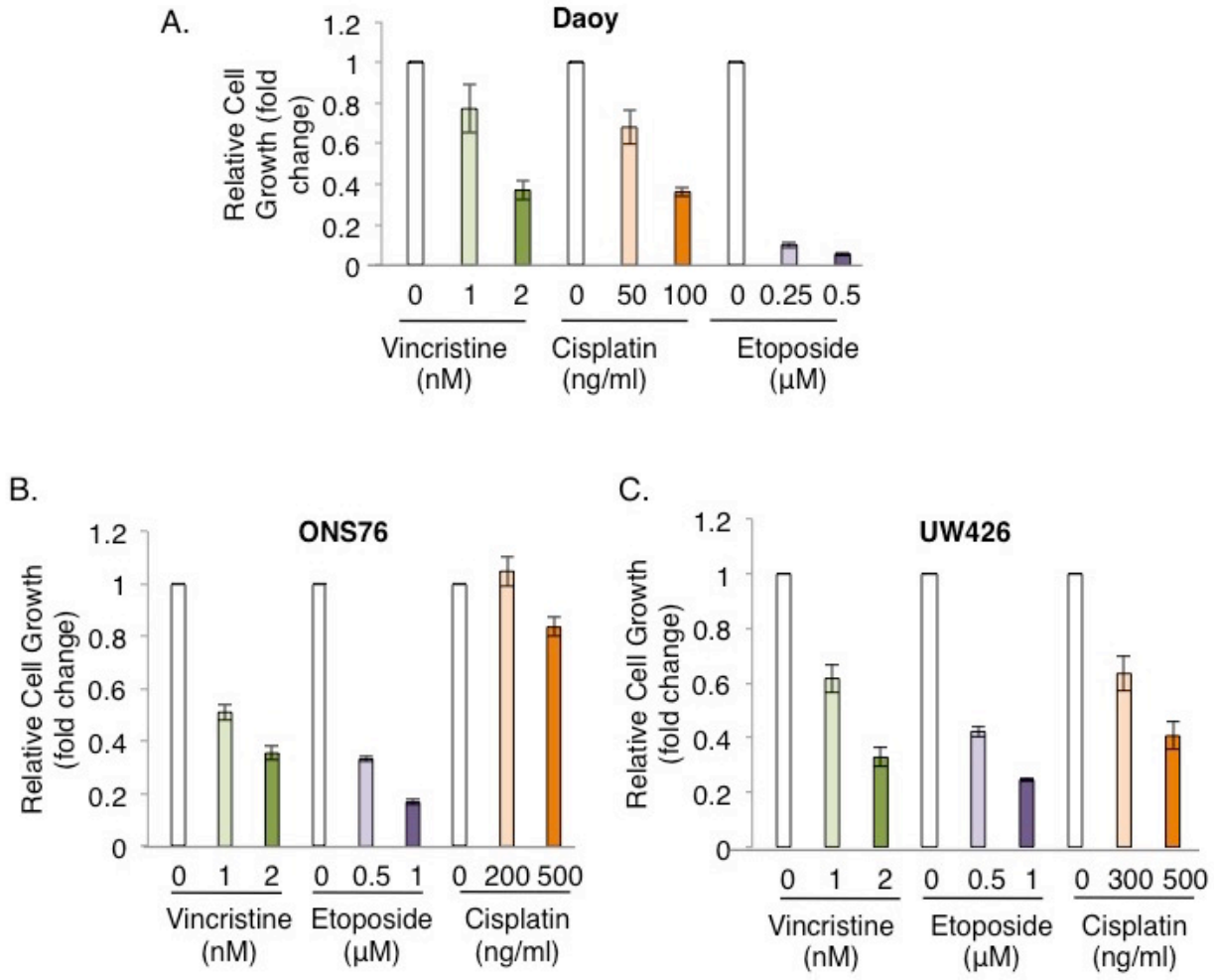

Figure 3.13 Growth effect of different anti-cancer drugs on MB cell lines.

(A) Daoy, **(B)** ONS76, and **(C)** UW426 cells treated with vincristine, cisplatin or etoposide in a 72 hour growth assay with Hoechst staining quantification. Cells were quantified using Hoechst staining and repeated in triplicate experiments.

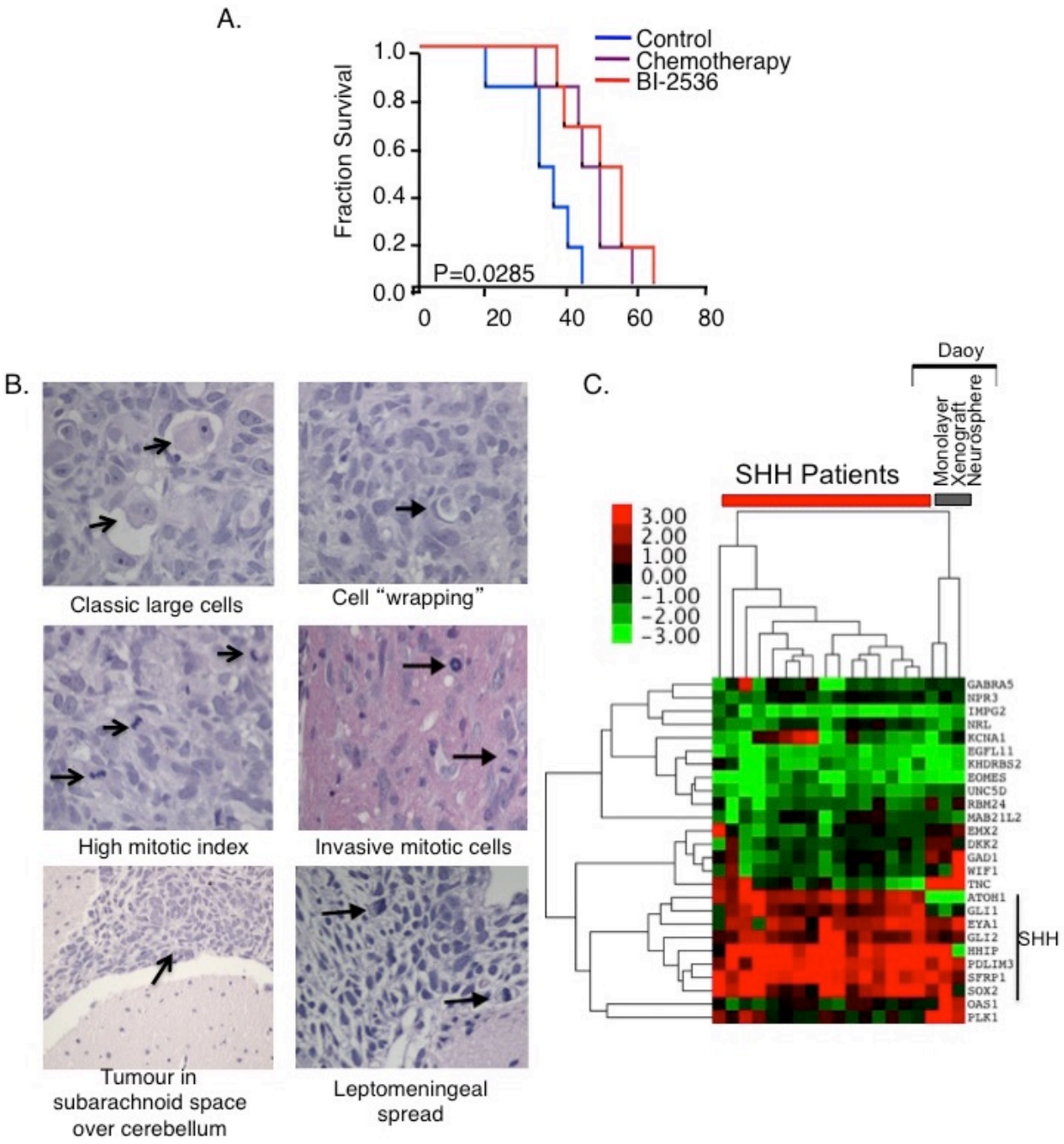

Figure 3.14 PLK1 inhibition delayed disease progression using xenograft model.

(A) Daoy cells were intracranially transplanted into NOD/SCID mice that were then treated with BI-2536 (n=6) or standard-of care chemotherapy (n=6) and compared to controls (n=6). BI-2536 (log rank, P= 0.0142) and chemotherapy (log rank, P=0.0336) treated mice lived longer than controls. No significant difference in survival was observed between BI-2536 and chemotherapy treated mice (log rank, P=0.4205). **(B)** The Daoy xenografts had large cellular morphology, cell wrapping, high mitotic activity, invasion into cerebellum and leptomeningies. **(C)** Daoy xenograft tumors resemble SHH patients from validation cohort in gene expression heatmap (green, low expression; red, high expression).

3.4 Discussion

In the present study we suggest a powerful role for PLK1 as a prognostic marker and anti-cancer drug target. We adopted the use of molecular subtyping to validate current diagnostic stratification methods. Further, we used this NanoString nCounter technology to measure *PLK1* in two independent patient cohorts, which demonstrated significant correlation to patient outcome. As a result, we found that primary patient-derived cells that express high levels of *PLK1* could be reduced in growth and self-renewal with PLK1 inhibitors. These studies provide significant insight into the gene expression pattern of *PLK1* in both primary and cell line models of MB, and demonstrate the efficacy of targeting PLK1 with small molecule inhibitors.

Previously published studies report the MB SHH subtype to have an intermediate prognosis (Kool et al., 2012; Northcott et al., 2011a, 2011b) and Group 3 MB to generally be the most aggressive subtype. While this held true for Group 3 in the cases we examined, it was interesting to note that the outcomes of the SHH subtype presented as high risk instead of intermediate. We suspect this could be attributed to age-associated treatment differences; for example, radiation is generally avoided in younger patients. The age of patients in the SHH subtype has a bimodal distribution of adult and infant cases that are associated with different survival outcomes. Our study only included pediatric MB whereas other reports include mixed cohorts of both pediatric and adult cases (Northcott et al., 2011b).

One of the limitations of our study was the availability of fresh primary MB tissues from different subtypes. Only primary SHH and Group 4 tumors were available to culture in the duration of this study. Nonetheless, PLK1 overexpression was an independent prognostic marker across all MB molecular subtypes in our assessment using FFPE. To this regard, we tested the MED8A cell line, which is reported to be Group 3 MB, and found it to be highly sensitive to BI-2536. It is interesting to note that our standard cell line models Daoy, ONS76, UW228 and UW426 were all associated with the SHH subtype, and this sparks curiosity to whether the nature of SHH MB is more ideally adapted to artificial culture conditions relative to other subtypes. As we continue culturing incoming patient cells we will extend our study to examine a greater variety of MB.

PLK1 is an oncogenic kinase with a central role in mitosis that confers a growth and survival advantage in cancer cells (Elez et al., 2000). Overexpression of PLK1 occurs in cancer

cells but not normal cell counterparts (Holtrich et al., 1994; Tokumitsu et al., 1999) and its inhibition specifically eliminates malignant cells while leaving non-malignant cells unharmed (Ahlfeld et al., 2013; Degenhardt and Lampkin, 2010; X. Liu et al., 2006). These attributes are highly sought after in the search for molecular targets for cancer therapeutics. We demonstrate that reducing the level of PLK1 in cells with siRNA can significantly reduce the proliferation of MB cells and initiate cell death. As well, the chemotherapeutics vincristine, cisplatin and etoposide, also had effects as monotherapies at relatively high concentrations. Although we did not test the *in vitro* effect of combining PLK1 inhibitors with these compounds, other groups report targeting PLK1 may enhance the efficacy of common chemotherapeutics. In breast cancer, siRNA knock down of PLK1 improves the sensitivity of cells towards Herceptin and paclitaxel in a synergistic manner (Spänkuch et al., 2007). Conversely, another *in vitro* study in colon cancer found that inhibiting PLK1 activity in combination with cisplatin only resulted in an additive effect (To et al., 2013). Modern treatment regimes for many forms of cancer now depend on the use of drug cocktails. Further work to establish the most beneficial combination of PLK1 inhibitors with standard-of care chemotherapeutics is necessary for clinical use.

Our present study also tested the PLK1 small molecule inhibitor, BI-2536, which as been evaluated in cancer patients (Frost et al., 2012; Steegmaier et al., 2007). However, there are various other small molecule PLK1 inhibitors that have been evaluated in phase I/II clinical trials including: BI-2536, BI-6727, Rigosertib and GSK461364 (Ma et al., 2012; Medema et al., 2011; Mross et al., 2008; Olmos et al., 2011; Rudolph et al., 2009). At this point, none of these trials have been designed to evaluate whether PLK1 inhibitors may be beneficial for brain tumor treatment. Our group has previously demonstrated that PLK1 inhibitors could be used to target glioblastoma (Lee et al., 2012b; Triscott et al., 2012) and other groups have published data agreeing with our findings in MB (Harris et al., 2012; Spaniol et al., 2011). We propose that PLK1 is a promising drug target for MB because 1) it is highly expressed in patient tumors relative to normal brain tissue and 2) small molecule inhibitors suppress primary MB cells and cell lines *in vitro* and *in vivo*.

In summary, MB patients that have tumors expressing very high levels of *PLK1* are considered to be at elevated risk for relapse and death. Since there are multiple PLK1 inhibitors in clinical trials for adult malignancies, we propose that these drugs may also provide benefit for

selected pediatric patients. Moving forward, it is feasible to predict that treatment of MB will be personalized by identifying *PLK1* high patients using technologies, like NanoString nCounter, that can also accurately assign subgroup affiliation in the rapid timeframe that meets the demands of clinical diagnosis (Northcott et al., 2012d). We also anticipate that PLK1 inhibitors may have fewer detrimental side effects, as it is not expressed at high levels in normal brain tissue. Therefore, incorporating PLK1 inhibition into treatment protocols could greatly improve the efficacy of current chemotherapies that can often cause long-term adverse effects (Dhall et al., 2008). These pre-clinical studies build the necessary foundation to develop PLK1 as a target for high-risk MB.

3.5 Experimental procedures

Medulloblastoma patient cohorts

Primary MBs were obtained from BC Children's Hospital (Vancouver, BC, Canada; discovery) and The Hospital for Sick Children (Toronto, ON, Canada; validation). In the discovery cohort we obtained 75 FFPE tumor blocks from patients diagnosed with MB between 1986 and 2012. Samples included both primary and relapse specimens, however only primary samples were assessed in this study. Medical charts were reviewed and pertinent clinicopathologic data was recorded (R. Rassekh, K. O'Halloran and C. Foster). Patient ages ranged from 3 months to 16.8 years; a review of this cohort is shown in Tables 3.1 and 3.2. Twelve of 75 patients excluded from survival analysis for the purpose of homogeneity of treatment. Three patient samples were retrospectively found not to be MB tumor tissue, and 9 other patients received treatment regimes conflicting with the standard-of-care. Dr. Michael D. Taylor from The Hospital for Sick Children generously provided the validation cohort of 61 MB patient RNA samples (Table 3.3 and 3.4). Four of 61 of these patients excluded from survival analysis for the purpose of homogeneity of treatment. All tumors were subtyped and the data analyzed according to Northcott and colleagues (Northcott et al., 2012d).

NanoString nCounter gene expression profiling

RNA was extracted from three 20μm scrolls of FFPE tissue using Qiagen RNeasy FFPE kit (Valencia, CA, USA). Exactly 250ng of RNA was run for each patient sample and RNA

quality was assessed using Nanodrop spectrometry. A 2100 Bioanalyzer (Agilent Technologies, Mississauga, ON, Canada) was used to spot-check RNA quality in random samples. MB cell lines were grown as tumorspheres, and subsequent mRNA analysis was performed in a similar manner to the FFPE tissues. Analysis using nCounter Gene Expression system was conducted at the Centre for Translational and Applied Genomics (CTAG) (BC Cancer Agency, Vancouver, BC). A custom codeset synthesized by NanoString Technologies (Seattle, WA, USA) was designed which included 22 MB specific subtyping gene probes (Northcott et al., 2012d) plus other genes of interest that specifically included *PLK1* (NM_005030.3). The recommendations outlined by NanoString Technologies were all followed regarding sample preparation, hybridization, detection, scanning, and data normalization.

Gene expression and subtype assignment analysis

NanoString gene expression data was analyzed as previously described (Northcott et al., 2012d; Tibshirani et al., 2002). Cell lines (grown as neurospheres) and xenograft tumor tissue was assigned subgroup classification using the 72 patient cohort as a training set. Cutoffs for *PLK1* expression were assigned based on z score deviation from the mean expression of the cohort. *PLK1* transcript counts below 400 (per 250ng patient RNA) were considered low in expression. Heatmaps were generated using unsupervised hierarchical clustering with average linkage using Cluster version 3.0 and Treeview version 1.60. RNA for qRT-PCR gene expression analysis was isolated using Qiagen RNeasy Mini Kit (Cat. #74106). Transcript expression was determined using qRT-PCR with PLK1 Assay on Demand (Applied Biosystems, cat. #4331182).

Immunofluorescence

Immunofluorescence staining was performed on Daoy cells according to the procedure we previously described (Fotovati et al., 2011). Primary antibodies include: alpha-tubulin (Abcam, ab18251), Pericentrin (Abcam, ab28144), anti-P-H2AX^{S139} (Abcam, ab26350), and PARP (Cell Signaling Technology). Images were taken using an Olympus FV10i confocal microscope on X60 magnification.

Drug library screen

The small-molecule targeted therapeutic agents were synthesized, purity checked and purchased from ChemieTek (Minneapolis, MN, USA). The Daoy cell line was seeded (3,000 cells/well) overnight then treated with 1μM and 10μM for 72 hours. Cells were fixed in 2% paraformaldehyde and stained with Hoechst 33342 (1μg/mL) (Sigma-Aldrich, Oakville, ON, Canada). Analysis was done with the ArrayScan high-content screening system (HCS; Thermo Fisher Scientific, Pittsburgh, PA, USA).

Cell culture and tumorsphere growth

Daoy cells were obtained from the American Tissue Culture Collection (ATCC, Manassas, VA, USA). MED8A cells were supplied from the lab of Dr. Michael D. Taylor (Toronto, ON). Primary brain tumor cells were isolated from BTX001 (SHH), BT006 (SHH), BT007 (SHH), BT008 (PNET), BT014 (Group 4), BT274, and BT025 (Group 4) and were grown as neurospheres as previously described (Lenkiewicz et al., 2009) using Neurocult media (Stem Cell technologies, Vancouver, BC, Canada)(Lee et al., 2012b). All primary cells were obtained through informed consent in abidance with the respective research ethics board guidelines at British Columbia Children's Hospital and The Hospital for Sick Children. A single-cell suspension of Daoy, MED8A, and patient-derived primary MB cells (BTX001, BT274, BT014, and BT025) were plated in tumorsphere assays as previously described (Lee et al., 2012b). Tumorspheres, plated in triplicate >50μm were quantified and photomicrographs were taken after 6 days of culture.

Transfection and western blotting

Small interfering RNA transfections were performed using scramble oligo controls and Lipofectamine RNAiMAX (Invitrogen, Burlington, ON, Canada) as previously described (Hu et al., 2009). Immunoblotting was conducted using anti-PLK1 (Sigma-Aldrich), anti-P-CDC25C^{Ser198}, anti-P-TCTP^{Ser46}, and anti-pan-actin (Cell Signaling Technology, Massachusetts, USA). Band densitometry was measured using ImageJ, v1.46r and normalized to Actin.

Cell cycle analysis

Cell cycle analysis was done following 24 hour siRNA or BI-2536 treatment using flow cytometry as described by Lee and colleagues (2012). Histone H3 phosphorylation was tested as previously described using P-histone $H3^{Ser10}$ (Cell Signaling Technology) (Stratford et al., 2012).

Annexin V staining and quantification of cell proliferation by hoechst staining

Daoy cells were treated with 2.5nM BI-2536 for 48 hours and stained with Annexin V (Promega, Wisconsin, USA) as previously described (Lee et al., 2008). To evaluate the effect of PLK1 inhibition on cell growth, Daoy or human neural stem cells (hNSC; H9, hESC-derived, GIBCO, Burlington, ON, Canada) were plated (3,000 cell/well) in 96-well plates also following previously outlined methods (Hu et al., 2009; Lee et al., 2008).

In vivo evaluation of BI-2536 compared to chemotherapy

Xenografts from Daoy cell line were injected into the right frontal lobe of 10 week old NOD-CB17-SCID mouse brains according to Research Ethics Board-approved protocols (n=18). Mice were injected with biological replicates consisting of 10^6 single-cell suspensions and randomly divided into three treatment groups (n=6) following engraftment of orthotopic tumors: control (0.1N HCl), chemotherapy (vincristine, cisplatin, cyclophosphamide), and treatment (BI-2536). Intraperitoneal injections were performed for delivery of all study group agents. Control group consisted of one weekly injection of 0.1N HCl for four weeks. Chemotherapy group consisted of one weekly injection of vincristine (1.05µg/kg) and cisplatin (2.5mg/kg) on day 1 followed by cyclophosphamide (0.0352mg/kg) on day 2 for three weeks. Treatment group consisted of one weekly injection of BI-2536 (62.5mg/kg, diluted in 0.1N HCl) for 4 weeks. The mice were observed until they displayed obvious signs of neurological deficits and appeared unwell. Tumors were removed at the end of the study, formalin-fixed, paraffin embedded (FFPE), stained with hematoxylin and eosin. The histopathology of the tumors was evaluated by a pediatric neuropathologist (C. Dunham).

Statistical analysis

All quantitative data presented were analyzed as mean value ± SE. Principal component analysis (PCA) was conducted for 2D modeling of dimensionality reduction of the 22 subtyping

genes (Northcott et al., 2012d, 2011b) using Partek Genomics Suite (Partek, St Louis, MO). For the clinical survival analysis and animal studies, log-rank analysis was performed on the Kaplan-Meier curve to determine statistical significance of the results. Multivariate survival analysis was conducted using Cox regression proportional hazards and a 95% confidence interval (CI). All survival analysis and Spearman's Rank correlation test were done using SPSS version 20.0 statistical software (IBM, Chicago, IL, USA). The number of samples used and the respective P-values are listed in the Figure legends. The level of significance for the *in vitro* cell growth/death data was determined by Student's two-tailed T-test and difference in PLK1 expression between subtypes was assessed using a Kruskal-Wallis test (*, P value<0.05; **, P value<0.01).

CHAPTER 4: THE ROLE OF PLK1 KINASE SUBSTRATE TCTP IN MEDULLOBLASTOMA

4.1 Overview

A common strategy of cancer cells is to up-regulate the expression and activity of mitotic kinases that drive proliferation. Polo-Like kinase 1 (PLK1) is one such kinase that is not only overexpressed, but is an indicator of poor outcome for the malignant brain tumor, medulloblastoma (MB). Fortunately, a great deal of promise lies in the therapeutic development of PLK1 specific inhibitors, such as BI-2536 and BI-6727; however, a knowledge gap remains in the explanation of why PLK1-high tumors are especially aggressive. In this study, we sought to characterize the oncogenic role of translationally controlled tumor protein (TCTP), a direct substrate of PLK1 kinase activity. Performing a detailed evaluation of TCTP in MB was especially attractive as transcript expression of TCTP positively correlated with p53 immunopositivity, which is an established indicator of p53 dysregulation in patient tissues. We discovered TCTP expression was enriched in the SHH subtype of MB and displayed a significant correlation with patient overall survival. Inhibition of TCTP using siRNA revealed an anti-proliferative effect in SHH MB cells. Further, siTCTP treatment triggered cell cycle shifts, as detected using flow cytometry, and blocked anchorage-independent colony formation. The preliminary data outlined here allude to a role for TCTP in cell cycle checkpoint activation. Finally, we generated a GFP-tagged system that overexpressed wild-type TCTP along with Ser46 mutants to simulate constitutively active and repressed phosphorylation by PLK1. This model was intended to investigate PLK1-TCTP signaling as a keystone regulator of PLK1-high MB treatment resistance, but unfortunately more extensive studies are required to optimize a fully functional system. By pinpointing critical factors that manipulate the molecular dynamics of poor prognosis MB, like TCTP, there can be a better understanding of the molecular consequences of inhibiting PLK1 for the treatment of cancer.

4.2 Introduction

MB is the most commonly occurring malignant pediatric brain tumor. This embryonic tumor occurs most frequently in young children and is thought to develop from oncogenic hijacking of developmental pathways of the cerebellum (Hallahan et al., 2004; Merve et al., 2014; Natarajan et al., 2013; Pei et al., 2012a). Although aggressive chemotherapy and radiation treatment protocols have significantly increased patient survival, this improvement comes at a price, and patients are frequently left with long-term negative side effects. Clinical trials considering the de-escalation of chemotherapy and radiation have revealed: (1) some patients do not require aggressive therapy, (2) others will not survive without it, and (3) many are resistant to currently available therapeutics regardless of dose or intensity (Grabenbauer et al., 1996; Jakacki et al., 2012). The present challenge is developing robust methods for patient stratification and prognostication that will ensure adequate treatment while preventing unwanted sequelae. As well, identify molecular pathways that can be used to better target the most resilient variations of MB.

MB is comprised of at least four distinct molecular subgroups based on gene expression profiling: WNT, SHH, Group 3, and Group 4. WNT cases are associated with having a good prognosis while Group 3 MB is frequently metastatic and associated with MYC amplification. Group 4 MB is generally considered to have an intermediate prognosis. However, this group remains the least understood. The SHH subgroup has a high frequency of infant cases, which are exceptionally difficult to treat and require radiation-sparing protocols due to negative consequences that radiation has on infant brain development (Northcott et al., 2011b; Taylor et al., 2011). We previously reported that the SHH subtype is associated with inferior survival much like Group 3 patients (Triscott et al., 2013). The aggressive nature of the SHH subtype is also reported by others (Kool et al., 2012).

Preclinical and clinical testing of SMO inhibitors that specifically target the SHH pathway have been less than promising and MB eventually develop drug resistance (Kim et al., 2013; Kool et al., 2014). This raises the question of what underlying factors are promoting tumorigenicity and how can they be targeted? Collaborative work involving patient cohorts from multiple institutions found that *TP53* mutation are enriched in SHH MB and is one of the most important risk factors for this subtype using multivariate analysis (Zhukova et al., 2013). Mutant

p53 can promote tumor development due to dysfunctional cell cycle control and DNA damage response signals, and a failure to induce cell cycle arrest, or apoptosis (Forbes et al., 2011; Vogelstein et al., 2000).

Recently our group and others have discovered that the mitotic kinase, PLK1, is useful as a prognostic marker and is a potential drug target for pediatric MB (Harris et al., 2012; Triscott et al., 2013). PLK1 is an essential serine/threonine kinase that is up-regulated during mitosis and phosphorylates various targets in the execution of mitotic entry, centrosome maturation, spindle assembly, chromosome segregation, and cytokinesis. (Elia et al., 2003b; Haren et al., 2009; Mardin et al., 2011; Petronczki et al., 2008). Similarly, PLK1 is an important factor in the DNA damage response pathway, as its inhibition in normal cells causes a pause in mitotic progression upon detection of single and double strand DNA breaks (Ando et al., 2004; Yata et al., 2012). Presently there are small molecule inhibitors (i.e., BI-2536 and BI-6727) that block PLK1 activity and are being tested in clinical trials for other cancer types (Ellis et al., 2013; Lin et al., 2014). The inhibition of PLK1 in cancer cells results in a G2/M arrest and the induction of cell death, but the overexpression of PLK1 promotes oncogenic transformation (Smith et al., 1997). MB expressing high levels of PLK1 is associated with tumor recurrence and poor overall survival (Triscott et al., 2013); however, the exact mechanism driving treatment resistance in PLK1-high cases is presently unknown.

Translationally controlled tumor protein (TCTP/TPT1) is a highly conserved and multifunctional protein that has been implicated in the regulation of cellular stress, proliferation, DNA damage repair, immune response, development, and tumor reversion (Chen et al., 2007; Cucchi et al., 2010; Gnanasekar et al., 2009; Schroeder et al., 1997; Tuynder et al., 2004; Xu et al., 1999; Yarm, 2002). Overexpression of TCTP protein relative to normal tissues has been reported in leukemia, lymphoma, hepatocellular carcinoma, colon, breast, and prostate cancer (Gnanasekar et al., 2009; Gu et al., 2013; Qiang et al., 2010; Tuynder et al., 2002; Zhu et al., 2008). Localization of TCTP occurs both in the nucleus and the cytoplasm, as well, it is tightly associated with components of the mitotic spindle. TCTP is suggested to function as a molecular chaperone that is capable of binding numerous different signaling proteins to either enhance, or inhibit, their function. We initially became interested in TCTP because (1) PLK1 phosphorylation of $TCTP^{Ser46}$ is a key modification in the metaphase-anaphase transition, and (2)

P-TCTP^{Ser46} is used as marker for PLK1 kinase activity (Cucchi et al., 2010; Yarm, 2002). In addition, TCTP is strongly linked to the obstruction of apoptotic cell death through multiple pathways, for example via interactions with Mcl-1, Bcl-xL, Bax, ATM, and p53 (Amson et al., 2011; Hong and Choi, 2013; Susini et al., 2008; Yang et al., 2005; Zhang et al., 2002). A reciprocal signaling loop with TCTP is suggested to regulate expression of p53. This may be the pivotal switch that dictates whether cells activate proper cell cycle checkpoints in the presence of chemotherapy and radiation, or proceed with improper duplication of error-prone oncogenomes (Amson et al., 2011).

The objective of the present study is to consider why PLK1 is associated with aggressive disease by asking whether its substrate TCTP drives proliferation and drug resistance. Herein we report that TCTP is a marker of MB outcome that strongly associates with the SHH subtype. We examine the association between TCTP and p53 immunopositivity, and question whether targeting TCTP can reduce proliferation and trigger cell cycle checkpoints in MB cell models.

4.3 Results

4.3.1 TCTP is expressed in MB and correlates with survival.

Elevated levels of TCTP expression in cancer is associated with more aggressive disease and is thought to influence treatment resistance (Gu et al., 2013; Kloc et al., 2012; Qiang et al., 2010). Gene expression using mRNA extracted from two independent pediatric MB patient cohorts was measured using the NanoString nCounter system. MB molecular subtype (WNT, SHH, Group 3 or Group 4) was assessed for the validation cohort (Table 4.1), and the subtypes for the discovery cohort have been previously described in chapter 3 (Triscott et al., 2013). High levels of TCTP transcript were detected in patients. Some MB patients overexpressed TCTP mRNA relative to normal cerebellum (37/134), however most patient samples (97/134) had lower levels (Figure 4.1A-B). A cut-off for high and low TCTP expressing cases was determined relative to the transcript expression of normal cerebellum (Figure 4.1A-B). SHH classified tumors had significantly elevated expression of TCTP compared to the other three subtypes in both the discovery (n=73; T-test, P=4.51E-09), and the validation cohorts (n=52; T-test,

P=3.51E-07) (Figure 4.2A-B). Protein expression was not assessed due to lack of specificity of immunohistochemical reagents and limited supply of archived tissue.

High levels of TCTP mRNA expression were associated with worse overall survival using a Kaplan-Meier univariate analysis for the discovery cohort (Figure 4.2C). In a multivariate cox regression analysis TCTP expression (HR, 4.893; 95% CI, 1.186-20.187), and presence of metastasis (HR, 5.305; 95% CI, 1.488-18.907), were determined to be independent factors affecting patient outcome. Although not significant in univariate analysis (see Chapter 3), treatment with radiation had a positive impact on survival in multivariate analysis (HR, 0.246; 95% CI, 0.066-0.913) (Table 4.2).

Immunopositive staining for p53 in patient tumor sections is an indication of p53 dysregulation and a marker of MB poor outcome (Tabori et al., 2010). Pediatric MB FFPE samples from the discovery cohort were assessed for p53 staining and quantified for signal intensity (Figure 4.3A). High p53 immunopositivity was significantly correlated with high levels of TCTP transcript expression, which was measured by NanoString (Figure 4.3B). In addition, high levels of PLK1 transcript expression were also associated with p53 immunopositivity (Figure 4.3C). Finally, cases that were ranked high in both PLK1 and TCTP expression did worse than cases only high in TCTP. PLK-low cases that were also low in TCTP demonstrated ~85% survival rate (Figure 4.3D). Together these findings allude to a PLK-TCTP-p53 relationship that might potentially be responsible for driving tumorigenicity.

Previously we have shown PLK1 to be an important prognostic marker in pediatric MB and TCTP is a direct substrate of PLK1 (Triscott et al., 2013; Yarm, 2002). Transcript expression of TCTP failed to correlate with PLK1 expression in both the discovery and validation cohorts using NanoString nCounter analysis (Figure 4.4). Both PLK1 and TCTP are significantly expressed in poor outcome MB, however the lack of transcript correlation emphasizes the post-translational relationship of these factors.

Sample Labels	Predicted Class	WNT	SHH	Group 3	Group 4
800A	Group4	1.19E-08	1.57E-04	3.58E-02	9.64E-01
801A	Group3	1.46E-09	3.35E-09	9.83E-01	1.72E-02
802A	Group3	2.65E-08	4.25E-09	9.98E-01	1.66E-03
803A	Group3	7.92E-08	2.35E-06	1.00E+00	1.99E-04
804A	Group4	1.59E-12	4.51E-08	2.01E-02	9.80E-01
805A	Group3	6.69E-10	6.72E-08	9.97E-01	2.87E-03
806A	Group4	1.02E-09	4.63E-06	1.77E-03	9.98E-01
807A	Group3	1.33E-07	9.87E-06	1.00E+00	1.82E-04
809A	Group4	3.08E-11	7.20E-08	2.05E-03	9.98E-01
810A	SHH	2.55E-03	9.97E-01	8.30E-07	6.34E-05
811A	SHH	8.49E-02	9.12E-01	2.27E-04	2.93E-03
812A	Group3	8.59E-08	1.81E-06	5.77E-01	4.23E-01
813A	SHH	1.48E-11	1.00E+00	1.13E-10	2.19E-10
814A	Group3	9.54E-07	5.39E-07	9.90E-01	1.02E-02
815A	Group4	4.67E-08	1.31E-05	5.26E-04	9.99E-01
817A	SHH	2.24E-12	1.00E+00	1.01E-09	1.37E-08
818A	Group4	1.83E-09	9.70E-07	8.19E-04	9.99E-01
819A	Group4	3.49E-05	3.37E-04	6.43E-02	9.35E-01
820A	Group3	6.89E-08	1.71E-08	9.00E-01	1.00E-01
821A	Group3	6.41E-03	7.77E-03	6.62E-01	3.24E-01
822A	Group4	3.09E-10	3.37E-06	2.50E-02	9.75E-01
823A	SHH	1.97E-10	1.00E+00	2.12E-10	1.98E-09
824A	Group4	2.07E-08	2.98E-08	5.98E-02	9.40E-01
825A	Group3	8.00E-09	1.03E-08	9.97E-01	2.78E-03
826A	SHH	4.34E-09	1.00E+00	5.35E-09	2.60E-07
827A	Group3	2.36E-10	1.70E-09	9.99E-01	1.14E-03
829A	WNT	1.00E+00	6.02E-05	4.87E-05	6.58E-05
830A	Group4	1.23E-09	2.17E-08	1.73E-02	9.83E-01
831A	Group3	4.24E-09	3.16E-08	8.19E-01	1.81E-01
832A	Group3	1.74E-10	5.02E-09	6.42E-01	3.58E-01
833A	Group3	2.00E-08	4.08E-08	1.00E+00	4.14E-05
834A	Group3	4.05E-08	1.90E-09	9.97E-01	2.79E-03
835A	Group4	9.24E-10	2.02E-08	9.28E-04	9.99E-01
836A	Group4	2.45E-12	1.81E-08	1.19E-04	1.00E+00
837A	SHH	2.49E-05	1.00E+00	1.33E-04	2.50E-04
838A	Group4	4.10E-09	1.40E-05	4.37E-04	1.00E+00
839A	Group4	3.86E-08	1.16E-06	2.62E-03	9.97E-01
840A	Group3	1.25E-05	7.40E-06	9.50E-01	5.01E-02
841A	SHH	1.27E-09	1.00E+00	2.22E-07	2.79E-07
842A	SHH	2.59E-03	9.97E-01	2.29E-04	2.04E-04
843A	WNT	1.00E+00	8.53E-06	1.06E-07	1.19E-07
844A	Group4	2.14E-08	5.59E-06	9.71E-03	9.90E-01
845A	WNT	1.00E+00	1.50E-07	3.82E-07	6.27E-08
846A	Group4	8.38E-10	2.86E-07	1.34E-03	9.99E-01
847A	SHH	1.50E-10	1.00E+00	3.06E-08	6.73E-08
848A	WNT	1.00E+00	5.19E-08	4.54E-04	2.44E-05
849A	SHH	1.28E-06	1.00E+00	5.68E-05	4.30E-04
850A	WNT	1.00E+00	5.23E-07	3.21E-04	9.31E-06
851A	Group3	1.54E-07	2.77E-05	1.00E+00	2.54E-04
852A	Group3	4.47E-09	1.05E-08	9.97E-01	2.82E-03
853A	SHH	3.13E-03	9.96E-01	8.33E-04	5.19E-04
BT034	SHH	5.83E-10	1.00E+00	2.04E-08	1.78E-07

Table 4.1 PAM class prediction validation for MB subgroup assignment of the CHEO validation cohort.

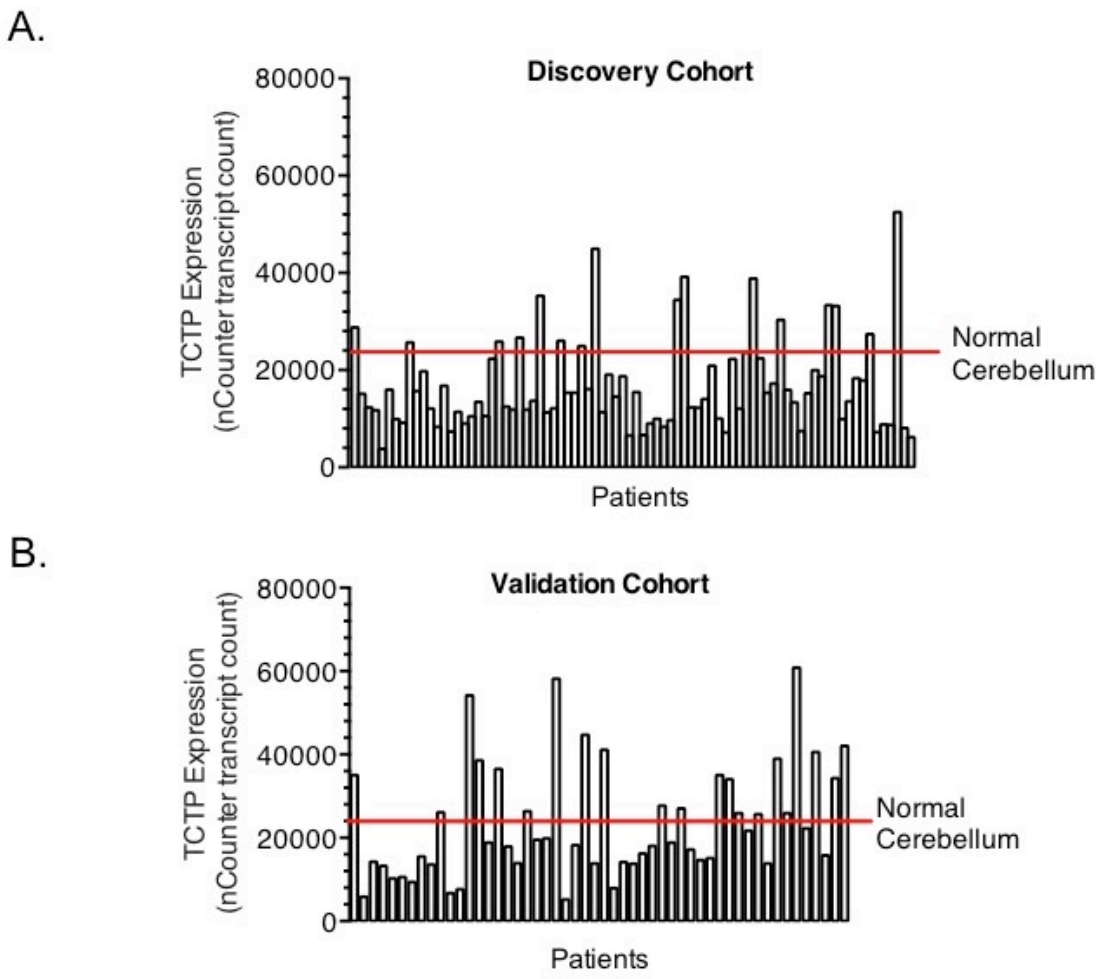

Figure 4.1 Distribution of *TCTP* transcript expression in discovery and validation cohorts.

NanoString nCounter analysis of patient samples (bars) shows *TCTP* mRNA is expressed in MB relative to normal cerebellum (red line) in **(A)** the discovery cohort (n=82), and **(B)** the validation cohort (n=52).

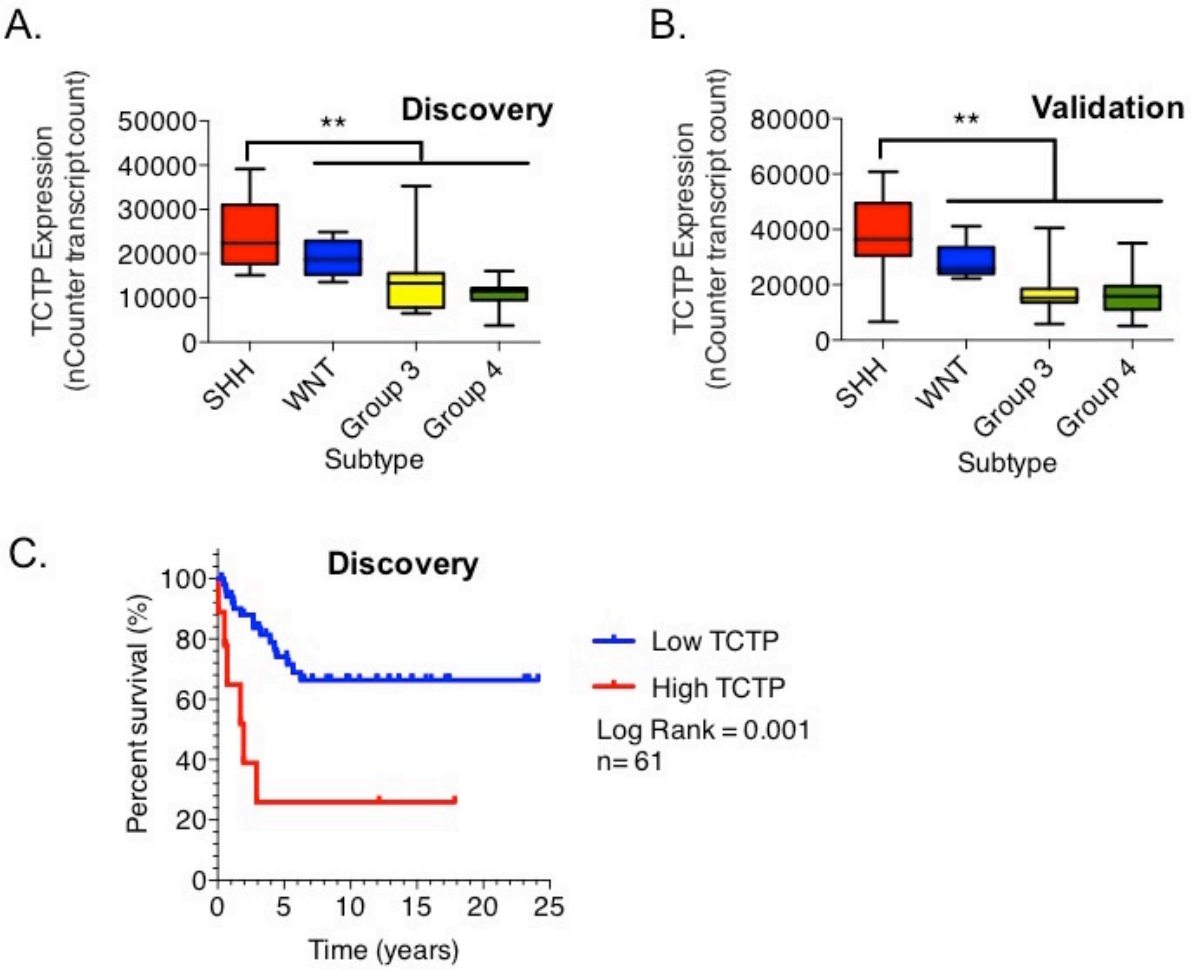

Figure 4.2 *TCTP* transcript expression associates with SHH MB and overall survival.

(A) *TCTP* expression is elevated in SHH MB in both the discovery cohort (n= 73; T-test, P=4.51E-09) and **(B)** validation cohort (n= 52; T-test, P=3.51E-07). **(C)** High *TCTP* mRNA expression predicts probability of poor overall survival (n=61, P=0.001).

Variable	No. (n=55)	Hazard ratio (95% confidence interval)	Cox regression analysis (p value)
Age			
< 3 years	11	1.040 (0.252 to 4.292)	0.957(n.s)
≥ 3 years	44		
Sex			
Male	33	0.659 (0.236 to 1.840)	0.426 (n.s)
Female	22		
Metastasis			
Present	25	5.305 (1.488 to 18.907)	**0.010**
Not Present	30		
Extent of Resection			
Gross Total Resection	44	1.474 (0.366 to 5.940)	0.585 (n.s)
Subtotal Resection or less	11		
Radiation			
Yes	41	0.246 (0.066 to 0.913)	**0.036**
No	14		
Chemotherapy			
Yes	51	0.289 (0.270 to 3.109)	0.306 (n.s)
No	4		
SHH Subtype			
SHH	14	3.365 (0.964 to 11.742)	0.057 (n.s)
Non SHH	41		
TCTP Transcript			
High	7	4.893 (1.1.86 to 20.187)	**0.028**
Low	47		

(n.s)= not significant

* Univariate assessment of clinical variables reported in Table 3.1 and 3.5

Table 4.2 Multivariate analyses of *TCTP* in relation to clinical, pathological and biological endpoints of the discovery cohort.

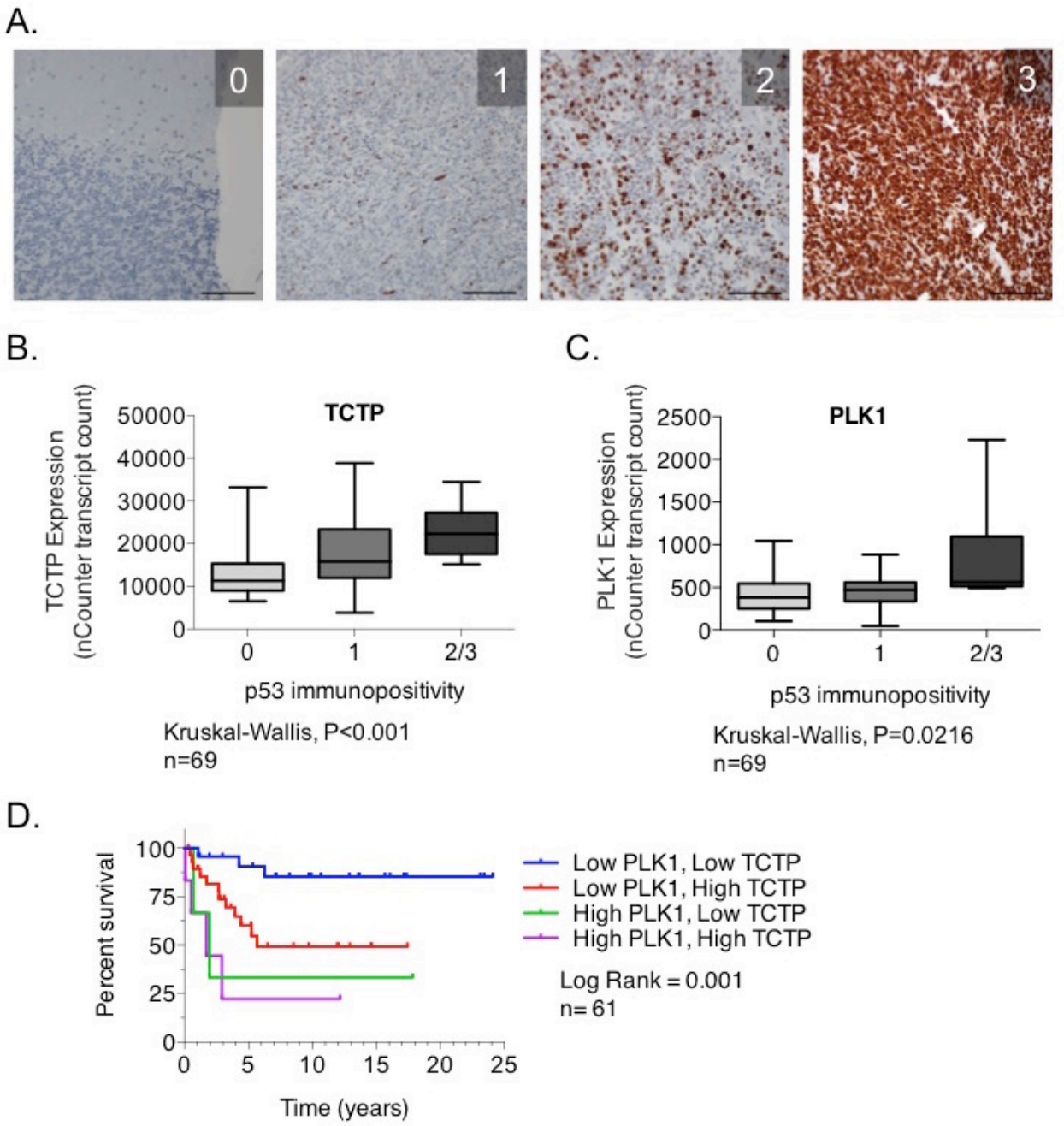

Figure 4.3 *TCTP* and *PLK1* expression correlate with p53 immunopositivity

(A) Protein expression of p53 was measured in discovery patient cohort through construction and staining of a tissue microarray. Immunopositivity was assessed on a scale using 0, 1, 2, and 3 at 20X magnification. **(B)** *TCTP* expression was associated with samples with high p53 IHC intensity (n=69; Kruskal-Wallis, P<0.001). **(C)** *PLK1* mRNA expressing MB was also elevated in p53 immunopositive MB (n=69; Kruskal-Wallis, P=0.0216). **(D)** Elevation of *PLK1* and *TCTP* predicts poor overall survival compared to cases elevated in one or neither transcripts (n=61, Log Rank, P=0.001).

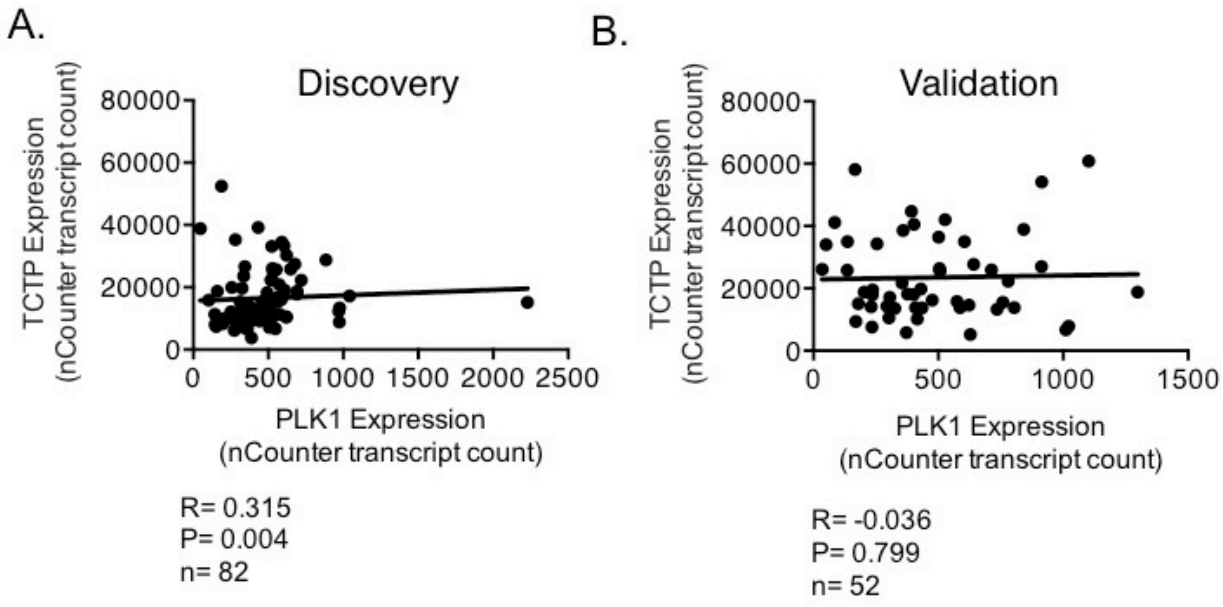

Figure 4.4 *TCTP* transcript correlation to *PLK1* in discovery and validation cohorts.

NanoString nCounter measurement of patient mRNA shows *TCTP* does not correlate with *PLK1* transcript expression in patient samples of the **(A)** discovery cohort (n=82, R=0.315), or **(B)** validation cohort (n=52, R=-0.036).

4.3.2 TCTP supports the growth and survival of SHH tumor cells.

Given that TCTP was associated with the SHH patient subtype and it correlated with more aggressive disease in survival analyses we asked the following questions. First, is TCTP a driver of tumor cell growth in SHH MB? Secondly, does it relate to poor outcomes in patients because it causes drug resistance? TCTP targeted siRNA was optimized to reduce transcript expression >95% (Figure 4.5A). As expected, silencing TCTP reduced both total and P-TCTP^{Ser46} following 48 hour treatment (Figure 4.5B, D). Loss of TCTP had no effect on PLK1 levels (Figure 4.5C-D). Interestingly, TCTP inhibition induced apoptosis in Daoy and ONS76 cells (Figure 4.5E-F). Inhibiting TCTP for 72 hours reduced the proliferation of Daoy SHH cells by 65.3% (T-test, P=2.03E-08) (Figure 4.6A). Similarly, ONS76 cell proliferation was inhibited by 61.7% (T-test, P=1.09E-06) with 96 hour siTCTP knockdown (Figure 4.6B). ONS76 cells are molecularly characterized as being of the SHH subtype as well (Triscott et al., 2013). Targeting TCTP in Daoy and ONS76 cells significantly inhibited SHH MB cell growth.

More importantly, siTCTP knockdown inhibited Daoy soft agar colony formation by greater than 80% (T-test, P=8.87E-39) (Figure 4.6C). TCTP expression is necessary for Daoy anchorage-independent growth. Unlike the Daoy cell line, ONS76 cells do not form colonies in soft agar assays. Therefore, we could not use this functional assay to assess the role of TCTP.

Independent of its relationship with PLK1, TCTP has been characterized in the regulation of DNA damage and cell survival pathways (Amson et al., 2011; Rho et al., 2011; Susini et al., 2008). Interestingly, siTCTP knockdown in Daoy cells resulted in a G2/M shift in the cell cycle using propidium iodide (PI) based flow cytometry (Figure 4.7A). This was further confirmed using fluorescent microscopy. Compared to control cells, there was a higher proportion of siTCTP treated Daoy cells frozen in metaphase (Figure 4.7B). Daoy cells have mutant p53. We also addressed the influence TCTP has on cell cycle when p53 is not mutated using ONS76 cells. In contrast, siTCTP knockdown caused a G1/S shift in the cell cycle of ONS76 at 48 and 72 hours (Figure 4.8A). Interestingly, fluorescent microscopy of ONS76 cells showed significant morphological changes as a result of TCTP inhibition. Cells lacking TCTP appeared extended with prolonged cytoskeletal appendages, and this was consistent independent of cell density (Figure 4.8B). These findings suggest inhibition of TCTP may affect the ability of ONS76 cells to undergo cell division by interfering with the G1/S checkpoint. As described above, p53 is

frequently mutated in SHH cells. Further, we show that blocking TCTP prevents Daoy cells from moving through G2/M. But how does it do this?

Daoy cells are reported to have mutant p53, and p53 dysregulation results in high protein detection (Tabori et al., 2010; Xu et al., 2015). Knockdown of TCTP in Daoy cells causes no change in p53 levels (Figure 4.9A). Conversely, ONS76 cells have wild-type p53 (Xu et al., 2015), which may contribute to its inability to form colonies in soft agar. Wild-type p53 has a short half-life and is normally undetectable by immunoblot in ONS76. Interestingly, 72-hour inhibition of TCTP caused a slight increase of detectable p53 in ONS76 cells (Figure 4.9B). These data suggest TCTP may have multiple cellular functions that affect cell cycle progression in a p53 dependent manner.

This prompted us to question whether the inhibition of TCTP could influence the efficacy of standard chemotherapy drugs against SHH MB. A 72 hour treatment of siTCTP Daoy cells with vincristine showed a significant additive effect with 37.8% (T-test, P=0.04) less growth in combination treated cells when compared to vincristine alone. As well, the combination of siTCTP with vincristine also reduced growth by 37.0% (T-test, P= 0.02) compared to siTCTP alone (Figure 4.10A). In contrast, ONS76 cells were also tested with the combination of siTCTP and vincristine and no additive cytotoxic effects were observed (Figure 4.10B). The sensitization to chemotherapy was restricted to vincristine on Daoy cells because siTCTP did not further enhance the response to etoposide either (data not shown).

Next, we tried temozolomide (TMZ), which is given as a second-line therapy when patients fail to respond to chemotherapies such as vincristine and etoposide. Daoy cells were resistant to TMZ at 5 and 10μM concentrations, but siTCTP significantly reduced their growth. There was no additional cytotoxicity from the combination with TMZ (Figure 4.10C). Thus, TCTP inhibitors could be used as a second-line therapy in place of TMZ.

From the studies described above, we concluded that TCTP is essential for controlling the growth of SHH MB cells. In this case, the entire protein was inhibited. However, we wondered if the well described post-translational modification of TCTP was specifically involved in carrying out the growth-promoting role of TCTP. Specifically, TCTP is phosphorylated at Ser46 by PLK1. $TCTP^{Ser46}$ is exclusively phosphorylated by PLK1 at the metaphase-anaphase transition of mitosis and is used as a functional marker of PLK1 kinase activity (Cucchi et al., 2010; Jaglarz et

al., 2012; Yarm, 2002). Therefore, we investigated TCTP phosphorylation further to address the role of phosphorylated TCTP^{Ser46} (P-TCTP^{Ser46}) on tumor cell growth.

Previously, Daoy, ONS76 and UW228 cells were shown to express high levels of PLK1 transcript (Triscott et al., 2013). In the present study, high PLK1 protein expression correlates with the detection of P-TCTP^{Ser46} for Daoy, ONS76, and UW228. BT027, which has low PLK1 transcript expression by NanoString and protein by immunoblotting, has no detectable P-TCTP^{Ser46} suggesting the PLK1-TCTP pathway is active in PLK1-high cells but not low (Figure 4.11A). Next, we went on to demonstrate the interdependency between PLK1 and TCTP phosphorylation. Inhibition of PLK1 expression with siRNA causes the downregulation of P-TCTP^{Ser46} in the Daoy MB cell line (Figure 4.11B). PLK1 high Daoy, ONS76, and UW228 cells undergo decreased growth proliferation and cell death when treated with PLK1 inhibitor BI-2536 (Triscott et al., 2013). Similarly, Daoy cells are extremely sensitive to BI-6727, which is the newer generation PLK1 kinase inhibitor. Treatment with 5nM BI-6727 for 72 hours significantly prevents MB cell growth and induces apoptosis (Figure 4.11C-D). Targeting the expression of TCTP has an impact on the growth of PLK1-high MB cell lines, but more work is required to establish the mechanism that drives the PLK1-TCTP pathway.

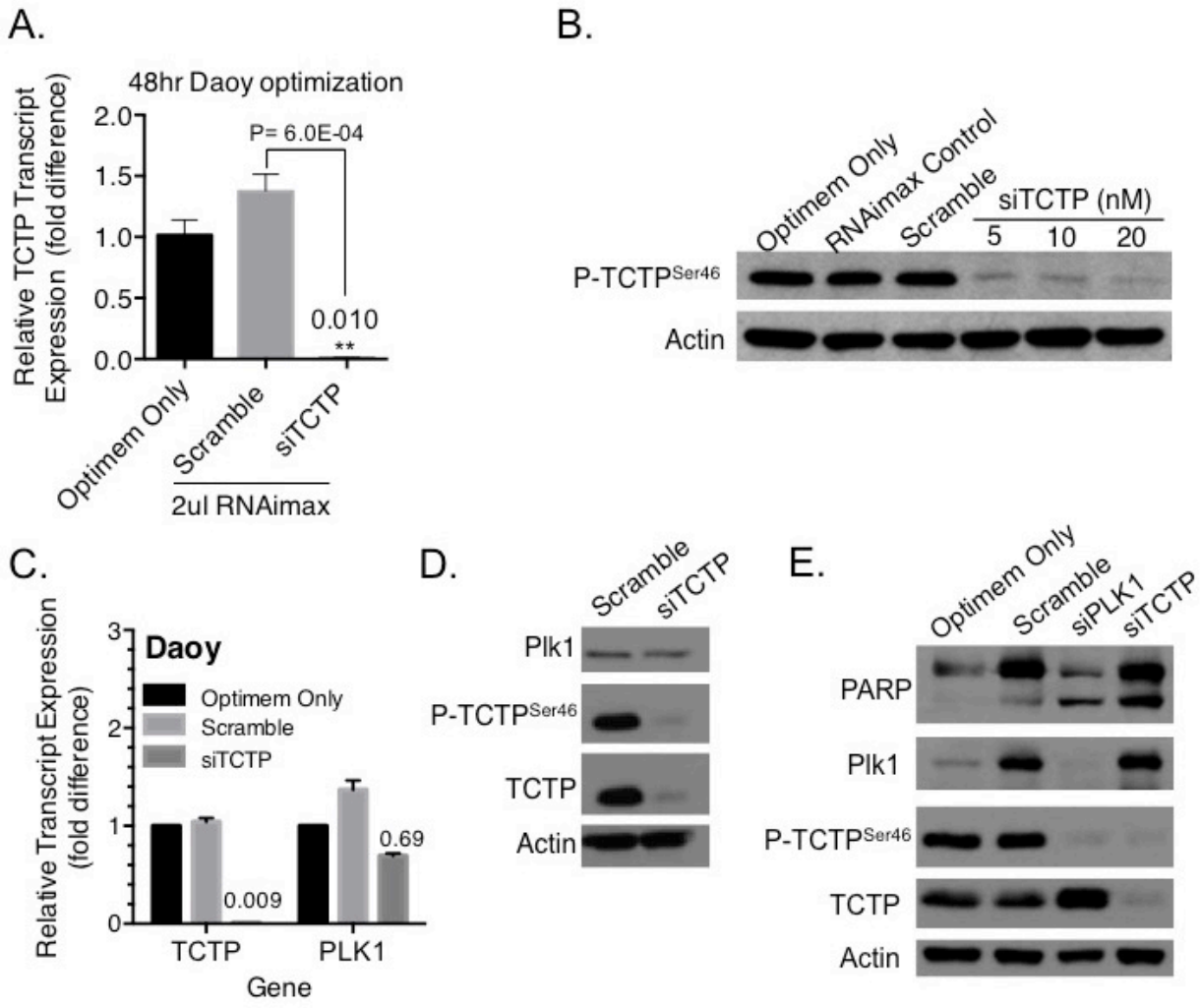

Dead cells:

Cells Alone	Scramble	siTCTP
1%	1%	16.8%

Figure 4.5 Small interfering RNA knockdown of TCTP reduces TCTP, and P-TCTP^{Ser46}, and induces death in MB cell lines.

TCTP siRNA knockdown was optimized following 48 hour treatment of Daoy cells. **(A)** qRT-PCR confirms downregulation of *TCTP* mRNA relative to scramble control (**, P<0.001), and **(B)** immunoblotting demonstrates knockdown conditions also reduce P-TCTP^{Ser46} protein expression. **(C)** Relative expression of PLK1 transcript in Daoy cells treated with siTCTP for 48 hours measured by qRT-PCR. As well, **(D)** immunoblotting shows PLK1 protein expression following 72 hour TCTP knockdown in Daoy cells. Cell death is demonstrated following 72 hour siTCTP treatment in **(E)** Daoy cells by immunoblot detection of PARP cleavage, and **(F)** flow cytometry in ONS76 cells. Relative mRNA expression was assessed using PPIA as an endogenous control.

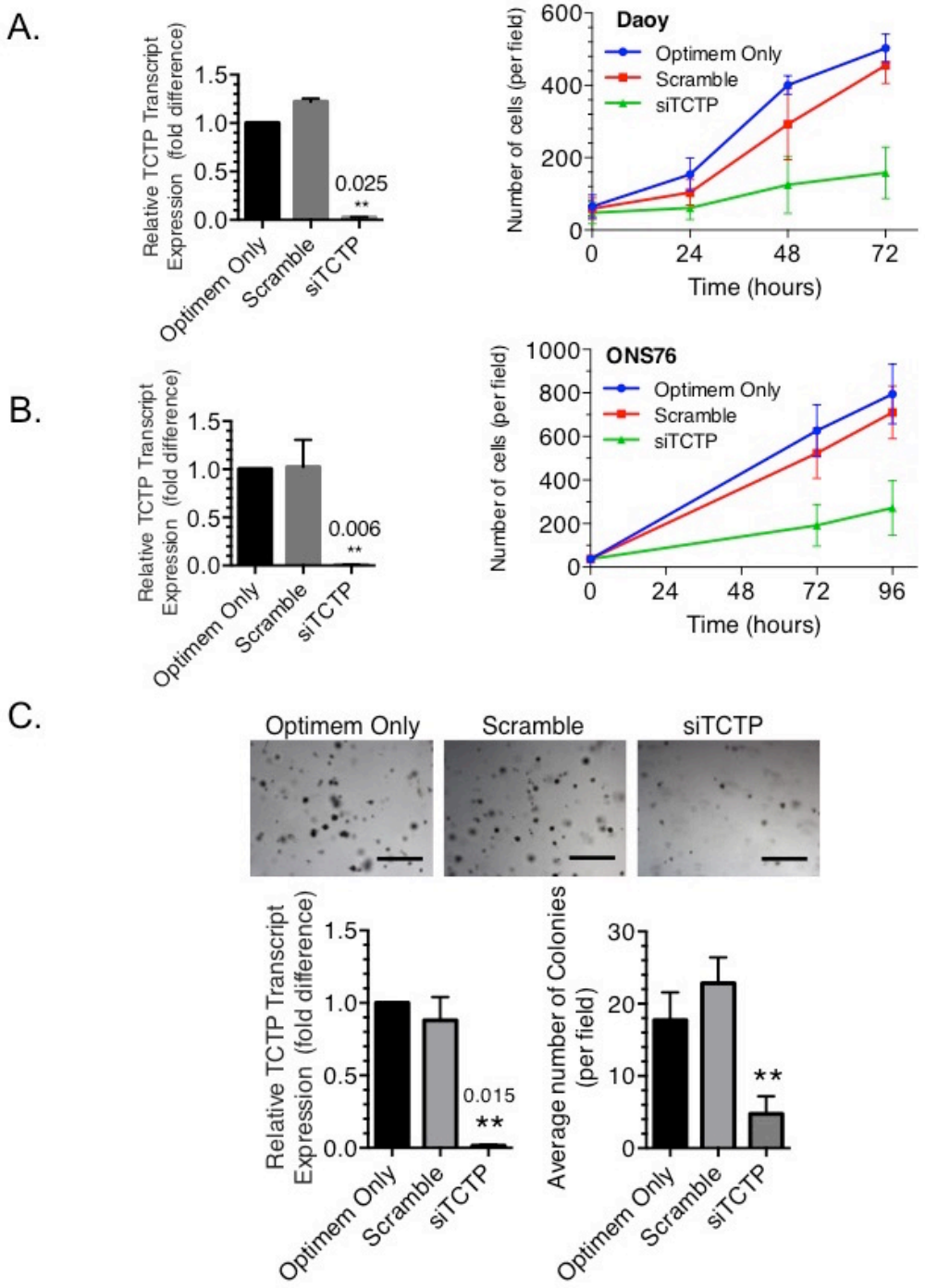

Figure 4.6 Daoy and ONS76 cell lines are sensitive to TCTP inhibition.

Cell proliferation was assessed using Hoechst staining following 10nM siTCTP treatment for **(A)** 24, 48, and 72 hours in Daoy, and **(B)** 72 and 96 hour treatment of ONS76 cells. **(C)** Daoy cells were treated with siTCTP for 48 hours in monolayer culture then plated into a 21-day soft agar colony formation assay testing anchorage independent growth. *TCTP* knockdown was assessed by qRT-PCR following 48 hour knockdown. (A-C) Data is representative of three independent experiments, scale bar= 400μm (**, P<0.001).

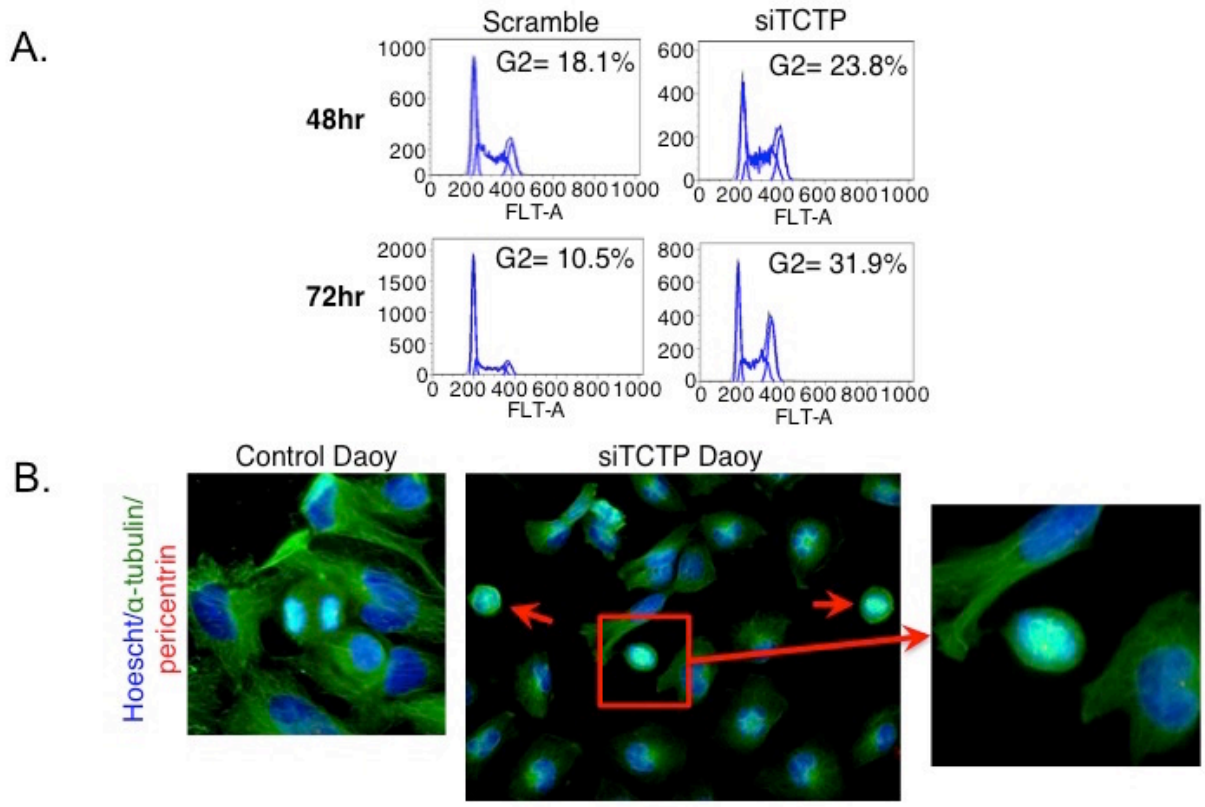

Figure 4.7 TCTP knockdown in Daoy cells causes G2/M arrest.

(A) Daoy cells treated with 10nM siTCTP for 48 and 72 hours were subjected to flow cytometry with propidium iodide for analysis of cell cycle profile. **(B)** Fluorescent microscopy of Daoy cells treated with siTCTP for 72 hours and stained for alpha-tubulin (green), pericentrin (red) and Hoechst nuclear staining (blue).

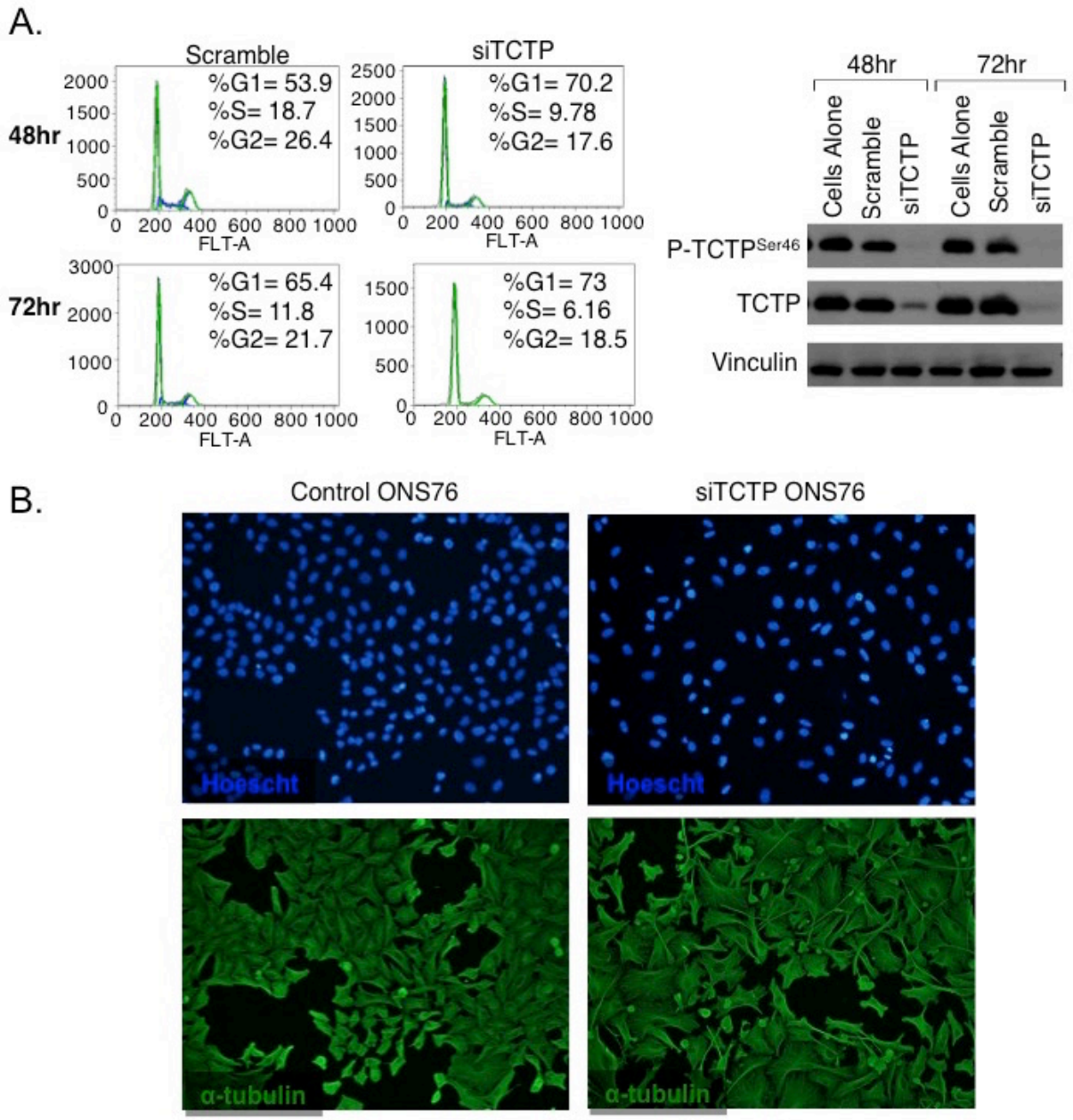

Figure 4.8 TCTP knockdown in ONS76 cells causes G1/S cell cycle shift and morphological changes.
(A) ONS76 cells treated with 10nM siTCTP for 48 and 72 hours were subjected to flow cytometry with propidium iodide for analysis of cell cycle profile. Immunoblotting confirmed knockdown of TCTP and P-TCTP^{S46} protein expression. Data is representative of three independent experiments. **(B)** Fluorescent microscopy of ONS76 cells treated with siTCTP for 96 hours and stained for alpha-tubulin (green), and Hoechst nuclear staining (blue).

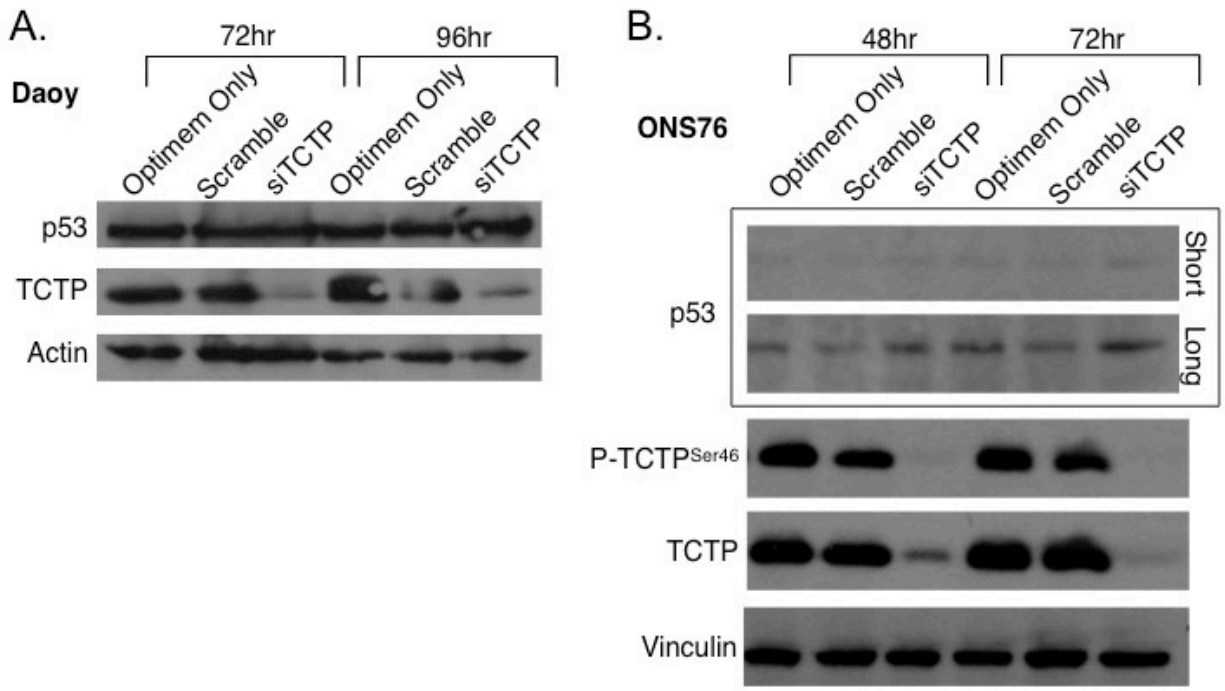

Figure 4.9 p53 expression following TCTP knockdown.

p53 protein was detected using immunoblotting following **(A)** 72 and 96 hour siTCTP knockdown in Daoy cells, and **(B)** 48 and 72 hour siTCTP treatment of ONS76 cells. Actin and vinculin were used for loading controls.

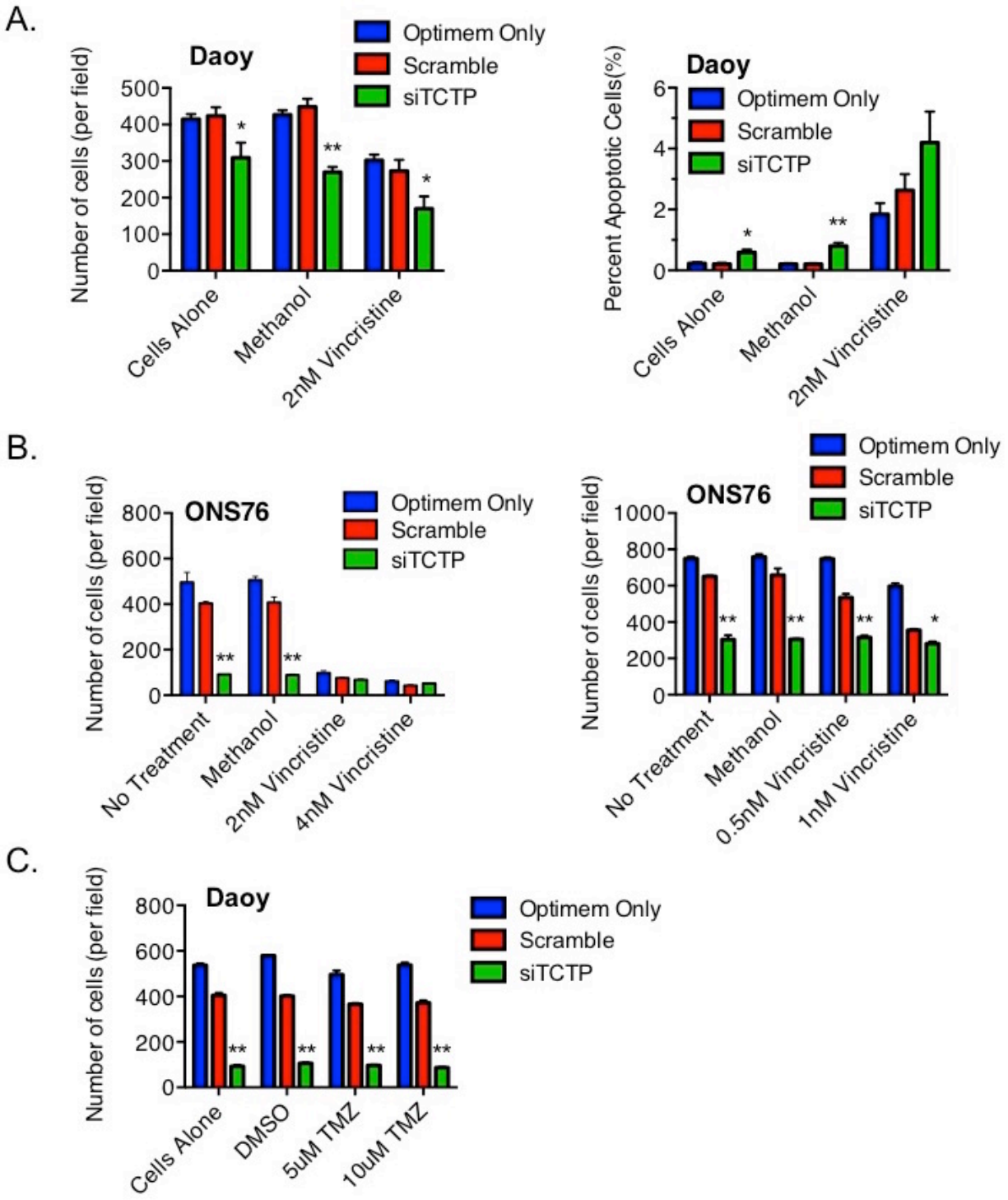

Figure 4.10 Proliferation assays testing the combination of siTCTP treated MB cells with chemotherapy. **(A)** TCTP was inhibited for 24 hours in Daoy cells and then treated for another 72 hours with 2nM vincristine. **(B)** ONS76 cells were treated with siTCTP for 24 hours then tested for growth in the presence of 0.5, 1, 2, and 4nM vincristine for another 72 hours. **(C)** TCTP was inhibited for 24 hours in Daoy cells and then treated for 72 hours

with 5 and 10μM TMZ. The data from (B) and (C) are representative of single experiments, while (A) is the cumulative data of two independent experiments. Growth and percent apoptosis was assessed using Hoechst staining and TCTP knockdown was confirmed with qRT-PCR or immunoblotting (*, P<0.05; **, P<0.001).

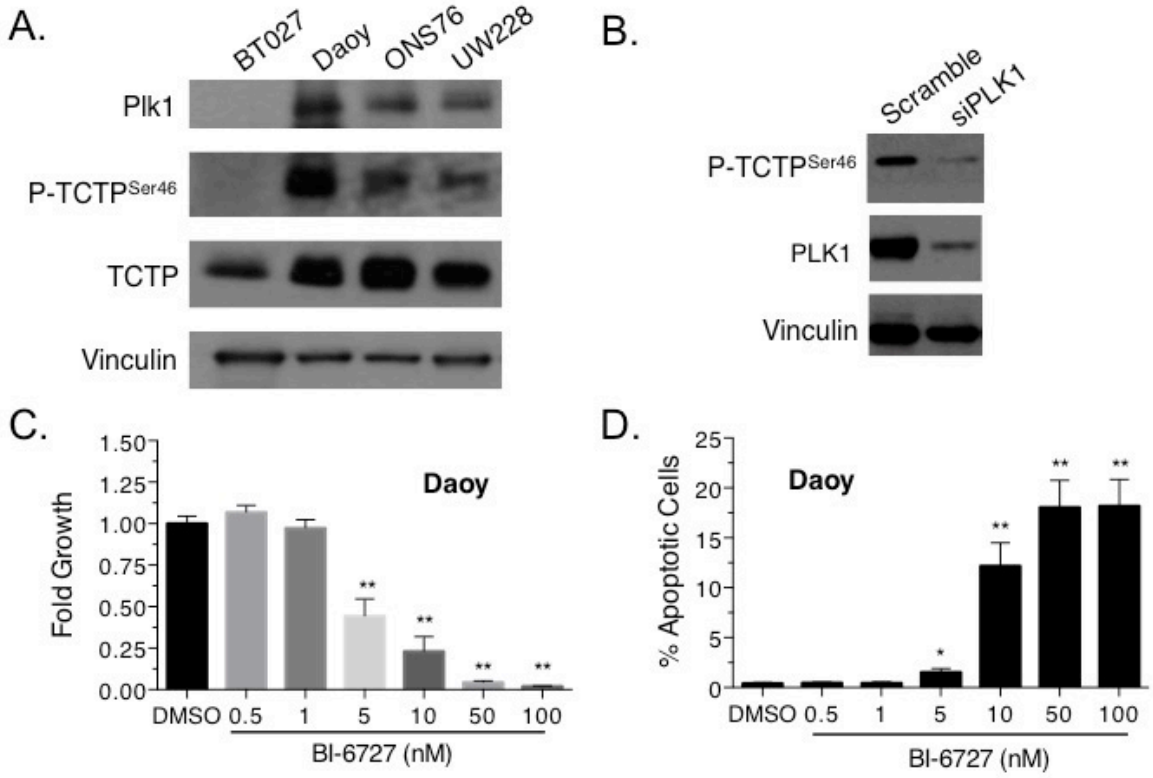

Figure 4.11 MB cells expressing high levels of PLK1 and P-TCTP^{Ser46} are sensitive to BI-6727.

(A) Protein expression of PLK1, P-TCTP^{ser46}, TCTP and vinculin loading control in a panel of MB cell lines. Daoy, ONS76, UW228 are PLK1-high SHH cells, and BT027 is derived from a PLK1-low Group 4 patient. **(B)** Daoy cells were treated with 5nM PLK1 siRNA for 24 hours. PLK1 knockdown and level of P-TCTP^{Ser46} was measured by immunoblotting. **(C-D)** Daoy cells were treated with 0.5-100nM BI-6727 for 72 hours then growth and apoptosis was assessed by Hoechst staining. Data is representative of three independent experiments (*, P<0.05; **, P<0.001).

4.3.3 Ectopic overexpression of mutant GFP-TCTPSer46 alone is not sufficient to modulate Daoy proliferation, or sensitivity to BI-6727 and vincristine.

Yarm and colleagues (2002) report that overexpression of wild-type and mutant TCTP in cancer cells causes mitotic defects and cell death that is similar to the effect of inhibiting PLK1. We assessed the importance of $TCTP^{Ser46}$ phosphorylation by PLK1 and asked whether modification of this residue can rescue drug-induced cell death. Site-directed mutagenesis of a GFP-tagged TCTP construct produced a serine to alanine phospho-null mutant (GFP-TCTPS46A), and a serine to aspartic acid phospho-mimic mutant (GFP-TCTPS46D) (Figure 4.12A). DNA sequencing of TCTP confirmed the correct base-pair modification for GFP-TCTPwt, GFP-TCTPS46A, and GFP-TCTPS46D (data not shown). Transient transfection of TCTP constructs - along with a control empty vector construct (GFP-EV) - was performed in the Daoy cells. GFP detection was used to confirm expression of the mutants and fluorescently activated cell sorting (FACS) was used to select for cell populations expressing the TCTP constructs (Figure 4.12B-C). siTCTP treatment of cells significantly down-regulated GFP signal in GFP-TCTPwt, GFP-TCTPS46A, and GFP-TCTPS46D cells while not affecting GFP-EV intensity in either the cytoplasm or the nucleus. This shows that GFP intensity is correlated to ectopic TCTP expression, as well, demonstrates the GFP-tagged constructs are not restricted in localization and capable of entering the nucleus, as would endogenous TCTP (Figure 4.12D). Further, immunoblotting showed GFP-TCTPwt can be phosphorylated at Ser46, and the band associated with the construct disappears with siTCTP treatment (Figure 4.13A). The addition of the constructs did not affect endogenous levels of TCTP or PLK1 (Figure 4.13A-B).

The established TCTP overexpression models were tested in functional assays. Compared to control Daoy cells, there was no effect on proliferation over 72 hours (Figure 4.14A). Overexpression of wild-type TCTP in Daoy cells also did not rescue the anti-proliferative effect of BI-6727 treatment. As well, expression of the phospho-null (S46A) or phospho-mimic (S46D) constructs also failed to modulate the response to BI-6727 (Figure 4.14B). This was also true for 72 hour BI-2536 treatment of construct expressing cells that all showed similar levels of apoptosis compared to control cells, as demonstrated by PARP cleavage (Figure 4.14C).

Knocking down TCTP in Daoy cells had an additive effect to vincristine cytotoxicity (Figure 4.10); therefore, we tested if Daoy cell death could be rescued using the TCTP

overexpression constructs. There was no significant difference in proliferative inhibition at 1, 2, and 4nM vincristine between GFP-EV, GFP-TCTPwt, GFP-TCTPS46A, and GFP-TCTPS46D cells (Figure 4.14D). The level of apoptosis assessed using PARP cleavage was also not different between the various construct expressing cells (Figure 4.14E, 4.13C).

The GFP-TCTP constructs did not significantly affect proliferation or rescue drug response in Daoy cells, therefore, we questioned if the mutation of S46 was affecting TCTP function. Phosphorylation of Ser46 has previously been reported to reduce the affinity of TCTP for cytoskeletal filaments, α-tubulin, and f-actin, and have a direct role in microtubule stabilization (Bazile et al., 2009). Confocal microscopy with fluorescent α-tubulin and Hoechst staining showed the GFP-TCTPwt construct strongly associated with the Daoy cytoskeletal structure. However, both GFP-TCTPS46A and GFP-TCTPS46D also had near identical fluorescent signal overlap with α-tubulin (Figure 4.15). As well, GFP-TCTPS46D continued to associate with mitotic structures during cell division regardless of S46 mutation (Figure 4.16). Based on these observations modification of $TCTP^{S46}$ alone may not be sufficient to model PLK1-TCTP signaling in MB.

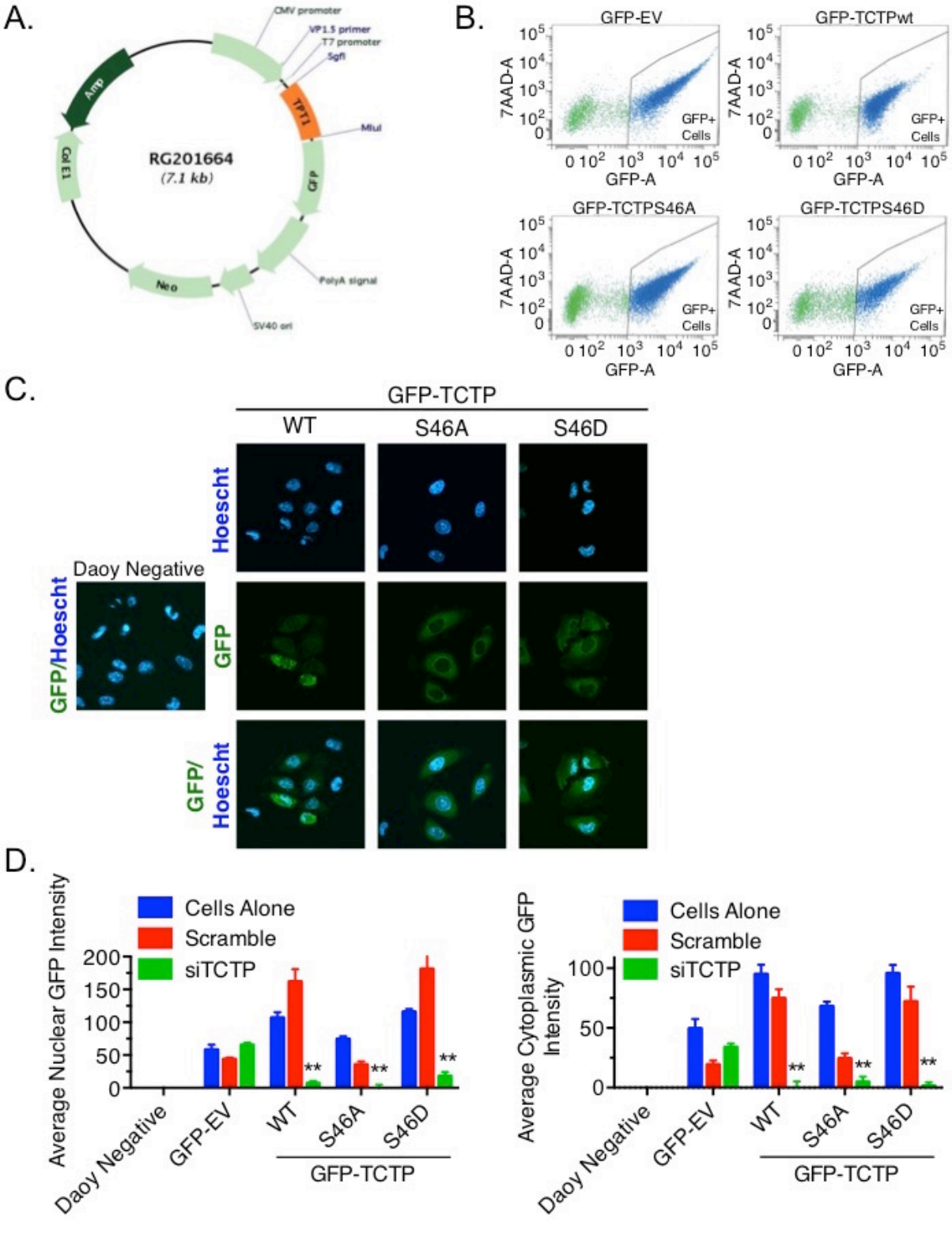
A.
CMV promoter
VP1.5 primer
T7 promoter
SgfI
TPT1
MluI
GFP
PolyA signal
SV40 ori
Neo
ColE1
Amp
RG201664
(7.1 kb)
B.
GFP-EV
GFP-TCTPwt
GFP-TCTPS46A
GFP-TCTPS46D
7AAD-A
GFP-A
GFP+ Cells
C.
GFP-TCTP
WT
S46A
S46D
Hoescht
Daoy Negative
GFP/Hoescht
GFP
GFP/ Hoescht
D.
Average Nuclear GFP Intensity
Average Cytoplasmic GFP Intensity
Cells Alone
Scramble
siTCTP
Daoy Negative
GFP-EV
WT
S46A
S46D
GFP-TCTP
**

Figure 4.12 GFP-TCTPwt, GFP-TCTPS46A, and GFP-TCTPS46D expression and localization in Daoy cells using fluorescence.

(A) A GFP-tagged human TCTP plasmid, pCMV6-AC-GFP-TCTP (GFP-TCTP) was used to perform site-directed mutagenesis and expressed in Daoy cells. **(B)** FACS sorting for enrichment of GFP-EV, GFP-TCTPwt, GFP-TCTPS46A, and GFP-TCTPS46D expressing Daoy cells, **(C)** which are quantified using fluorescent microscopy. **(D)** Nuclear and cytoplasmic detection of GFP is reduced following 72 hour TCTP knockdown using high-content screening methods for quantification. GFP intensity was normalized to Daoy negative control cell background levels (**, $P<0.001$).

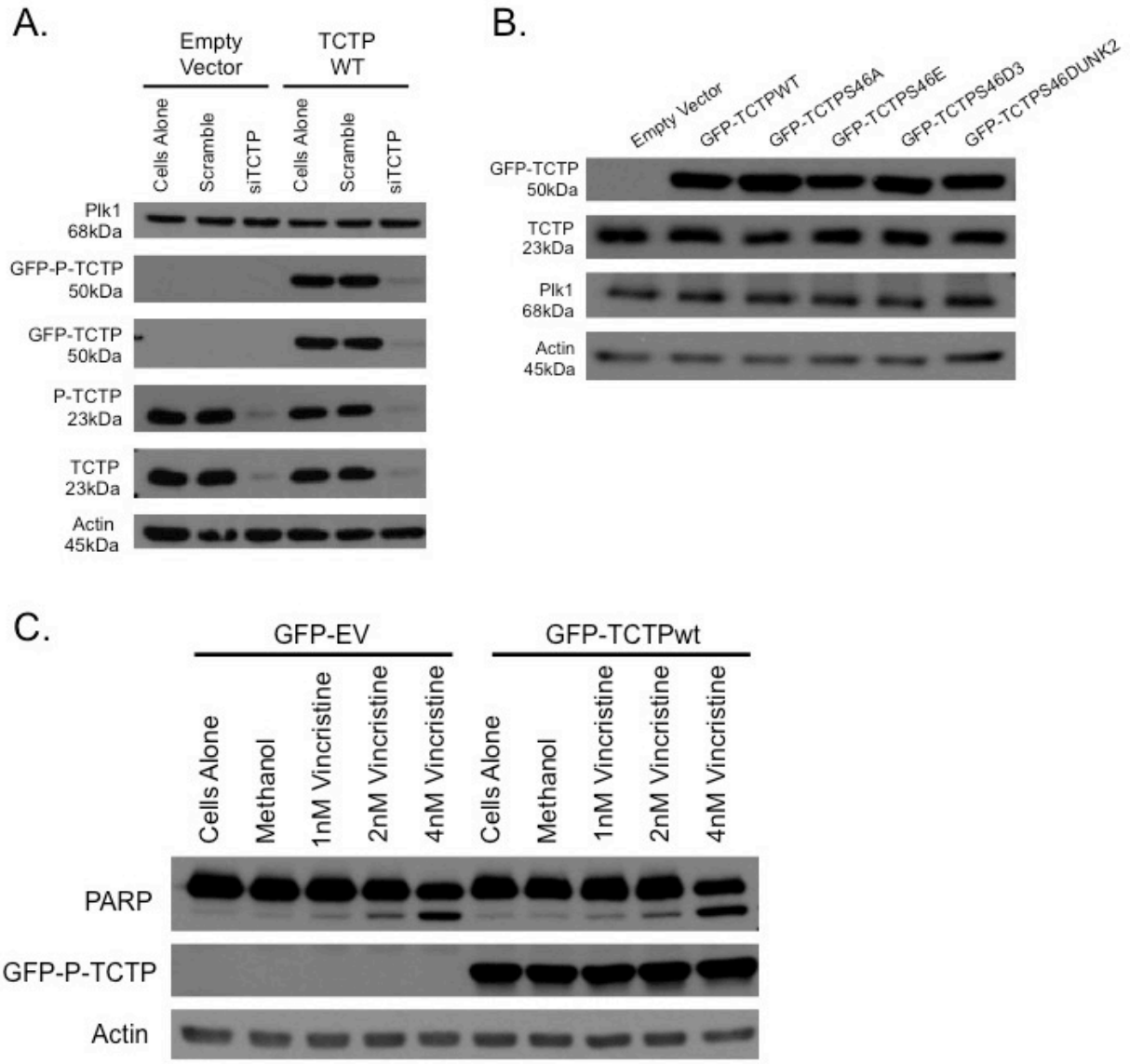

Figure 4.13 GFP-TCTPwt, GFP-TCTPS46A, and GFP-TCTPS46D expression in Daoy cells using immunoblotting.

(A) Daoy expression of the GFP-TCTPwt is detected as a 50kDa band using immunoblotting that can be probed with TCTP and P-TCTP^{Ser46} antibodies. 72 hour TCTP siRNA treatment causes a reduction of endogenous TCTP and GFP-TCTPwt protein expression. Expression of GFP-TCTPwt does not affect endogenous levels of PLK1 and **(B)** neither does expression of GFP-EV, GFP-TCTPS46A, or GFP-TCTPS46D constructs. Endogenous TCTP protein expression is also not altered by the presence of ectopic overexpression vectors. **(C)** Daoy cells expressing either control GFP-EV or GFP-TCTPwt TCTP overexpression vector were treated with 1, 2, or 4nM vincristine for 72 hours. Apoptosis was assessed using immunoblot detection of PARP cleavage. Presence of the GFP-TCTPwt construct shown through detection of 50kDa band using a TCTP specific antibody.

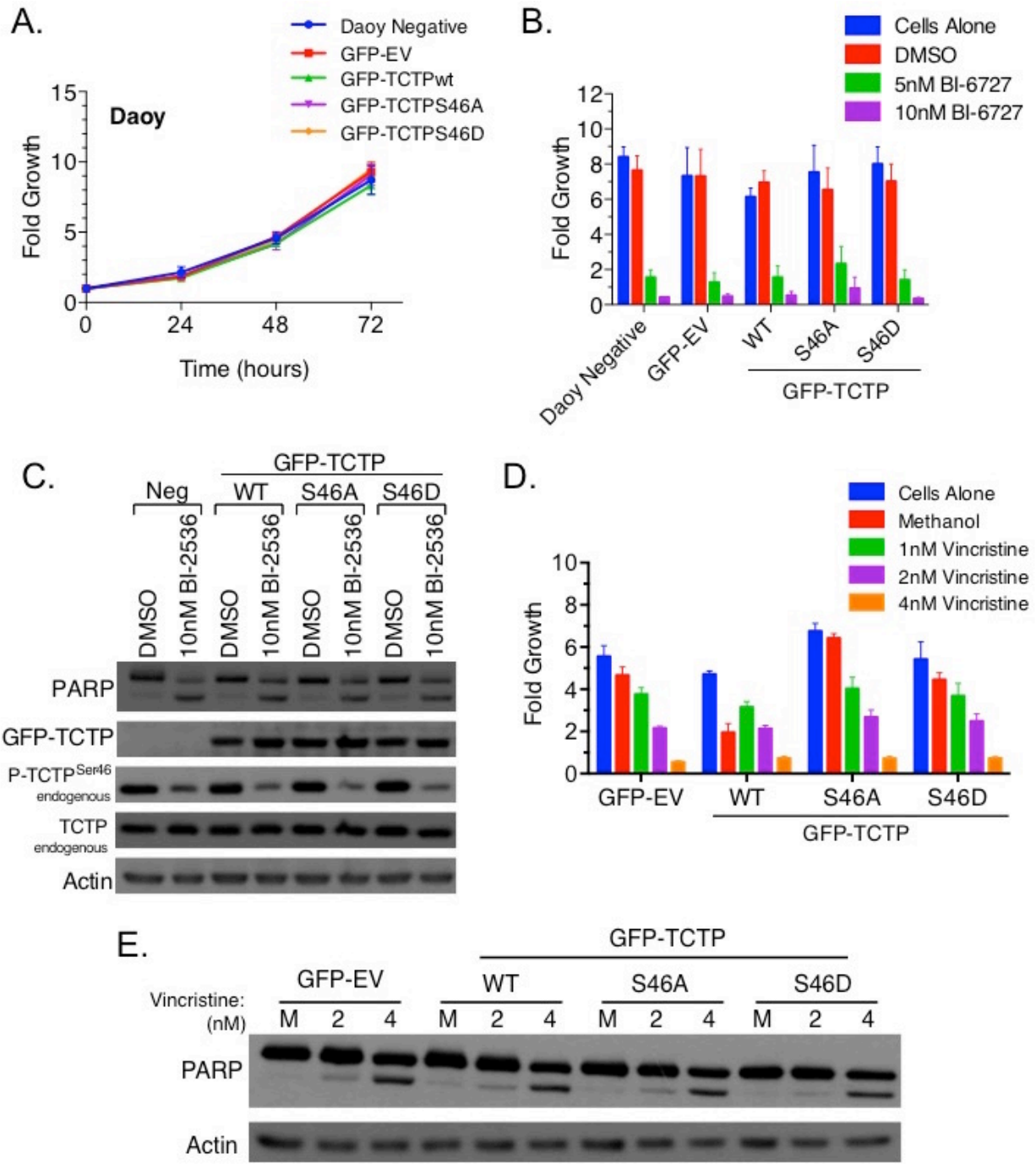

Figure 4.14 Overexpression of GFP-TCTPSer46 mutant constructs does not influence Daoy cell growth and drug sensitivity.

Daoy cells expressing GFP-TCTPwt, GFP-TCTPS46A, GFP-TCTPS46D, and GFP-EV were grown in G418 selective medium and **(A)** tested for differences in proliferation over a 24, 48, and 72 hours using Hoechst staining compared to untransfected Daoy negative cells. As well, **(B)** GFP-TCTP mutant overexpressing cells were treated with 5 and 10nM BI-6727 over 72 hours and assessed for growth relative to untreated and DMSO solvent control.

(C) Immunoblotting was used to detect endogenous and GFP-tagged TCTP, as well, show P-TCTP^{Ser46} downregulation, and PARP cleavage with PLK1 inhibition following 72 hour treatment. **(D)** GFP-EV, GFP-TCTPwt, GFP-TCTPS46A, and GFP-S46D overexpressing Daoy cells were treated with 1, 2, and 4nM vincristine for 72 hours and examined for growth using Hoechst staining and **(E)** immunoblotting was used to detect apoptosis using detection of PARP cleavage. A, B, and D Figures are representative of three independent experiments.

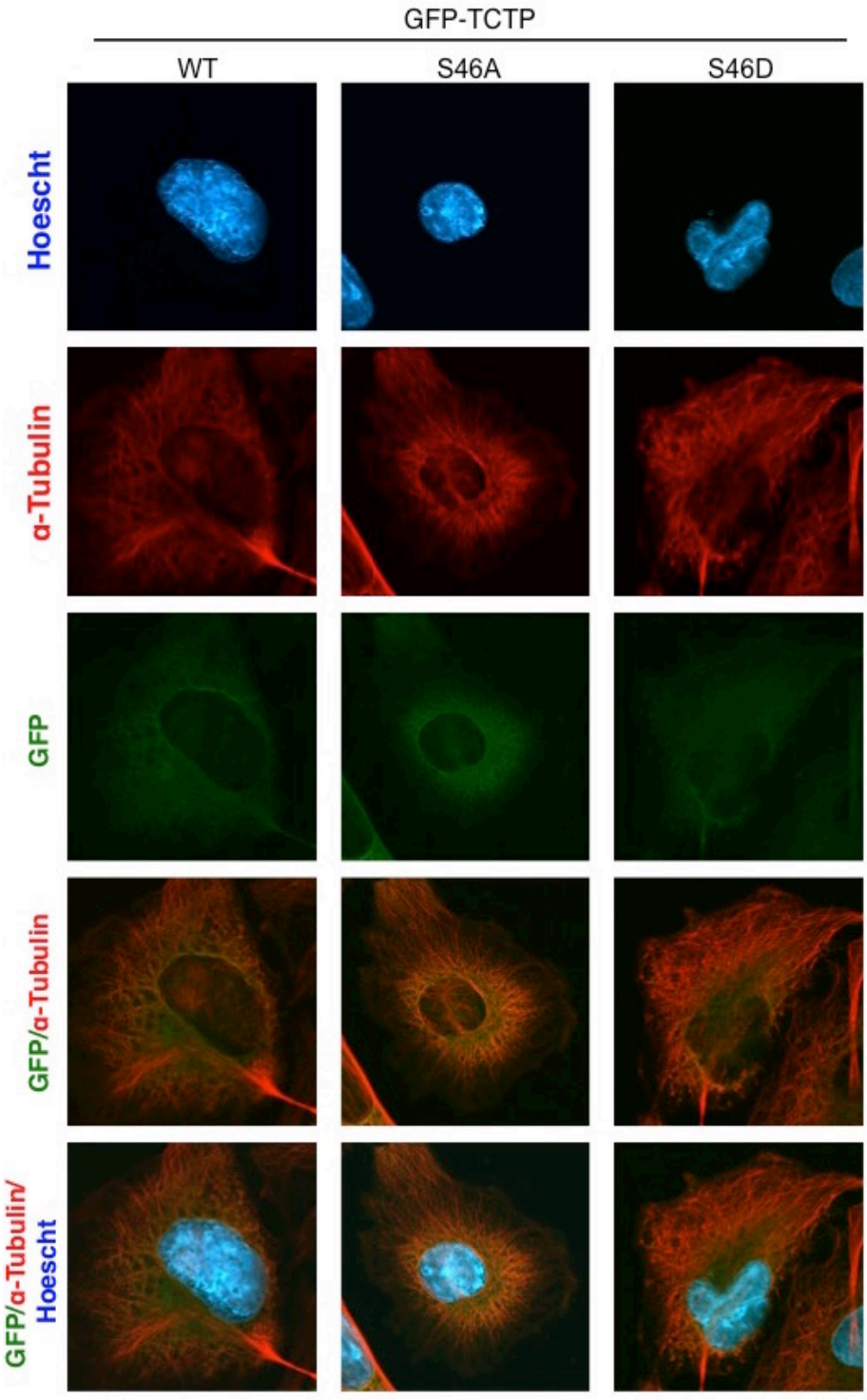

Figure 4.15 GFP-tagged mutant TCTPSer46 constructs co-localize with Daoy cell cytoskeleton.

Daoy cells expressing GFP-TCTPwt, GFP-TCTPS46A, and GFP-TCTPS46D (green) were grown in selective G418 medium and fluorescently stained for alpha-tubulin (red), and Hoechst nuclear staining (blue).

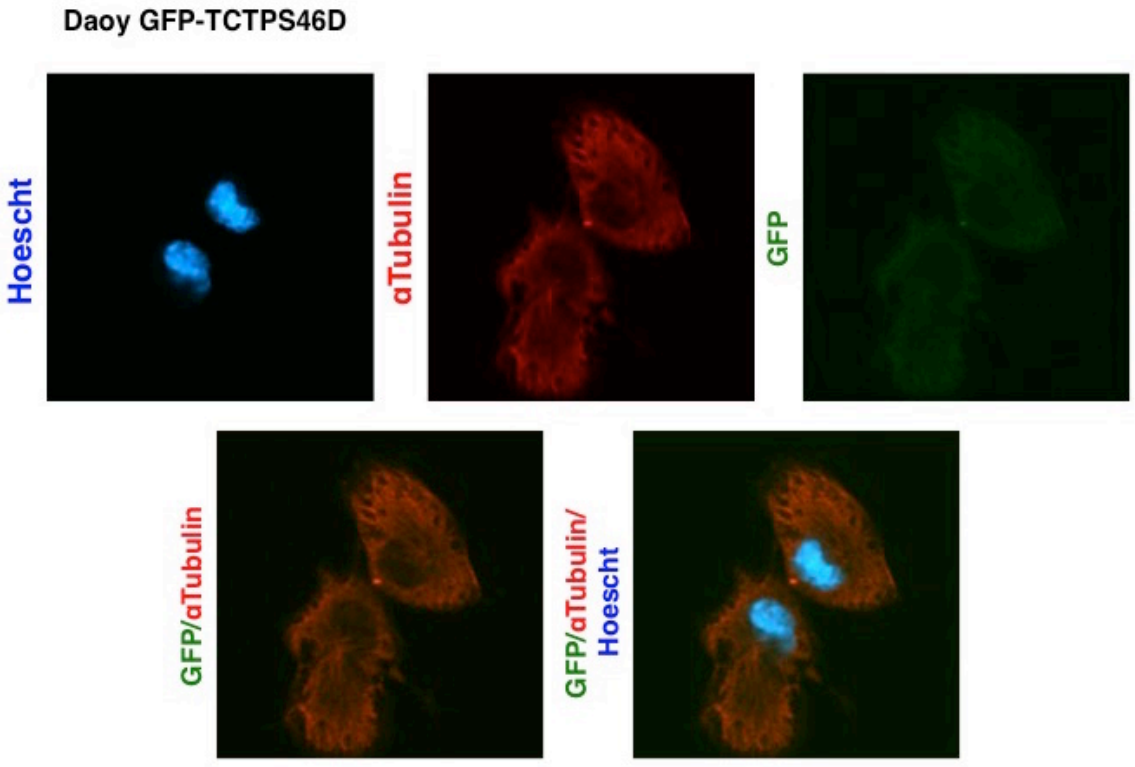

Figure 4.16 GFP-TCTPS46D associates with alpha tubulin during cell division.

Daoy expressing GFP-TCTPS46D (green) were grown in selective G418 medium and fluorescently stained for alpha-tubulin (red), and Hoechst nuclear staining (blue).

4.4 Discussion

The objective of this study was to evaluate the PLK1 substrate, TCTP, and assess what factors are involved in driving MB therapy resistance and relapse. TCTP transcript expression was enriched in SHH patients that demonstrated especially dismal survival outcomes. Although PLK1 and TCTP transcript expression was not associated, both TCTP and PLK1-high cases correlated with high p53 immunopositivity and poor overall survival. Therefore, we question whether a key regulatory pathway exists between PLK1 and TCTP that influences the aggressiveness of MB. To do this, the functionality of TCTP needs to be better understood.

High TCTP expression has also been found to correlate with worse patient survival in other types of cancer (Amson et al., 2011; Gu et al., 2013). We found that targeting TCTP had a significant impact on MB cell proliferation and anchorage-independent growth. The knockdown of TCTP using siRNA reduces proliferation in multiple cancer cell lines including melanoma, non-Hodgkins lymphoma, osteosarcoma, glioma, and prostate cancer (Bae et al., 2015; Gnanasekar et al., 2009; Gu et al., 2013; He et al., 2015; Shen et al., 2014). Shen and colleagues also observed a dramatic reduction in colony formation in anchorage-independent growth conditions similar to our findings in Daoy cells (Shen et al., 2014).

TCTP has been reported to have multiple cellular functions involving cell cycle, stress response, apoptosis, and tumor reversion (Baylot et al., 2012; Susini et al., 2008; Tuynder et al., 2004; Yarm, 2002; J. Zhang et al., 2012). Therefore, we questioned whether inhibiting TCTP could enhance the efficacy of chemotherapy. Although these early experiments did not show an additive effect with TMZ or etoposide, a modest decrease was observed following the treatment of Daoy siTCTP cells with vincristine. This may be due to the microtubule-targeted mode of action of vincristine that may overlap with TCTP's involvement in the regulation of the cytoskeleton. Other groups have reported that inhibition of TCTP increases sensitivity to γ-radiation and suggest an anti-apoptotic relationship between TCTP and DNA damage repair signaling (Amson et al., 2011; Hong and Choi, 2013; J. Zhang et al., 2012). This suggests that modulating TCTP in cancer could potentially increase the efficacy of radiation therapy. Expansion of our preliminary work to consider the role of TCTP in γ-radiation sensitization could help minimize the negative impact of radiation treatment of pediatric brain tumor patients.

The inhibition of PLK1 in MB results in a G2/M cell cycle arrest (Triscott et al., 2013) and we were interested to find that TCTP knockdown in Daoy cells also resulted in a G2/M shift. Conversely, siTCTP treatment of ONS76 cells caused a G1/S cell cycle shift, which was also observed in a study using siTCTP knockdown in osteosarcoma cell lines (Shen et al., 2014). Other groups suggest this effect may result from the inactivation of the anti-apoptotic enhancement of TCTP on proteins like Mcl-1 and Bcl-2 (He et al., 2015; Liu et al., 2005). Of note, developmental work on TCTP in *Drosophila melanogaster* found that aberrant TCTP could manipulate the G2/M checkpoint in response to γ-irradiation. Further, the same study demonstrated mutant TCTP in a different cell compartment could also activate G1/S cell cycle arrest upon radiation exposure (Hong and Choi, 2013). This is especially interesting because we observed different checkpoint activation in Daoy and ONS76 cells following TCTP knockdown. Zhang and colleagues also observed both a G1/S and G2/M delay following irradiation of human fibroblast cells treated with siTCTP. They suggest that the loss of checkpoint control from TCTP depletion disrupts DNA repair programs and is an early step in carcinogenesis (J. Zhang et al., 2012). While we speculate that the *TP53* mutation status of our MB cell lines might indicate which checkpoint is activated, more work needs to be done to better characterize TCTP within specific cell types. Together, this information suggests that TCTP may play a role in facilitating cell cycle checkpoint progression and may be crucial for maintenance of genomic stability.

TCTP depletion in ONS76 cells also resulted in a dramatic morphological shape change. Other groups have also observed this following modification of TCTP expression (Bazile et al., 2009; Gachet et al., 1999). Similar to our study, cells became elongated and formed protrusions while proliferation slowed with siTCTP treatment, and long cables of microtubules formed in the cytoplasm (Bazile et al., 2009). TCTP is involved in facilitating microtubule stability and suppression of its expression may dramatically affect microtubule dynamics of the cytoskeleton.

In both normal and cancer cells, TCTP is localized to the cytoskeleton in the cytoplasm and nucleus (Kloc et al., 2013). Quantification using GFP demonstrated expression of GFP-TCTPwt, GFP-TCTPS46A, and GFP-TCTPS46D in both cellular compartments. We observed an association with our GFP-tagged TCTP constructs similar to microtubule localization patterns established by other groups (Gachet et al., 1999; Jaglarz et al., 2012). We were surprised to see that overexpression of GFP-TCTPwt did not affect the rate of Daoy cell proliferation or enhance

anti-apoptotic function in drug combination studies. He and colleagues also used a GFP-tagged TCTP construct and observed a significant difference in cell viability (He et al., 2015). Also, overexpression of TCTP by another group increased *in vitro* and *in vivo* growth of glioma cells (Gu et al., 2013). The non-effect observed in our study could also be attributed to a number of technical factors. Although we demonstrated that our GFP-TCTP construct was able to localize in the nucleus and be phosphorylated at the $TCTP^{Ser46}$ site, it remains possible that the GFP-tag obstructed TCTP functions; for example protein-protein interactions. Another strong possibility is that we incorporated our overexpression system in the Daoy cell model that already had high endogenous levels of TCTP. We speculate that the cells may have already been saturated with TCTP, and moving forward will consider testing TCTP overexpression paired with a conditional knockout system.

PLK1 phosphorylation of TCTP reduces its association with microtubules (Yarm, 2002). We hypothesized that site-directed mutagenesis of the residue targeted by PLK1 would either enhance or reduce the GFP-TCTP construct association with Daoy cell cytoskeleton. This was not the case however, and the phospho- null (GFP-TCTPS46A) and phospho- mimic (GFP-TCTPS46D) mutants did not appear to differ in microtubule co-localization from the GFP-TCTPwt construct using fluorescent microscopy. A possible explanation for these results is that phosphorylation of $TCTP^{S46A}$ alone is not sufficient to alter the function of TCTP. PLK1 has been shown to phosphorylate a second residue on TCTP. Phosphorylation of the second residue is dependent on the initial phosphorylation of Ser46 by PLK1. Initially, Ser64 was reported to be the second PLK1 target site (Yarm, 2002), however, more recently Thr65 has been suggested as the secondary phosphorylation site (Cucchi et al., 2010). $TCTP^{Ser46}$ is more consistently reported as the main target site for PLK1, which is why we choose to focus on its role in MB, but manipulation of the second PLK1 phosphosite might be necessary to modify TCTP functionality. In future studies, we will test the effect of a TCTP double mutant.

In conclusion, this work highlights a previously undiscovered relationship between the anti-apoptotic protein TCTP and aggressive malignant brain tumors. Further exploration of TCTP as a target in MB may provide valuable insight into the mechanisms that drive treatment resistance.

4.5 Experimental procedures

Medulloblastoma patient cohorts

Primary MBs were obtained from BC Children's Hospital (BCCH) (Vancouver, BC, Canada; discovery) and Children's Hospital of Eastern Ontario (CHEO) (Ottawa, ON, Canada; validation). Molecular subtyping and clinical attributes of the BCCH discovery cohort have previously been published (Triscott et al., 2013). Drs. Jean Michaud and Donna Johnston from CHEO generously provided the validation cohort of 53 primary MB patient FFPE samples. Two of 53 of these samples failed to produce enough high quality RNA and clinical outcomes data was not available at this time. All tumors were subtyped and the data analyzed according to Northcott and colleagues (Table 4.1) (Northcott et al., 2012d).

NanoString nCounter sample preparation and codeset

RNA was extracted from three 20μm scrolls of FFPE tissue, exactly 250ng of RNA was run for each patient sample, and RNA quality was assessed using Nanodrop spectrometry as previously described (Triscott et al., 2013). Analysis using the NanoString nCounter Gene Expression system was conducted at the Centre for Translational and Applied Genomics (CTAG) (BC Cancer Agency, Vancouver, BC). A custom codeset synthesized by NanoString Technologies (Seattle, WA, USA) was designed which included 22 MB specific subtyping gene probes (Northcott et al., 2012d) plus other genes of interest that specifically included *PLK1* (NM_005030.3), and *TCTP* (NM_003295.2). The recommendations outlined by NanoString Technologies were all followed regarding sample preparation, hybridization, detection, scanning, and data normalization.

Immunohistochemical staining

A tissue microarray (TMA) was subsequently constructed from the original FFPE blocks; triplicate 1mm cores extracted from every tumor resection performed on the patients. TMA slides were incubated with CitriSolvTM for de-paraffinization. The slides were dehydrated in 100% ethanol and rehydrated using an ethanol gradient then steam-heated in 0.1 mol/L citrate buffer for 20 minutes for antigen retrieval. Endogenous peroxidase activity was quenched by incubating with 3% v/v H2O2, at room temperature. The slides were rinsed by 3 × 5-minute

washes in PBS containing 0.2% (v/v) Triton X-100. The sections were treated with DAKO protein block for 10 minutes and incubated overnight with anti- mouse anti-p53 (Bp53-11) primary antibody, Ventana (cat. 760-2542), diluted (1:200) in PBS containing 0.3% (v/v) Triton X-100 and 0.1% (w/v) bovine serum albumin. All slides were counterstained with hematoxylin for 40 seconds and rinsed with tap water. Images were acquired using a Nikon Eclipse 50i light microscope and a Digital-Sight DS-Fi1 camera (Nikon, Japan). P53 was scored semi-quantitatively using a 4 point scale (0-3) that took into consideration the intensity and the diffusivity of the staining.

NanoString gene expression and qRT-PCR analysis

NanoString gene expression data was analyzed as previously described (Triscott et al., 2013). Heatmaps were generated using unsupervised hierarchical clustering with average linkage using Cluster version 3.0 and Treeview version 1.60. RNA for qRT-PCR gene expression analysis was isolated using Qiagen RNeasy Mini Kit (Cat. #74106). Transcript expression was determined using qRT-PCR with *PLK1* and *TCTP (TPT1)* Assay on Demand (Applied Biosystems, cat. #4331182; Hs00153444_m1 and Hs02621289_g1).

Cell culture

Daoy cells were obtained from the American Tissue Culture Collection (ATCC, Manassas, VA, USA) while ONS76, and UW228 were kindly provided by Dr. Sheila K. Singh (McMaster University, Hamilton, ON). Primary brain tumor cells were isolated from BT027 (Group 4) and were grown as neurospheres as previously described (Lenkiewicz et al., 2009) using Neurocult media (Stem Cell technologies, Vancouver, BC, Canada) (Lee et al., 2012b). Samples from BT027 were obtained through informed consent in abidance with the respective research ethics board guidelines at British Columbia Children's Hospital.

siRNA transfection and western blotting

TCTP small interfering RNA transfections were performed using Lipofectamine RNAiMAX (Invitrogen, Burlington, ON, Canada). RNA oligos T1, T2, and T3 were acquired from Ambion/Life Technologies (#AM16708; 289422, 13153, 12966) and transfected as

previously reported using 10nM RNA transfection concentrations (Hu et al., 2009). Immunoblotting was conducted using anti-PLK1 (Sigma-Aldrich), anti-P-TCTP^{Ser46}, anti-TCTP, anti-poly (ADP-ribose) polymerase (PARP) (Cell Signaling Technology), anti-vinculin (Upstate) and anti-pan-actin (Cell Signaling Technology, Massachusetts, USA). Band quantification was done using densitometry that was measured using ImageJ, v1.46r and normalized to Actin.

Cell proliferation assays

To evaluate the effect of PLK1 and TCTP inhibition on cell growth, MB cells were plated (750 cells/well) in 96-well plates, fixed using 2% paraformaldehyde and stained with Hoechst nuclear dye (1ug/mL). The plates were analyzed and the images were taken on the ArrayScan VTI Reader (Cellomics, Pittsburgh, USA) using previously outlined methods (Hu et al., 2009; Triscott et al., 2013). Growth assays involving siRNA or drug treatment were plated overnight and treated the following day after cells had adhered to culture plates.

GFP-TCTP^{Ser46} plasmid site-directed mutagenesis

A GFP-tagged human TCTP plasmid, pCMV6-AC-GFP-TCTP (GFP-TCTP) (Origene, RG201664), and control plasmid, pCMV6-AC-GFP (GFP-EV) (Origene, PS100010) was obtained. Site-directed mutagenesis was performed using the QuikChange II Site-Directed Mutagenesis Kits (Stratagene) according to instructions outlined by the manufacturer. Table 4.3 includes primer sequences and mutated TCTP target sequence that was confirmed using DNA sequencing. Daoy cells were transfected with Lipofectamine 2000 (Invitrogen) and then maintained in selective medium containing G418.

Fluorescence-activated cell sorting (FACs) and cell cycle analysis

Single cell suspensions of Daoy cells expressing GFP-EV, GFP-TCTP, GFP-TCTPwt, GFP-TCTPS46A, or GFP-TCTPS46D were fixed with ethanol. Cells were sorted for the top 10% GFP expressers and data acquisition was performed on a BD FACS Calibur using Cell Quest Pro software then analyzed using FlowJo software. No additional staining was necessary and re-sorting was done every 5-8 passages to attempt to control for changes in GFP construct

expression over time. Cell cycle analysis was done following 24 to 96 hour siRNA or BI-2536 treatment using flow cytometry as described by Lee and colleagues (2012).

Fluorescent marker screening and microscopy

GFP expression of GFP-EV and TCTP expressing cells quantified using high-content screening with the ArrayScan VTI Reader (Cellomics, Pittsburgh, USA). Cells were plated in 96-well format, fixed with 2% paraformaldehyde and stained with Hoechst (1ug/mL). Both nuclear and cytoplasmic intensity was measured relative to Daoy negative GFP cells. Immunofluorescence microscopy was performed on Daoy cells according to the procedure we previously described (Fotovati et al., 2011; Triscott et al., 2013). Primary antibodies include: alpha-tubulin (Abcam, ab18251), Pericentrin (Abcam, ab28144), anti-P-H2AX^{S139} (Abcam, ab26350), and PARP (Cell Signaling Technology). Images were taken using an Olympus FV10i confocal microscope on X60 lens magnification.

Anchorage-independent soft agar growth

Daoy cells were treated with scramble control and TCTP siRNA for 48 hours then plated at a density of 5000 and 10 000 cells/well in a 24- well plate in 0.6% agar cell layer with a 1.2% agar feeder layer composed of 2X DMEM + FBS medium. Colonies developed over 21 days and each experiment was performed in replicates of four and repeated thrice. Plate wells were divided into quadrants and 4 fields were counted per each well then averaged across replicates.

Statistical analysis

For the clinical survival analysis, log-rank analysis was performed on the Kaplan-Meier curve to determine statistical significance of the results. Multivariate survival analysis was conducted using Cox regression proportional hazards and a 95% confidence interval (CI). All survival analysis and Spearman's Rank correlation test were done using SPSS version 20.0 statistical software (IBM, Chicago, IL, USA). The number of samples used and the respective P-values are listed in the Figure legends. The level of significance for the *in vitro* cell growth/death data was determined by Student's two-tailed T-test and difference in TCTP expression between subtypes was assessed using one-way ANOVA (*, P value<0.05; **, P value<0.01).

4.6 Supplementary data

Mutation	Template Strand	Primer Sequence	Length (nt)
TCTPS46 Serine to Alaine	Sense	5'-CATTTCCACCAATGAGCGCGTCATCAATGTTACCTTC-3'	37
TCG to GCG	Antisense	5'-GAAGGTAACATTGATGACGCGCTCATTGGTGGAAATG-3'	37
TCTPS46 Serine to Aspartic acid	Sense	5'-GACAGAAGGTAACATTGATGACGATCTCATTGGTGGAAATGCCTCCG-3'	47
TCG to GAT	Antisense	5'-CGGAGGCATTTCCACCAATGAGATCGTCATCAATGTTACCTTCTGTC-3'	47

Table 4.3 Primers used for site-directed mutagenesis of GFP-TCTPSer46.

CHAPTER 5: CONCLUDING REMARKS

5.1 Summary

There is still an immense need to improve therapeutic development for high-grade brain tumors. GBM is the most commonly occurring malignant brain tumor in adults and is a diagnosis that leaves virtually no survivors. MB - the most common malignant brain tumor in children- has a survival rate that has improved to >70%; however, the negative sequelae associated with treatment often transforms this childhood cancer into a life-long disability. While there has been an expansion of surgical technologies that assist the removal of tumor tissue, the delicate and essential nature of the human brain always results in a subtotal resection. Thus, there is a requirement for additional modalities of treatment such as radiation and chemotherapy. Recent work in the field has demonstrated that treatments that target the proliferative tumor bulk are not sufficient to prevent the relapse of brain tumors (Bao et al., 2006; Burkhardt et al., 2011). The discovery of brain tumor CSC populations created a fundamental requirement for treatments to not only prevent cell proliferation, but also have the capacity to eliminate the self-renewal of CSCs. Unfortunately, the development of novel therapeutics is exceedingly complicated for brain malignancies due to the tightly regulated BBB that restricts access of most chemicals. Further, the astronomic investment of resources that is required to translate a therapeutic from the research bench to clinical bedside results in few experimental options being tested in clinical trials. The objective of this thesis was to identify, and preclinically evaluate, new drug targets that have the potential to overcome these challenges.

Our approach has been to target kinases for improving cancer treatment, and these are among the most plausible drug targets. There have been 26 kinase inhibitors approved for the treatment of cancer to date; this is more than any other drug class. Preceding this thesis our group conducted a kinome-wide screen and reported that inhibiting PLK1 with siRNA suppressed the growth of a wide range of pediatric solid tumors including glioma cells (Hu et al., 2009). Following this, we examined the potential of targeting PLK1 in GBM cells. We found PLK1 expression was associated with aggressive disease, and its inhibition prevented CSC self-renewal (Lee et al., 2012b). These early results encouraged us to explore the feasibility of

targeting PLK1 in the context of TMZ-resistant GBM, as well as expanding its promise as a molecular target into MB. The purpose of this project was to evaluate the importance of PLK1 in aggressive brain tumor models, with the goal of establishing the preclinical groundwork necessary to promote testing of PLK1 inhibitors in patients.

The studies presented in this thesis implicate PLK1 as a cornerstone kinase that orchestrates the oncogenic program characteristic of poor outcome disease. In chapter 2, we queried whether off-patent drugs could be repurposed for the treatment of TMZ-resistant GBM. In doing so, we found that treatment of GBM cells with standard-of-care TMZ failed to eliminate highly proliferative PLK1 expressing cells. Alternatively, we discovered that DSF, an off-patent drug clinically approved for substance abuse, could completely abolish the growth and self-renewal of TMZ-resistant cells. We observed comparable efficacy when we targeted PLK1 with BI-2536 or siRNA. In stark contrast to TMZ, we were the first to show that DSF treatment caused a downregulation of PLK1 expression; therefore it might offer a novel approach to targeting drug-resistant GBM. This *in vitro* based study demonstrated that the chemical downregulation of PLK1 - either with DSF or specific kinase inhibitors - could be key in the prevention of tumor relapse (Triscott et al., 2012).

In chapter 3, we used a bioinformatic approach to stratify pediatric MB patients using NanoString gene expression technology. Based on our findings in GBM, we assessed the importance of PLK1 expression and discovered this highly overexpressed oncogene was also correlated significantly with relapse and overall patient survival. Further testing of primary patient samples was used to demonstrate that PLK1-high cases responded to BI-2536, whereas PLK1-low did not. PLK1 inhibition in MB cell lines triggered G2/M arrest and apoptosis at low concentrations. As well, BI-2536 had comparable efficacy to standard-of-care chemotherapy as it extended the survival of xenograft bearing mice. The work presented here was one of the first of its kind to independently validate MB molecular subtyping, as well, introduce a personalized means to identify and treat poor prognosis patients by targeting PLK1 (Triscott et al., 2013).

Chapters 2 and 3 demonstrated that high-grade brain tumors that have high PLK1- or belong to the SHH MB subtype- corresponded with treatment resistance. Therefore, in chapter 4, we sought to identify the molecular pathways responsible for making these tumors especially resilient. TCTP transcript expression was enriched in SHH MB patient samples and significantly

correlated with p53 positive immunostaining. Inhibition of TCTP using siRNA activated G1/S and G2/M cell cycle shifts, eliminated colony formation in soft agar, and dramatically reduced MB cell line proliferation. The approach of inhibiting TCTP could effectively block growth in cells that failed to respond to TMZ. Additionally, being a PLK1 phospho- substrate, we evaluated whether the mutation of the $TCTP^{S46}$ residue alone was sufficient to rescue the anti-cancer effects observed in the siTCTP assays. The work presented in this chapter positions TCTP as a marker of PLK1 kinase activity for inhibitor studies, but more importantly introduces it to have a impact on brain tumor cell growth that is independent of its relationship with PLK1.

Taken together, the significance of this work lies in the discovery that the mitotic kinase, PLK1, can be utilized as a marker for treatment-resistant disease that can be safely targeted in patients. These studies were the first to attempt to characterize the functionality of the PLK1 substrate, TCTP, in a brain tumor model and will have added value in the mechanistic depiction of SHH MB. Finally, the highly promising new purpose for DSF in cancer treatment is also an important contribution of this research as this compound is already available for clinical use.

5.2 Discussion and future directions

DSF is a promising off-patent drug for the treatment of GBM

Following publication of the work included in chapter 2, other groups have also reported the potential of DSF against GBM CSCs using cell lines (P. Liu et al., 2012) and a high content screening approach (Hothi et al., 2012). Our findings are especially valuable in that we were the first to test the efficacy of DSF against fresh primary GBM samples in the context of TMZ resistance. The significance of this has direct clinical application as we demonstrate that DSF may be a powerful inhibitor for both MGMT methylated and unmethylated tumors.

The value of DSF has also been explored in other studies. In T98G GBM cells that are TMZ-resistant, Paranipe et al. recently reported that DSF down-regulates MGMT in xenografts implanted subcutaneously (Paranjpe et al., 2014). They suggest that DSF could, therefore, be used to treat gliomas because it crosses the BBB, but they did not perform intracranial injections of T98G cells. However, Choi et al. recently published a study in atypical teratoid rhabdoid tumors (AT/RT) that demonstrated DSF crosses the BBB in mice and can reduce AT/RT CSCs

(Choi et al., 2014a). AT/RT are a rare yet deadly type of pediatric brain tumor where improved therapies are most certainly needed. Of note, they reported that DSF reduced ALDH *in vitro* by ~75% and in tumors. It also inhibited EdU incorporation and tumor cell proliferation based on Ki67 staining. AT/RT CSCs were more sensitive to DSF than clinically used drugs such as ifosfamide. Likewise, ifosfamide had no survival benefit in mice whereas DSF did prolong survival. There were no adverse effects of DSF reported in the mice. Thus, DSF is promising for the treatment of brain tumors because it crosses the BBB and suppresses the growth of brain tumors yet additional studies are needed to understand how widespread the effect will be.

Interestingly, treatment of primary GBM cells with DSF *in vitro* reduced the expression of kinases such as PLK1 protein and mRNA (chapter 2). The exact mechanism driving DSF induced PLK1 down-regulation still requires further investigation. However, these findings suggest DSF to be capable of targeting aggressive PLK1-high cell populations, which may be responsible for driving tumor relapse.

There are additional anticancer properties of DSF. For example, it also suppresses the proteasome and NFkB pathways (Chen et al., 2006; Liu et al., 2014; P. Liu et al., 2012; Yip et al., 2011; Zha et al., 2014). In the body, the DSF molecule is converted into a smaller metabolite called diethyldithiocarbamate. This metabolite has been shown to chelate into complexes when in combination with copper or zinc ions. These complexes are suggested to inhibit proteasome activity, and elevate reactive oxygen species (Yip et al., 2011). Under this premise, many cancer studies use DSF in combination with copper (Cen et al., 2002; Liu et al., 2013; Yip et al., 2011).

DSF has also been shown to impinge on epigenetic pathways. In prostate cancer, DSF can act as a DNA demethylating agent through inhibition of DNA methyltransferase 1 (DNMT1) (Lin et al., 2011). More recently studies on the fusion protein NUP98-PHF23 shows DSF treatment can reduce its chromatin modifying potential and induce cell death in acute myeloid leukemia. Interestingly, transcriptional availability of CSC signature genes, such as Hoxa, Hoxb and Meis1, is blocked by DSF (Gough et al., 2014). These observations further exemplify the potential anti-cancer activity of DSF.

Although incredibly promising, there is a collection of limitations in our assessment of DSF in GBM that can be addressed in future studies. First, the availability of primary tumor tissue that had finite growth capacity when passaged using *in vitro* culture. We were fortunate to

acquire BT74, GBM4, BT241, aBT001 and aBT003 but were limited in the size and number of experiments that could be conducted. A second consideration is that the availability of pediatric GBM samples is exceedingly limited. While we were able to examine the effects of PLK1 inhibition on the established pediatric cell line, SF188, at that point in the study there were no primary pediatric samples available. In future work, we wish to address whether DSF could specifically benefit childhood gliomas. In this regard, DSF has demonstrated decades of clinical safety and low side effects that may be better tolerated by children compared to highly toxic and minimally effective chemotherapies. Thirdly, previous work by our group provided an elegant study showing the efficacy of BI-2536 at extending the survival of a GBM xenograft model (Lee et al., 2012b). Although we report that DSF is effective at eliminating GBM cells using tissue culture, we have not yet tested DSF *in vivo*. However, it can be argued that extensive animal testing might not be essential because DSF is already an established clinical compound.

A final technical limitation from chapter 2, that is also relevant to all subsequent data chapters, is the accuracy of the ArrayScan HCS system (Thermo Fisher Scientific) at measuring cell proliferation. This high-content screening technology was used to quantify the number of cells remaining in cell culture plates after drug or siRNA treatment of various cell lines using the detection of a Hoechst 33342 nuclear stain. Issues may arise when comparing cells with different rates of proliferation. As well, whether a cell is counted depends on its ability to adhere to the culture plate following fixation with paraformaldehyde, and PBS washes. This system was also used to estimate the number of apoptotic cells remaining on the plate using thresholds for dye intensity and nuclear morphology, but the presence of confounding factors- like binucleated cells- may complicate the automated interpretation of the plate reader (Haney et al., 2006). More extensive proliferation screens that test multiple timepoints and a larger range of drug concentrations may be necessary to overcome these technical limitations. As well, pairing the results collected from high-content screening with western blot or flow cytometry markers of cell cycle progression could provide additional evidence of proliferative affects.

PLK1 is a molecular target for treatment and prognostication of MB.

We discovered that the measurement of PLK1 using the NanoString nCounter system could be an informative prognostic tool that may be used in the selection of personalized

treatments. There are other studies that have examined the efficacy of inhibiting PLK1 in MB. One *in vitro* study tested the early generation PLK1 inhibitor, GW843682X, against a panel of 18 pediatric tumor cells lines. Similar to the findings of our study, this work showed that PLK1 inhibition could be used to block the proliferation of cell lines that are highly resistant to common cancer drugs (Spaniol et al., 2011). Specifically in MB, Harris and colleagues (2012) show that PLK1 is highly overexpressed compared to normal tissue and is uniformly distributed across molecular subtypes. The data reported in the aforementioned study further compliments the findings from our work. They also show that targeted PLK1 knockdown significantly reduced Daoy and ONS76 proliferation (Harris et al., 2012). This was correlated with enhanced apoptosis and inhibition of colony formation. Using a 72 hour Daoy cell growth assay, this group found the IC_{50} of BI-2536 to be between 5 and 10nM concentrations, which is near identical to the findings from chapter 3 of this thesis (Harris et al., 2012). In addition, Markant and colleagues (2013) published a notable study showing the benefit of PLK1 inhibition specifically in a SHH MB. They found that BI-2536 treatment also caused an elevation of P-histone H3 in cells isolated from a mutant PTCH mouse model. Using concentrations of 100nM BI-2536, they also observed a dramatic G2/M cell cycle shift in this GEM cells *in vitro*. Similar to our findings, targeting PLK1 inhibited the proliferation of patient-derived MB cells, and also reduced tumor volume of the mutant PTCH mouse model compared to saline controls. Interestingly, a 10nM dose of BI-2536 had an additive effect that significantly decreased the IC_{50} vincristine for an anti-proliferative effect on SHH MB cells (Markant et al., 2013). Both groups show the PLK1 inhibitor BI-2536 can target MB CSC populations through the measurement of SOX2, or the assessment of CD15+ populations (Harris et al., 2012; Markant et al., 2013).

The work conducted by our group is unique because it (1) provides evidence suggesting that PLK1-high MB patients have poor clinical outcome, (2) recommends PLK1 inhibition as a targetable therapy based on the results of bioinformatic classification, (3) demonstrates the retention of subtype-specific characteristics of primary cultured cells, and (4) directly compares *in vivo* efficacy of BI-2536 relative to a chemotherapy cocktail that models current clinical protocols. The importance of these findings can be further exemplified by other brain tumor and cancer models that provide additional support to the premise of this work.

Cancer cells almost always demonstrate an oncogenic addiction to PLK1 as a cornerstone of mitotic regulation. Relative to normal tissues, PLK1 is overexpressed in GBM, medulloblastoma, breast, ovarian, prostate, colorectal, non-small-cell lung, and other cancer types (Harris et al., 2012; Lee et al., 2012b; Liu et al., 2011; Takahashi et al., 2003; Takai et al., 2005; Wolf et al., 1997). Interestingly, PLK1 protein detection increases with severity of histopathological grade of astrocytoma (Dietzmann et al., 2001). In an analysis of 343 glioma cases high levels of *PLK1* transcript were significantly associated with worse overall survival, as well, there is an enrichment of expression within the especially aggressive proliferative category of GBM (Lee et al., 2012a, 2012b; Phillips et al., 2006). Another gene expression analysis using The TCGA identified *PLK1* as the only overexpressed gene that significantly correlated with *TP53* mutation in GBM. This suggests a synthetic lethal interaction between Plk1 and p53, one of the most deregulated oncogenes in cancer (Degenhardt et al., 2010; Masica and Karchin, 2011).

In a screen of siRNAs representing the human kinome, PLK1 inhibition reduced cell proliferation, disrupted cell cycle, and induced mitotic arrest (Pezuk et al., 2013; Tandle et al., 2013). Reducing PLK1 activity with both siRNA or kinase inhibitors increased sensitivity to GBM to radiotherapy but without affecting normal cells (Tandle et al., 2013). Primary neural stem cells and normal human astrocytes express less *PLK1* then glioma cells. The PLK1 small molecule BI-2536 similarly inhibited the growth of glioma cells and PLK1 inhibition had the added benefit of suppressing self-renewal and the expression of the CSC marker SOX2 (Lee et al., 2012b). BI-2536 also did not inhibit the growth of primary hematopoietic stem cells at concentrations that killed cancer stem cells. Multiple preclinical studies also reported that PLK1 inhibitors suppress the growth of glioma CSCs and primary cell growth in both adult and pediatric brain tumors (Danovi et al., 2013; Lee et al., 2012b; Pezuk et al., 2013). The reliance of many cancer cells on PLK1 is unquestionable and, as a result, several small molecule inhibitors have been developed against this important drug target. Targeting PLK1 in cancer has been used to overcome resistance to chemotherapy and has potential to improve the efficacy of current therapies (Gleixner et al., 2010).

As previously discussed in chapter 3, we were limited in the number and variety of primary MB surgical samples. Whether our model of BI-2536 sensitivity being dictated by high

PLK1 expression can be generalized to all four MB subgroups has yet to be determined. We only had access to primary SHH and Group 4 cells (Triscott et al., 2013), but the evaluation of the commonly metastatic Group 3 subgroup could have valuable implications for patient treatment. Further investigation of the characteristics of PLK1-low cells could also be explored. While our group and others have extensively tested the effects of inhibiting PLK1 in MB, an important proof-of-concept experiment would be to overexpress PLK1 in PLK1-low cells. Constitutive overexpression of PLK1 has been shown to cause neoplasm formation, which could suggest this may amplify tumorigenesis as well (Smith et al., 1997). This approach will further validate the therapeutic potential of PLK1 inhibitors, and provide clues into the accompanying signaling pathways that make PLK1-high brain tumors especially aggressive.

TCTP supports the growth and survival of SHH MB.

This is the first study to assess the importance of TCTP in MB. To our knowledge, this is also the first report of an association of TCTP expression and the SHH pathway in cancer. Like most of the pathways implicated in MB tumorigenesis, TCTP has distinct roles in developmental regulation. In mice, E9.5 TCTP knockout embryos have significantly reduced *Shh* at the posterior end, and are embryonic lethal (Chen et al., 2007). TCTP may have implications in signaling of other MB subtypes as it has also been reported to enhance WNT and β-catenin signaling (Bae et al., 2015; Gu et al., 2013). We are particularly interested in the association with the SHH subtype because patients from this group have poor survival outcomes with standard of care (Triscott et al., 2013).

It is important to note that the MB patient samples assessed in chapter 4 were exclusively pediatric patients. Outside of the confines of this study, we also had access to a very limited cohort of young adult MB cases. These cases were molecularly subtyped (data not shown) and, as expected from the literature (Northcott et al., 2011b), a majority was classified as SHH MB. Although low in number, the overall survival of adult SHH MB was dramatically better than the pediatric cases (Appendix A). The available clinical data showed a 79% and 25% 5-year survival rate for adult and pediatric SHH MB, respectively (n=29; Log Rank=0.029). It has previously been shown that pediatric and adult MBs are characteristically distinct (Northcott et al., 2011a), and may potentially originate from different cells of origin (Palma et al., 2005). An interesting

study would be to examine whether TCTP is also important in adult MB, and consider which oncogenic traits of the SHH subgroup it is responsible for driving.

An estimated 21% of SHH MB have *TP53* mutations (Zhukova et al., 2013); this includes both sporadic and familial Li-Fraumeni patients. Adding to this, p53 deactivation has previously been shown to activate SHH signaling in MB (Po et al., 2010). Our group and others suggest that targeting TCTP may promote the activation of cell cycle checkpoints, of which regulatory control is lost during carcinogenesis. The ability to re-activate apoptotic control checkpoints in cancer cells with dysfunctional DNA damage responses could help facilitate successful de-escalation of aggressive treatment regimes. More work needs to be done to test how targeting TCTP could improve the efficacy of radiation protocols and further determine whether TCTP functionality is linked directly to PLK1 kinase activity. The PLK1-TCTP pathway might offer an explanation to (1) why PLK1-high cases have a considerably worse outcome, (2) to better understand the molecular genesis of SHH subgroup of MB, and (3) further depict the relevance of PLK1 upregulation in p53 mutant cancers. A better understanding of TCTP signaling could offer an approach to overcome p53 suppression and promote the cell death of aggressive SHH MB.

In chapter 4 we present a promising preliminary assessment of TCTP in MB, but we were restricted by a number of limitations. We were privileged to have access to two independent patient cohorts, but, unfortunately, the accompanying clinical data were not available for the validation cases. A more robust analysis of the significance of TCTP in MB prognostication is needed and this will be addressed in continuing work. Additionally, we observed an interesting association between TCTP expression and p53 immunopositivity in patients. Although elevated levels of p53 in tissue is an established marker of its dysregulation (Tabori et al., 2010), it is unclear whether the cases in our study harbor mutations in *TP53*. If considered feasible, and based on the availability of tumor tissue, this can be evaluated by DNA sequencing or with one of many mutation-specific p53 IHC antibodies. Finally, chapter 4 uses the Daoy and ONS76 cell lines as models of p53 mutant and wild-type MB. Expansion of our work to multiple cell lines and primary patient-derived cells could have added value to support the findings of our study. Regardless, the evidence presented in this thesis proposes a crucial role for TCTP in the promotion of SHH MB.

Future work

Within this body of work, we associated PLK1 with poor prognosis and treatment-resistant disease. Moving forward, one goal would be to directly test whether targeting the PLK1 pathway can prevent tumor growth in a model of MB relapse. One future research model could involve the pretreatment of tumor-bearing mice with the chemotherapy cocktail used in chapter 3. Previous use of a Daoy cell orthotopic xenograft demonstrates that tumors will initially respond to chemotherapy but then fatally relapse (Triscott et al. 2013). We would want to examine how standard-of-care treatment influences changes in the expression of PLK1 and it's substrate P-TCTP^{Ser46}. Further, we need to collect further evidence showing that the new generation PLK1 inhibitor, BI-6727, can be used to overcome chemotherapy-resistant MB.

In order to conduct this research, we need to develop a robust animal model of MB that accurately reflects clinical disease, and is capable of accurate monitoring of tumor growth. Therefore, we were the first group in our institute to optimize an intracranial xenograft model that incorporates both luciferase and fluorescent labeling of Daoy MB cells. Appendix B outlines a technical report summarizing the work to date that has contributed the establishment of (1) a Luc2=tdT Daoy labeled system, (2) a surgical protocol, and (3) optimization of tumor monitoring. This animal model could be used to extend our current drug screening methods and provide a preclinical assessment of desirable dose and treatment scheduling for promising therapeutics like BI-6727 and DSF.

5.3 Clinical implications

The presented work has been conducted with the intent for direct clinical relevance to patient treatment. We were not only one of the first groups to independently validate the use of NanoString nCounter MB subtyping, but we were able to expand the original protocols with improved methods for FFPE RNA extraction (Northcott et al., 2012d, 2011b). Northcott and colleagues (2012d) had previously reported that RNA extracted from FFPE older than eight years could not be accurately subtyped; however, our group successfully classified cases using material older than 26 years. Accordingly, reproducibility is of the upmost importance in the development of diagnostic tests. Our initial subgroup classification (WNT, SHH, Group 3, and

Group 4) of retrospective cases was so effective that we were able to adapt our methods to allow subtyping of incoming MB patient tumors at BCCH.

The benefit of molecular subtyping has already been observed in other cancer types. Another group has successfully established the use of the NanoString nCounter system for the Prosigna™ breast cancer prognostic assay. This assay has recently been approved for clinical use in the United States and uses a 50 gene PAM50 signature to assign one of four possible molecular subtypes (Dowsett et al., 2013; Nielsen et al., 2010). Although not yet incorporated into standard decision-making for brain tumors, molecular subtyping will soon refine traditional techniques used by pathologists. This is imperative in the context of pediatric brain tumors. For example, a child with the diagnosis of a WNT MB could be spared from intensive radiation protocols, while a case classified as Group 3 could quickly be identified as a candidate for intensive therapy and/or Group 3 specific treatment being examined in clinical trials.

One of the goals of subclassification of brain tumors is to identify critical oncogenic pathways so that treatments can be personalized for specific subtypes. Although some tumor subtypes may favor the upregulation of a specific pathway (i.e., WNT or SHH), a major caveat of this approach is that no cellular pathway operates autonomously from other signals. This concept is exemplified with SMO inhibitors for the treatment of SHH MB (Low and De Sauvage, 2010). While targeting the signaling pathway that initially drove tumorigenesis provides a preliminary response, secondary pathways such as PI3K/AKT signaling have been reported to bypass this effect and activate GLI transcript activity even in the presence of SMO agonists (Buonamici et al., 2010; Dijkgraaf et al., 2011; Kool et al., 2014). Similarly, EGFR is commonly mutated in Classic and Neural subgroups of GBM; therefore, it is logical to assume EGFR specific inhibitors would benefit patients with these classifications (Libermann et al., 1984; Wong et al., 1992). Surprisingly, cancer is not this transparent and the survival benefit reported in trials that test the EGFR inhibitors, erlotinib, and gefitinib, for GBM also remains marginal (Brown et al., 2008; Franceschi et al., 2007; Prados et al., 2009; Rich et al., 2004).

This leads to the second point of this study's clinical importance. There remains a need for markers of prognosis that could be effectively targeted even in molecular subgroups that lack a "low hanging" signaling pathway. In chapter 3 we discovered that level *PLK1* transcript expression associated with poor outcome MB indiscriminate to subtype, and could be assessed

concurrently with the 22 gene minimal marker system used for molecular subtyping (Northcott et al., 2012d; Triscott et al., 2013). Also, in chapter 2 we showed that PLK1 was overexpressed in TMZ-resistant GBM cells (Triscott et al., 2012). Herein we propose incorporating PLK1 expression for the purpose of patient risk stratification. We provide evidence of the value of PLK1 as both a prognostic marker, and molecular target, by demonstrating the efficacy of PLK1 specific inhibitors.

There have been several clinical trials testing PLK1 inhibitors in cancer, most in the refractory setting where patients have failed all else (Table 5.1). To date, Phase I/II clinical trials using BI-2536 have mostly been tested in advanced metastatic tumors (Hofheinz et al.; Mross et al., 2008), followed by small cell carcinoma (Ellis et al., 2013), prostate cancer (Vose et al., 2013), leukemia (Müller-Tidow et al., 2013), lymphoma and non-small-cell lung carcinoma (NSCLC) (Gandhi et al., 2009). Phase I dose-establishing trials found 200mg treatments could produce high tissue distribution and total clearance with a promising pharmacokinetic profile (Mross et al., 2008; Vose et al., 2013). However, Phase II study results with BI-2536 as a monotherapy were not as promising and had a number of dose-limiting side effects such as neutropenia, nausea and anemia (Müller-Tidow et al., 2013; Sebastian et al., 2010). Further studies have therefore tested the efficacy of combinatorial treatments of BI-2536 with other chemotherapeutics. For example, one phase I clinical trial combined BI-2536 with pemetrexed in the treatment of non-small cell lung cancer patients (Ellis et al., 2013). Of the 41 patients involved in the trial, 54% had stable disease after the second cycle of pemetrexed (500mg/m^2) and BI-2536 once a week for three weeks. Two of these patients were reported to have confirmed partial responses to this combination (Ellis et al., 2013). While BI-2536 demonstrated some anti-tumoral promise in clinical tests, the suggested benefits were overshadowed by dose-limiting toxicities. As a result, this lead to the development of a second-generation PLK1 inhibitor, BI-6727.

BI-6727 is a small molecule with structural similarities to BI-2536. Interestingly, preclinical studies demonstrated multidrug resistance enhanced by CSC drivers such as ABC transport proteins might be overridden with the use of BI-6727. Drug screens of colon cancer *in vitro* suggest BI-6727 to be moderately synergistic with mitroxantrone and highly synergistic with paclitaxel (To et al., 2013). Similarly, work in prostate cancer suggests *in vitro* synergism

between BI-6727 and HDAC inhibitors; a relationship that warrants further clinical exploration (Wissing et al., 2010). A recent Phase I study established maximum tolerated dose using intravenous injection of BI-6727 in advanced solid malignancies. The inhibitor was generally well tolerated with partial responses evident in patients (Lin et al., 2014). Another Phase II clinical trial with BI-6727 as a single agent in metastatic urothelial cancer seemed less promising and suggests the inhibitor is best suited as a second-line treatment (Stadler et al., 2014). While there was no reported cumulative toxicity from the drug in either BI-6727 study, the greatest challenge is dose-limiting toxicities evident by thrombocytopenia and neutropenia (Lin et al., 2014; Sapkota et al., 2007; Stadler et al., 2014). Yet, this has not prevented the approval of PLK1 inhibitors by the Food and Drug Administration. In a press release last year, Volasertib was approved by the FDA and notably it was granted a Breakthrough Therapy designation (Aggarwal, 2014).

A single Phase I clinical trial has been conducted using GSK461364 as a monotherapy in order to characterize its pharmacodynamic and safety profile (Olmos et al., 2011). This PLK1 inhibitor has been recommended for advancement in further clinical testing. As well, a final ATP-competitive inhibitor has completed a Phase I clinical trail for NSM-1286937. TKM-080301 was then implemented in Phase I clinical trials that showed a promising toxicity profile and confirmed RNAi effect in patients with liver cancer (Ramanathan et al., 2013). Although Phase II trials are presently being conducted for neuroendocrine and liver malignancies, this option has not been examined for brain tumors (Table 5.1).

A third clinical implication of this study was an unanticipated result from the mechanistic characterization of the PLK1 substrate, TCTP. The phosphorylation of TCTP is a useful marker of PLK1 kinase activity (Cucchi et al., 2010), and we are the first group to validate P-TCTP^{Ser46} for this purpose in MB. In future clinical trials, P-TCTP^{Ser46} levels could be used to gauge the efficacy of PLK1 inhibitor activity in patient tissues. Perhaps more importantly, the studies in chapter 4 introduce TCTP as a significant marker of overall survival for pediatric MB that correlates with possible p53 dysregulation and is enriched in the SHH subtype. Although preliminary, our work suggests that the inhibition of TCTP may re-enable cell cycle checkpoint activation in both *TP53* mutant and wild-type tumor models. This could have wide-spread implications as *TP53* is the most commonly mutated genes across a multitude of cancer types

(Forbes et al., 2011; Vogelstein et al., 2000). Manipulation of p53 via TCTP may be a future approach to enhancing the efficacy of standard treatment (Amson et al., 2011; Hong and Choi, 2013; J. Zhang et al., 2012) and even trigger apoptosis in PLK1-high cancer cells. More work needs to be done to examine further the functional role (1) of the PLK1-TCTP pathway in regard to p53 signaling, and (2) of TCTP in response to γ-radiation in MB.

A final, and perhaps most translatable, clinical implication resulting from this thesis is the proposed repurposing the anti-alcoholism drug, DSF, for the treatment of brain tumors. While PLK1 inhibitors are attractive for many reasons, their downside is dose-limiting toxicities. The main side effect is neutropenia. DSF on the other hand is not commonly associated with neutropenia suggesting that its mode of action, while reported to reduce PLK1 expression levels by ~50% (Triscott et al., 2012), has a better safety profile. In fact, the safety profile of DSF has been put to practice for decades. Researchers are now attempting to establish which DSF dosing schedule and chemotherapeutic combination will deliver the greatest inhibitory response from tumor cells. *In vitro* studies suggest that there is an additive effect that results from the combination of DSF with buthionine sulfoximine, a gamma-glutamyl-cysteine synthase inhibitor (Cen et al., 2002). As well, combining DSF with copper can act synergistically with cisplatin to prevent lung cancer proliferation (Duan et al., 2014). Recently it was shown that the survival of patients with stage IV non-small cell lung cancer could be prolonged by combining DSF with current cisplatin and vinorelbrine protocols (Nechushtan et al., 2015). Our preclinical studies that combined DSF with TMZ did not demonstrate an additive or synergistic effect, but DSF treatment alone was sufficient to almost completely eliminate GBM cell proliferation. The only adverse side effect reported is hepatotoxicity when DSF is prescribed at high doses. An added benefit is that the cost to treat a patient for a year with DSF is estimated to be approximately $550 (Cvek, 2011), which is less than 1% the estimated cost of treating the average cancer patient with current protocols (Fojo and Grady, 2009; Wasserfallen et al., 2005). Following the publication of the content in chapter 2 (Triscott et al., 2012), two ongoing clinical trials have been initiated which test DSF in GBM (ClinicalTrials.gov Identifiers NCT01907165 and NCT01777919) (Table 5.2). Both of these trials will test the combination of DSF with TMZ compared to patients treated with only the standard TMZ protocols.

Concluding remarks

Malignancies of the brain are not only life-threatening, but the manner in which patients are treated has implications that are unlike any other cancer type. The brain is "the seat of an individual's literal sense of identity", the manifestation of behavior, and cognizance of one's existence (Lipsman et al., 2007). The tragedy of high-grade brain tumors has recently been exemplified in a highly publicized case of GBM whereby the patient chose to end her own life as an alternative to enduring the disease and its anticipated treatment protocols (Printz, 2015). Adding to this, the efficacy of successful therapies for pediatric MB charges a high cost to quality of life and cognitive function. Therefore, the goal of this work has been to identify key molecular factors that can refine prognostication and be targeted with preexisting compounds already tested in clinical trials.

The present findings outlined in this thesis prompt the development of PLK1 directed therapeutics for the treatment of GBM and MB. We show that PLK1 is up-regulated in poor prognosis disease, and its expression persists following standard chemotherapy treatments, such as TMZ. The measurement of PLK1 provides a marker of prognostication that could be used to dictate the de-escalation of high-intensity therapy for pediatric patients. Similarly, we discovered that PLK1-high cases could be targeted with specific inhibitors that are capable of crossing the BBB. Adding to this, we characterized the PLK1 substrate, TCTP and provide preliminary findings that implicate TCTP in the tumorigenesis of SHH MB. Taken together, this work adds to the growing body of knowledge on targetable molecules that can contribute to the personalization of cancer treatment.

Here we provide preclinical evidence that supports the use of PLK1 inhibitors for clinical trials in high-grade brain tumors. But, perhaps most importantly, we discovered that the off-patent drug DSF eliminates PLK1-high tumor cells and has the potential to be immediately translated into clinical use. In summary, our work encourages the investigation of PLK1 in high-grade brain tumors and emphasizes the practice of fighting cancer with repurposed drugs in order to pave the way for future targeted options.

Compound	Clinical Trial Indentifier	Disease	Study Phase	Status	Sponsor
BI-2536	NCT02211872	Advanced, non resectable, or metastatic tumors	Phase I	Completed	Boehringer Ingelheim
	NCT02211833	NSCLC	Phase I	Completed	Boehringer Ingelheim
	NCT02215044	Pancreatic Neoplasms	Phase I	Terminated	Boehringer Ingelheim
	NCT02211859	Advanced solid tumors	Phase I	Completed	Boehringer Ingelheim
	NCT00243087	Lymphoma	Phase I	Completed	Boehringer Ingelheim
	NCT00710710	Pancreatic Neoplasms	Phase II	Completed	Boehringer Ingelheim
	NCT00376623	NSCLC	Phase II	Completed	Boehringer Ingelheim
	NCT00701766	AML	Phase II	Completed	Boehringer Ingelheim
	NCT00706498	Prostate Cancer	Phase II	Completed	Boehringer Ingelheim
	NCT00526149	Breast, Endometrial, Head & Neck, Ovarian cancers, Sarcoma, Melanoma	Phase II	Completed	EORTC
	NCT00412880	Carcinoma, Small Cell	Phase II	Completed	Boehringer Ingelheim
BI-6727, Volasertib	NCT00969761	Advanced solid tumors	Phase I	Completed	Boehringer Ingelheim
	NCT01022853	Advanced solid tumors	Phase I	Completed	Boehringer Ingelheim
	NCT01145885	Advanced solid tumors	Phase I	Completed	Boehringer Ingelheim
	NCT01206816	Advanced solid tumors	Phase I	Completed	Boehringer Ingelheim
	NCT01348347	Advanced solid tumors	Phase I	Completed	Boehringer Ingelheim
	NCT01662505	AML	Phase I	Active	Boehringer Ingelheim
	NCT02003573	AML	Phase I	Active	Boehringer Ingelheim
	NCT00969553	Solid tumors	Phase I	Completed	Boehringer Ingelheim
	NCT02273388	Advanced solid tumors	Phase I	Completed	Boehringer Ingelheim
	NCT02201329	CMML	Phase I	Active	Boehringer Ingelheim
	NCT01957644	CMML	Phase I	Active	Boehringer Ingelheim
	NCT01971476	Advanced pediatric cancers	Phase I	Active	Boehringer Ingelheim
	NCT00804856	AML	Phase II	Active	Boehringer Ingelheim
	NCT00824408	NSCLC	Phase II	Active	Boehringer Ingelheim
	NCT01023958	Urothelial cancer	Phase II	Completed	Boehringer Ingelheim
	NCT01121406	Ovarian Cancer	Phase II	Completed	Boehringer Ingelheim
	NCT02198482	AML	Phase II	Not open yet	University of Ulm
	NCT01721876	AML	Phase III	Active	Boehringer Ingelheim
GSK461364	NCT00536835	Advanced Solid Tumor, Lymphoma, Non-Hodgkin, Non-Hodgkin's Lymphoma	Phase I	Completed	GlaxoSmithKline
TAK-960	NCT01179399	Advanced Nonhematological Malignancies	Phase I	Terminated	Millennium Pharmaceuticals, Inc.
NMS-1286937	NCT01014429	Metastatic solid tumors	Phase I	Completed	Nerviano Medical Sciences
TKM-080301	NCT01437007	Liver Cancer	Phase I	Completed	National Cancer Institute (NCI)
	NCT01262235	Neuroendocrine tumors, Adrenocortical Carcinoma	Phase I/ II	Active	Tekmira Pharmaceuticals Corporation
	NCT02191878	Hepatocellular carcinoma, Hepatoma, Liver Cancer, Liver Cell Carcinoma	Phase I/ II	Active	Tekmira Pharmaceuticals Corporation

Identifiers in reference to www.clinicaltrials.gov online database, accessed April 2014

Table 5.1 Clinical trials of PLK1 inhibitors in cancer.

Clinical Trial Identifier*	Disease	Study Phase	Sponsor	Enrollment	Status	Start/Completion Dates
NCT00742911	Advanced Solid malignancy with liver metastasis	Phase I	University of Utah	21	Completed	July 2008-March 2013
NCT00571116	Metastatic Melanoma	Phase I	University of California, Irvine	15	Terminated**	September 2006-August 2012
NCT00256230	Metastatic Melanoma	Phase I/II	University of California, Irvine	7	Completed	January 2002-August 2007
NCT01777919	Glioblastoma	Phase II	Olympion Medical Center	TBD	Not active yet	September 2015-Septembr 2018
NCT00312819	NSCLC	Phase II/III	Hadassah Medical Organization	60	Completed	March 2006-December 2009
NCT01118741	Prostate Cancer	Phase I/II	Johns Hopkins University	19	Completed	May 2010-June 2012
NCT01907165	Glioblastoma	Phase II	Washington University School of Medicine	TBD	Active	October 2013-December 2017

*Identifiers in reference to www.clinicaltrials.gov online database, accessed September 2014
** Lack of study funding and slow accrual
Adapted from (Triscott et al., 2015)
TBD: to be determined

Table 5.2 Clinical trials involving DSF in cancer.

REFERENCES

Adamson, D.C., Shi, Q., Wortham, M., Northcott, P.A., Di, C., Duncan, C.G., Li, J., McLendon, R.E., Bigner, D.D., Taylor, M.D., Yan, H., 2009. OTX2 Is Critical for the Maintenance and Progression of Shh-Independent Medulloblastomas. Cancer Res. 70, 181–191.

Agarwal, S., Manchanda, P., Vogelbaum, M. a., Ohlfest, J.R., Elmquist, W.F., 2013. Function of the blood-brain barrier and restriction of drug delivery to invasive glioma cells: Findings in an orthotopic rat xenograft model of glioma. Drug Metab. Dispos. 41, 33–39.

Aggarwal, S.R., 2014. A survey of breakthrough therapy designations. Nat. Biotechnol. 32, 323–30.

Ahlfeld, J., Favaro, R., Pagella, P., Kretzschmar, H. a, Nicolis, S., Schüller, U., 2013. Sox2 requirement in Sonic hedgehog-associated medulloblastoma. Cancer Res. 73, 3796–3807.

Alcantara Llaguno, S., Chen, J., Kwon, C.H., Jackson, E.L., Li, Y., Burns, D.K., Alvarez-Buylla, A., Parada, L.F., 2009. Malignant Astrocytomas Originate from Neural Stem/Progenitor Cells in a Somatic Tumor Suppressor Mouse Model. Cancer Cell 15, 45–56.

Alder, J., Lee, K.J., Jessell, T.M., Hatten, M.E., 1999. Generation of cerebellar granule neurons in vivo by transplantation of BMP-treated neural progenitor cells. Nat. Neurosci. 2, 535–540.

Althaus, F.R., Kleczkowska, H.E., Malanga, M., Müntener, C.R., Pleschke, J.M., Ebner, M., Auer, B., 1999. Poly ADP-ribosylation: a DNA break signal mechanism. Mol. Cell. Biochem. 193, 5–11.

Amson, R., Pece, S., Lespagnol, A., Vyas, R., Mazzarol, G., Tosoni, D., Colaluca, I., Viale, G., Rodrigues-Ferreira, S., Wynendaele, J., Chaloin, O., Hoebeke, J., Marine, J.-C., Di Fiore, P.P., Telerman, A., 2011. Reciprocal repression between P53 and TCTP. Nat. Med. 18, 91–99.

Ando, K., Ozaki, T., Yamamoto, H., Furuya, K., Hosoda, M., Hayashi, S., Fukuzawa, M., Nakagawara, A., 2004. Polo-like kinase 1 (Plk1) inhibits p53 function by physical interaction and phosphorylation. J. Biol. Chem. 279, 25549–61.

Angley, C., Kumar, M., Dinsio, K.J., Hall, A.K., Siegel, R.E., 2003. Signaling by bone morphogenetic proteins and Smad1 modulates the postnatal differentiation of cerebellar cells. J. Neurosci. 23, 260–268.

Archambault, V., Lépine, G., Kachaner, D., 2015. Understanding the Polo Kinase machine. Oncogene 1–9.

Arnaud, L., Pines, J., Nigg, E. a., 1998. GFP tagging reveals human Polo-like kinase 1 at the kinetochore/centromere region of mitotic chromosomes. Chromosoma 107, 424–429.

Bae, S., Kim, H.J., Lee, K., Lee, K., 2015. Translationally Controlled Tumor Protein induces epithelial to mesenchymal transition and promotes cell migration , invasion and metastasis 1–9.

Bai, R., Siu, I.-M., Tyler, B.M., Staedtke, V., Gallia, G.L., Riggins, G.J., 2010. Evaluation of retinoic acid therapy for OTX2-positive medulloblastomas. Neuro. Oncol. 12, 655–663.

Baker, S.D., Wirth, M., Statkevich, P., Reidenberg, P., Alton, K., Sartorius, S.E., Dugan, M., Cutler, D., Batra, V., Grochow, L.B., Donehower, R.C., Rowinsky, E.K., 1999. Absorption, metabolism, and excretion of 14C-temozolomide following oral administration to patients with advanced cancer. Clin. cancer Res. 5, 309–317.

Bao, S., Wu, Q., McLendon, R.E., Hao, Y., Shi, Q., Hjelmeland, A.B., Dewhirst, M.W., Bigner, D.D., Rich, J.N., 2006. Glioma stem cells promote radioresistance by preferential activation of the DNA damage response. Nature 444, 756–60.

Barker, F.C., Chang, S.M., Gutin, P.H., Malec, M.K., McDermott, M.W., Prados, M.D., Wilson, C.B., 1998. Survival and functional status after resection of recurrent glioblastoma multiforme. Neurosurgery 42, 709–723.

Barth, R.F., 1998. Rat brain tumor models in experimental neuro-oncology: the 9L, C6, T9, F98, RG2 (D74), RT-2 and CNS-1 gliomas. J. Neurooncol. 36, 91–102.

Bartlett, F., Kortmann, R., Saran, F., 2013. Medulloblastoma. Clin. Oncol. (R. Coll. Radiol). 25, 36–45.

Bassermann, F., Frescas, D., Guardavaccaro, D., Busino, L., Peschiaroli, A., Pagano, M., 2008. The Cdc14B-Cdh1-Plk1 axis controls the G2 DNA-damage-response checkpoint. Cell 134, 256–67.

Bastos, R.N., Barr, F.A., 2010. Plk1 negatively regulates Cep55 recruitment to the midbody to ensure orderly abscission. J. Cell Biol. 191, 751–60.

Baylot, V., Katsogiannou, M., Andrieu, C., Taieb, D., Acunzo, J., Giusiano, S., Fazli, L., Gleave, M., Garrido, C., Rocchi, P., 2012. Targeting TCTP as a new therapeutic strategy in castration-resistant prostate cancer. Mol. Ther. 20, 2244–2256.

Bazile, F., Pascal, A., Arnal, I., Le Clainche, C., Chesne, F., Kubiak, J.Z., 2009. Complex relationship between TCTP, microtubules and actin microfilaments regulates cell shape in normal and cancer cells. Carcinogenesis 30, 555–565.

Beck, J., Maerki, S., Posch, M., Metzger, T., Persaud, A., Scheel, H., Hofmann, K., Rotin, D., Pedrioli, P., Swedlow, J.R., Peter, M., Sumara, I., 2013. Ubiquitylation-dependent localization of PLK1 in mitosis. Nat. Cell Biol. 15, 430–439.

Begley, D.J., 2004. ABC transporters and the blood-brain barrier. Curr. Pharm. Des. 10, 1295–1312.

Bhatia, R., Tahir, M., Chandler, C.L., 2009. The management of hydrocephalus in children with posterior fossa tumours: the role of pre-resectional endoscopic third ventriculostomy. Pediatr. Neurosurg. 45, 186–91.

Blough, M.D., Westgate, M.R., Beauchamp, D., Kelly, J.J., Stechishin, O., Ramirez, A.L., Weiss, S., Cairncross, J.G., 2010. Sensitivity to temozolomide in brain tumor initiating cells. Neuro. Oncol. 12, 756 – 760.

Brinster, R.L., Chen, H.Y., Messing, A., van Dyke, T., Levine, A.J., Palmiter, R.D., 1984. Transgenic mice harboring SV40 T-antigen genes develop characteristic brain tumors. Cell 37, 367–79.

Brosh, R., Rotter, V., 2009. When mutants gain new powers: news from the mutant p53 field. Nat. Rev. Cancer 9, 701–13.

Brown, P.D., Krishnan, S., Sarkaria, J.N., Wu, W., Jaeckle, K. a., Uhm, J.H., Geoffroy, F.J., Arusell, R., Kitange, G., Jenkins, R.B., Kugler, J.W., Morton, R.F., Rowland, K.M., Mischel, P., Yong, W.H., Scheithauer, B.W., Schiff, D., Giannini, C., Buckner, J.C., 2008. Phase I/II trial of erlotinib and temozolomide with radiation therapy in the treatment of newly diagnosed glioblastoma multiforme: North central cancer treatment group study N0177. J. Clin. Oncol. 26, 5603–5609.

Budman, D.R., Calabro, A., 2002. In vitro search for synergy and antagonism: Evaluation of docetaxel combinations in breast cancer cell lines. Breast Cancer Res. Treat. 74, 41–46.

Bunt, J., Hasselt, N.A., Zwijnenburg, D.A., Koster, J., Versteeg, R., Kool, M., 2013. OTX2 sustains a bivalent-like state of OTX2-bound promoters in medulloblastoma by maintaining their H3K27me3 levels. Acta Neuropathol. 125, 385–94.

Buonamici, S., Williams, J., Morrissey, M., Wang, A., Guo, R., Vattay, A., Hsiao, K., Yuan, J., Green, J., Ospina, B., Yu, Q., Ostrom, L., Fordjour, P., Anderson, D.L., Monahan, J.E., Kelleher, J.F., Peukert, S., Pan, S., Wu, X., Maira, S.-M., García-Echeverría, C., Briggs, K.J., Watkins, D.N., Yao, Y., Lengauer, C., Warmuth, M., Sellers, W.R., Dorsch, M., 2010. Interfering with resistance to smoothened antagonists by inhibition of the PI3K pathway in medulloblastoma. Sci. Transl. Med. 2, 51ra70.

Burkhardt, J.-K., Shin, B.J., Boockvar, J.A., 2011. Neural Stem Cells and Glioma Stem-like Cells Respond Differently to Chemotherapeutic Drugs: Selectivity at the Cellular Level. Neurosugery 68, N21–22.

Burton, E.C., Lamborn, K.R., Forsyth, P., Scott, J., O'Campo, J., Uyehara-Lock, J., Prados, M., Berger, M., Passe, S., Uhm, J., O'Neill, B.P., Jenkins, R.B., Aldape, K.D., 2002. Aberrant p53, mdm2, and proliferation differ in glioblastomas from long-term compared with typical survivors. Clin. Cancer Res. 8, 180–187.

Cahill, D.P., Levine, K.K., Betensky, R. a., Codd, P.J., Romany, C. a., Reavie, L.B., Batchelor, T.T., Futreal, P.A., Stratton, M.R., Curry, W.T., Lafrate, a. J., Louis, D.N., 2007. Loss of the mismatch repair protein MSH6 in human glioblastomas is associated with tumor progression during temozolomide treatment. Clin. Cancer Res. 13, 2038–2045.

Carmena, M., Pinson, X., Platani, M., Salloum, Z., Xu, Z., Clark, A., MacIsaac, F., Ogawa, H., Eggert, U., Glover, D.M., Archambault, V., Earnshaw, W.C., 2012. The Chromosomal Passenger Complex Activates Polo Kinase at Centromeres. PLoS Biol. 10, e1001250.

Carrie, C., Hoffstetter, S., Gomez, F., Moncho, V., Doz, F., Alapetite, C., Murraciole, X., Maire, J.P., Benhassel, M., Chapet, S., Quetin, P., Kolodie, H., Lagrange, J.L., Cuillere, J.C., Habrand, J.L., 1999. Impact of targeting deviations on outcome in medulloblastoma: study of the French Society of Pediatric Oncology (SFOP). Int. J. Radiat. Oncol. Biol. Phys. 45, 435–9.

Carvalho-Santos, Z., Machado, P., Branco, P., Tavares-Cadete, F., Rodrigues-Martins, A., Pereira-Leal, J.B., Bettencourt-Dias, M., 2010. Stepwise evolution of the centriole-assembly pathway. J. Cell Sci. 123, 1414–1426.

Casenghi, M., Barr, F.A., Nigg, E.A., 2005. Phosphorylation of Nlp by Plk1 negatively regulates its dynein-dynactin-dependent targeting to the centrosome. J. Cell Sci. 118, 5101–8.

Casenghi, M., Meraldi, P., Weinhart, U., Duncan, P.I., Körner, R., Nigg, E.A., 2003. Polo-like kinase 1 regulates Nlp, a centrosome protein involved in microtubule nucleation. Dev. Cell 5, 113–25.

Cen, D., Gonzalez, R.I., Buckmeier, J.A., Kahlon, R.S., Tohidian, N.B., Meyskens, F.L., 2002. Disulfiram Induces Apoptosis in Human Melanoma Cells : A Redox-related Process. Drugs 1, 197–204.

Cha, S., 2006. Update on brain tumor imaging: from anatomy to physiology. AJNR. Am. J. Neuroradiol. 27, 475–87.

Chang, C.H., Housepian, E.M., Herbert, C., 1969. An Operative Staging System and a Megavoltage Radiotherapeutic Technic for Cerebellar Medulloblastomas 1. Radiology 93, 1351–1359.

Chen, D., Cui, Q.C., Yang, H., Dou, Q.P., 2006. Disulfiram, a clinically used anti-alcoholism drug and copper-binding agent, induces apoptotic cell death in breast cancer cultures and xenografts via inhibition of the proteasome activity. Cancer Res. 66, 10425–33.

Chen, H., Li, X., Li, W., Zheng, H., 2015. miR-130a can predict response to temozolomide in patients with glioblastoma multiforme, independently of O6-methylguanine-DNA methyltransferase. J. Transl. Med. 13, 69.

Chen, J., Li, Y., Yu, T.-S., McKay, R.M., Burns, D.K., Kernie, S.G., Parada, L.F., 2012. A restricted cell population propagates glioblastoma growth after chemotherapy. Nature 488, 522–526.

Chen, S.H., We, P.-S., Chou, C.-H., Yan, Y.-T., Liu, H., Weng, S.-Y., Yang-Yen, H.-F., 2007. A knockout mouse approach reveals that TCTP functions as an essential factor for cell proliferation and survival in a tissue- or cell type- specific manner. Mol. Biol. Cell 18, 2525–2532.

Chen, W., 2007. Clinical applications of PET in brain tumors. J. Nucl. Med. 48, 1468–81.

Chi, S.N., Gardner, S.L., Levy, A.S., Knopp, E. a., Miller, D.C., Wisoff, J.H., Weiner, H.L., Finlay, J.L., 2004. Feasibility and response to induction chemotherapy intensified with high-dose methotrexate for young children with newly diagnosed high-risk disseminated medulloblastoma. J. Clin. Oncol. 22, 4881–4887.

Cho, Y.-J., Tsherniak, A., Tamayo, P., Santagata, S., Ligon, A., Greulich, H., Berhoukim, R., Amani, V., Goumnerova, L., Eberhart, C.G., Lau, C.C., Olson, J.M., Gilbertson, R.J., Gajjar, A., Delattre, O., Kool, M., Ligon, K., Meyerson, M., Mesirov, J.P., Pomeroy, S.L., 2011. Integrative genomic analysis of medulloblastoma identifies a molecular subgroup that drives poor clinical outcome. J. Clin. Oncol. 29, 1424–30.

Choi, S.A., Choi, J.W., Wang, K.-C., Phi, J.H., Lee, J.Y., Park, K.D., Eum, D., Park, S.-H., Kim, I.H., Kim, S.-K., 2014a. Disulfiram modulates stemness and metabolism of brain tumor initiating cells in atypical teratoid/rhabdoid tumors. Neuro. Oncol. 1–11.

Choi, S.A., Lee, J.Y., Phi, J.H., Wang, K.-C., Park, C.-K., Park, S.-H., Kim, S.-K., 2014b. Identification of brain tumour initiating cells using the stem cell marker aldehyde dehydrogenase. Eur. J. Cancer 50, 137–49.

Chong, C.R., Sullivan, D.J., 2007. New uses for old drugs. Nature 448, 645–646.

Chu, Y., Yao, P.Y., Wang, W., Wang, D., Wang, Z., Zhang, L., Huang, Y., Ke, Y., Ding, X., Yao, X., 2011. Aurora B kinase activation requires survivin priming phosphorylation by PLK1. J. Mol. Cell Biol. 3, 260–7.

Ciani, L., Salinas, P.C., 2005. WNTs in the vertebrate nervous system: from patterning to neuronal connectivity. Nat. Rev. Neurosci. 6, 351–62.

Coloma, M.J., Lee, H.J., Kurihara, A., Landaw, E.M., Boado, R.J., Morrison, S.L., Pardridge, W.M., 2000. Transport across the primate blood-brain barrier of a genetically engineered chimeric monoclonal antibody to the human insulin receptor. Pharm Res 17, 266–274.

Corti, S., Locatelli, F., Papadimitriou, D., Donadoni, C., Salani, S., Del Bo, R., Strazzer, S., Bresolin, N., Comi, G.P., 2006. Identification of a primitive brain-derived neural stem cell population based on aldehyde dehydrogenase activity. Stem Cells 24, 975–85.

Costello, J.F., Berger, M.S., Huang, H.S., Cavenee, W.K., 1996. Silencing of p16/CDKN2 expression in human gliomas by methylation and chromatin condensation. Cancer Res. 56, 2405–10.

Cowan, R., Hoban, P., Kelsey, A., Birch, J.M., Gattamaneni, R., Evans, D.G., 1997. The gene for the naevoid basal cell carcinoma syndrome acts as a tumour-suppressor gene in medulloblastoma. Br. J. Cancer 76, 141–145.

Crawford, J.R., MacDonald, T.J., Packer, R.J., 2007. Medulloblastoma in childhood: new biological advances. Lancet. Neurol. 6, 1073–85.

Cucchi, U., Gianellini, L.M., De Ponti, A., Sola, F., Alzani, R., Patton, V., Pezzoni, A., Troiani, S., Saccardo, M.B., Rizzi, S., Giorgini, M.L., Cappella, P., Beria, I., Valsasina, B., 2010. Phosphorylation of TCTP as a marker for polo-like kinase-1 activity in vivo. Anticancer Res. 30, 4973–85.

Cvek, B., 2011. Nonprofit drugs as the salvation of the world's healthcare systems: the case of Antabuse (disulfiram). Drug Discov. Today 17, 409–412.

Dahmane, N., Lee, J., Robins, P., Heller, P., Ruiz i Altaba, A., 1997. Activation of the transcription factor Gli1 and the Sonic hedgehog signalling pathway in skin tumours. Nature 389, 876–81.

Dang, L., White, D.W., Gross, S., Bennett, B.D., Bittinger, M.A., Driggers, E.M., Fantin, V.R., Jang, H.G., Jin, S., Keenan, M.C., Marks, K.M., Prins, R.M., Ward, P.S., Yen, K.E., Liau, L.M., Rabinowitz, J.D., Cantley, L.C., Thompson, C.B., Vander Heiden, M.G., Su, S.M., 2009. Cancer-associated IDH1 mutations produce 2-hydroxyglutarate. Nature 462, 739–744.

Danovi, D., Folarin, A., Gogolok, S., Ender, C., Elbatsh, A.M.O., Engström, P.G., Stricker, S.H., Gagrica, S., Georgian, A., Yu, D., U, K.P., Harvey, K.J., Ferretti, P., Paddison, P.J., Preston, J.E., Abbott, N.J., Bertone, P., Smith, A., Pollard, S.M., 2013. A High-Content Small Molecule Screen Identifies Sensitivity of Glioblastoma Stem Cells to Inhibition of Polo-Like Kinase 1. PLoS One 8, e77053.

Degenhardt, Y., Greshock, J., Laquerre, S., Gilmartin, A.G., Jing, J., Richter, M., Zhang, X., Bleam, M., Halsey, W., Hughes, A., Moy, C., Liu-Sullivan, N., Powers, S., Bachman, K., Jackson, J., Weber, B., Wooster, R., 2010. Sensitivity of cancer cells to Plk1 inhibitor GSK461364A is associated with loss of p53 function and chromosome instability. Mol. Cancer Ther. 9, 2079–89.

Degenhardt, Y., Lampkin, T., 2010. Targeting polo-like kinase in cancer therapy. Clin. Cancer Res. 16, 384–389.

Deleyrolle, L.P., Harding, A., Cato, K., Siebzehnrubl, F. a, Rahman, M., Azari, H., Olson, S., Gabrielli, B., Osborne, G., Vescovi, A., Reynolds, B. a, 2011. Evidence for label-retaining tumour-initiating cells in human glioblastoma. Brain 134, 1331–1343.

Deleyrolle, L.P., Reynolds, B.A., 2009. Isolation, expansion, and differentiation of adult Mammalian neural stem and progenitor cells using the neurosphere assay. Methods Mol Biol 549, 91–101.

Dell'Albani, P., 2008. Stem cell markers in gliomas. Neurochem Res 33, 2407–2415.

Delmore, J.E., Issa, G.C., Lemieux, M.E., Rahl, P.B., Shi, J., Jacobs, H.M., Kastritis, E., Gilpatrick, T., Paranal, R.M., Qi, J., Chesi, M., Schinzel, A.C., McKeown, M.R., Heffernan, T.P., Vakoc, C.R., Bergsagel, P.L., Ghobrial, I.M., Richardson, P.G., Young, R. a., Hahn, W.C., Anderson, K.C., Kung, A.L., Bradner, J.E., Mitsiades, C.S., 2011. BET bromodomain inhibition as a therapeutic strategy to target c-Myc. Cell 146, 904–917.

Dhall, G., Grodman, H., Ji, L., Sands, S., Gardner, S., Dunkel, I.J., McCowage, G.B., Diez, B., Allen, J.C., Gopalan, A., Cornelius, A.S., Termuhlen, A., Abromowitch, M., Sposto, R., Finlay, J.L., 2008. Outcome of children less than three years old at diagnosis with non-metastatic medulloblastoma treated with chemotherapy on the "Head Start" I and II protocols. Pediatr. Blood Cancer 50, 1169–75.

Diehn, M., Cho, R.W., Lobo, N. a, Kalisky, T., Dorie, M.J., Kulp, A.N., Qian, D., Lam, J.S., Ailles, L.E., Wong, M., Joshua, B., Kaplan, M.J., Wapnir, I., Dirbas, F.M., Somlo, G., Garberoglio, C., Paz, B., Shen, J., Lau, S.K., Quake, S.R., Brown, J.M., Weissman, I.L., Clarke, M.F., 2009. Association of reactive oxygen species levels and radioresistance in cancer stem cells. Nature 458, 780–3.

Dietzmann, K., Kirches, E., Bossanyi, P. von, Jachau, K., Mawrin, C., 2001. Increased Human Polo-Like Kinase-1 Expression in Gliomas. J. Neurooncol. 53, 1–11.

Dijkgraaf, G.J.P., Alicke, B., Weinmann, L., Januario, T., West, K., Modrusan, Z., Burdick, D., Goldsmith, R., Robarge, K., Sutherlin, D., Scales, S.J., Gould, S.E., Yauch, R.L., De Sauvage, F.J., 2011. Small molecule inhibition of GDC-0449 refractory smoothened mutants and downstream mechanisms of drug resistance. Cancer Res. 71, 435–444.

DiMasi, J. a., Hansen, R.W., Grabowski, H.G., 2003. The price of innovation: New estimates of drug development costs. J. Health Econ. 22, 151–185.

Donson, A.M., Addo-yobo, S.O., Handler, M.H., Gore, L., Foreman, N.K., 2007. MGMT Promoter Methylation Correlates With Survival Benefit and Sensitivity to Temozolomide in Pediatric Glioblastoma. Pediatr. Blood Cancer 403–407.

Down, C.F., Millour, J., Lam, E.W.-F., Watson, R.J., 2012. Binding of FoxM1 to G2/M gene promoters is dependent upon B-Myb. Biochim. Biophys. Acta 1819, 855–62.

Dowsett, M., Sestak, I., Lopez-Knowles, E., Sidhu, K., Dunbier, A.K., Cowens, J.W., Ferree, S., Storhoff, J., Schaper, C., Cuzick, J., 2013. Comparison of PAM50 risk of recurrence score with oncotype DX and IHC4 for predicting risk of distant recurrence after endocrine therapy. J. Clin. Oncol. 31, 2783–90.

Duan, L., Shen, H., Zhao, G., Yang, R., Cai, X., Zhang, L., Jin, C., Huang, Y., 2014. Inhibitory effect of Disulfiram/copper complex on non-small cell lung cancer cells. Biochem. Biophys. Res. Commun. 446, 1010–6.

Dubuc, A.M., Remke, M., Korshunov, A., Northcott, P. a, Zhan, S.H., Mendez-Lago, M., Kool, M., Jones, D.T.W., Unterberger, A., Morrissy, a S., Shih, D., Peacock, J., Ramaswamy, V., Rolider, A., Wang, X., Witt, H., Hielscher, T., Hawkins, C., Vibhakar, R., Croul, S., Rutka, J.T., Weiss, W. a, Jones, S.J.M., Eberhart, C.G., Marra, M. a, Pfister, S.M., Taylor, M.D., 2012. Aberrant patterns of H3K4 and H3K27 histone lysine methylation occur across subgroups in medulloblastoma. Acta Neuropathol. 125, 373–384.

Duffner, P.K., Horowitz, M.E., Krischer, J.P., Friedman, H.S., Burger, P.C., Cohen, M.E., Sanford, R.A., Mulhern, R.K., James, H.E., Freeman, C.R., 1993. Postoperative chemotherapy and delayed radiation in children less than three years of age with malignant brain tumors. N. Engl. J. Med. 328, 1725–31.

Duncan, C.G., Killela, P.J., Payne, C.A., Chen, W.C., Liu, J., Solomon, D., Waldman, T., Aaron, J., Gregory, S.G., Mcdonald, K.L., Mclendon, R.E., Darell, D., 2010. Integrated genomic analyses identify ERRFI1 and TACC3 as glioblastoma- targeted genes ABSTRACT : 1, 265–277.

Dupuy, A.J., Akagi, K., Largaespada, D.A., Copeland, N.G., Jenkins, N.A., 2005. Mammalian mutagenesis using a highly mobile somatic Sleeping Beauty transposon system. Nature 436, 221–6.

Eberhart, C.G., 2012. Three down and one to go: modeling medulloblastoma subgroups. Cancer Cell 21, 137–8.

Eberhart, C.G., 2008. Even Cancers Want Commitment: Lineage Identity and Medulloblastoma Formation. Cancer Cell 14, 105–107.

Eberhart, C.G., Kepner, J.L., Goldthwaite, P.T., Kun, L.E., Duffner, P.K., Friedman, H.S., Strother, D.R., Burger, P.C., 2002. Histopathologic grading of medulloblastomas: A Pediatric Oncology Group study. Cancer 94, 552–560.

Eberhart, C.G., Tihan, T., Burger, P.C., 2000. Nuclear localization and mutation of beta-catenin in medulloblastomas. J. Neuropathol. Exp. Neurol. 59, 333–7.

Ekstrand, A.J., James, C.D., Cavenee, W.K., Seliger, B., Pettersson, R.F., Collins, V.P., 1991. Genes for epidermal growth factor receptor, transforming growth factor alpha, and epidermal growth factor and their expression in human gliomas in vivo. Cancer Res 51, 2164–2172.

Elez, R., Piiper, A., Giannini, C.D., Brendel, M., Zeuzem, S., 2000. Polo-like kinase1, a new target for antisense tumor therapy. Biochem. Biophys. Res. Commun. 269, 352–356.

Elia, A.E.H., Cantley, L.C., Yaffe, M.B., 2003a. Proteomic screen finds pSer/pThr-binding domain localizing Plk1 to mitotic substrates. Science 299, 1228–31.

Elia, A.E.H., Rellos, P., Haire, L.F., Chao, J.W., Ivins, F.J., Hoepker, K., Mohammad, D., Cantley, L.C., Smerdon, S.J., Yaffe, M.B., 2003b. The molecular basis for phosphodependent substrate targeting and regulation of Plks by the Polo-box domain. Cell 115, 83–95.

Ellinger-Ziegelbauer, H., Karasuyama, H., Yamada, E., Tsujikawa, K., Todokoro, K., Nishida, E., 2000. Ste20-like kinase (SLK), a regulatory kinase for polo-like kinase (Plk) during the G2/M transition in somatic cells. Genes Cells 5, 491–8.

Ellis, P.M., Chu, Q.S., Leighl, N., Laurie, S.A., Fritsch, H., Gaschler-Markefski, B., Gyorffy, S., Munzert, G., 2013. A phase I open-label dose-escalation study of intravenous BI 2536 together with pemetrexed in previously treated patients with non-small-cell lung cancer. Clin. Lung Cancer 14, 19–27.

Ellison, D.W., Dalton, J., Kocak, M., Nicholson, S.L., Fraga, C., Neale, G., Kenney, A.M., Brat, D.J., Perry, A., Yong, W.H., Taylor, R.E., Bailey, S., Clifford, S.C., Gilbertson, R.J., 2011. Medulloblastoma: clinicopathological correlates of SHH, WNT, and non-SHH/WNT molecular subgroups. Acta Neuropathol. 121, 381–96.

Ellison, D.W., Onilude, O.E., Lindsey, J.C., Lusher, M.E., Weston, C.L., Taylor, R.E., Pearson, A.D., Clifford, S.C., 2005. Beta-catenin status predicts a favorable outcome in childhood medulloblastoma: The United Kingdom Children's Cancer Study Group Brain Tumour Committee. J. Clin. Oncol. 23, 7951–7957.

Eneanya, D.L., Bianchine, J.R., Duran, D.O., Andresen, B.D., 1981. The actions and metabolic fate of disulfiram. Annu. Rev. Pharmacol. Toxicol.

Eramo, a, Ricci-Vitiani, L., Zeuner, a, Pallini, R., Lotti, F., Sette, G., Pilozzi, E., Larocca, L.M., Peschle, C., De Maria, R., 2006. Chemotherapy resistance of glioblastoma stem cells. Cell Death Differ. 13, 1238–1241.

Esteller, M., Garcia-Foncillas, J., Andion, E., Goodman, S.N., Hidalgo, O.F., Vanaclocha, V., Baylin, S.B., Herman, J.G., 2000. Inactivation of the DNA-repair gene MGMT and the clinical response of gliomas to alkylating agents. N. Engl. J. Med. 343, 1350–1354.

Faiman, M.D., Artman, L., Haya, K.H., 1980. Disulfiram Distribution and Elimination in the Rat After Oral and Intraperitoneal Administration. Alcohol. Clin. Exp. Res. 4, 412–419.

Fangusaro, J., Finlay, J., Sposto, R., Ji, L., Saly, M., Zacharoulis, S., Asgharzadeh, S., Abromowitch, M., Olshefshi, R., Halpern, S., Dubowy, R., Comito, M., Diez, B., Kellie, S., Hukin, J., Rosenblum, M., Dunkel, I., Miller, D.C., Allen, J., Gardner, S., 2008. Intensive Chemotherapy Followed by Consolidative Myeloablative Chemotherapy With Autologous Hematopoietic Cell Rescue (AuHCR) in Young Children With Newly Diagnosed Supra tentorial Primitive Neuroectodermal Tumors (sPNETs): Report of the Head Start I and . Pediatr. Blood Cancer 50, 312–318.

Fernandez, P., Solenthaler, M., Spertini, O., Quarroz, S., Rovo, A., Lovey, P.-Y., Leoncini, L., Ruault-Jungblut, S., D'Asaro, M., Schaad, O., Docquier, M., Descombes, P., Matthes, T., 2012. Using digital RNA counting and flow cytometry to compare mRNA with protein expression in acute leukemias. PLoS One 7, e49010.

Fisher, G.H., Orsulic, S., Holland, E., Hively, W.P., Li, Y., Lewis, B.C., Williams, B.O., Varmus, H.E., 1999. Development of a flexible and specific gene delivery system for production of murine tumor models. Oncogene 18, 5253–5260.

Fisher, J.L., Schwartzbaum, J.A., Wrensch, M., Wiemels, J.L., 2007. Epidemiology of brain tumors. Neurol. Clin. 25, 867–90, vii.

Fishman, J.B., Rubin, J.B., Handrahan, J. V, Connor, J.R., Fine, R.E., 1987. Receptor-mediated transcytosis of transferrin across the blood-brain barrier. J. Neurosci. Res. 18, 299–304.

Fogarty, M.P., Kessler, J.D., Wechsler-Reya, R.J., 2005. Morphing into cancer: The role of developmental signaling pathways in brain tumor formation. J. Neurobiol. 64, 458–475.

Fojo, T., Grady, C., 2009. How much is life worth: Cetuximab, non-small cell lung cancer, and the $440 billion question. J. Natl. Cancer Inst. 101, 1044–1048.

Forbes, S.A., Bindal, N., Bamford, S., Cole, C., Kok, C.Y., Beare, D., Jia, M., Shepherd, R., Leung, K., Menzies, A., Teague, J.W., Campbell, P.J., Stratton, M.R., Futreal, P.A., 2011. COSMIC: mining complete cancer genomes in the Catalogue of Somatic Mutations in Cancer. Nucleic Acids Res. 39, D945–50.

Fotovati, A., Abu-Ali, S., Wang, P.-S., Deleyrolle, L.P., Lee, C., Triscott, J., Chen, J.Y., Franciosi, S., Nakamura, Y., Sugita, Y., Uchiumi, T., Kuwano, M., Leavitt, B.R., Singh, S.K., Jury, A., Jones, C., Wakimoto, H., Reynolds, B. a, Pallen, C.J., Dunn, S.E., 2011. YB-1 bridges neural stem cells and brain-tumor initiating cells via its roles in differentiation and cell growth. Cancer Res. 71, 5569–5578.

Fouladi, M., Gilger, E., Kocak, M., Wallace, D., Buchanan, G., Reeves, C., Robbins, N., Merchant, T., Kun, L.E., Khan, R., Gajjar, A., Mulhern, R., 2005. Intellectual and functional outcome of children 3 years old or younger who have CNS malignancies. J. Clin. Oncol. 23, 7152–7160.

Francescangeli, F., Patrizii, M., Signore, M., Federici, G., Di Franco, S., Pagliuca, A., Baiocchi, M., Biffoni, M., Ricci Vitiani, L., Todaro, M., De Maria, R., Zeuner, A., 2012. Proliferation State and Polo-Like Kinase1 Dependence of Tumorigenic Colon Cancer Cells. Stem Cells 30, 1819–1830.

Franceschi, E., Cavallo, G., Lonardi, S., Magrini, E., Tosoni, A., Grosso, D., Scopece, L., Blatt, V., Urbini, B., Pession, A., Tallini, G., Crinò, L., Brandes, A.A., 2007. Gefitinib in patients with progressive high-grade gliomas: a multicentre phase II study by Gruppo Italiano Cooperativo di Neuro-Oncologia (GICNO). Br. J. Cancer 96, 1047–1051.

Frange, P., Alapetite, C., Gaboriaud, G., Bours, D., Zucker, J.M., Zerah, M., Brisse, H., Chevignard, M., Mosseri, V., Bouffet, E., Doz, F., 2009. From childhood to adulthood: long-term outcome of medulloblastoma patients. The Institut Curie experience (1980-2000). J. Neurooncol. 95, 271–9.

Frederick, L., Wang, X.Y., Eley, G., James, C.D., 2000. Diversity and frequency of epidermal growth factor receptor mutations in human glioblastomas. Cancer Res. 60, 1383–1387.

Friedman, H.S., Kerby, T., Calvert, H., 2000. Temozolomide and treatment of malignant glioma. Clin. Cancer Res. 6, 2585–2597.

Friedman, H.S., McLendon, R.E., Kerby, T., Dugan, M., Bigner, S.H., Henry, A.J., Ashley, D.M., Krischer, J., Lovell, S., Rasheed, K., Marchev, F., Seman, A.J., Cokgor, I., Rich, J., Stewart, E., Colvin, O.M., Provenzale, J.M., Bigner, D.D., Haglund, M.M., Friedman, A.H., Modrich, P.L., 1998. DNA mismatch repair and O6-alkylguanine-DNA alkyltransferase analysis and response to Temodal in newly diagnosed malignant glioma. J. Clin. Oncol. 16, 3851–7.

Friedman, H.S., Prados, M.D., Wen, P.Y., Mikkelsen, T., Schiff, D., Abrey, L.E., Yung, W.K.A., Paleologos, N., Nicholas, M.K., Jensen, R., Vredenburgh, J., Huang, J., Zheng, M., Cloughesy, T., 2009. Bevacizumab alone and in combination with irinotecan in recurrent glioblastoma. J. Clin. Oncol. 27, 4733–4740.

Friedrich, C., Von Bueren, A.O., Von Hoff, K., Kwiecien, R., Pietsch, T., Warmuth-Metz, M., Hau, P., Deinlein, F., Kuehl, J., Kortmann, R.D., Rutkowski, S., 2013. Treatment of adult nonmetastatic medulloblastoma patients according to the paediatric HIT 2000 protocol: A prospective observational multicentre study. Eur. J. Cancer 49, 893–903.

Frost, a, Mross, K., Steinbild, S., Hedbom, S., Unger, C., Kaiser, R., Trommeshauser, D., Munzert, G., 2012. Phase i study of the Plk1 inhibitor BI 2536 administered intravenously on three consecutive days in advanced solid tumours. Curr. Oncol. 19, e28–35.

Fu, D., Calvo, J.A., Samson, L.D., 2012. Balancing repair and tolerance of DNA damage caused by alkylating agents. Nat. Rev. Cancer 12, 104–20.

Furnari, F.B., Fenton, T., Bachoo, R.M., Mukasa, A., Stommel, J.M., Stegh, A., Hahn, W.C., Ligon, K.L., Louis, D.N., Brennan, C., Chin, L., DePinho, R.A., Cavenee, W.K., 2007. Malignant astrocytic glioma: Genetics, biology, and paths to treatment. Genes Dev. 21, 2683–2710.

Gabathuler, R., 2010. Approaches to transport therapeutic drugs across the blood-brain barrier to treat brain diseases. Neurobiol. Dis. 37, 48–57.

Gachet, Y., Tournier, S., Lee, M., Lazaris-Karatzas, a, Poulton, T., Bommer, U. a, 1999. The growth-related, translationally controlled protein P23 has properties of a tubulin binding protein and associates transiently with microtubules during the cell cycle. J. Cell Sci. 112 (Pt 8, 1257–71.

Gajjar, A.J., Robinson, G.W., 2014. Medulloblastoma—translating discoveries from the bench to the bedside. Nat. Rev. Clin. Oncol. 11, 714–722.

Galli, R., Binda, E., Orfanelli, U., Cipelletti, B., Gritti, A., De Vitis, S., Fiocco, R., Foroni, C., Dimeco, F., Vescovi, A., 2004. Isolation and characterization of tumorigenic, stem-like neural precursors from human glioblastoma. Cancer Res. 64, 7011–21.

Gandhi, L., Chu, Q.S., Stephenson, J., Johnson, B.E., Govindan, R., Bonomi, P., Eaton, K., Fritsch, H., Munzert, G., Socinski, M., 2009. An open label phase II trial of the Plk1 inhibitor BI 2536, in patients with sensitive relapse small cell lung cancer (SCLC). ASCO Meet. Abstr. 27, 8108.

Gandola, L., Massimino, M., Cefalo, G., Solero, C., Spreafico, F., Pecori, E., Riva, D., Collini, P., Pignoli, E., Giangaspero, F., Luksch, R., Berretta, S., Poggi, G., Biassoni, V., Ferrari, A., Pollo, B., Favre, C., Sardi, I., Terenziani, M., Fossati-Bellani, F., 2009. Hyperfractionated accelerated radiotherapy in the Milan strategy for metastatic medulloblastoma. J. Clin. Oncol. 27, 566–71.

Gao, Y., Fotovati, A., Lee, C., Wang, M., Cote, G., Guns, E., Toyota, B., Faury, D., Jabado, N., Dunn, S.E., 2009. Inhibition of Y-box binding protein-1 slows the growth of glioblastoma

multiforme and sensitizes to temozolomide independent O6-methylguanine-DNA methyltransferase. Mol. Cancer Ther. 8, 3276–84.

Garrè, M.L., Cama, A., Bagnasco, F., Morana, G., Giangaspero, F., Brisigotti, M., Gambini, C., Forni, M., Rossi, A., Haupt, R., Nozza, P., Barra, S., Piatelli, G., Viglizzo, G.M., Capra, V., Bruno, W., Pastorino, L., Massimino, M., Tumolo, M., Fidani, P., Dallorso, S., Schumacher, R.F., Milanaccio, C., Pietsch, T., 2009. Medulloblastoma variants: Age-dependent occurrence and relation to gorlin syndrome-a new clinical perspective. Clin. Cancer Res. 15, 2463–2471.

Garuti, L., Roberti, M., Bottegoni, G., 2012. Polo-Like Kinases Inhibitors. Curr. Med. Chem. 19, 3937–3948.

Gatta, G., Zigon, G., Capocaccia, R., Coebergh, J.W., Desandes, E., Kaatsch, P., Pastore, G., Peris-Bonet, R., Stiller, C.A., 2009. Survival of European children and young adults with cancer diagnosed 1995-2002. Eur. J. Cancer 45, 992–1005.

Geiss, G.K., Bumgarner, R.E., Birditt, B., Dahl, T., Dowidar, N., Dunaway, D.L., Fell, H.P., Ferree, S., George, R.D., Grogan, T., James, J.J., Maysuria, M., Mitton, J.D., Oliveri, P., Osborn, J.L., Peng, T., Ratcliffe, A.L., Webster, P.J., Davidson, E.H., Hood, L., Dimitrov, K., 2008. Direct multiplexed measurement of gene expression with color-coded probe pairs. Nat. Biotechnol. 26, 317–25.

Genovesi, L. a, Ng, C.G., Davis, M.J., Remke, M., Taylor, M.D., Adams, D.J., Rust, A.G., Ward, J.M., Ban, K.H., Jenkins, N. a, Copeland, N.G., Wainwright, B.J., 2013. Sleeping Beauty mutagenesis in a mouse medulloblastoma model defines networks that discriminate between human molecular subgroups. Proc. Natl. Acad. Sci. U. S. A. 110, E4325–34.

Gerber, N.U., Mynarek, M., von Hoff, K., Friedrich, C., Resch, a., Rutkowski, S., 2014. Recent developments and current concepts in Medulloblastoma. Cancer Treat. Rev. 40, 356–365.

Gerstner, E.R., Yip, S., Wang, D.L., Louis, D.N., Iafrate, A.J., Batchelor, T.T., 2009. Mgmt methylation is a prognostic biomarker in elderly patients with newly diagnosed glioblastoma. Neurology 73, 1509–10.

Gibson, P., Tong, Y., Robinson, G., Thompson, M.C., Currle, D.S., Eden, C., Kranenburg, T. a, Hogg, T., Poppleton, H., Martin, J., Finkelstein, D., Pounds, S., Weiss, A., Patay, Z., Scoggins, M., Ogg, R., Pei, Y., Yang, Z.-J., Brun, S., Lee, Y., Zindy, F., Lindsey, J.C., Taketo, M.M., Boop, F. a, Sanford, R. a, Gajjar, A., Clifford, S.C., Roussel, M.F., McKinnon, P.J., Gutmann, D.H., Ellison, D.W., Wechsler-Reya, R., Gilbertson, R.J., 2010. Subtypes of medulloblastoma have distinct developmental origins. Nature 468, 1095–9.

Gilbert, M.R., Dignam, J.J., Armstrong, T.S., Wefel, J.S., Blumenthal, D.T., Vogelbaum, M. a, Colman, H., Chakravarti, A., Pugh, S., Won, M., Jeraj, R., Brown, P.D., Jaeckle, K. a, Schiff, D., Stieber, V.W., Brachman, D.G., Werner-Wasik, M., Tremont-Lukats, I.W.,

Sulman, E.P., Aldape, K.D., Curran, W.J., Mehta, M.P., 2014. A randomized trial of bevacizumab for newly diagnosed glioblastoma. N. Engl. J. Med. 370, 699–708.

Gilmartin, A.G., Bleam, M.R., Richter, M.C., Erskine, S.G., Kruger, R.G., Madden, L., Hassler, D.F., Smith, G.K., Gontarek, R.R., Courtney, M.P., Sutton, D., Diamond, M.A., Jackson, J.R., Laquerre, S.G., 2009. Distinct concentration-dependent effects of the polo-like kinase 1-specific inhibitor GSK461364A, including differential effect on apoptosis. Cancer Res. 69, 6969–77.

Giovannini, E., Lazzeri, P., Milano, A., Gaeta, M.C., Ciarmiello, A., 2015. Clinical applications of Choline PET/CT in Brain Tumors. Curr. Pharm. Des. 21, 121–127.

Glantz, M., Chamberlain, M., Liu, Q., Litofsky, N.S., Recht, L.D., 2003. Temozolomide as an alternative to irradiation for elderly patients with newly diagnosed malignant gliomas. Cancer 97, 2262–2266.

Gleixner, K. V, Ferenc, V., Peter, B., Gruze, A., Meyer, R.A., Hadzijusufovic, E., Cerny-Reiterer, S., Mayerhofer, M., Pickl, W.F., Sillaber, C., Valent, P., 2010. Polo-like kinase 1 (Plk1) as a novel drug target in chronic myeloid leukemia: overriding imatinib resistance with the Plk1 inhibitor BI 2536. Cancer Res. 70, 1513–23.

Gnanasekar, M., Thirugnanam, S., Zheng, G., Chen, A., Ramaswamy, K., 2009. Gene silencing of translationally controlled tumor protein (TCTP) by siRNA inhibits cell growth and induces apoptosis of human prostate cancer cells. Int. J. Oncol. 34, 1241–1246.

Godard, S., Getz, G., Delorenzi, M., Farmer, P., Kobayashi, H., Desbaillets, I., Nozaki, M., Diserens, A.C., Hamou, M.F., Dietrich, P.Y., Regli, L., Janzer, R.C., Bucher, P., Stupp, R., De Tribolet, N., Domany, E., Hegi, M.E., 2003. Classification of Human Astrocytic Gliomas on the Basis of Gene Expression: A Correlated Group of Genes with Angiogenic Activity Emerges As a Strong Predictor of Subtypes. Cancer Res. 63, 6613–6625.

Golding, S.E., Morgan, R.N., Adams, B.R., Hawkins, A.J., Povirk, L.F., Valerie, K., 2009. Pro-survival AKT and ERK signaling from EGFR and mutant EGFRvIII enhances DNA double-strand break repair in human glioma cells. Cancer Biol. Ther. 8, 730–738.

Goldowitz, D., Hamre, K., 1998. The cells and molecules that make a cerebellum. Trends Neurosci. 21, 375–382.

Golsteyn, R.M., Golsteyn, R.M., Mundt, K.E., Mundt, K.E., Fry, a M., Fry, a M., Nigg, E. a, Nigg, E. a, 1995. Cell-Cycle Regulation of the Activity and Subcellular-Localization of Plk1, A Human Protein-Kinase Implicated in Mitotic Spindle Function. J. Cell Biol. 129, 1617–1628.

Goodrich, L. V, Milenkovic, L., Higgins, K.M., Scott, M.P., 1997. Altered Neural Cell Fates and Medulloblastoma in Mouse patched Mutants. Science (80-.). 5329, 1109–1113.

Goschzik, T., Zur Mühlen, A., Kristiansen, G., Haberler, C., Stefanits, H., Friedrich, C., von Hoff, K., Rutkowski, S., Pfister, S.M., Pietsch, T., 2014. Molecular stratification of medulloblastoma: Comparison of histological and genetic methods to detect Wnt activated tumors. Neuropathol. Appl. Neurobiol. 135–144.

Goto, H., Kiyono, T., Tomono, Y., Kawajiri, A., Urano, T., Furukawa, K., Nigg, E. a, Inagaki, M., 2006. Complex formation of Plk1 and INCENP required for metaphase-anaphase transition. Nat. Cell Biol. 8, 180–187.

Gough, S.M., Lee, F., Yang, F., Walker, R.L., Zhu, Y.J., Pineda, M., Onozawa, M., Chung, Y.J., Bilke, S., Wagner, E.K., Denu, J.M., Ning, Y., Xu, B., Wang, G.G., Meltzer, P.S., Aplan, P.D., 2014. NUP98-PHF23 is a chromatin-modifying oncoprotein that causes a wide array of leukemias sensitive to inhibition of PHD histone reader function. Cancer Discov. 4, 564–77.

Grabenbauer, G.G., Beck, J.D., Erhardt, J., Seegenschmiedt, M.H., Seyer, H., Thierauf, P., Sauer, R., 1996. Postoperative radiotherapy of medulloblastoma. Impact of radiation quality on treatment outcome. Am. J. Clin. Oncol. 19, 73–7.

Greig, N.H., Brossi, A., Pei, X.-F., Ingram, D.K., Soncrant, T.T., 1995. Designing drugs for optimal nervous system activity, in: Greenwood, J., Begley, D.J., Segal, M.B. (Eds.), New Concepts of a Blood—Brain Barrier. Springer US, Boston, MA, pp. 251–264.

Grill, J., Sainte-Rose, C., Jouvet, A., Gentet, J.C., Lejars, O., Frappaz, D., Doz, F., Rialland, X., Pichon, F., Bertozzi, A.I., Chastagner, P., Couanet, D., Habrand, J.L., Raquin, M.A., Le Deley, M.C., Kalifa, C., 2005. Treatment of medulloblastoma with postoperative chemotherapy alone: An SFOP prospective trial in young children. Lancet Oncol. 6, 573–580.

Grinshtein, N., Datti, A., Fujitani, M., Uehling, D., Prakesch, M., Isaac, M., Irwin, M.S., Wrana, J.L., Al-Awar, R., Kaplan, D.R., 2011. Small molecule kinase inhibitor screen identifies polo-like kinase 1 as a target for neuroblastoma tumor-initiating cells. Cancer Res. 71, 1385–95.

Gu, X., Yao, L., Ma, G., Cui, L., Li, Y., Liang, W., Zhao, B., Li, K., 2013. TCTP promotes glioma cell proliferation in vitro and in vivo via enhanced β-catenin/TCF-4 transcription. Neuro. Oncol. 16, 217–227.

Guo, X., Xu, B., Pandey, S., Goessl, E., Brown, J., Armesilla, A.L., Darling, J.L., Wang, W., 2010. Disulfiram/copper complex inhibiting NFkappaB activity and potentiating cytotoxic effect of gemcitabine on colon and breast cancer cell lines. Cancer Lett. 290, 104–113.

Guthrie, G.D., Eljamel, S., 2013. Impact of particular antiepileptic drugs on the survival of patients with glioblastoma multiforme. J. Neurosurg. 118, 859–865.

Hald, J., Jacobsen, E., 1948. A drug sensitizing the organism to ethyl alcohol. Lancet 2, 1001–4.

Hallahan, A.R., Pritchard, J.I., Hansen, S., Benson, M., Stoeck, J., Hatton, B. a., Russell, T.L., Ellenbogen, R.G., Bernstein, I.D., Beachy, P. a., Olson, J.M., 2004. The SmoA1 mouse model reveals that notch signaling is critical for the growth and survival of Sonic Hedgehog-induced medulloblastomas. Cancer Res. 64, 7794–7800.

Hambardzumyan, D., Amankulor, N.M., Helmy, K.Y., Becher, O.J., Holland, E.C., 2009. Modeling Adult Gliomas Using RCAS/t-va Technology. Transl. Oncol. 2, 89–95.

Hambardzumyan, D., Becher, O.J., Rosenblum, M.K., Pandolfi, P.P., Manova-Todorova, K., Holland, E.C., 2008. PI3K pathway regulates survival of cancer stem cells residing in the perivascular niche following radiation in medulloblastoma in vivo. Genes Dev. 22, 436–448.

Hamilton, S.R., Liu, B., Parsons, R.E., Papadopoulos, N., Jen, J., Powell, S.M., Krush, A.J., Berk, T., Cohen, Z., Tetu, B., 1995. The molecular basis of Turcot's syndrome. N. Engl. J. Med. 332, 839–47.

Haney, S. a., LaPan, P., Pan, J., Zhang, J., 2006. High-content screening moves to the front of the line. Drug Discov. Today 11, 889–894.

Hansen, D. V, Loktev, A. V, Ban, K.H., Jackson, P.K., 2004. Plk1 Regulates Activation of the Anaphase Promoting Complex by Phosphorylating and Triggering SCF TrCP - dependent Destruction of the APC Inhibitor Emi1 15, 5623–5634.

Haren, L., Stearns, T., Lüders, J., 2009. Plk1-Dependent Recruitment of γ-Tubulin Complexes to Mitotic Centrosomes Involves Multiple PCM Components. PLoS One 4, e5976.

Hargrave, D., Bartels, U., Bouffet, E., 2006. Diffuse brainstem glioma in children: Critical review of clinical trials. Lancet Oncol. 7, 241–248.

Harris, P.S., Venkataraman, S., Alimova, I., Birks, D.K., Donson, A.M., Knipstein, J., Dubuc, A., Taylor, M.D., Handler, M.H., Foreman, N.K., Vibhakar, R., 2012. Polo-like kinase 1 (PLK1) inhibition suppresses cell growth and enhances radiation sensitivity in medulloblastoma cells. BMC Cancer 12, 80.

Hatton, B. a., Villavicencio, E.H., Tsuchiya, K.D., Pritchard, J.I., Ditzler, S., Pullar, B., Hansen, S., Knoblaugh, S.E., Lee, D., Eberhart, C.G., Hallahan, A.R., Olson, J.M., 2008. The Smo/Smo model: Hedgehog-induced medulloblastoma with 90% incidence and leptomeningeal spread. Cancer Res. 68, 1768–1776.

He, S., Huang, Y., Wang, Y., Tang, J., Song, Y., Yu, X., Ma, J., Wang, S., Yin, H., Li, Q., Ji, L., Xu, X., 2015. Histamine-releasing factor/translationally controlled tumor protein plays a

role in induced cell adhesion, apoptosis resistance and chemoresistance in non-Hodgkin lymphomas. Leuk. Lymphoma 1–9.

Hegi, M.E., Diserens, A.-C., Gorlia, T., Hamou, M.-F., de Tribolet, N., Weller, M., Kros, J.M., Hainfellner, J.A., Mason, W., Mariani, L., Bromberg, J.E.C., Hau, P., Mirimanoff, R.O., Cairncross, J.G., Janzer, R.C., Stupp, R., 2005. MGMT gene silencing and benefit from temozolomide in glioblastoma. N. Engl. J. Med. 352, 997–1003.

Heimberger, A.B., Hlatky, R., Suki, D., Yang, D., Weinberg, J., Gilbert, M., Sawaya, R., Aldape, K., 2005. Prognostic effect of epidermal growth factor receptor and EGFRvIII in glioblastoma multiforme patients. Clin. Cancer Res. 11, 1462–1466.

Hipkens, J.H., Struck, R.F., Gurtoo, H.L., 1981. Role of Aldehyde Dehydrogenase in the Metabolism-dependent Biological Activity of Cyclophosphamide Role of Aldehyde Dehydrogenase in the Metabolism-dependent Activity of Cyclophosphamide1. Cancer Res. 3571–3583.

Hirose, Y., Hirose, Y., Berger, M.S., Berger, M.S., Pieper, R.O., Pieper, R.O., 2001. p53 Effects Both the Duration of G 2 /M Arrest and the Fate of Temozolomide-treated Human Glioblastoma Cells 1. Cancer 1957–1963.

Hochberg, F.H., Pruitt, A., 1980. Assumptions in the radiotherapy of glioblastoma. Neurology 30, 907–911.

Hofheinz, R.-D., Al-Batran, S.-E., Hochhaus, A., Jäger, E., Reichardt, V.L., Fritsch, H., Trommeshauser, D., Munzert, G.,. An open-label, phase I study of the polo-like kinase-1 inhibitor, BI 2536, in patients with advanced solid tumors. Clin. Cancer Res. 16, 4666–74.

Holtrich, U.W.E., Wolf, G., Brauninger, A., Karnq, T., Bohme, B., Rjbsamen-waigmann, H., Strebhardt, K., 1994. Induction and down-regulation of PLK, a human serine/threonine kinase expressed in proliferating cells and tumors. Proc. Natl. Acad. Sci. 91, 1736–1740.

Hong, S.-T., Choi, K.-W., 2013. TCTP directly regulates ATM activity to control genome stability and organ development in Drosophila melanogaster. Nat. Commun. 4.

Horten, B., Basler, G.A., Shapiro, W.R., 1981. Xenograft of Human Malignant Glial Tumors into Brains of Nude Mice A Histopathological Study. J. Neuropathol. Exp. Neurol. 40, 493–511.

Horton, J.K., Wilson, S.H., 2007. Hypersensitivity phenotypes associated with genetic and synthetic inhibitor-induced base excision repair deficiency. DNA Repair (Amst). 6, 530–43.

Hothi, P., Martins, T.J., Chen, L., Deleyrolle, L., Yoon, J.-G., Reynolds, B., Foltz, G., 2012. High-throughput chemical screens identify disulfiram as an inhibitor of human glioblastoma stem cells. Oncotarget 3, 1124–1136.

Hu, C.-K., Coughlin, M., Mitchison, T.J., 2012. Midbody assembly and its regulation during cytokinesis. Mol. Biol. Cell 23, 1024–34.

Hu, K., Lee, C., Qiu, D., Fotovati, A., Davies, A., Abu-Ali, S., Wai, D., Lawlor, E.R., Triche, T.J., Pallen, C.J., Dunn, S.E., 2009. Small interfering RNA library screen of human kinases and phosphatases identifies polo-like kinase 1 as a promising new target for the treatment of pediatric rhabdomyosarcomas. Mol. Cancer Ther. 8, 3024–35.

Hulleman, E., Helin, K., 2005. Molecular mechanisms in gliomagenesis. Adv. Cancer Res. 94, 1–27.

Huse, J.T., Holland, E.C., 2009. Genetically engineered mouse models of brain cancer and the promise of preclinical testing. Brain Pathol. 19, 132–143.

Huttner, A.J., Kieran, M.W., Yao, X., Cruz, L., Ladner, J., Quayle, K., Goumnerova, L.C., Irons, M.B., Ullrich, N.J., 2010. Clinicopathologic study of glioblastoma in children with neurofibromatosis type 1. Pediatr. Blood Cancer 54, 890–6.

Iljin, K., Ketola, K., Vainio, P., Halonen, P., Kohonen, P., Fey, V., Grafström, R.C., Perälä, M., Kallioniemi, O., 2009. High-throughput cell-based screening of 4910 known drugs and drug-like small molecules identifies disulfiram as an inhibitor of prostate cancer cell growth. Clin. Cancer Res. 15, 6070–8.

Ingham, P.W., Nakano, Y., Seger, C., 2011. Mechanisms and functions of Hedgehog signalling across the metazoa. Nat. Rev. Genet. 12, 393–406.

Iwamoto, F.M., Abrey, L.E., Beal, K., Gutin, P.H., Rosenblum, M.K., Reuter, V.E., Deangelis, L.M., Lassman, A.B., 2009. Patterns of relapse and prognosis after bevacizumab failure in recurrent glioblastoma. Neurology 73, 1200–1206.

Jackman, M., Lindon, C., Nigg, E.A., Pines, J., 2003. Active cyclin B1-Cdk1 first appears on centrosomes in prophase. Nat. Cell Biol. 5, 143–8.

Jaglarz, M.K., Bazile, F., Laskowska, K., Polanski, Z., Chesnel, F., Borsuk, E., Kloc, M., Kubiak, J.Z., 2012. Association of TCTP with centrosome and microtubules. Biochem. Res. Int. 2012.

Jakacki, R.I., Burger, P.C., Zhou, T., Holmes, E.J., Kocak, M., Onar, A., Goldwein, J., Mehta, M., Packer, R.J., Tarbell, N., Fitz, C., Vezina, G., Hilden, J., Pollack, I.F., 2012. Outcome of children with metastatic medulloblastoma treated with carboplatin during craniospinal radiotherapy: A children's oncology group phase I/II study. J. Clin. Oncol. 30, 2648–2653.

Jang, Y.-J., Lin, C.-Y., Ma, S., Erikson, R.L., 2002. Functional studies on the role of the C-terminal domain of mammalian polo-like kinase. Proc. Natl. Acad. Sci. U. S. A. 99, 1984–9.

Jang, Y.J., Ma, S., Terada, Y., Erikson, R.L., 2002. Phosphorylation of threonine 210 and the role of serine 137 in the regulation of mammalian polo-like kinase. J. Biol. Chem. 277, 44115–44120.

Jansen, M.H.A., van Vuurden, D.G., Vandertop, W.P., Kaspers, G.J.L., 2012. Diffuse intrinsic pontine gliomas: a systematic update on clinical trials and biology. Cancer Treat. Rev. 38, 27–35.

Janzer, R.C., Raff, M.C., 1987. Astrocytes induce blood-brain barrier properties in endothelial cells. Nature 325, 253–7.

Jiang, F., Qiu, Q., Khanna, A., Todd, N.W., Deepak, J., Xing, L., Wang, H., Liu, Z., Su, Y., Stass, S.A., Katz, R.L., 2009. Aldehyde dehydrogenase 1 is a tumor stem cell-associated marker in lung cancer. Mol. Cancer Res. 7, 330–8.

Jones, D.T.W., Jäger, N., Kool, M., Zichner, T., Hutter, B., Sultan, M., Cho, Y.-J., Pugh, T.J., Hovestadt, V., Stütz, A.M., Rausch, T., Warnatz, H.-J., Ryzhova, M., Bender, S., Sturm, D., Pleier, S., Cin, H., Pfaff, E., Sieber, L., Wittmann, A., Remke, M., Witt, H., Hutter, S., Tzaridis, T., Weischenfeldt, J., Raeder, B., Avci, M., Amstislavskiy, V., Zapatka, M., Weber, U.D., Wang, Q., Lasitschka, B., Bartholomae, C.C., Schmidt, M., von Kalle, C., Ast, V., Lawerenz, C., Eils, J., Kabbe, R., Benes, V., van Sluis, P., Koster, J., Volckmann, R., Shih, D., Betts, M.J., Russell, R.B., Coco, S., Paolo Tonini, G., Schüller, U., Hans, V., Graf, N., Kim, Y.-J., Monoranu, C., Roggendorf, W., Unterberg, A., Herold-Mende, C., Milde, T., Kulozik, A.E., von Deimling, A., Witt, O., Maass, E., Rössler, J., Ebinger, M., Schuhmann, M.U., Frühwald, M.C., Hasselblatt, M., Jabado, N., Rutkowski, S., von Bueren, A.O., Williamson, D., Clifford, S.C., McCabe, M.G., Peter Collins, V., Wolf, S., Wiemann, S., Lehrach, H., Brors, B., Scheurlen, W., Felsberg, J., Reifenberger, G., Northcott, P. a., Taylor, M.D., Meyerson, M., Pomeroy, S.L., Yaspo, M.-L., Korbel, J.O., Korshunov, A., Eils, R., Pfister, S.M., Lichter, P., 2012. Dissecting the genomic complexity underlying medulloblastoma. Nature 488, 100–105.

Jones, D.T.W., Northcott, P. a, Kool, M., Pfister, S.M., 2013. The role of chromatin remodeling in medulloblastoma. Brain Pathol. 23, 193–9.

Jordan, P.W., Karppinen, J., Handel, M.A., 2012. Polo-like kinase is required for synaptonemal complex disassembly and phosphorylation in mouse spermatocytes. J. Cell Sci. 125, 5061–5072.

Kachaner, D., Pinson, X., El Kadhi, K. Ben, Normandin, K., Talje, L., Lavoie, H., Lépine, G., Carréno, S., Kwok, B.H., Hickson, G.R., Archambault, V., 2014. Interdomain allosteric regulation of Polo kinase by Aurora B and Map205 is required for cytokinesis. J. Cell Biol. 207, 201–11.

Kanai, R., Rabkin, S.D., Yip, S., Sgubin, D., Zaupa, C.M., Hirose, Y., Louis, D.N., Wakimoto, H., Martuza, R.L., 2012. Oncolytic virus-mediated manipulation of DNA damage

responses: synergy with chemotherapy in killing glioblastoma stem cells. J. Natl. Cancer Inst. 104, 42–55.

Karamehic, J., Ridic, O., Ridic, G., Jukic, T., Coric, J., Subasic, D., Panjeta, M., Saban, A., Zunic, L., Masic, I., 2013. Financial aspects and the future of the pharmaceutical industry in the United States of america. Mater. Sociomed. 25, 286–90.

Karpov, P.A., Nadezhdina, E.S., Yemets, A.I., Matusov, V.G., Nyporko, A., Shashina, N., Blume, Y.B., 2010. Bioinformatic search of plant microtubule-and cell cycle related serine-threonine protein kinases. BMC Genomics 11, S14.

Kast, R.E., Belda-Iniesta, C., 2009. Suppressing Glioblastoma Stem Cell Function by Aldehyde Dehydrogenase Inhibition with Chloramphenicol or Disulfiram as a New Treatment Adjunct: A Hypothesis. Curr. Stem Cell Res. Ther. 4, 314–317.

Kato, H., Kato, S., Kumabe, T., Sonoda, Y., Yoshimoto, T., Kato, S., Han, S., Suzuki, T., Shibata, H., Kanamaru, R., Ishioka, C., 2000. Functional evaluation of p53 and PTEN gene mutations in gliomas. Clin. Cancer Res. 6, 3937–3943.

Kawauchi, D., Robinson, G., Uziel, T., Gibson, P., Rehg, J., Gao, C., Finkelstein, D., Qu, C., Pounds, S., Ellison, D.W., Gilbertson, R.J., Roussel, M.F., 2012. A mouse model of the most aggressive subgroup of human medulloblastoma. Cancer Cell 21, 168–80.

Kelm, O., 2002. Cell Cycle-regulated Phosphorylation of the Xenopus Polo-like Kinase Plx1. J. Biol. Chem. 277, 25247–25256.

Kenney, A.M., Rowitch, D.H., 2000. Sonic hedgehog promotes G(1) cyclin expression and sustained cell cycle progression in mammalian neuronal precursors. Mol. Cell. Biol. 20, 9055–9067.

Kim, J., Aftab, B.T., Tang, J.Y., Kim, D., Lee, A.H., Rezaee, M., Kim, J., Chen, B., King, E.M., Borodovsky, A., Riggins, G.J., Epstein, E.H., Beachy, P.A., Rudin, C.M., 2013. Itraconazole and Arsenic Trioxide Inhibit Hedgehog Pathway Activation and Tumor Growth Associated with Acquired Resistance to Smoothened Antagonists. Cancer Cell 23, 23–34.

Kim, J.H., Shin, J.H., Kim, I.H., 2004. Susceptibility and radiosensitization of human glioblastoma cells to trichostatin A, a histone deacetylase inhibitor. Int. J. Radiat. Oncol. Biol. Phys. 59, 1174–80.

Kippin, T.E., Martens, D.J., Van Der Kooy, D., 2005. p21 loss compromises the relative quiescence of forebrain stem cell proliferation leading to exhaustion of their proliferation capacity. Genes Dev. 19, 756–767.

Klerk, C.P., Overmeer, R.M., Niers, T.M., Versteeg, H.H., Richel, D.J., Buckle, T., Van Noorden, C.J., van Tellingen, O., 2007. Validity of bioluminescence measurements for noninvasive in vivo imaging of tumor load in small animals. Biotechniques 43, 7–13.

Kloc, M., Tejpal, N., Sidhu, J., Ganachari, M., Flores-Villanueva, P., Jennings, N.B., Sood, A.K., Kubiak, J.Z., Ghobrial, R.M., 2012. Inverse relationship between TCTP/RhoA and p53 /cyclin A/actin expression in ovarian cancer cells. Folia Histochem. Cytobiol. 50, 358–67.

Kloc, M., Tejpal, N., Sidhu, J., Ganachari, M., Flores-Villanueva, P., Jennings, N.B., Sood, A.K., Kubiak, J.Z., Ghobrial, R.M., Manuscript, A., 2013. Inverse relationship between TCTP/RhoA and p53/cyclin A/actin expression in ovarian cancer cells. Folia Histochem Cytobiol. 50, 358–367.

Kohsaka, S., Wang, L., Yachi, K., Mahabir, R., Narita, T., Itoh, T., Tanino, M., Kimura, T., Nishihara, H., Tanaka, S., 2012. STAT3 Inhibition Overcomes Temozolomide Resistance in Glioblastoma by Downregulating MGMT Expression. Mol. Cancer Ther. 11, 1289–1299.

Kong, D., Farmer, V., Shukla, A., James, J., Gruskin, R., Kiriyama, S., Loncarek, J., 2014. Centriole maturation requires regulated Plk1 activity during two consecutive cell cycles. J. Cell Biol. 206, 855–65.

Kool, M., Jones, D.T.W., Jäger, N., Northcott, P. a, Pugh, T.J., Hovestadt, V., Piro, R.M., Esparza, L.A., Markant, S.L., Remke, M., Milde, T., Bourdeaut, F., Ryzhova, M., Sturm, D., Pfaff, E., Stark, S., Hutter, S., Seker-Cin, H., Johann, P., Bender, S., Schmidt, C., Rausch, T., Shih, D., Reimand, J., Sieber, L., Wittmann, A., Linke, L., Witt, H., Weber, U.D., Zapatka, M., König, R., Beroukhim, R., Bergthold, G., van Sluis, P., Volckmann, R., Koster, J., Versteeg, R., Schmidt, S., Wolf, S., Lawerenz, C., Bartholomae, C.C., von Kalle, C., Unterberg, A., Herold-Mende, C., Hofer, S., Kulozik, A.E., von Deimling, A., Scheurlen, W., Felsberg, J., Reifenberger, G., Hasselblatt, M., Crawford, J.R., Grant, G. a, Jabado, N., Perry, A., Cowdrey, C., Croul, S., Zadeh, G., Korbel, J.O., Doz, F., Delattre, O., Bader, G.D., McCabe, M.G., Collins, V.P., Kieran, M.W., Cho, Y.-J., Pomeroy, S.L., Witt, O., Brors, B., Taylor, M.D., Schüller, U., Korshunov, A., Eils, R., Wechsler-Reya, R.J., Lichter, P., Pfister, S.M., 2014. Genome Sequencing of SHH Medulloblastoma Predicts Genotype-Related Response to Smoothened Inhibition. Cancer Cell 25, 393–405.

Kool, M., Korshunov, A., Remke, M., Jones, D.T.W., Schlanstein, M., Northcott, P. a., Cho, Y.J., Koster, J., Schouten-Van Meeteren, A., Van Vuurden, D., Clifford, S.C., Pietsch, T., Von Bueren, A.O., Rutkowski, S., McCabe, M., Collins, V.P., Bäcklund, M.L., Haberler, C., Bourdeaut, F., Delattre, O., Doz, F., Ellison, D.W., Gilbertson, R.J., Pomeroy, S.L., Taylor, M.D., Lichter, P., Pfister, S.M., 2012. Molecular subgroups of medulloblastoma: An international meta-analysis of transcriptome, genetic aberrations, and clinical data of WNT, SHH, Group 3, and Group 4 medulloblastomas. Acta Neuropathol. 123, 473–484.

Kool, M., Koster, J., Bunt, J., Hasselt, N.E., Lakeman, A., van Sluis, P., Troost, D., Meeteren, N.S., Caron, H.N., Cloos, J., Mrsić, A., Ylstra, B., Grajkowska, W., Hartmann, W., Pietsch,

T., Ellison, D., Clifford, S.C., Versteeg, R., 2008. Integrated genomics identifies five medulloblastoma subtypes with distinct genetic profiles, pathway signatures and clinicopathological features. PLoS One 3, e3088.

Korah, M.P., Esiashvili, N., Mazewski, C.M., Hudgins, R.J., Tighiouart, M., Janss, A.J., Schwaibold, F.P., Crocker, I.R., Curran, W.J., Marcus, R.B., 2010. Incidence, Risks, and Sequelae of Posterior Fossa Syndrome in Pediatric Medulloblastoma. Int. J. Radiat. Oncol. 77, 106–112.

Kothe, M., Kohls, D., Low, S., Coli, R., Cheng, A.C., Jacques, S.L., Johnson, T.L., Lewis, C., Loh, C., Nonomiya, J., Sheils, A.L., Verdries, K.A., Wynn, T.A., Kuhn, C., Ding, Y.-H., 2007. Structure of the catalytic domain of human polo-like kinase 1. Biochemistry 46, 5960–71.

Kraft, C., Herzog, F., Gieffers, C., Mechtler, K., Hagting, A., Pines, J., Peters, J.-M., 2003. Mitotic regulation of the human anaphase-promoting complex by phosphorylation. EMBO J. 22, 6598–609.

Krause, K., Wasner, M., Reinhard, W., Haugwitz, U., Dohna, C.L., Mössner, J., Engeland, K., 2000. The tumour suppressor protein p53 can repress transcription of cyclin B. Nucleic Acids Res. 28, 4410–8.

Kulkarni, A. V, Piscione, J., Shams, I., Bouffet, E., 2013. Long-term quality of life in children treated for posterior fossa brain tumors. J. Neurosurg. Pediatr. 12, 235–240.

Lane, H.A., Nigg, E.A., 1996. Antibody microinjection reveals an essential role for human polo-like kinase 1 (Plk1) in the functional maturation of mitotic centrosomes. J. Cell Biol. 135, 1701–13.

Langdon, J. a, Lamont, J.M., Scott, D.K., Dyer, S., Prebble, E., Bown, N., Grundy, R.G., Ellison, D.W., Clifford, S.C., 2006. Combined genome-wide allelotyping and copy number analysis identify frequent genetic losses without copy number reduction in medulloblastoma. Genes. Chromosomes Cancer 45, 47–60.

Lauth, M., Bergström, A., Shimokawa, T., Toftgård, R., 2007. Inhibition of GLI-mediated transcription and tumor cell growth by small-molecule antagonists. Proc. Natl. Acad. Sci. U. S. A. 104, 8455–8460.

Lawrence, T., Ten Haken, R., Giaccia, A., 2008. Principles of Radiation Oncology, in: Principles of Practice of Oncology, 8th Ed.

Lee, C., Dhillon, J., Wang, M.Y.C., Gao, Y., Hu, K., Park, E., Astanehe, A., Hung, M.-C.C., Eirew, P., Eaves, C.J., Dunn, S.E., 2008. Targeting YB-1 in HER-2 overexpressing breast cancer cells induces apoptosis via the mTOR/STAT3 pathway and suppresses tumor growth in mice. Cancer Res. 68, 8661–6.

Lee, C., Dunn, S.E., Yip, S., 2012a. Stem cells in brain tumour development and therapy- two-sides of the same coin. Can. J. Neurol. Sci. 39, 145–56.

Lee, C., Fotovati, A., Triscott, J., Chen, J., 2012b. Polo-Like Kinase 1 Inhibition Kills Glioblastoma Multiforme Brain Tumor Cells in Part Through Loss of SOX2 and Delays Tumor Progression in Mice. Stem Cells 30, 1064–1075.

Lee, J., Kotliarova, S., Kotliarov, Y., Li, A., Su, Q., Donin, N.M., Pastorino, S., Purow, B.W., Christopher, N., Zhang, W., Park, J.K., Fine, H. a., 2006. Tumor stem cells derived from glioblastomas cultured in bFGF and EGF more closely mirror the phenotype and genotype of primary tumors than do serum-cultured cell lines. Cancer Cell 9, 391–403.

Lee, K.S., Grenfell, T.Z., Yarm, F.R., Erikson, R.L., 1998. Mutation of the polo-box disrupts localization and mitotic functions of the mammalian polo kinase Plk. Proc. Natl. Acad. Sci. U. S. A. 95, 9301–6.

Lénárt, P., Petronczki, M., Steegmaier, M., Di Fiore, B., Lipp, J.J., Hoffmann, M., Rettig, W.J., Kraut, N., Peters, J.M., 2007. The Small-Molecule Inhibitor BI 2536 Reveals Novel Insights into Mitotic Roles of Polo-like Kinase 1. Curr. Biol. 17, 304–315.

Lenkiewicz, M., Li, N., Singh, S.K., 2009. Culture and isolation of brain tumor initiating cells, in: Current Protocols in Stem Cell Biology.

Leung, C., Lingbeek, M., Shakhova, O., Liu, J., Tanger, E., Saremaslani, P., Van Lohuizen, M., Marino, S., 2004. Bmi1 is essential for cerebellar development and is overexpressed in human medulloblastomas. Nature 428, 337–41.

Li, J., Yen, C., Liaw, D., Podsypanina, K., Bose, S., Wang, S.I., Puc, J., Miliaresis, C., Rodgers, L., McCombie, R., Bigner, S.H., Giovanella, B.C., Ittmann, M., Tycko, B., Hibshoosh, H., Wigler, M.H., Parsons, R., 1997. PTEN, a putative protein tyrosine phosphatase gene mutated in human brain, breast, and prostate cancer. Science 275, 1943–1947.

Libermann, T.A., Razon, N., Bartal, A.D., Yarden, Y., Schlessinger, J., Soreq, H., 1984. Expression of epidermal growth factor receptors in human brain tumors. Cancer Res 44, 753–760.

Limbo, O., Porter-Goff, M.E., Rhind, N., Russell, P., 2011. Mre11 nuclease activity and Ctp1 regulate Chk1 activation by Rad3ATR and Tel1ATM checkpoint kinases at double-strand breaks. Mol. Cell. Biol. 31, 573–83.

Lin, C.-C., Su, W.-C., Yen, C.-J., Hsu, C.-H., Su, W.-P., Yeh, K.-H., Lu, Y.-S., Cheng, A.-L., Huang, D.C.-L., Fritsch, H., Voss, F., Taube, T., Yang, J.C.-H., 2014. A phase I study of two dosing schedules of volasertib (BI 6727), an intravenous polo-like kinase inhibitor, in patients with advanced solid malignancies. Br. J. Cancer 110, 2434–2440.

Lin, H.-R., Ting, N.S.Y., Qin, J., Lee, W.-H., 2003. M phase-specific phosphorylation of BRCA2 by Polo-like kinase 1 correlates with the dissociation of the BRCA2-P/CAF complex. J. Biol. Chem. 278, 35979–87.

Lin, J., Haffner, M.C., Zhang, Y., Lee, B.H., Brennen, W.N., Britton, J., Kachhap, S.K., Shim, J.S., Liu, J.O., Nelson, W.G., Yegnasubramanian, S., Carducci, M.A., 2011. Disulfiram Is a DNA Demethylating Agent and Inhibits Prostate Cancer Cell Growth. Prostate, The 71, 333–343.

Lindon, C., 2004. Ordered proteolysis in anaphase inactivates Plk1 to contribute to proper mitotic exit in human cells. J. Cell Biol. 164, 233–241.

Lipsky, J.J., Shen, M.L., Naylor, S., 2001. Overview--in vitro inhibition of aldehyde dehydrogenase by disulfiram and metabolites. Chem. Biol. Interact. 130-132, 81–91.

Lipsman, N., Skanda, A., Kimmelman, J., Bernstein, M., 2007. The attitudes of brain cancer patients and their caregivers towards death and dying: a qualitative study. BMC Palliat. Care 6, 7.

Litofsky, N.S., Farace, E., Anderson, F., Meyers, C.A., Huang, W., Laws, E.R., Kaplan, A.I., Brem, H., Berger, M.S., Westphal, M., 2004. Depression in Patients with High-grade Glioma: Results of the Glioma Outcomes Project. Neurosurgery 54, 358–367.

Liu, D., Davydenko, O., Lampson, M.A., 2012. Polo-like kinase-1 regulates kinetochore-microtubule dynamics and spindle checkpoint silencing. J. Cell Biol. 198, 491–9.

Liu, G., Yuan, X., Zeng, Z., Tunici, P., Ng, H., Abdulkadir, I.R., Lu, L., Irvin, D., Black, K.L., Yu, J.S., 2006. Analysis of gene expression and chemoresistance of CD133+ cancer stem cells in glioblastoma. Mol. Cancer 5, 67.

Liu, H., Peng, H.-W., Cheng, Y.-S., Yuan, H.S., Yang-Yen, H.-F., 2005. Stabilization and enhancement of the antiapoptotic activity of mcl-1 by TCTP. Mol. Cell. Biol. 25, 3117–3126.

Liu, L., Markowitz, S., Gerson, S.L., 1996. Mismatch repair mutations override alkyltransferase in conferring resistance to temozolomide but not to 1,3-bis(2-chloroethyl)nitrosourea. Cancer Res. 56, 5375–9.

Liu, P., Brown, S., Goktug, T., Channathodiyil, P., Kannappan, V., Hugnot, J.-P., Guichet, P.-O., Bian, X., Armesilla, A.L., Darling, J.L., Wang, W., 2012. Cytotoxic effect of disulfiram/copper on human glioblastoma cell lines and ALDH-positive cancer-stem-like cells. Br. J. Cancer 107, 1488–97.

Liu, P., Kumar, I.S., Brown, S., Kannappan, V., Tawari, P.E., Tang, J.Z., Jiang, W., Armesilla, a L., Darling, J.L., Wang, W., 2013. Disulfiram targets cancer stem-like cells and reverses

resistance and cross-resistance in acquired paclitaxel-resistant triple-negative breast cancer cells. Br. J. Cancer 1–10.

Liu, P., Wang, Z., Brown, S., Kannappan, V., Tawari, P.E., Jiang, W., Irache, J.M., Tang, J.Z., Armesilla, A.L., Darling, J.L., Tang, X., Wang, W., 2014. Liposome encapsulated Disulfiram inhibits NFκB pathway and targets breast cancer stem cells in vitro and in vivo. Oncotarget 5, 7471–85.

Liu, X., Lei, M., Erikson, R.L., 2006. Normal cells, but not cancer cells, survive severe Plk1 depletion. Mol. Cell. Biol. 26, 2093–108.

Liu, X.S., Song, B., Elzey, B.D., Ratliff, T.L., Konieczny, S.F., Cheng, L., Ahmad, N., Liu, X., 2011. Polo-like kinase 1 facilitates loss of Pten tumor suppressor-induced prostate cancer formation. J. Biol. Chem. 286, 35795–800.

Lottaz, C., Beier, D., Meyer, K., Kumar, P., Hermann, A., Schwarz, J., Junker, M., Oefner, P.J., Bogdahn, U., Wischhusen, J., Spang, R., Storch, A., Beier, C.P., 2010. Transcriptional profiles of CD133+ and CD133- glioblastoma-derived cancer stem cell lines suggest different cells of origin. Cancer Res. 70, 2030–40.

Louis, D.N., Ohgaki, H., Wiestler, O.D., Cavenee, W.K., Burger, P.C., Jouvet, A., Scheithauer, B.W., Kleihues, P., 2007. The 2007 WHO classification of tumours of the central nervous system. Acta Neuropathol. 114, 97–109.

Low, J.A., De Sauvage, F.J., 2010. Clinical experience with hedgehog pathway inhibitors. J. Clin. Oncol. 28, 5321–5326.

Lu, L.-Y., Wood, J.L., Minter-Dykhouse, K., Ye, L., Saunders, T.L., Yu, X., Chen, J., 2008. Polo-like kinase 1 is essential for early embryonic development and tumor suppression. Mol. Cell. Biol. 28, 6870–6876.

Ma, W.W., Messersmith, W. a., Dy, G.K., Weekes, C.D., Whitworth, A., Ren, C., Maniar, M., Wilhelm, F., Eckhardt, S.G., Adjei, A. a., Jimeno, A., 2012. Phase I study of rigosertib, an inhibitor of the phosphatidylinositol 3-kinase and polo-like kinase 1 pathways, combined with gemcitabine in patients with solid tumors and pancreatic cancer. Clin. Cancer Res. 18, 2048–2055.

Mabbott, D.J., Spiegler, B.J., Greenberg, M.L., Rutka, J.T., Hyder, D.J., Bouffet, E., 2005. Serial evaluation of academic and behavioral outcome after treatment with cranial radiation in childhood. J. Clin. Oncol. 23, 2256–2263.

Macůrek, L., Lindqvist, A., Lim, D., Lampson, M.A., Klompmaker, R., Freire, R., Clouin, C., Taylor, S.S., Yaffe, M.B., Medema, R.H., 2008. Polo-like kinase-1 is activated by aurora A to promote checkpoint recovery. Nature 455, 119–23.

Magni, M., Shammah, S., Schiró, R., Mellado, W., Dalla-Favera, R., Gianni, a M., 1996. Induction of cyclophosphamide-resistance by aldehyde-dehydrogenase gene transfer. Blood 87, 1097–103.

Maj, J., Grabowska, M., Kweik, J., 1970. The effect of disulfiram, diethyldithiocarbamate and dimethyldithiocarbamate on serotonin and 5-hydroxyindole-3-acetic acid brain levels in rats. Biochem. Pharmacol. 19, 2517–2519.

Malanga, M., Althaus, F.R., 2005. The role of poly(ADP-ribose) in the DNA damage signaling network. Biochem. Cell Biol. 83, 354–364.

Malkin, D., Li, F.P., Strong, L.C., Fraumeni, J.F., Nelson, C.E., Kim, D.H., Kassel, J., Gryka, M.A., Bischoff, F.Z., Tainsky, M.A., 1990. Germ line p53 mutations in a familial syndrome of breast cancer, sarcomas, and other neoplasms. Science 250, 1233–8.

Malkov, V. a, Serikawa, K. a, Balantac, N., Watters, J., Geiss, G., Mashadi-Hossein, A., Fare, T., 2009. Multiplexed measurements of gene signatures in different analytes using the Nanostring nCounter Assay System. BMC Res. Notes 2, 80.

Mamely, I., van Vugt, M.A., Smits, V.A.J., Semple, J.I., Lemmens, B., Perrakis, A., Medema, R.H., Freire, R., 2006. Polo-like kinase-1 controls proteasome-dependent degradation of Claspin during checkpoint recovery. Curr. Biol. 16, 1950–5.

Mandal, R., Strebhardt, K., 2013. Plk1: unexpected roles in DNA replication. Cell Res. 23, 1251–3.

Manoranjan, B., Wang, X., Hallett, R.M., Venugopal, C., Mack, S.C., McFarlane, N., Nolte, S.M., Scheinemann, K., Gunnarsson, T., Hassell, J. a., Taylor, M.D., Lee, C., Triscott, J., Foster, C.M., Dunham, C., Hawkins, C., Dunn, S.E., Singh, S.K., 2013. Foxg1 interacts with bmi1 to regulate self-renewal and tumorigenicity of Medulloblastoma stem cells. Stem Cells 31, 1266–1277.

Marcato, P., Dean, C., Pan, D., Araslanova, R., 2011. Aldehyde dehydrogenase activity of breast cancer stem cells is primarily due to isoform ALDH1A3 and its expression is predictive of metastasis. Stem Cells 32–45.

Mardin, B.R., Agircan, F.G., Lange, C., Schiebel, E., 2011. Plk1 controls the Nek2A-PP1γ antagonism in centrosome disjunction. Curr. Biol. 21, 1145–51.

Mardin, B.R., Lange, C., Baxter, J.E., Hardy, T., Scholz, S.R., Fry, A.M., Schiebel, E., 2010. Components of the Hippo pathway cooperate with Nek2 kinase to regulate centrosome disjunction. Nat. Cell Biol. 12, 1166–76.

Markant, S.L., Esparza, L. a, Sun, J., Barton, K., McCoig, L.M., Grant, G. a, Crawford, J.R., Levy, M.L., Northcott, P., Shih, D., Remke, M., Taylor, M.D., Wechsler-Reya, R.J., 2013.

Targeting Sonic Hedgehog-associated medulloblastoma through inhibition of Aurora and Polo-Like Kinases. Cancer Res. 73, 6310–6322.

Masica, D.L., Karchin, R., 2011. Correlation of somatic mutation and expression identifies genes important in human glioblastoma progression and survival. Cancer Res. 71, 4550–61.

Mayo, L.D., Dixon, J.E., Durden, D.L., Tonks, N.K., Donner, D.B., 2002. PTEN protects p53 from Mdm2 and sensitizes cancer cells to chemotherapy. J. Biol. Chem. 277, 5484–5489.

McGowan, C.H., Russell, P., 1995. Cell cycle regulation of human WEE1. EMBO J. 14, 2166–75.

McInnes, C., Estes, K., Baxter, M., Yang, Z., Farag, D.B., Johnston, P., Lazo, J.S., Wang, J., Wyatt, M.D., 2012. Targeting subcellular localization through the polo-box domain: non-ATP competitive inhibitors recapitulate a PLK1 phenotype. Mol. Cancer Ther. 11, 1683–92.

McInnes, C., Wyatt, M.D., 2011. PLK1 as an oncology target: current status and future potential. Drug Discov. Today 16, 619–25.

McManamy, C.S., Pears, J., Weston, C.L., Hanzely, Z., Ironside, J.W., Taylor, R.E., Grundy, R.G., Clifford, S.C., Ellison, D.W., 2007. Nodule formation and desmoplasia in medulloblastomas - Defining the nodular/desmoplastic variant and its biological behavior. Brain Pathol. 17, 151–164.

Medema, R.H., Lin, C.-C., Yang, J.C.-H., 2011. Polo-like Kinase 1 Inhibitors and Their Potential Role in Anticancer Therapy, with a Focus on NSCLC. Clin. Cancer Res. 17, 6459–6466.

Meropol, N.J., Schulman, K. a., 2007. Cost of cancer care: Issues and implications. J. Clin. Oncol. 25, 180–186.

Merve, A., Dubuc, A.M., Zhang, X., Remke, M., Baxter, P.A., Li, X.-N., Taylor, M.D., Marino, S., 2014. Polycomb group gene BMI1 controls invasion of medulloblastoma cells and inhibits BMP-regulated cell adhesion. Acta Neuropathol. Commun. 2, 10.

Milde, T., Lodrini, M., Savelyeva, L., Korshunov, A., Kool, M., Brueckner, L.M., Antunes, A.S.L.M., Oehme, I., Pekrun, A., Pfister, S.M., Kulozik, A.E., Witt, O., Deubzer, H.E., 2012. HD-MB03 is a novel Group 3 medulloblastoma model demonstrating sensitivity to histone deacetylase inhibitor treatment. J. Neurooncol. 110, 335–348.

Milne, C.P., Bruss, J.B., 2008. The economics of pediatric formulation development for off-patent drugs. Clin. Ther. 30, 2133–2145.

Mimeault, M., Batra, S.K., 2008. Recent advances in the development of novel anti-cancer drugs targeting cancer stem/progenitor cells. Drug Dev. Res. 69, 415–430.

Min, H.S., Lee, J.Y., Kim, S.-K., Park, S.-H., 2013. Genetic grouping of medulloblastomas by representative markers in pathologic diagnosis. Transl. Oncol. 6, 265–72.

Mischel, P.S., Nelson, S.F., Cloughesy, T.F., 2003. Molecular analysis of glioblastoma: Pathway profiling and its implications for patient therapy. Cancer Biol. Ther. 2, 242–247.

Mizoguchi, M., Guan, Y., Yoshimoto, K., Hata, N., Amano, T., Nakamizo, A., Sasaki, T., 2013. Clinical implications of microRNAs in human glioblastoma. Front. Oncol. 3, 19.

Molofsky, A. V, Pardal, R., Iwashita, T., Park, I.-K., Clarke, M.F., Morrison, S.J., 2003. Bmi-1 dependence distinguishes neural stem cell self-renewal from progenitor proliferation. Nature 425, 962–967.

Morgello, S., Uson, R.R., Schwartz, E.J., Haber, R.S., 1995. The human blood-brain barrier glucose transporter (GLUT1) is a glucose transporter of gray matter astrocytes. Glia 14, 43–54.

Morrison, S.J., White, P.M., Zock, C., Anderson, D.J., 1999. Prospective identification, isolation by flow cytometry, and in vivo self-renewal of multipotent mammalian neural crest stem cells. Cell 96, 737–749.

Moshe, Y., Boulaire, J., Pagano, M., Hershko, A., 2004. Role of Polo-like kinase in the degradation of early mitotic inhibitor 1, a regulator of the anaphase promoting complex/cyclosome. Proc. Natl. Acad. Sci. U. S. A. 101, 7937–42.

Mross, K., Frost, A., Steinbild, S., Hedbom, S., Rentschler, J., Kaiser, R., Rouyrre, N., Trommeshauser, D., Hoesl, C.E., Munzert, G., 2008. Phase I dose escalation and pharmacokinetic study of BI 2536, a novel Polo-like kinase 1 inhibitor, in patients with advanced solid tumors. J. Clin. Oncol. 26, 5511–7.

Mueller, P.R., Coleman, T.R., Kumagai, A., Dunphy, W.G., 1995. Myt1: a membrane-associated inhibitory kinase that phosphorylates Cdc2 on both threonine-14 and tyrosine-15. Science 270, 86–90.

Muller, P. a J., Vousden, K.H., 2013. P53 Mutations in Cancer. Nat. Cell Biol. 15, 2–8.

Müller-Tidow, C., Bug, G., Lübbert, M., Krämer, A., Krauter, J., Valent, P., Nachbaur, D., Berdel, W.E., Ottmann, O.G., Fritsch, H., Munzert, G., Garin-Chesa, P., Fleischer, F., Taube, T., Döhner, H., 2013. A randomized, open-label, phase I/II trial to investigate the maximum tolerated dose of the Polo-like kinase inhibitor BI 2536 in elderly patients with refractory/relapsed acute myeloid leukaemia. Br. J. Haematol. 163, 214–22.

Mundt, K.E., Golsteyn, R.M., Lane, H. a, Nigg, E. a, 1997. On the regulation and function of human polo-like kinase 1 (PLK1): effects of overexpression on cell cycle progression. Biochem. Biophys. Res. Commun. 239, 377–385.

Muñoz, D.M., Guha, A., 2011. Mouse Models to Interrogate the Implications of the Differentiation Status in the Ontogeny of Gliomas 2, 590–598.

Musacchio, J.M., Goldstein, M., Anagnoste, B., Poch, G., Kopin, I.J., 1966. Inhibition of dopamine-beta-hydroxylase by disulfiram in vivo. J. Pharmacol. Exp. Ther. 152, 56–61.

Nakajima, H., Toyoshima-Morimoto, F., Taniguchi, E., Nishida, E., 2003. Identification of a consensus motif for Plk (Polo-like kinase) phosphorylation reveals Myt1 as a Plk1 substrate. J. Biol. Chem. 278, 25277–80.

Nakamura, M., Watanabe, T., Yonekawa, Y., Kleihues, P., Ohgaki, H., 2001. Promoter methylation of the DNA repair gene MGMT in astrocytomas is frequently associated with G:C --> A:T mutations of the TP53 tumor suppressor gene. Carcinogenesis 22, 1715–1719.

Narita, Y., Nagane, M., Mishima, K., Huang, H.-J.S., Furnari, F.B., Cavenee, W.K., 2002. Mutant epidermal growth factor receptor signaling down-regulates p27 through activation of the phosphatidylinositol 3-kinase/Akt pathway in glioblastomas. Cancer Res. 62, 6764–9.

Natarajan, S., Li, Y., Miller, E.E., Shih, D.J., Taylor, M.D., Stearns, T.M., Bronson, R.T., Ackerman, S.L., Yoon, J.K., Yun, K., 2013. Notch1-induced brain tumor models the sonic hedgehog subgroup of human medulloblastoma. Cancer Res. 73, 5381–90.

Nechushtan, H., Hamamreh, Y., Nidal, S., Gotfried, M., Baron, A., Shalev, Y.I., Nisman, B., Pereta, T., Peylan-Ramu, N., 2015. Clinical Trial Results A Phase IIb Trial Assessing the Addition of Disulfiram to Chemotherapy for the Treatment of Metastatic Non-Small Cell Lung Cancer. Oncologist 20, 366–367.

Neef, R., Gruneberg, U., Kopajtich, R., Li, X., Nigg, E.A., Sillje, H., Barr, F.A., 2007. Choice of Plk1 docking partners during mitosis and cytokinesis is controlled by the activation state of Cdk1. Nat. Cell Biol. 9, 436–44.

Neyns, B., Sadones, J., Joosens, E., Bouttens, F., Verbeke, L., Baurain, J.F., D'Hondt, L., Strauven, T., Chaskis, C., In't Veld, P., Michotte, a., De Greve, J., 2009. Stratified phase II trial of cetuximab in patients with recurrent high-grade glioma. Ann. Oncol. 20, 1596–1603.

Nicklas, R.B., Ward, S.C., 1994. Elements of error correction in mitosis: microtubule capture, release, and tension. J. Cell Biol. 126, 1241–53.

Nielsen, T.O., Parker, J.S., Leung, S., Voduc, D., Ebbert, M., Vickery, T., Davies, S.R., Snider, J., Stijleman, I.J., Reed, J., Cheang, M.C.U., Mardis, E.R., Perou, C.M., Bernard, P.S., Ellis, M.J., 2010. A comparison of PAM50 intrinsic subtyping with immunohistochemistry and clinical prognostic factors in tamoxifen-treated estrogen receptor-positive breast cancer. Clin. Cancer Res. 16, 5222–32.

Nogueira, L., Ruiz-Ontañon, P., Vazquez-Barquero, A., Moris, F., Fernandez-Luna, J.L., 2011. The NFκB pathway: a therapeutic target in glioblastoma. Oncotarget 2, 646–53.

Northcott, P.A., Hielscher, T., Dubuc, A., Mack, S., Shih, D., Remke, M., Al-Halabi, H., Albrecht, S., Jabado, N., Eberhart, C.G., Grajkowska, W., Weiss, W. a, Clifford, S.C., Bouffet, E., Rutka, J.T., Korshunov, A., Pfister, S., Taylor, M.D., 2011a. Pediatric and adult sonic hedgehog medulloblastomas are clinically and molecularly distinct. Acta Neuropathol. 122, 231–40.

Northcott, P.A., Jones, D.T.W., Kool, M., Robinson, G.W., Gilbertson, R.J., Cho, Y.-J., Pomeroy, S.L., Korshunov, A., Lichter, P., Taylor, M.D., Pfister, S.M., 2012a. Medulloblastomics: the end of the beginning. Nat. Rev. Cancer 12, 818–834.

Northcott, P.A., Korshunov, A., Pfister, S.M., Taylor, M.D., 2012b. The clinical implications of medulloblastoma subgroups. Nat. Rev. Neurol. 8, 340–351.

Northcott, P.A., Korshunov, A., Witt, H., Hielscher, T., Eberhart, C.G., Mack, S., Bouffet, E., Clifford, S.C., Hawkins, C.E., French, P., Rutka, J.T., Pfister, S., Taylor, M.D., 2011b. Medulloblastoma comprises four distinct molecular variants. J. Clin. Oncol. 29, 1408–14.

Northcott, P.A., Lee, C., Zichner, T., Stütz, A.M., Erkek, S., Kawauchi, D., Shih, D.J.H., Hovestadt, V., Zapatka, M., Sturm, D., Jones, D.T.W., Kool, M., Remke, M., Cavalli, F.M.G., Zuyderduyn, S., Bader, G.D., VandenBerg, S., Esparza, L.A., Ryzhova, M., Wang, W., Wittmann, A., Stark, S., Sieber, L., Seker-Cin, H., Linke, L., Kratochwil, F., Jäger, N., Buchhalter, I., Imbusch, C.D., Zipprich, G., Raeder, B., Schmidt, S., Diessl, N., Wolf, S., Wiemann, S., Brors, B., Lawerenz, C., Eils, J., Warnatz, H.-J., Risch, T., Yaspo, M.-L., Weber, U.D., Bartholomae, C.C., von Kalle, C., Turányi, E., Hauser, P., Sanden, E., Darabi, A., Siesjö, P., Sterba, J., Zitterbart, K., Sumerauer, D., van Sluis, P., Versteeg, R., Volckmann, R., Koster, J., Schuhmann, M.U., Ebinger, M., Grimes, H.L., Robinson, G.W., Gajjar, A., Mynarek, M., von Hoff, K., Rutkowski, S., Pietsch, T., Scheurlen, W., Felsberg, J., Reifenberger, G., Kulozik, A.E., von Deimling, A., Witt, O., Eils, R., Gilbertson, R.J., Korshunov, A., Taylor, M.D., Lichter, P., Korbel, J.O., Wechsler-Reya, R.J., Pfister, S.M., 2014. Enhancer hijacking activates GFI1 family oncogenes in medulloblastoma. Nature 511, 428–34.

Northcott, P.A., Shih, D.J.H., Peacock, J., Garzia, L., Sorana Morrissy, A., Zichner, T., Stütz, A.M., Korshunov, A., Reimand, J., Schumacher, S.E., Beroukhim, R., Ellison, D.W., Marshall, C.R., Lionel, A.C., Mack, S., Dubuc, A., Yao, Y., Ramaswamy, V., Luu, B., Rolider, A., Cavalli, F.M.G., Wang, X., Remke, M., Wu, X., Chiu, R.Y.B., Chu, A., Chuah, E., Corbett, R.D., Hoad, G.R., Jackman, S.D., Li, Y., Lo, A., Mungall, K.L., Ming Nip, K., Qian, J.Q., Raymond, A.G.J., Thiessen, N., Varhol, R.J., Birol, I., Moore, R. a., Mungall, A.J., Holt, R., Kawauchi, D., Roussel, M.F., Kool, M., Jones, D.T.W., Witt, H., Fernandez-L, A., Kenney, A.M., Wechsler-Reya, R.J., Dirks, P., Aviv, T., Grajkowska, W. a., Perek-Polnik, M., Haberler, C.C., Delattre, O., Reynaud, S.S., Doz, F.F., Pernet-Fattet, S.S., Cho, B.-K., Kim, S.-K., Wang, K.-C., Scheurlen, W., Eberhart, C.G., Fèvre-Montange, M.,

Jouvet, A., Pollack, I.F., Fan, X., Muraszko, K.M., Yancey Gillespie, G., Di Rocco, C., Massimi, L., Michiels, E.M.C., Kloosterhof, N.K., French, P.J., Kros, J.M., Olson, J.M., Ellenbogen, R.G., Zitterbart, K., Kren, L., Thompson, R.C., Cooper, M.K., Lach, B., McLendon, R.E., Bigner, D.D., Fontebasso, A., Albrecht, S., Jabado, N., Lindsey, J.C., Bailey, S., Gupta, N., Weiss, W. a., Bognár, L., Klekner, A., Van Meter, T.E., Kumabe, T., Tominaga, T., Elbabaa, S.K., Leonard, J.R., Rubin, J.B., Liau, L.M., Van Meir, E.G., Fouladi, M., Nakamura, H., Cinalli, G., Garami, M., Hauser, P., Saad, A.G., Iolascon, A., Jung, S., Carlotti, C.G., Vibhakar, R., Shin Ra, Y., Robinson, S., Zollo, M., Faria, C.C., Chan, J. a., Levy, M.L., Sorensen, P.H.B., Meyerson, M., Pomeroy, S.L., Cho, Y.-J., Bader, G.D., Tabori, U., Hawkins, C.E., Bouffet, E., Scherer, S.W., Rutka, J.T., Malkin, D., Clifford, S.C., Jones, S.J.M., Korbel, J.O., Pfister, S.M., Marra, M. a., Taylor, M.D., 2012c. Subgroup-specific structural variation across 1,000 medulloblastoma genomes. Nature 488, 49–56.

Northcott, P.A., Shih, D.J.H., Remke, M., Cho, Y.-J., Kool, M., Hawkins, C., Eberhart, C.G., Dubuc, A., Guettouche, T., Cardentey, Y., Bouffet, E., Pomeroy, S.L., Marra, M., Malkin, D., Rutka, J.T., Korshunov, A., Pfister, S., Taylor, M.D., 2012d. Rapid, reliable, and reproducible molecular sub-grouping of clinical medulloblastoma samples. Acta Neuropathol. 123, 615–626.

Noushmehr, H., Weisenberger, D.J., Diefes, K., Phillips, H.S., Pujara, K., Berman, B.P., Pan, F., Pelloski, C.E., Sulman, E.P., Bhat, K.P., Verhaak, R.G.W., Hoadley, K. a., Hayes, D.N., Perou, C.M., Schmidt, H.K., Ding, L., Wilson, R.K., Van Den Berg, D., Shen, H., Bengtsson, H., Neuvial, P., Cope, L.M., Buckley, J., Herman, J.G., Baylin, S.B., Laird, P.W., Aldape, K., 2010. Identification of a CpG Island Methylator Phenotype that Defines a Distinct Subgroup of Glioma. Cancer Cell 17, 510–522.

O'Brien, A., Barber, J.E.B., Reid, S., Niknejad, N., Dimitroulakos, J., 2012. Enhancement of cisplatin cytotoxicity by disulfiram involves activating transcription factor 3. Anticancer Res. 32, 2679–2688.

Odent, S., Atti-Bitach, T., Blayau, M., Mathieu, M., Aug, J., Delezo de, A.L., Gall, J.Y., Le Marec, B., Munnich, A., David, V., Vekemans, M., 1999. Expression of the Sonic hedgehog (SHH) gene during early human development and phenotypic expression of new mutations causing holoprosencephaly. Hum. Mol. Genet. 8, 1683–9.

Ohgaki, H., Dessen, P., Jourde, B., Horstmann, S., Nishikawa, T., Di Patre, P.L., Burkhard, C., Schüler, D., Probst-Hensch, N.M., Maiorka, P.C., Baeza, N., Pisani, P., Yonekawa, Y., Yasargil, M.G., Lütolf, U.M., Kleihues, P., 2004. Genetic pathways to glioblastoma: A population-based study. Cancer Res. 64, 6892–6899.

Ohgaki, H., Kleihues, P., 2007. Genetic pathways to primary and secondary glioblastoma. Am. J. Pathol. 170, 1445–1453.

Oldendorf, W.H., 1974. Lipid solubility and drug penetration of the blood brain barrier. Proc. Soc. Exp. Biol. Med. 147, 813–815.

Oliver, T.G., Grasfeder, L.L., Carroll, A.L., Kaiser, C., Gillingham, C.L., Lin, S.M., Wickramasinghe, R., Scott, M.P., Wechsler-Reya, R.J., 2003. Transcriptional profiling of the Sonic hedgehog response: a critical role for N-myc in proliferation of neuronal precursors. Proc. Natl. Acad. Sci. U. S. A. 100, 7331–6.

Olmos, D., Barker, D., Sharma, R., Brunetto, A.T., Yap, T.A., Taegtmeyer, A.B., Barriuso, J., Medani, H., Degenhardt, Y.Y., Allred, A.J., Smith, D.A., Murray, S.C., Lampkin, T.A., Dar, M.M., Wilson, R., de Bono, J.S., Blagden, S.P., 2011. Phase I study of GSK461364, a specific and competitive Polo-like kinase 1 inhibitor, in patients with advanced solid malignancies. Clin. Cancer Res. 17, 3420–30.

Oskarsson, A., 1984. Dithiocarbamate-induced redistribution and increased brain uptake of lead in rats. Neurotoxicology 5, 283–293.

Ostermann, S., Csajka, C., Buclin, T., Leyvraz, S., Lejeune, F., Decosterd, L. a, Stupp, R., 2004. Plasma and cerebrospinal fluid population pharmacokinetics of temozolomide in malignant glioma patients. Clin. Cancer Res. 10, 3728–3736.

Ostrom, Q.T., Gittleman, H., Liao, P., Rouse, C., Chen, Y., Dowling, J., Wolinsky, Y., Kruchko, C., Barnholtz-Sloan, J., 2014. CBTRUS Statistical Report: Primary Brain and Central Nervous System Tumors Diagnosed in the United States in 2007–2011. Neuro. Oncol. 16, iv1–iv63.

Packer, R.J., Gajjar, A., Vezina, G., Rorke-Adams, L., Burger, P.C., Robertson, P.L., Bayer, L., LaFond, D., Donahue, B.R., Marymont, M.H., Muraszko, K., Langston, J., Sposto, R., 2006. Phase III study of craniospinal radiation therapy followed by adjuvant chemotherapy for newly diagnosed average-risk medulloblastoma. J. Clin. Oncol. 24, 4202–4208.

Pallini, R., Ricci-Vitiani, L., Banna, G.L., Signore, M., Lombardi, D., Todaro, M., Stassi, G., Martini, M., Maira, G., Larocca, L.M., De Maria, R., 2008. Cancer Stem Cell Analysis and Clinical Outcome in Patients with Glioblastoma Multiforme. Clin. Cancer Res. 14, 8205–8212.

Palma, V., Lim, D. a, Dahmane, N., Sánchez, P., Brionne, T.C., Herzberg, C.D., Gitton, Y., Carleton, A., Alvarez-Buylla, A., Ruiz i Altaba, A., 2005. Sonic hedgehog controls stem cell behavior in the postnatal and adult brain. Development 132, 335–344.

Pan, Y., Bai, C.B., Joyner, A.L., Wang, B., 2006. Sonic hedgehog signaling regulates Gli2 transcriptional activity by suppressing its processing and degradation. Mol. Cell. Biol. 26, 3365–77.

Pandita, A., Aldape, K.D., Zadeh, G., Guha, A., James, C.D., 2004. Contrasting in vivo and in vitro fates of glioblastoma cell subpopulations with amplified EGFR. Genes. Chromosomes Cancer 39, 29–36.

Pangalos, M.N., Schechter, L.E., Hurko, O., 2007. Drug development for CNS disorders: strategies for balancing risk and reducing attrition. Nat. Rev. Drug Discov. 6, 521–532.

Paranjpe, A., Zhang, R., Ali-Osman, F., Bobustuc, G.C., Srivenugopal, K.S., 2014. Disulfiram is a direct and potent inhibitor of human O6-methylguanine-DNA methyltransferase (MGMT) in brain tumor cells and mouse brain and markedly increases the alkylating DNA damage. Carcinogenesis 35, 692–702.

Park, D.M., Rich, J.N., 2009. Biology of glioma cancer stem cells. Mol. Cells 28, 7–12.

Park, T.S., Hoffman, H.J., Hendrick, E.B., Humphreys, R.P., Becker, L.E., 1983. Medulloblastoma: clinical presentation and management. Experience at the hospital for sick children, toronto, 1950-1980. J. Neurosurg. 58, 543–52.

Parsons, D.W., Li, M., Zhang, X., Jones, S., Leary, R.J., Lin, J.C.-H., Boca, S.M., Carter, H., Samayoa, J., Bettegowda, C., Gallia, G.L., Jallo, G.I., Binder, Z. a, Nikolsky, Y., Hartigan, J., Smith, D.R., Gerhard, D.S., Fults, D.W., VandenBerg, S., Berger, M.S., Marie, S.K.N., Shinjo, S.M.O., Clara, C., Phillips, P.C., Minturn, J.E., Biegel, J. a, Judkins, A.R., Resnick, A.C., Storm, P.B., Curran, T., He, Y., Rasheed, B.A., Friedman, H.S., Keir, S.T., McLendon, R., Northcott, P. a, Taylor, M.D., Burger, P.C., Riggins, G.J., Karchin, R., Parmigiani, G., Bigner, D.D., Yan, H., Papadopoulos, N., Vogelstein, B., Kinzler, K.W., Velculescu, V.E., 2011. The genetic landscape of the childhood cancer medulloblastoma. Science 331, 435–9.

Pasquali, S.K., Lam, W.K., Chiswell, K., Kemper, A.R., Li, J.S., 2012. Status of the pediatric clinical trials enterprise: an analysis of the US ClinicalTrials.gov registry. Pediatrics 130, e1269–77.

Pei, Y., Brun, S.N., Markant, S.L., Lento, W., Gibson, P., Taketo, M.M., Giovannini, M., Gilbertson, R.J., Wechsler-Reya, R.J., 2012a. WNT signaling increases proliferation and impairs differentiation of stem cells in the developing cerebellum. Development 139, 1724–1733.

Pei, Y., Moore, C.E., Wang, J., Tewari, A.K., Eroshkin, A., Cho, Y.-J., Witt, H., Korshunov, A., Read, T.-A., Sun, J.L., Schmitt, E.M., Miller, C.R., Buckley, A.F., McLendon, R.E., Westbrook, T.F., Northcott, P.A., Taylor, M.D., Pfister, S.M., Febbo, P.G., Wechsler-Reya, R.J., 2012b. An Animal Model of MYC-Driven Medulloblastoma. Cancer Cell 21, 155–167.

Perry, J., Chambers, A., Spithoff, K., Laperriere, N., 2007. Gliadel wafers in the treatment of malignant glioma: a systematic review. Curr. Oncol. 14, 189–194.

Petronczki, M., Glotzer, M., Kraut, N., Peters, J.-M., 2007. Polo-like kinase 1 triggers the initiation of cytokinesis in human cells by promoting recruitment of the RhoGEF Ect2 to the central spindle. Dev. Cell 12, 713–25.

Petronczki, M., Lénárt, P., Peters, J.M., 2008. Polo on the Rise-from Mitotic Entry to Cytokinesis with Plk1. Dev. Cell 14, 646–659.

Pezuk, J. a, Brassesco, M.S., Morales, a G., de Oliveira, J.C., de Paula Queiroz, R.G., Machado, H.R., Carlotti, C.G., Neder, L., Scrideli, C. a, Tone, L.G., 2013. Polo-like kinase 1 inhibition causes decreased proliferation by cell cycle arrest, leading to cell death in glioblastoma. Cancer Gene Ther. 20, 499–506.

Pfister, S., Remke, M., Benner, A., Mendrzyk, F., Toedt, G., Felsberg, J., Wittmann, A., Devens, F., Gerber, N.U., Joos, S., Kulozik, A., Reifenberger, G., Rutkowski, S., Wiestler, O.D., Radlwimmer, B., Scheurlen, W., Lichter, P., Korshunov, A., 2009. Outcome prediction in pediatric medulloblastoma based on DNA copy-number aberrations of chromosomes 6q and 17q and the MYC and MYCN loci. J. Clin. Oncol. 27, 1627–1636.

Phillips, H.S., Kharbanda, S., Chen, R., Forrest, W.F., Soriano, R.H., Wu, T.D., Misra, A., Nigro, J.M., Colman, H., Soroceanu, L., Williams, P.M., Modrusan, Z., Feuerstein, B.G., Aldape, K., 2006. Molecular subclasses of high-grade glioma predict prognosis, delineate a pattern of disease progression, and resemble stages in neurogenesis. Cancer Cell 9, 157–173.

Piccirillo, S.G.M., Reynolds, B. a, Zanetti, N., Lamorte, G., Binda, E., Broggi, G., Brem, H., Olivi, a, Dimeco, F., Vescovi, a L., 2006. Bone morphogenetic proteins inhibit the tumorigenic potential of human brain tumour-initiating cells. Nature 444, 761–5.

Piccirillo, S.G.M., Vescovi, A.L., 2007. Brain tumour stem cells: possibilities of new therapeutic strategies. Expert Opin. Biol. Ther. 7, 1129–35.

Pietsch, T., Schmidt, R., Remke, M., Korshunov, A., Hovestadt, V., Jones, D.T.W., Felsberg, J., Kaulich, K., Goschzik, T., Kool, M., Northcott, P. a., Von Hoff, K., Von Bueren, A.O., Friedrich, C., Mynarek, M., Skladny, H., Fleischhack, G., Taylor, M.D., Cremer, F., Lichter, P., Faldum, A., Reifenberger, G., Rutkowski, S., Pfister, S.M., 2014. Prognostic significance of clinical, histopathological, and molecular characteristics of medulloblastomas in the prospective HIT2000 multicenter clinical trial cohort. Acta Neuropathol. 128, 137–149.

Pilkinton, M., Sandoval, R., Colamonici, O.R., 2007. Mammalian Mip/LIN-9 interacts with either the p107, p130/E2F4 repressor complex or B-Myb in a cell cycle-phase-dependent context distinct from the Drosophila dREAM complex. Oncogene 26, 7535–43.

Pizer, B., Donachie, P.H.J., Robinson, K., Taylor, R.E., Michalski, A., Punt, J., Ellison, D.W., Picton, S., 2011. Treatment of recurrent central nervous system primitive neuroectodermal

tumours in children and adolescents: Results of a Children's Cancer and Leukaemia Group study. Eur. J. Cancer 47, 1389–1397.

Pletsas, D., Garelnabi, E. a E., Li, L., Phillips, R.M., Wheelhouse, R.T., 2013. Synthesis and quantitative structure-activity relationship of imidazotetrazine prodrugs with activity independent of O6-methylguanine-DNA- methyltransferase, DNA mismatch repair, and p53. J. Med. Chem. 56, 7120–7132.

Po, A., Ferretti, E., Miele, E., De Smaele, E., Paganelli, A., Canettieri, G., Coni, S., Di Marcotullio, L., Biffoni, M., Massimi, L., Di Rocco, C., Screpanti, I., Gulino, A., 2010. Hedgehog controls neural stem cells through p53-independent regulation of Nanog. EMBO J. 29, 2646–2658.

Pomeroy, S.L., Tamayo, P., Gaasenbeek, M., Sturla, L.M., Angelo, M., McLaughlin, M.E., Kim, J.Y.H., Goumnerova, L.C., Black, P.M., Lau, C., Allen, J.C., Zagzag, D., Olson, J.M., Curran, T., Wetmore, C., Biegel, J. a, Poggio, T., Mukherjee, S., Rifkin, R., Califano, A., Stolovitzky, G., Louis, D.N., Mesirov, J.P., Lander, E.S., Golub, T.R., 2002. Prediction of central nervous system embryonal tumour outcome based on gene expression. Nature 415, 436–442.

Pöschl, J., Stark, S., Neumann, P., Gröbner, S., Kawauchi, D., Jones, D.T.W., Northcott, P. a, Lichter, P., Pfister, S.M., Kool, M., Schüller, U., 2014. Genomic and transcriptomic analyses match medulloblastoma mouse models to their human counterparts. Acta Neuropathol. 128, 123–136.

Prados, M.D., Berger, M.S., Wilson, C.B., 1998. Primary central nervous system tumors: advances in knowledge and treatment. CA. Cancer J. Clin. 48, 331–360, 321.

Prados, M.D., Chang, S.M., Butowski, N., Deboer, R., Parvataneni, R., Carliner, H., Kabuubi, P., Ayers-Ringler, J., Rabbitt, J., Page, M., Fedoroff, A., Sneed, P.K., Berger, M.S., McDermott, M.W., Parsa, A.T., Vandenberg, S., James, C.D., Lamborn, K.R., Stokoe, D., Haas-Kogan, D. a., 2009. Phase II study of erlotinib plus temozolomide during and after radiation therapy in patients with newly diagnosed glioblastoma multiforme or gliosarcoma. J. Clin. Oncol. 27, 579–584.

Preston-Martin, S., Yu, M.C., Benton, B., Henderson, B.E., 1982. N-Nitroso compounds and childhood brain tumors: a case-control study. Cancer Res. 42, 5240–5.

Printz, C., 2015. Death with dignity: Young patient with brain tumor puts a face on the right-to-die movement. Cancer 121, 641–643.

Provias, J.P., Becker, L.E., 1996. Cellular and molecular pathology of medulloblastoma. J. Neurooncol. 29, 35–43.

Pugh, T.J., Weeraratne, S.D., Archer, T.C., Pomeranz Krummel, D. a., Auclair, D., Bochicchio, J., Carneiro, M.O., Carter, S.L., Cibulskis, K., Erlich, R.L., Greulich, H., Lawrence, M.S., Lennon, N.J., McKenna, A., Meldrim, J., Ramos, A.H., Ross, M.G., Russ, C., Shefler, E., Sivachenko, A., Sogoloff, B., Stojanov, P., Tamayo, P., Mesirov, J.P., Amani, V., Teider, N., Sengupta, S., Francois, J.P., Northcott, P. a., Taylor, M.D., Yu, F., Crabtree, G.R., Kautzman, A.G., Gabriel, S.B., Getz, G., Jäger, N., Jones, D.T.W., Lichter, P., Pfister, S.M., Roberts, T.M., Meyerson, M., Pomeroy, S.L., Cho, Y.-J., 2012. Medulloblastoma exome sequencing uncovers subtype-specific somatic mutations. Nature 4–8.

Purow, B.W., Haque, R.M., Noel, M.W., Su, Q., Burdick, M.J., Lee, J., Sundaresan, T., Pastorino, S., Park, J.K., Mikolaenko, I., Maric, D., Eberhart, C.G., Fine, H. a., 2005. Expression of Notch-1 and its ligands, Delta-like-1 and Jagged=1, is critical for glioma cell survival and proliferation. Cancer Res. 65, 2353–2363.

Pursche, S., Schleyer, E., von Bonin, M., Ehninger, G., Said, S.M., Prondzinsky, R., Illmer, T., Wang, Y., Hosius, C., Nikolova, Z., Bornhäuser, M., Dresemann, G., 2008. Influence of enzyme-inducing antiepileptic drugs on trough level of imatinib in glioblastoma patients. Curr. Clin. Pharmacol. 3, 198–203.

Qian, Y., Hua, E., Bisht, K., Woditschka, S., Skordos, K.W., Liewehr, D.J., Steinberg, S.M., Brogi, E., Akram, M.M., Killian, J.K., Edelman, D.C., Pineda, M., Scurci, S., Degenhardt, Y.Y., Laquerre, S., Lampkin, T. a, Meltzer, P.S., Camphausen, K., Steeg, P.S., Palmieri, D., 2011. Inhibition of Polo-like kinase 1 prevents the growth of metastatic breast cancer cells in the brain. Clin. Exp. Metastasis 28, 899–908.

Qiang, M., Yan, G., Weiwen, X., Yingsong, W., Fuli, H., Wen, S., Maoliang, H., Hongyan, D., Ming, L., 2010. The role of translationally controlled tumor protein in tumor growth and metastasis of colon adenocarcinoma cells. J. Proteome Res. 9, 40–49.

Quan, N., Banks, W.A., 2007. Brain-immune communication pathways. Brain. Behav. Immun. 21, 727–735.

Raghavan, R., Steart, P. V, Weller, R.O., 1990. Cell proliferation patterns in the diagnosis of astrocytomas, anaplastic astrocytomas and glioblastoma multiforme: a Ki-67 study. Neuropathol. Appl. Neurobiol. 16, 123–33.

Ramanathan, R.K., Hamburg, S.I., Borad, M.J., Seetharam, M., Kundranda, M.N., Lee, P., Fredlund, P., Gilbert, M., Mast, C., Semple, S.C., Judge, A.D., Crowell, B., Vocila, L., MacLachlan, I., Northfelt, D.W., 2013. Abstract LB-289: A phase I dose escalation study of TKM-080301, a RNAi therapeutic directed against PLK1, in patients with advanced solid tumors. Cancer Res. 73, LB–289–LB–289.

Rapley, J., Baxter, J.E., Blot, J., Wattam, S.L., Casenghi, M., Meraldi, P., Nigg, E.A., Fry, A.M., 2005. Coordinate Regulation of the Mother Centriole Component Nlp by Nek2 and Plk1 Protein Kinases. Mol. Cell. Biol. 25, 1309–1324.

Rasper, M., Schäfer, A., Piontek, G., Teufel, J., Brockhoff, G., Ringel, F., Heindl, S., Zimmer, C., Schlegel, J., 2010. Aldehyde dehydrogenase 1 positive glioblastoma cells show brain tumor stem cell capacity. Neuro. Oncol. 12, 1024–33.

Rausch, T., Jones, D.T.W., Zapatka, M., Stütz, A.M., Zichner, T., Weischenfeldt, J., Jäger, N., Remke, M., Shih, D., Northcott, P. a., Pfaff, E., Tica, J., Wang, Q., Massimi, L., Witt, H., Bender, S., Pleier, S., Cin, H., Hawkins, C., Beck, C., Von Deimling, A., Hans, V., Brors, B., Eils, R., Scheurlen, W., Blake, J., Benes, V., Kulozik, A.E., Witt, O., Martin, D., Zhang, C., Porat, R., Merino, D.M., Wasserman, J., Jabado, N., Fontebasso, A., Bullinger, L., Rücker, F.G., Döhner, K., Döhner, H., Koster, J., Molenaar, J.J., Versteeg, R., Kool, M., Tabori, U., Malkin, D., Korshunov, A., Taylor, M.D., Lichter, P., Pfister, S.M., Korbel, J.O., 2012. Genome sequencing of pediatric medulloblastoma links catastrophic DNA rearrangements with TP53 mutations. Cell 148, 59–71.

Read, T., Fogarty, M.P., Markant, S.L., Mclendon, R.E., Wei, Z., Ellison, D.W., Febbo, P.G., Wechsler-reya, R.J., 2009. Identification of CD15 as a Marker for Tumor-Propagating Cells in a Mouse Model of Medulloblastoma. Cancer 15, 135–147.

Reilly, K.M., Loisel, D.A., Bronson, R.T., McLaughlin, M.E., Jacks, T., 2000. Nf1;Trp53 mutant mice develop glioblastoma with evidence of strain-specific effects. Nat. Genet. 26, 109–113.

Remke, M., Hielscher, T., Korshunov, A., Northcott, P. a, Bender, S., Kool, M., Westermann, F., Benner, A., Cin, H., Ryzhova, M., Sturm, D., Witt, H., Haag, D., Toedt, G., Wittmann, A., Schöttler, A., von Bueren, A.O., von Deimling, A., Rutkowski, S., Scheurlen, W., Kulozik, A.E., Taylor, M.D., Lichter, P., Pfister, S.M., 2011a. FSTL5 Is a Marker of Poor Prognosis in Non-WNT/Non-SHH Medulloblastoma. J. Clin. Oncol. 29, 3852–61.

Remke, M., Hielscher, T., Northcott, P. a., Witt, H., Ryzhova, M., Wittmann, A., Benner, A., Von Deimling, A., Scheurlen, W., Perry, A., Croul, S., Kulozik, A.E., Lichter, P., Taylor, M.D., Pfister, S.M., Korshunov, A., 2011b. Adult medulloblastoma comprises three major molecular variants. J. Clin. Oncol. 29, 2717–2723.

Reynolds, B. a, Weiss, S., 1992. Generation of neurons and astrocytes from isolated cells of the adult mammalian central nervous system. Science 255, 1707–10.

Rho, S.B., Lee, J.H., Park, M.S., Byun, H.J., Kang, S., Seo, S.S., Kim, J.Y., Park, S.Y., 2011. Anti-apoptotic protein TCTP controls the stability of the tumor suppressor p53. FEBS Lett. 585, 29–35.

Rich, J.N., Reardon, D.A., Peery, T., Dowell, J.M., Quinn, J.A., Penne, K.L., Wikstrand, C.J., Van Duyn, L.B., Dancey, J.E., McLendon, R.E., Kao, J.C., Stenzel, T.T., Ahmed Rasheed, B.K., Tourt-Uhlig, S.E., Herndon, J.E., Vredenburgh, J.J., Sampson, J.H., Friedman, A.H., Bigner, D.D., Friedman, H.S., 2004. Phase II trial of gefitinib in recurrent glioblastoma. J. Clin. Oncol. 22, 133–142.

Rios, I., Alvarez-Rodríguez, R., Martí, E., Pons, S., 2004. Bmp2 antagonizes sonic hedgehog-mediated proliferation of cerebellar granule neurones through Smad5 signalling. Development 131, 3159–3168.

Ris, B.M.D., Packer, R., Goldwein, J., Jones-wallace, D., Boyett, J.M., 2014. Intellectual Outcome After Reduced-Dose Radiation Therapy Plus Adjuvant Chemotherapy for Medulloblastoma : A Children ' s Cancer Group Study 19, 3470–3476.

Roa, W., Brasher, P.M.A., Bauman, G., Anthes, M., Bruera, E., Chan, A., Fisher, B., Fulton, D., Gulavita, S., Hao, C., Husain, S., Murtha, A., Petruk, K., Stewart, D., Tai, P., Urtasun, R., Cairncross, J.G., Forsyth, P., 2004. Abbreviated course of radiation therapy in older patients with glioblastoma multiforme: a prospective randomized clinical trial. J. Clin. Oncol. 22, 1583–1588.

Roberts, R.O., Lynch, C.F., Jones, M.P., Hart, M.N., 1991. Medulloblastoma: a population-based study of 532 cases. J. Neuropathol. Exp. Neurol. 50, 134–44.

Robinson, G., Parker, M., Kranenburg, T. a., Lu, C., Chen, X., Ding, L., Phoenix, T.N., Hedlund, E., Wei, L., Zhu, X., Chalhoub, N., Baker, S.J., Huether, R., Kriwacki, R., Curley, N., Thiruvenkatam, R., Wang, J., Wu, G., Rusch, M., Hong, X., Becksfort, J., Gupta, P., Ma, J., Easton, J., Vadodaria, B., Onar-Thomas, A., Lin, T., Li, S., Pounds, S., Paugh, S., Zhao, D., Kawauchi, D., Roussel, M.F., Finkelstein, D., Ellison, D.W., Lau, C.C., Bouffet, E., Hassall, T., Gururangan, S., Cohn, R., Fulton, R.S., Fulton, L.L., Dooling, D.J., Ochoa, K., Gajjar, A., Mardis, E.R., Wilson, R.K., Downing, J.R., Zhang, J., Gilbertson, R.J., 2012. Novel mutations target distinct subgroups of medulloblastoma. Nature 488, 43–48.

Rock, K., Mcardle, O., Forde, P., Dunne, M., Fitzpatrick, D., O'Neill, B., Faul, C., 2012. A clinical review of treatment outcomes in glioblastoma multiforme--thevalidation in a non-trial population of the results of a randomised PhaseIII clinical trial: has a more radical approach improved survival? Br. J. Radiol. 85, e729–e733.

Rorke, L.B., 1983. The cerebellar medulloblastoma and its relationship to primitive neuroectodermal tumors. J. Neuropathol. Exp. Neurol. 42, 1–15.

Roshak, A.K., Capper, E.A., Imburgia, C., Fornwald, J., Scott, G., Marshall, L.A., 2000. The human polo-like kinase, PLK, regulates cdc2/cyclin B through phosphorylation and activation of the cdc25C phosphatase. Cell. Signal. 12, 405–11.

Roy, N.S., Wang, S., Jiang, L., Kang, J., Benraiss, A., Harrison-Restelli, C., Fraser, R.A., Couldwell, W.T., Kawaguchi, A., Okano, H., Nedergaard, M., Goldman, S.A., 2000. In vitro neurogenesis by progenitor cells isolated from the adult human hippocampus. Nat. Med. 6, 271–277.

Rudolph, D., Steegmaier, M., Hoffmann, M., Grauert, M., Baum, A., Quant, J., Haslinger, C., Garin-Chesa, P., Adolf, G.R., 2009. BI 6727, a Polo-like kinase inhibitor with improved pharmacokinetic profile and broad antitumor activity. Clin. Cancer Res. 15, 3094–102.

Ruiz i Altaba, A., Palma, V., Dahmane, N., 2002. Hedgehog-Gli signalling and the growth of the brain. Nat. Rev. Neurosci. 3, 24–33.

Rutkowski, S., Bode, U., Deinlein, F., Ottensmeir, H., Warmuth-Metz, M., Soerensen, N., Graf, N., Emser, A., Pietsch, T., Wolff, J.E.., Kortmann, R.D., Kuehl, J., 2005. Treatment of early childhood medulloblastoma by postoperative chemotherapy alone. N. Engl. J. Med. 352, 978–986.

Rutkowski, S., Von Hoff, K., Emser, A., Zwiener, I., Pietsch, T., Figarella-Branger, D., Giangaspero, F., Ellison, D.W., Garre, M.L., Biassoni, V., Grundy, R.G., Finlay, J.L., Dhall, G., Raquin, M.A., Grill, J., 2010. Survival and prognostic factors of early childhood medulloblastoma: An international meta-analysis. J. Clin. Oncol. 28, 4961–4968.

Sadasivam, S., Duan, S., DeCaprio, J.A., 2012. The MuvB complex sequentially recruits B-Myb and FoxM1 to promote mitotic gene expression. Genes Dev. 26, 474–489.

Sadetzki, S., Bruchim, R., Oberman, B., Armstrong, G.N., Lau, C.C., Claus, E.B., Barnholtz-Sloan, J.S., Il'yasova, D., Schildkraut, J., Johansen, C., Houlston, R.S., Shete, S., Amos, C.I., Bernstein, J.L., Olson, S.H., Jenkins, R.B., Lachance, D., Vick, N.A., Merrell, R., Wrensch, M., Davis, F.G., McCarthy, B.J., Lai, R., Melin, B.S., Bondy, M.L., 2013. Description of selected characteristics of familial glioma patients - results from the Gliogene Consortium. Eur. J. Cancer 49, 1335–45.

Sæther, C.A., Torsteinsen, M., Torp, S.H., Sundstrøm, S., Unsgård, G., Solheim, O., 2012. Did survival improve after the implementation of intraoperative neuronavigation and 3D ultrasound in glioblastoma surgery? A retrospective analysis of 192 primary operations. J. Neurol. Surg. A. Cent. Eur. Neurosurg. 73, 73–78.

Sands, S. a, Pasichow, K.P., Weiss, R., Garvin, J., Gardner, S., Dunkel, I.J., Finlay, J.L., 2011. Quality of life and behavioral follow-up study of Head Start I pediatric brain tumor survivors. J. Neurooncol. 101, 287–95.

Sanson, M., Marie, Y., Paris, S., Idbaih, A., Laffaire, J., Ducray, F., Hallani, S. El, Boisselier, B., Mokhtari, K., Hoang-Xuan, K., Delattre, J.Y., 2009. Isocitrate dehydrogenase 1 codon 132 mutation is an important prognostic biomarker in gliomas. J. Clin. Oncol. 27, 4150–4154.

Santagata, S., Eberlin, L.S., Norton, I., Calligaris, D., Feldman, D.R., Ide, J.L., Liu, X., Wiley, J.S., Vestal, M.L., Ramkissoon, S.H., Orringer, D. a, Gill, K.K., Dunn, I.F., Dias-Santagata, D., Ligon, K.L., Jolesz, F. a, Golby, A.J., Cooks, R.G., Agar, N.Y.R., 2014. Intraoperative mass spectrometry mapping of an onco-metabolite to guide brain tumor surgery. Proc. Natl. Acad. Sci. U. S. A. 111, 1–6.

Santamaria, A., Neef, R., Eberspächer, U., Eis, K., Husemann, M., Mumberg, D., Prechtl, S., Schulze, V., Siemeister, G., Wortmann, L., Barr, F.A., Nigg, E.A., 2007. Use of the novel Plk1 inhibitor ZK-thiazolidinone to elucidate functions of Plk1 in early and late stages of mitosis. Mol. Biol. Cell 18, 4024–36.

Sapkota, G.P., Cummings, L., Newell, F.S., Armstrong, C., Bain, J., Frodin, M., Grauert, M., Hoffmann, M., Schnapp, G., Steegmaier, M., Cohen, P., Alessi, D.R., 2007. BI-D1870 is a specific inhibitor of the p90 RSK (ribosomal S6 kinase) isoforms in vitro and in vivo. Biochem. J. 401, 29–38.

Schäfer, A., Teufel, J., Ringel, F., Bettstetter, M., Hoepner, I., Rasper, M., Gempt, J., Koeritzer, J., Schmidt-Graf, F., Meyer, B., Beier, C.P., Schlegel, J., 2012. Aldehyde dehydrogenase 1A1--a new mediator of resistance to temozolomide in glioblastoma. Neuro. Oncol. 14, 1452–64.

Schmidek, H.H., Nielsen, S.L., Schiller, A.L., Messer, J., 1971. Morphological studies of rat brain tumors induced by N-nitrosomethylurea. J. Neurosurg. 34, 335–40.

Schroeder, J.T., Lichtenstein, L.M., MacDonald, S.M., 1997. Recombinant histamine-releasing factor enhances IgE-dependent IL-4 and IL-13 secretion by human basophils. J. Immunol. 159, 447–452.

Schüller, U., Heine, V.M., Mao, J., Kho, A.T., Dillon, A.K., Han, Y.-G.G., Huillard, E., Sun, T., Ligon, A.H., Qian, Y., Ma, Q., Alvarez-Buylla, A., McMahon, A.P., Rowitch, D.H., Ligon, K.L., 2008. Acquisition of Granule Neuron Precursor Identity Is a Critical Determinant of Progenitor Cell Competence to Form Shh-Induced Medulloblastoma. Cancer Cell 14, 123–134.

Schwartzentruber, J., Korshunov, A., Liu, X.-Y., Jones, D.T.W., Pfaff, E., Jacob, K., Sturm, D., Fontebasso, A.M., Quang, D.-A.K., Tönjes, M., Hovestadt, V., Albrecht, S., Kool, M., Nantel, A., Konermann, C., Lindroth, A., Jäger, N., Rausch, T., Ryzhova, M., Korbel, J.O., Hielscher, T., Hauser, P., Garami, M., Klekner, A., Bognar, L., Ebinger, M., Schuhmann, M.U., Scheurlen, W., Pekrun, A., Frühwald, M.C., Roggendorf, W., Kramm, C., Dürken, M., Atkinson, J., Lepage, P., Montpetit, A., Zakrzewska, M., Zakrzewski, K., Liberski, P.P., Dong, Z., Siegel, P., Kulozik, A.E., Zapatka, M., Guha, A., Malkin, D., Felsberg, J., Reifenberger, G., von Deimling, A., Ichimura, K., Collins, V.P., Witt, H., Milde, T., Witt, O., Zhang, C., Castelo-Branco, P., Lichter, P., Faury, D., Tabori, U., Plass, C., Majewski, J., Pfister, S.M., Jabado, N., 2012. Driver mutations in histone H3.3 and chromatin remodelling genes in paediatric glioblastoma. Nature 482, 226–31.

Sdelci, S., Schütz, M., Pinyol, R., Bertran, M.T., Regué, L., Caelles, C., Vernos, I., Roig, J., 2012. Nek9 phosphorylation of NEDD1/GCP-WD contributes to Plk1 control of γ-tubulin recruitment to the mitotic centrosome. Curr. Biol. 22, 1516–23.

Sebastian, M., Reck, M., Waller, C.F., Kortsik, C., Frickhofen, N., Schuler, M., Fritsch, H., Gaschler-Markefski, B., Hanft, G., Munzert, G., von Pawel, J., 2010. The Efficacy and Safety of BI 2536 , a Novel Plk-1 Inhibitor , in Patients with Stage IIIB / IV Non-small Cell Lung Cancer. J. Thorac. Oncol. 5, 4–6.

Seki, A., Coppinger, J.A., Jang, C.-Y., Yates, J.R., Fang, G., 2008. Bora and the kinase Aurora a cooperatively activate the kinase Plk1 and control mitotic entry. Science 320, 1655–8.

Seligman, A.M., Shear, M.J., Alexander, L., 1939. Studies in carcinogenesis: VIII. Experimental production of brain tumors in mice with methylcholanthrene. Am. J. Cancer 37, 364–395.

Semple, S.C., Judge, A.D., Robbins, M., Klimuk, S., Eisenhardt, M., Crosley, E., Leung, A., Kwok, R., Ambegia, E., McClintock, K., MacLachlan, I., 2011. Abstract 2829: Preclinical characterization of TKM-080301, a lipid nanoparticle formulation of a small interfering RNA directed against polo-like kinase 1. Cancer Res. 71, 2829–2829.

Seong, Y.-S., 2002. A Spindle Checkpoint Arrest and a Cytokinesis Failure by the Dominant-negative Polo-box Domain of Plk1 in U-2 OS Cells. J. Biol. Chem. 277, 32282–32293.

Shapiro, W.R., Basler, G.A., Chernik, N.L., Posner, J.B., 1979. Human brain tumor transplantation into nude mice. J. Natl. Cancer Inst. 62, 447–53.

Shen, J.-H., Qu, C., Chu, H., Cui, M.-Y., Wang, Y.-L.Y.-I., Sun, Y., Song, Y., Li, G., Shi, F., 2014. siRNA targeting TCTP suppresses osteosarcoma cell growth and induces apoptosis in vitro and in vivo. Biotechnol. Appl. Biochem. [Epub ahead of print].

Shi, L., Chen, J., Yang, J., Pan, T., Zhang, S., Wang, Z., 2010. MiR-21 protected human glioblastoma U87MG cells from chemotherapeutic drug temozolomide induced apoptosis by decreasing Bax/Bcl-2 ratio and caspase-3 activity. Brain Res. 1352, 255–64.

Shih, D.J.H., Northcott, P. a., Remke, M., Korshunov, A., Ramaswamy, V., Kool, M., Luu, B., Yao, Y., Wang, X., Dubuc, A.M., Garzia, L., Peacock, J., Mack, S.C., Wu, X., Rolider, A., Morrissy, a. S., Cavalli, F.M.G., Jones, D.T.W., Zitterbart, K., Faria, C.C., Schüller, U., Kren, L., Kumabe, T., Tominaga, T., Ra, Y.S., Garami, M., Hauser, P., Chan, J. a., Robinson, S., Bognár, L., Klekner, A., Saad, A.G., Liau, L.M., Albrecht, S., Fontebasso, A., Cinalli, G., De Antonellis, P., Zollo, M., Cooper, M.K., Thompson, R.C., Bailey, S., Lindsey, J.C., Di Rocco, C., Massimi, L., Michiels, E.M.C., Scherer, S.W., Phillips, J.J., Gupta, N., Fan, X., Muraszko, K.M., Vibhakar, R., Eberhart, C.G., Fouladi, M., Lach, B., Jung, S., Wechsler-Reya, R.J., Fèvre-Montange, M., Jouvet, A., Jabado, N., Pollack, I.F., Weiss, W. a., Lee, J.Y., Cho, B.K., Kim, S.K., Wang, K.C., Leonard, J.R., Rubin, J.B., De Torres, C., Lavarino, C., Mora, J., Cho, Y.J., Tabori, U., Olson, J.M., Gajjar, A., Packer, R.J., Rutkowski, S., Pomeroy, S.L., French, P.J., Kloosterhof, N.K., Kros, J.M., Van Meir, E.G., Clifford, S.C., Bourdeaut, F., Delattre, O., Doz, F.F., Hawkins, C.E., Malkin, D., Grajkowska, W. a., Perek-Polnik, M., Bouffet, E., Rutka, J.T., Pfister, S.M., Taylor, M.D.,

2014. Cytogenetic prognostication within medulloblastoma subgroups. J. Clin. Oncol. 32, 886–896.

Shu, Q., Antalffy, B., Su, J.M.F., Adesina, A., Ou, C.-N., Pietsch, T., Blaney, S.M., Lau, C.C., Li, X.-N., 2006. Valproic Acid prolongs survival time of severe combined immunodeficient mice bearing intracerebellar orthotopic medulloblastoma xenografts. Clin. Cancer Res. 12, 4687–94.

Singec, I., Knoth, R., Meyer, R.P., Maciaczyk, J., Volk, B., Nikkhah, G., Frotscher, M., Snyder, E.Y., 2006. Defining the actual sensitivity and specificity of the neurosphere assay in stem cell biology. Nat. Methods 3, 801–6.

Singh, S.K., Clarke, I.D., Hide, T., Dirks, P.B., 2004a. Cancer stem cells in nervous system tumors. Oncogene 23, 7267–73.

Singh, S.K., Clarke, I.D., Terasaki, M., Bonn, V.E., Hawkins, C., Squire, J., Dirks, P.B., 2003. Identification of a Cancer Stem Cell in Human Brain Tumors. Cancer Res. 5821–5828.

Singh, S.K., Hawkins, C., Clarke, I.D., Squire, J.A., Bayani, J., Hide, T., Henkelman, R.M., Cusimano, M.D., Dirks, P.B., 2004b. Identification of human brain tumour initiating cells. Nature 432, 396–401.

Sirachainan, N., Nuchprayoon, I., Thanarattanakorn, P., Pakakasama, S., Lusawat, A., Visudibhan, A., Dhanachai, M., Larbcharoensub, N., Amornfa, J., Shotelersuk, K., Katanyuwong, K., Tangkaratt, S., Hongeng, S., 2011. Outcome of medulloblastoma in children treated with reduced-dose radiation therapy plus adjuvant chemotherapy. J. Clin. Neurosci. 18, 515–519.

Sládek, N.E., Kollander, R., Sreerama, L., Kiang, D.T., 2002. Cellular levels of aldehyde dehydrogenases (ALDH1A1 and ALDH3A1) as predictors of therapeutic responses to cyclophosphamide-based chemotherapy of breast cancer: a retrospective study. Rational individualization of oxazaphosphorine-based cancer chemotherap. Cancer Chemother. Pharmacol. 49, 309–21.

Sloan, A.E., Ahluwalia, M.S., Valerio-Pascua, J., Manjila, S., Torchia, M.G., Jones, S.E., Sunshine, J.L., Phillips, M., Griswold, M. a, Clampitt, M., Brewer, C., Jochum, J., McGraw, M. V, Diorio, D., Ditz, G., Barnett, G.H., 2013. Results of the NeuroBlate System first-in-humans Phase I clinical trial for recurrent glioblastoma: clinical article. J. Neurosurg. 118, 1202–19.

Slotty, P.J., Siantidis, B., Beez, T., Steiger, H.J., Sabel, M., 2013. The impact of improved treatment strategies on overall survival in glioblastoma patients. Acta Neurochir. (Wien). 155, 959–963.

Smith, E., Hégarat, N., Vesely, C., Roseboom, I., Larch, C., Streicher, H., Straatman, K., Flynn, H., Skehel, M., Hirota, T., Kuriyama, R., Hochegger, H., 2011. Differential control of Eg5-dependent centrosome separation by Plk1 and Cdk1. EMBO J. 30, 2233–45.

Smith, J.S., Tachibana, I., Passe, S.M., Huntley, B.K., Borell, T.J., Iturria, N., O'Fallon, J.R., Schaefer, P.L., Scheithauer, B.W., James, C.D., Buckner, J.C., Jenkins, R.B., 2001. PTEN mutation, EGFR amplification, and outcome in patients with anaplastic astrocytoma and glioblastoma multiforme. J. Natl. Cancer Inst. 93, 1246–1256.

Smith, M.R., Wilson, M.L., Hamanaka, R., Chase, D., Kung, H., Longo, D.L., Ferris, D.K., 1997. Malignant transformation of mammalian cells initiated by constitutive expression of the polo-like kinase. Biochem. Biophys. Res. Commun. 234, 397–405.

Smits, M., Nilsson, J., Mir, S.E., Stoop, P.M. Van Der, Hulleman, E., Niers, J.M., Hamer, P.C.D.W., Marquez, V.E., Cloos, J., Krichevsky, A.M., Noske, D.P., Tannous, B.A., Würdinger, T., 2010. miR- 101 is down- regulated in glioblastoma resulting in EZH2-induced proliferation, migration, and angiogenesis. Oncotarget 1, 710–720.

Smits, V. a, Klompmaker, R., Arnaud, L., Rijksen, G., Nigg, E. a, Medema, R.H., 2000. Polo-like kinase-1 is a target of the DNA damage checkpoint. Nat. Cell Biol. 2, 672–676.

Solecki, D.J., Liu, X., Tomoda, T., Fang, Y., Hatten, M.E., 2001. Activated Notch2 signaling inhibits differentiation of cerebellar granule neuron precursors by maintaining proliferation. Neuron 31, 557–568.

Son, M.J., Woolard, K., Nam, D.-H., Lee, J., Fine, H.A., 2009. SSEA-1 is an enrichment marker for tumor-initiating cells in human glioblastoma. Cell Stem Cell 4, 440–52.

Spaniol, K., Boos, J., Lanvers-Kaminsky, C., 2011. An in-vitro evaluation of the polo-like kinase inhibitor GW843682X against paediatric malignancies. Anticancer. Drugs 22, 531–542.

Spänkuch, B., Kurunci-Csacsko, E., Kaufmann, M., Strebhardt, K., 2007. Rational combinations of siRNAs targeting Plk1 with breast cancer drugs. Oncogene 26, 5793–5807.

Stadler, W.M., Vaughn, D.J., Sonpavde, G., Vogelzang, N.J., Tagawa, S.T., Petrylak, D.P., Rosen, P., Lin, C.-C., Mahoney, J., Modi, S., Lee, P., Ernstoff, M.S., Su, W.-C., Spira, A., Pilz, K., Vinisko, R., Schloss, C., Fritsch, H., Zhao, C., Carducci, M. a, 2014. An open-label, single-arm, phase 2 trial of the Polo-like kinase inhibitor volasertib (BI 6727) in patients with locally advanced or metastatic urothelial cancer. Cancer 120, 976–82.

Stea, B., Falsey, R., Kislin, K., Patel, J., Glanzberg, H., Carey, S., Ambrad, A.A., Meuillet, E.J., Martinez, J.D., 2003. Time and dose-dependent radiosensitization of the glioblastoma multiforme U251 cells by the EGF receptor tyrosine kinase inhibitor ZD1839 ('Iressa'). Cancer Lett. 202, 43–51.

Steegmaier, M., Hoffmann, M., Baum, A., Lénárt, P., Petronczki, M., Krššák, M., Gürtler, U., Garin-Chesa, P., Lieb, S., Quant, J., Grauert, M., Adolf, G.R., Kraut, N., Peters, J.-M.M., Rettig, W.J., Krssák, M., Gürtler, U., Garin-Chesa, P., Lieb, S., Quant, J., Grauert, M., Adolf, G.R., Kraut, N., Peters, J.-M.M., Rettig, W.J., 2007. BI 2536, a potent and selective inhibitor of polo-like kinase 1, inhibits tumor growth in vivo. Curr. Biol. 17, 316–22.

Stern, B.M., Murray, A.W., 2001. Lack of tension at kinetochores activates the spindle checkpoint in budding yeast. Curr. Biol. 11, 1462–7.

Stiles, C.D., Rowitch, D.H., 2008. Glioma stem cells: a midterm exam. Neuron 58, 832–46.

Strano, S., Dell'Orso, S., Di Agostino, S., Fontemaggi, G., Sacchi, a, Blandino, G., 2007. Mutant p53: an oncogenic transcription factor. Oncogene 26, 2212–2219.

Stratford, A.L., Reipas, K., Hu, K., Fotovati, A., Brough, R., Frankum, J., Takhar, M., Watson, P., Ashworth, A., Lord, C.J., Lasham, A., Print, C.G., Dunn, S.E., 2012. Targeting p90 Ribosomal S6 Kinase (RSK) Eliminates Tumor-Initiating Cells by Inactivating Y-Box Binding Protein-1 (YB-1) in Triple-Negative Breast Cancers. Stem Cells 30, 1338–1348.

Stummer, W., Pichlmeier, U., Meinel, T., Wiestler, O.D., Zanella, F., Reulen, H.-J., 2006. Fluorescence-guided surgery with 5-aminolevulinic acid for resection of malignant glioma: a randomised controlled multicentre phase III trial. Lancet Oncol. 7, 392–401.

Stupp, R., Mason, W.P., van den Bent, M.J., Weller, M., Fisher, B., Taphoorn, M.J.B., Belanger, K., Brandes, A. a, Marosi, C., Bogdahn, U., Curschmann, J., Janzer, R.C., Ludwin, S.K., Gorlia, T., Allgeier, A., Lacombe, D., Cairncross, J.G., Eisenhauer, E., Mirimanoff, R.O., 2005. Radiotherapy plus concomitant and adjuvant temozolomide for glioblastoma. N. Engl. J. Med. 352, 987–96.

Sturm, D., Witt, H., Hovestadt, V., Jones, D.T.W., Sill, M., Bender, S., Kool, M., Zapatka, M., Konermann, C., Pfaff, E., To, M., Becker, N., Zucknick, M., Hielscher, T., Liu, X., Fontebasso, A.M., Ryzhova, M., Albrecht, S., Jacob, K., Wolter, M., Ebinger, M., Schuhmann, M.U., Meter, T. Van, Fru, M.C., Hartmann, C., Wiestler, B., Wick, W., Milde, T., Witt, O., Lindroth, A.M., Schwartzentruber, J., Faury, D., Fleming, A., Zakrzewska, M., 2012. Hotspot Mutations in H3F3A and IDH1 Define Distinct Epigenetic and Biological Subgroups of Glioblastoma. Cancer Cell 22, 425–437.

Stylli, S.S., Kaye, a H., Novak, U., 2000. Induction of CD44 expression in stab wounds of the brain: long term persistence of CD44 expression. J. Clin. Neurosci. 7, 137–140.

Stylli, S.S., Luwor, R.B., Ware, T.M.B., Tan, F., Kaye, A.H., 2015. Mouse models of glioma. J. Clin. Neurosci. 22, 619–626.

Suh, J.J., Pettinati, H.M., Kampman, K.M., O'Brien, C.P., 2006. The status of disulfiram: a half of a century later. J. Clin. Psychopharmacol. 26, 290–302.

Suneja, G., 2011. Outcome of infants and young children with newly diagnosed medulloblastoma treated on Head Start III protocol | Oncolink - Cancer Resources [WWW Document]. URL http://www.oncolink.org/conferences/article.cfm?id=6639 (accessed 3.18.15).

Susini, L., Besse, S., Duflaut, D., Lespagnol, A., Beekman, C., Fiucci, G., Atkinson, A.R., Busso, D., Poussin, P., Marine, J.-C., Martinou, J.-C., Cavarelli, J., Moras, D., Amson, R., Telerman, A., 2008. TCTP protects from apoptotic cell death by antagonizing bax function. Cell Death Differ. 15, 1211–1220.

Sütterlin, C., Lin, C.Y., Feng, Y., Ferris, D.K., Erikson, R.L., Malhotra, V., 2001. Polo-like kinase is required for the fragmentation of pericentriolar Golgi stacks during mitosis. Proc. Natl. Acad. Sci. U. S. A. 98, 9128–9132.

Swartling, F.J., Grimmer, M.R., Hackett, C.S., Northcott, P. a., Fan, Q.W., Goldenberg, D.D., Lau, J., Masic, S., Nguyen, K., Yakovenko, S., Zhe, X.N., Flynn Gilmer, H.C., Collins, R., Nagaoka, M., Phillips, J.J., Jenkins, R.B., Tihan, T., Vandenberg, S.R., James, C.D., Tanaka, K., Taylor, M.D., Weiss, W. a., Chesler, L., 2010. Pleiotropic role for MYCN in medulloblastoma. Genes Dev. 24, 1059–1072.

Tabori, U., Baskin, B., Shago, M., Alon, N., Taylor, M.D., Ray, P.N., Bouffet, E., Malkin, D., Hawkins, C., 2010. Universal poor survival in children with medulloblastoma harboring somatic TP53 mutations. J. Clin. Oncol. 28, 1345–50.

Tabori, U., Sung, L., Hukin, J., Laperriere, N., Crooks, B., Carret, A.S., Silva, M., Odame, I., Mpofu, C., Strother, D., Wilson, B., Samson, Y., Bouffet, E., 2006. Distinctive clinical course and pattern of relapse in adolescents with medulloblastoma. Int. J. Radiat. Oncol. Biol. Phys. 64, 402–407.

Taillandier, L., Blonski, M., Carrie, C., Bernier, V., Bonnetain, F., Bourdeaut, F., Thomas, I.-C., Chastagner, P., Dhermain, F., Doz, F., Frappaz, D., Grill, J., Guillevin, R., Idbaih, A., Jouvet, A., Kerr, C., Donadey, F.-L., Padovani, L., Pallud, J., Sunyach, M.-P., 2011. Medulloblastomas: review. Rev. Neurol. (Paris). 167, 431–48.

Takahashi, T., Sano, B., Nagata, T., Kato, H., Sugiyama, Y., Kunieda, K., Kimura, M., Okano, Y., Saji, S., 2003. Polo-like kinase 1 (PLK1) is overexpressed in primary colorectal cancers. Cancer Sci. 94, 148–52.

Takai, N., Hamanaka, R., Yoshimatsu, J., Miyakawa, I., 2005. Polo-like kinases (Plks) and cancer. Oncogene 24, 287–91.

Takanaga, H., Tamai, I., Inaba, S., Sai, Y., Higashida, H., Yamamoto, H., Tsuji, A., 1995. cDNA cloning and functional characterization of rat intestinal monocarboxylate transporter. Biochem. Biophys. Res. Commun. 217, 370–377.

Takaoka, M., Saito, H., Takenaka, K., Miki, Y., Nakanishi, A., 2014. BRCA2 phosphorylated by PLK1 moves to the midbody to regulate cytokinesis mediated by non-muscle myosin IIC. Cancer Res. 74, 1518–1528.

Tan, B.T., Park, C.Y., Ailles, L.E., Weissman, I.L., 2006. The cancer stem cell hypothesis: a work in progress. Lab. Invest. 86, 1203–1207.

Tandle, A.T., Kramp, T., Kil, W.J., Halthore, A., Gehlhaus, K., Shankavaram, U., Tofilon, P.J., Caplen, N.J., Camphausen, K., 2013. Inhibition of polo-like kinase 1 in glioblastoma multiforme induces mitotic catastrophe and enhances radiosensitisation. Eur. J. Cancer 49, 3020–3028.

Taniguchi, E., Toyoshima-Morimoto, F., Nishida, E., 2002. Nuclear translocation of plk1 mediated by its bipartite nuclear localization signal. J. Biol. Chem. 277, 48884–48888.

Taylor, M.D., Liu, L., Raffel, C., Hui, C., Mainprize, T.G., Zhang, X., Agatep, R., Chiappa, S., Gao, L., Lowrance, A., Hao, A., Goldstein, A.M., Stavrou, T., Scherer, S.W., Dura, W.T., Wainwright, B., Squire, J.A., Rutka, J.T., Hogg, D., 2002. Mutations in SUFU predispose to medulloblastoma. Nat. Genet. 31, 306–310.

Taylor, M.D., Northcott, P. a, Korshunov, A., Remke, M., Cho, Y.-J., Clifford, S.C., Eberhart, C.G., Parsons, D.W., Rutkowski, S., Gajjar, A., Ellison, D.W., Lichter, P., Gilbertson, R.J., Pomeroy, S.L., Kool, M., Pfister, S.M., 2012. Molecular subgroups of medulloblastoma: the current consensus. Acta Neuropathol. 123, 465–472.

Thompson, M.C., Fuller, C., Hogg, T.L., Dalton, J., Finkelstein, D., Lau, C.C., Chintagumpala, M., Adesina, A., Ashley, D.M., Kellie, S.J., Taylor, M.D., Curran, T., Gajjar, A., Gilbertson, R.J., 2006. Genomics identifies medulloblastoma subgroups that are enriched for specific genetic alterations. J. Clin. Oncol. 24, 1924–1931.

Thompson, P.M., Stein, J.L., Medland, S.E., Hibar, D.P., Vasquez, A.A., Renteria, M.E., Toro, R., Jahanshad, N., Schumann, G., Franke, B., Wright, M.J., Martin, N.G., Agartz, I., Alda, M., Alhusaini, S., Almasy, L., Almeida, J., Alpert, K., Andreasen, N.C., Andreassen, O. a., Apostolova, L.G., Appel, K., Armstrong, N.J., Aribisala, B., Bastin, M.E., Bauer, M., Bearden, C.E., Bergmann, Ø., Binder, E.B., Blangero, J., Bockholt, H.J., Bøen, E., Bois, C., Boomsma, D.I., Booth, T., Bowman, I.J., Bralten, J., Brouwer, R.M., Brunner, H.G., Brohawn, D.G., Buckner, R.L., Buitelaar, J., Bulayeva, K., Bustillo, J.R., Calhoun, V.D., Cannon, D.M., Cantor, R.M., Carless, M. a., Caseras, X., Cavalleri, G.L., Chakravarty, M.M., Chang, K.D., Ching, C.R.K., Christoforou, A., Cichon, S., Clark, V.P., Conrod, P., Coppola, G., Crespo-Facorro, B., Curran, J.E., Czisch, M., Deary, I.J., de Geus, E.J.C., den Braber, A., Delvecchio, G., Depondt, C., de Haan, L., de Zubicaray, G.I., Dima, D., Dimitrova, R., Djurovic, S., Dong, H., Donohoe, G., Duggirala, R., Dyer, T.D., Ehrlich, S., Ekman, C.J., Elvsåshagen, T., Emsell, L., Erk, S., Espeseth, T., Fagerness, J., Fears, S., Fedko, I., Fernández, G., Fisher, S.E., Foroud, T., Fox, P.T., Francks, C., Frangou, S., Frey, E.M., Frodl, T., Frouin, V., Garavan, H., Giddaluru, S., Glahn, D.C., Godlewska, B.,

Goldstein, R.Z., Gollub, R.L., Grabe, H.J., Grimm, O., Gruber, O., Guadalupe, T., Gur, R.E., Gur, R.C., Göring, H.H.H., Hagenaars, S., Hajek, T., Hall, G.B., Hall, J., Hardy, J., Hartman, C. a., Hass, J., Hatton, S.N., Haukvik, U.K., Hegenscheid, K., Heinz, A., Hickie, I.B., Ho, B.C., Hoehn, D., Hoekstra, P.J., Hollinshead, M., Holmes, A.J., Homuth, G., Hoogman, M., Hong, L.E., Hosten, N., Hottenga, J.J., Hulshoff Pol, H.E., Hwang, K.S., Jack, C.R., Jenkinson, M., Johnston, C., Jönsson, E.G., Kahn, R.S., Kasperaviciute, D., Kelly, S., Kim, S., Kochunov, P., Koenders, L., Krämer, B., Kwok, J.B.J., Lagopoulos, J., Laje, G., Landen, M., Landman, B. a., Lauriello, J., Lawrie, S.M., Lee, P.H., Le Hellard, S., Lemaître, H., Leonardo, C.D., Li, C.S., Liberg, B., Liewald, D.C., Liu, X., Lopez, L.M., Loth, E., Lourdusamy, A., Luciano, M., Macciardi, F., Machielsen, M.W.J., MacQueen, G.M., Malt, U.F., Mandl, R., Manoach, D.S., Martinot, J.L., Matarin, M., Mather, K. a., Mattheisen, M., Mattingsdal, M., Meyer-Lindenberg, A., McDonald, C., McIntosh, A.M., McMahon, F.J., McMahon, K.L., Meisenzahl, E., Melle, I., Milaneschi, Y., Mohnke, S., Montgomery, G.W., Morris, D.W., Moses, E.K., Mueller, B. a., Muñoz Maniega, S., Mühleisen, T.W., Müller-Myhsok, B., Mwangi, B., Nauck, M., Nho, K., Nichols, T.E., Nilsson, L.G., Nugent, A.C., Nyberg, L., Olvera, R.L., Oosterlaan, J., Ophoff, R. a., Pandolfo, M., Papalampropoulou-Tsiridou, M., Papmeyer, M., Paus, T., Pausova, Z., Pearlson, G.D., Penninx, B.W., Peterson, C.P., Pfennig, A., Phillips, M., Pike, G.B., Poline, J.B., Potkin, S.G., Pütz, B., Ramasamy, A., Rasmussen, J., Rietschel, M., Rijpkema, M., Risacher, S.L., Roffman, J.L., Roiz-Santiañez, R., Romanczuk-Seiferth, N., Rose, E.J., Royle, N. a., Rujescu, D., Ryten, M., Sachdev, P.S., Salami, A., Satterthwaite, T.D., Savitz, J., Saykin, A.J., Scanlon, C., Schmaal, L., Schnack, H.G., Schork, A.J., Schulz, S.C., Schür, R., Seidman, L., Shen, L., Shoemaker, J.M., Simmons, A., Sisodiya, S.M., Smith, C., Smoller, J.W., Soares, J.C., Sponheim, S.R., Sprooten, E., Starr, J.M., Steen, V.M., Strakowski, S., Strike, L., Sussmann, J., Sämann, P.G., Teumer, A., Toga, A.W., Tordesillas-Gutierrez, D., Trabzuni, D., Trost, S., Turner, J., Van den Heuvel, M., van der Wee, N.J., van Eijk, K., van Erp, T.G.M., van Haren, N.E.M., van 't Ent, D., van Tol, M.J., Valdés Hernández, M.C., Veltman, D.J., Versace, A., Völzke, H., Walker, R., Walter, H., Wang, L., Wardlaw, J.M., Weale, M.E., Weiner, M.W., Wen, W., Westlye, L.T., Whalley, H.C., Whelan, C.D., White, T., Winkler, A.M., Wittfeld, K., Woldehawariat, G., Wolf, C., Zilles, D., Zwiers, M.P., Thalamuthu, A., Schofield, P.R., Freimer, N.B., Lawrence, N.S., Drevets, W., 2014. The ENIGMA Consortium: Large-scale collaborative analyses of neuroimaging and genetic data. Brain Imaging Behav. 8, 153–182.

Tibshirani, R., Hastie, T., Narasimhan, B., Chu, G., 2002. Diagnosis of multiple cancer types by shrunken centroids of gene expression. Proc. Natl. Acad. Sci. U. S. A. 99, 6567–72.

To, K.K.., Poon, D.C., Chen, X.., Fu, L.., 2013. Volasertib (BI 6727), a novel polo-like kinase inhibitor, reverses ABCB1 and ABCG2-mediated multidrug resistance in cancer cells. J. Cancer Ther. Res. 2, 13.

Tokumitsu, Y., Mori, M., Tanaka, S., Akazawa, K., Nakano, S., Niho, Y., 1999. Prognostic significance of polo-like kinase expression in esophageal carcinoma. Int.J.Oncol. 15, 687–692.

Toyoshima-Morimoto, F., 2002. Plk1 promotes nuclear translocation of human Cdc25C during prophase. EMBO Rep. 3, 341–348.

Toyoshima-Morimoto, F., Taniguchi, E., Shinya, N., Iwamatsu, A., Nishida, E., 2001. Polo-like kinase 1 phosphorylates cyclin B1 and targets it to the nucleus during prophase. Nature 410, 215–20.

Toyota, M., Ohe-Toyota, M., Ahuja, N., Issa, J.P., 2000. Distinct genetic profiles in colorectal tumors with or without the CpG island methylator phenotype. Proc. Natl. Acad. Sci. U. S. A. 97, 710–5.

Triscott, J., Lee, C., Foster, C., Manoranjan, B., Pambid, M.R., Berns, R., Fotovati, A., Venugopal, C., O'Halloran, K., Narendran, A., Hawkins, C., Ramaswamy, V., Bouffet, E., Taylor, M.D., Singhal, A., Hukin, J., Rassekh, R., Yip, S., Northcott, P., Singh, S.K., Dunham, C., Dunn, S.E., 2013. Personalizing the treatment of pediatric medulloblastoma: Polo-like kinase 1 as a molecular target in high-risk children. Cancer Res. 73, 6734–6744.

Triscott, J., Lee, C., Hu, K., Fotovati, A., Berns, R., Pambid, M., Luk, M., Kast, R.E., Kong, E., Toyota, E., Yip, S., Toyota, B., Dunn, S.E., 2012. Disulfiram, a drug widely used to control alcoholism, suppresses the self-renewal of glioblastoma and over-rides resistance to temozolomide. Oncotarget 3, 1112–1123.

Triscott, J., Pambid, M.R., Dunn, S.E., 2015. Bullseye : Targeting Cancer Stem Cells to Improve the Treatment of Gliomas by Repurposing Disulfiram. Stem Cells 33, 1042–1046.

Trivedi, R.N., Almeida, K.H., Fornsaglio, J.L., Schamus, S., Sobol, R.W., 2005. The Role of Base Excision Repair in the Sensitivity and Resistance to Temozolomide-Mediated Cell Death Resistance to Temozolomide-Mediated Cell Death 6394–6400.

Tsou, M.-F.B., Wang, W.-J., George, K.A., Uryu, K., Stearns, T., Jallepalli, P. V, 2009. Polo kinase and separase regulate the mitotic licensing of centriole duplication in human cells. Dev. Cell 17, 344–54.

Tubbs, J.L., Pegg, A.E., Tainer, J.A., 2007. DNA binding, nucleotide flipping, and the helix-turn-helix motif in base repair by O6-alkylguanine-DNA alkyltransferase and its implications for cancer chemotherapy. DNA Repair (Amst). 6, 1100–1115.

Tuynder, M., Fiucci, G., Prieur, S., Lespagnol, A., Géant, A., Beaucourt, S., Duflaut, D., Besse, S., Susini, L., Cavarelli, J., Moras, D., Amson, R., Telerman, A., 2004. Translationally controlled tumor protein is a target of tumor reversion. Proc. Natl. Acad. Sci. U. S. A. 101, 15364–15369.

Tuynder, M., Susini, L., Prieur, S., Besse, S., Fiucci, G., Amson, R., Telerman, A., 2002. Biological models and genes of tumor reversion: cellular reprogramming through tpt1/TCTP and SIAH-1. Proc. Natl. Acad. Sci. U. S. A. 99, 14976–14981.

Uchiumi, T., Longo, D.L., Ferris, D.K., 1997. Cell Cycle Regulation of the Human Polo-like Kinase (PLK) Promoter. J. Biol. Chem. 272, 9166–9174.

Uhrbom, L., Hesselager, G., Nister, M., Westermark, B., 1998. Induction of brain tumors in mice using a recombinant platelet-derived growth factor B-chain retrovirus. Cancer Res 58, 5275–5279.

Ujifuku, K., Mitsutake, N., Takakura, S., Matsuse, M., Saenko, V., Suzuki, K., Hayashi, K., Matsuo, T., Kamada, K., Nagata, I., Yamashita, S., 2010. miR-195, miR-455-3p and miR-10a(*) are implicated in acquired temozolomide resistance in glioblastoma multiforme cells. Cancer Lett. 296, 241–8.

Valsasina, B., Beria, I., Alli, C., Alzani, R., Avanzi, N., Ballinari, D., Cappella, P., Caruso, M., Casolaro, A., Ciavolella, A., Cucchi, U., De Ponti, A., Felder, E., Fiorentini, F., Galvani, A., Gianellini, L.M., Giorgini, M.L., Isacchi, A., Lansen, J., Pesenti, E., Rizzi, S., Rocchetti, M., Sola, F., Moll, J., 2012. NMS-P937, an orally available, specific small-molecule polo-like kinase 1 inhibitor with antitumor activity in solid and hematologic malignancies. Mol. Cancer Ther. 11, 1006–16.

Van de Weerdt, B.C.M., van Vugt, M.A.T.M., Lindon, C., Kauw, J.J.W., Rozendaal, M.J., Klompmaker, R., Wolthuis, R.M.F., Medema, R.H., 2005. Uncoupling anaphase-promoting complex/cyclosome activity from spindle assembly checkpoint control by deregulating polo-like kinase 1. Mol. Cell. Biol. 25, 2031–44.

Van den Boom, J., Wolter, M., Kuick, R., Misek, D.E., Youkilis, A.S., Wechsler, D.S., Sommer, C., Reifenberger, G., Hanash, S.M., 2003. Characterization of gene expression profiles associated with glioma progression using oligonucleotide-based microarray analysis and real-time reverse transcription-polymerase chain reaction. Am J Pathol 163, 1033–1043.

Van Vugt, M.A.T.M., Gardino, A.K., Linding, R., Ostheimer, G.J., Reinhardt, H.C., Ong, S.-E., Tan, C.S., Miao, H., Keezer, S.M., Li, J., Pawson, T., Lewis, T.A., Carr, S.A., Smerdon, S.J., Brummelkamp, T.R., Yaffe, M.B., 2010. A mitotic phosphorylation feedback network connects Cdk1, Plk1, 53BP1, and Chk2 to inactivate the G(2)/M DNA damage checkpoint. PLoS Biol. 8, e1000287.

Van Vugt, M.A.T.M., van de Weerdt, B.C.M., Vader, G., Janssen, H., Calafat, J., Klompmaker, R., Wolthuis, R.M.F., Medema, R.H., 2004. Polo-like kinase-1 is required for bipolar spindle formation but is dispensable for anaphase promoting complex/Cdc20 activation and initiation of cytokinesis. J. Biol. Chem. 279, 36841–54.

Venugopal, C., Wang, X.S., Manoranjan, B., McFarlane, N., Nolte, S., Li, M., Murty, N., Siu, K.W.M., Singh, S.K., 2012. GBM secretome induces transient transformation of human neural precursor cells. J. Neurooncol. 457–466.

Verhaak, R.G.W., Hoadley, K. a, Purdom, E., Wang, V., Qi, Y., Wilkerson, M.D., Miller, C.R., Ding, L., Golub, T., Mesirov, J.P., Alexe, G., Lawrence, M., O'Kelly, M., Tamayo, P., Weir, B. a, Gabriel, S., Winckler, W., Gupta, S., Jakkula, L., Feiler, H.S., Hodgson, J.G., James, C.D., Sarkaria, J.N., Brennan, C., Kahn, A., Spellman, P.T., Wilson, R.K., Speed, T.P., Gray, J.W., Meyerson, M., Getz, G., Perou, C.M., Hayes, D.N., 2010. Integrated genomic analysis identifies clinically relevant subtypes of glioblastoma characterized by abnormalities in PDGFRA, IDH1, EGFR, and NF1. Cancer Cell 17, 98–110.

Verma, S., Stewart, D.J., Maroun, J.A., Nair, R.C., 1990. A randomized phase II study of cisplatin alone versus cicplatin plus disulfiram. Am. J. Clin. Oncol. Cancer Clin. Trials 13, 119–124.

Vescovi, A.L., Galli, R., Reynolds, B.A., 2006. Brain tumour stem cells. Nat. Rev. Cancer 6, 425–436.

Vieira, W.A., Weltman, E., Chen, M.J., da Silva, N.S., Cappellano, A.M., Pereira, L.D., Gonçalves, M.I.R., Ferrigno, R., Hanriot, R.M., Nadalin, W., Odone Filho, V., Petrilli, A.S., 2014. Ototoxicity evaluation in medulloblastoma patients treated with involved field boost using intensity-modulated radiation therapy (IMRT): a retrospective review. Radiat. Oncol. 9, 158.

Vogelstein, B., Lane, D., Levine, A.J., 2000. Surfing the p53 network. Nature 408, 307–310.

Von Deimling, A., Louis, D.N., Wiestler, O.D., 1995. Molecular pathways in the formation of gliomas. Glia 15, 328–338.

Von Hoff, K., Hinkes, B., Gerber, N.U., Deinlein, F., Mittler, U., Urban, C., Benesch, M., Warmuth-Metz, M., Soerensen, N., Zwiener, I., Goette, H., Schlegel, P.G., Pietsch, T., Kortmann, R.D., Kuehl, J., Rutkowski, S., 2009. Long-term outcome and clinical prognostic factors in children with medulloblastoma treated in the prospective randomised multicentre trial HIT'91. Eur. J. Cancer 45, 1209–17.

Von Hoff, K., Rutkowski, S., 2012. Medulloblastoma. Curr. Treat. Options Neurol. 14, 416–426.

Vose, J.M., Friedberg, J.W., Waller, E.K., Cheson, B.D., Juvvigunta, V., Fritsch, H., Petit, C., Munzert, G., Younes, A., 2013. The Plk1 inhibitor BI 2536 in patients with refractory or relapsed non-Hodgkin lymphoma: a phase I, open-label, single dose-escalation study. Leuk. Lymphoma 54, 708–13.

Wakimoto, H., Kesari, S., Farrell, C.J., Curry, W.T., Zaupa, C., Aghi, M., Kuroda, T., Stemmer-Rachamimov, A., Shah, K., Liu, T.-C., Jeyaretna, D.S., Debasitis, J., Pruszak, J., Martuza, R.L., Rabkin, S.D., 2009. Human glioblastoma-derived cancer stem cells: establishment of invasive glioma models and treatment with oncolytic herpes simplex virus vectors. Cancer Res. 69, 3472–81.

Wakimoto, H., Mohapatra, G., Kanai, R., Curry, W.T., Yip, S., Nitta, M., Patel, A.P., Barnard, Z.R., Stemmer-Rachamimov, A.O., Louis, D.N., Martuza, R.L., Rabkin, S.D., 2011. Maintenance of primary tumor phenotype and genotype in glioblastoma stem cells. Neuro. Oncol. 02114, 132–44.

Wang, H., Ouyang, Y., Somers, W.G., Chia, W., Lu, B., 2007. Polo inhibits progenitor self-renewal and regulates Numb asymmetry by phosphorylating Pon. Nature 449, 96–100.

Wang, J., Sakariassen, P.Ø., Tsinkalovsky, O., Immervoll, H., Bøe, S.O., Svendsen, A., Prestegarden, L., Røsland, G., Thorsen, F., Stuhr, L., Molven, A., Bjerkvig, R., Enger, P.Ø., 2008. CD133 negative glioma cells form tumors in nude rats and give rise to CD133 positive cells. Int. J. Cancer 122, 761–8.

Wang, M., Dignam, J.J., Won, M., Curran, W., Mehta, M., Gilbert, M.R., 2015. Variation over time and interdependence between disease progression and death among patients with glioblastoma on RTOG 0525. Neuro. Oncol. 1–8.

Wang, V.Y., Zoghbi, H.Y., 2001. Genetic regulation of cerebellar development. Nat. Rev. Neurosci. 2, 484–491.

Wang, W., McLeod, H.L., Cassidy, J., 2003. Disulfiram-mediated inhibition of NF-kappaB activity enhances cytotoxicity of 5-fluorouracil in human colorectal cancer cell lines. Int. J. Cancer 104, 504–511.

Wang, X., Venugopal, C., Manoranjan, B., McFarlane, N., O'Farrell, E., Nolte, S., Gunnarsson, T., Hollenberg, R., Kwiecien, J., Northcott, P., Taylor, M.D., Hawkins, C., Singh, S.K., 2011. Sonic hedgehog regulates Bmi1 in human medulloblastoma brain tumor-initiating cells. Oncogene 187–199.

Ward, P.S., Patel, J., Wise, D.R., Abdel-Wahab, O., Bennett, B.D., Coller, H. a., Cross, J.R., Fantin, V.R., Hedvat, C. V., Perl, A.E., Rabinowitz, J.D., Carroll, M., Su, S.M., Sharp, K. a., Levine, R.L., Thompson, C.B., 2010. The Common Feature of Leukemia-Associated IDH1 and IDH2 Mutations Is a Neomorphic Enzyme Activity Converting α-Ketoglutarate to 2-Hydroxyglutarate. Cancer Cell 17, 225–234.

Warmuth-Metz, M., Blashofer, S., Von Bueren, A.O., Von Hoff, K., Bison, B., Pohl, F., Kortmann, R.D., Pietsch, T., Rutkowski, S., 2011. Recurrence in childhood medulloblastoma. J. Neurooncol. 103, 705–711.

Wäsch, R., Hasskarl, J., Schnerch, D., Lübbert, M., 2010. BI_2536-targeting the mitotic kinase Polo-like kinase 1 (Plk1), Small Molecules in Oncology. Springer Berline Heidelberg, Recent Results in Cancer Research. Springer Berlin Heidelberg, Berlin, Heidelberg.

Wasserfallen, J.-B., Ostermann, S., Leyvraz, S., Stupp, R., 2005. Cost of temozolomide therapy and global care for recurrent malignant gliomas followed until death. Neuro. Oncol. 7, 189–195.

Watanabe, K., Tachibana, O., Sata, K., Yonekawa, Y., Kleihues, P., Ohgaki, H., 1996. Overexpression of the EGF receptor and p53 mutations are mutually exclusive in the evolution of primary and secondary glioblastomas. Brain Pathol. 6, 217–223.

Watanabe, N., Arai, H., Nishihara, Y., Taniguchi, M., Watanabe, N., Hunter, T., Osada, H., 2004. M-phase kinases induce phospho-dependent ubiquitination of somatic Wee1 by SCFbeta-TrCP. Proc. Natl. Acad. Sci. U. S. A. 101, 4419–24.

Weber, G.L., Parat, M.-O., Binder, Z.A., Gallia, G.L., 2011. Abrogation of PIK3CA or PIK3R1 reduces proliferation, migration, and invasion in glioblastoma multiforme cells. Oncotarget 2, 833–849.

Weiler, M., Blaes, J., Pusch, S., Sahm, F., Czabanka, M., Luger, S., Bunse, L., Solecki, G., Eichwald, V., Jugold, M., Hodecker, S., Osswald, M., Meisner, C., Hielscher, T., Rübmann, P., Pfenning, P.-N., Ronellenfitsch, M., Kempf, T., Schnölzer, M., Abdollahi, A., Lang, F., Bendszus, M., von Deimling, A., Winkler, F., Weller, M., Vajkoczy, P., Platten, M., Wick, W., 2014. mTOR target NDRG1 confers MGMT-dependent resistance to alkylating chemotherapy. Proc. Natl. Acad. Sci. U. S. A. 111, 409–414.

Wen, H., Andrejka, L., Ashton, J., Karess, R., Lipsick, J.S., 2008. Epigenetic regulation of gene expression by Drosophila Myb and E2F2-RBF via the Myb-MuvB/dREAM complex. Genes Dev. 22, 601–14.

Wen, P., Kesari, S., 2008. Malignant Gliomas in Adults. N. Engl. J. Med. 359, 492–507.

Wen, P.Y., Schiff, D., Kesari, S., Drappatz, J., Gigas, D.C., Doherty, L., 2006. Medical management of patients with brain tumors. J. Neurooncol. 80, 313–332.

Westphal, M., Hilt, D.C., Bortey, E., Delavault, P., Olivares, R., Warnke, P.C., Whittle, I.R., Jääskeläinen, J., Ram, Z., 2003. A phase 3 trial of local chemotherapy with biodegradable carmustine (BCNU) wafers (Gliadel wafers) in patients with primary malignant glioma. Neuro. Oncol. 5, 79–88.

Wetmore, C., Eberhart, D.E., Curran, T., 2000. The normal patched allele is expressed in medulloblastomas from mice with heterozygous germ-line mutation of patched. Cancer Res. 60, 2239–2246.

Winkles, J.A., Alberts, G.F., 2005. Differential regulation of polo-like kinase 1, 2, 3, and 4 gene expression in mammalian cells and tissues. Oncogene 24, 260–6.

Wirtz, C.R., Knauth, M., Staubert, A., Bonsanto, M.M., Sartor, K., Kunze, S., Tronnier, V.M., 2000. Clinical evaluation and follow-up results for intraoperative magnetic resonance imaging in neurosurgery. Neurosurgery 46, 1112–1122.

Wissing, M.D., Rosmus, N., Gonzalez, M., Hammers, H., Carducci, M.A., Kachhap, S.K., 2010. Targeting prostate cancer through a combination of Polo-like kinase inhibitors and histone deacetylase inhibitors. Cancer Res. 70, 5414–5414.

Wolf, A., Agnihotri, S., Guha, A., 2010. Targeting metabolic remodeling in glioblastoma multiforme. Oncotarget 1, 552–62.

Wolf, G., Elez, R., Doermer, A., Holtrich, U., Ackermann, H., Stutte, H.J., Altmannsberger, H.M., Rübsamen-Waigmann, H., Strebhardt, K., 1997. Prognostic significance of polo-like kinase (PLK) expression in non-small cell lung cancer. Oncogene 14, 543–9.

Wong, A.J., Ruppert, J.M., Bigner, S.H., Grzeschik, C.H., Humphrey, P.A., Bigner, D.S., Vogelstein, B., 1992. Structural alterations of the epidermal growth factor receptor gene in human gliomas. Proc. Natl. Acad. Sci. U. S. A. 89, 2965–2969.

Wong, S.T.S., Zhang, X.Q., Zhuang, J.T.F., Chan, H.L., Li, C.H., Leung, G.K.K., 2012. MicroRNA-21 inhibition enhances in vitro chemosensitivity of temozolomide-resistant glioblastoma cells. Anticancer Res. 32, 2835–2842.

Wu, X., Northcott, P. a, Dubuc, A., Dupuy, A.J., Shih, D.J.H., Witt, H., Croul, S., Bouffet, E., Fults, D.W., Eberhart, C.G., Garzia, L., Van Meter, T., Zagzag, D., Jabado, N., Schwartzentruber, J., Majewski, J., Scheetz, T.E., Pfister, S.M., Korshunov, A., Li, X.-N., Scherer, S.W., Cho, Y.-J., Akagi, K., MacDonald, T.J., Koster, J., McCabe, M.G., Sarver, A.L., Collins, V.P., Weiss, W. a, Largaespada, D. a, Collier, L.S., Taylor, M.D., 2012. Clonal selection drives genetic divergence of metastatic medulloblastoma. Nature 482, 529–33.

Xiao, A., Wu, H., Pandolfi, P.P., Louis, D.N., Van Dyke, T., 2002. Astrocyte inactivation of the pRb pathway predisposes mice to malignant astrocytoma development that is accelerated by PTEN mutation. Cancer Cell 1, 157–168.

Xu, A., Bellamy, A.R., Taylor, J.A., 1999. Expression of translationally controlled tumour protein is regulated by calcium at both the transcriptional and post-transcriptional level. Biochem. J. 342 Pt 3, 683–689.

Xu, J., Margol, A., Asgharzadeh, S., Erdreich-Epstein, A., 2015. Pediatric Brain Tumor Cell Lines. J. Cell. Biochem. 116, 218–224.

Xu, J., Shen, C., Wang, T., Quan, J., 2013. Structural basis for the inhibition of Polo-like kinase 1. Nat. Struct. Mol. Biol. 1–8.

Xu-Welliver, M., Pegg, A.E., 2002. Degradation of the alkylated form of the DNA repair protein, O(6)-alkylguanine-DNA alkyltransferase. Carcinogenesis 23, 823–30.

Yamashiro, S., Yamakita, Y., Totsukawa, G., Goto, H., Kaibuchi, K., Ito, M., Hartshorne, D.J., Matsumura, F., 2008. Myosin phosphatase-targeting subunit 1 regulates mitosis by antagonizing polo-like kinase 1. Dev. Cell 14, 787–97.

Yan, H., Parsons, D.W., Jin, G., McLendon, R., Rasheed, B.A., Yuan, W., Kos, I., Batinic-Haberle, I., Jones, S., Riggins, G.J., Friedman, H., Friedman, A., Reardon, D., Herndon, J., Kinzler, K.W., Velculescu, V.E., Vogelstein, B., Bigner, D.D., 2009. IDH1 and IDH 2 Mutations in Gliomas. N. Engl. J. Med. 360, 765–773.

Yang, Y., Yang, F., Xiong, Z., Yan, Y., Wang, X., Nishino, M., Mirkovic, D., Nguyen, J., Wang, H., Yang, X.-F., 2005. An N-terminal region of translationally controlled tumor protein is required for its antiapoptotic activity. Oncogene 24, 4778–88.

Yang, Y.P., Chien, Y., Chiou, G.Y., Cherng, J.Y., Wang, M.L., Lo, W.L., Chang, Y.L., Huang, P.I., Chen, Y.W., Shih, Y.H., Chen, M.T., Chiou, S.H., 2012. Inhibition of cancer stem cell-like properties and reduced chemoradioresistance of glioblastoma using microRNA145 with cationic polyurethane-short branch PEI. Biomaterials 33, 1462–1476.

Yang, Z.-J.J., Ellis, T., Markant, S.L., Read, T.-A.A., Kessler, J.D., Bourboulas, M., Schüller, U., Machold, R., Fishell, G., Rowitch, D.H., Wainwright, B.J., Wechsler-Reya, R.J., 2008. Medulloblastoma Can Be Initiated by Deletion of Patched in Lineage-Restricted Progenitors or Stem Cells. Cancer Cell 14, 135–145.

Yarm, F.R., 2002. Plk Phosphorylation Regulates the Microtubule-Stabilizing Protein TCTP. Mol. Cell. Biol. 22, 6209–6221.

Yata, K., Lloyd, J., Maslen, S., Bleuyard, J.Y., Skehel, M., Smerdon, S.J., Esashi, F., 2012. Plk1 and CK2 Act in Concert to Regulate Rad51 during DNA Double Strand Break Repair. Mol. Cell 45, 371–383.

Yauch, R.L., Dijkgraaf, G.J.P., Alicke, B., Januario, T., Ahn, C.P., Holcomb, T., Pujara, K., Stinson, J., Callahan, C.A., Tang, T., Bazan, J.F., Kan, Z., Seshagiri, S., Hann, C.L., Gould, S.E., Low, J.A., Rudin, C.M., de Sauvage, F.J., 2009. Smoothened mutation confers resistance to a Hedgehog pathway inhibitor in medulloblastoma. Science 326, 572–574.

Ying, M., Wang, S., Sang, Y., Sun, P., Lal, B., Goodwin, C.R., Guerrero-Cazares, H., Quinones-Hinojosa, a, Laterra, J., Xia, S., 2011. Regulation of glioblastoma stem cells by retinoic acid: role for Notch pathway inhibition. Oncogene 30, 3454–67.

Yip, N.C., Fombon, I, S., Liu, P., Brown, S., Kannappan, V., Armesilla, A.L., Xu, B., Cassidy, J., Darling, J.L., Wang, W., 2011. Disulfiram modulated ROS-MAPK and NFκB pathways

and targeted breast cancer cells with cancer stem cell-like properties. Br. J. Cancer 104, 1564–74.

Yip, S., Miao, J., Cahill, D.P., Iafrate, a J., Aldape, K., Nutt, C.L., Louis, D.N., 2009. MSH6 mutations arise in glioblastomas during temozolomide therapy and mediate temozolomide resistance. Clin. Cancer Res. 15, 4622–9.

Yoon, K., Gaiano, N., 2005. Notch signaling in the mammalian central nervous system: insights from mouse mutants. Nat. Neurosci. 8, 709–15.

Young, G.S., 2007. Advanced MRI of adult brain tumors. Neurol. Clin. 25, 947–73, viii.

Yuan, J., Hörlin, A., Hock, B., Stutte, H.J., Rübsamen-Waigmann, H., Strebhardt, K., 1997. Polo-like kinase, a novel marker for cellular proliferation. Am. J. Pathol. 150, 1165–72.

Zechner, D., Fujita, Y., Hülsken, J., Müller, T., Walther, I., Taketo, M.M., Crenshaw, E.B., Birchmeier, W., Birchmeier, C., 2003. beta-Catenin signals regulate cell growth and the balance between progenitor cell expansion and differentiation in the nervous system. Dev. Biol. 258, 406–18.

Zha, J., Chen, F., Dong, H., Shi, P., Yao, Y., Zhang, Y., Li, R., Wang, S., Li, P., Wang, W., Xu, B., 2014. Disulfiram targeting lymphoid malignant cell lines via ROS-JNK activation as well as Nrf2 and NF-kB pathway inhibition. J. Transl. Med. 12, 163.

Zhang, C., Sun, X., Ren, Y., Lou, Y., Zhou, J., Liu, M., Li, D., 2012. Validation of Polo-like kinase 1 as a therapeutic target in pancreatic cancer cells. Cancer Biol. Ther. 13, 1214–1220.

Zhang, D., Li, F., Weidner, D., Mnjoyan, Z.H., Fujise, K., 2002. Physical and functional interaction between myeloid cell leukemia 1 protein (MCL1) and fortilin. The potential role of MCL1 as a fortilin chaperone. J. Biol. Chem. 277, 37430–37438.

Zhang, J., de Toledo, S.M., Pandey, B.N., Guo, G., Pain, D., Li, H., Azzam, E.I., Toledo, S.M. De, Pandey, B.N., Guo, G., Pain, D., Li, H., 2012. Role of the translationally controlled tumor protein in DNA damage sensing and repair. Proc. Natl. Acad. Sci. U. S. A. 109, E926–33.

Zhang, J., Stevens, M.F.G., Laughton, C.A., Madhusudan, S., Bradshaw, T.D., 2010. Acquired resistance to temozolomide in glioma cell lines: Molecular mechanisms and potential translational applications. Oncology 78, 103–114.

Zhang, N., Panigrahi, A.K., Mao, Q., Pati, D., 2011. Interaction of Sororin protein with polo-like kinase 1 mediates resolution of chromosomal arm cohesion. J. Biol. Chem. 286, 41826–37.

Zhao, H., Ayrault, O., Zindy, F., Kim, J., Roussel, M.F., 2008. Post-transcriptional down-regulation of Atoh1 / Math1 by bone morphogenic proteins suppresses medulloblastoma development service Post-transcriptional down-regulation of Atoh1 / Math1 by bone morphogenic proteins suppresses medulloblastoma development 722–727.

Zhu, W.L., Cheng, H.X., Han, N., Liu, D.L., Zhu, W.X., Fan, B.L., Duan, F.L., 2008. Messenger RNA expression of translationally controlled tumor protein (TCTP) in liver regeneration and cancer. Anticancer Res. 28, 1575–1580.

Zhu, Y., Guignard, F., Zhao, D., Liu, L., Burns, D.K., Mason, R.P., Messing, A., Parada, L.F., 2005. Early inactivation of p53 tumor suppressor gene cooperating with NF1 loss induces malignant astrocytoma. Cancer Cell 8, 119–130.

Zhukova, N., Ramaswamy, V., Remke, M., Pfaff, E., Shih, D.J.H., Martin, D.C., Castelo-Branco, P., Baskin, B., Ray, P.N., Bouffet, E., von Bueren, a. O., Jones, D.T.W., Northcott, P. a., Kool, M., Sturm, D., Pugh, T.J., Pomeroy, S.L., Cho, Y.-J., Pietsch, T., Gessi, M., Rutkowski, S., Bognar, L., Klekner, A., Cho, B.-K., Kim, S.-K., Wang, K.-C., Eberhart, C.G., Fevre-Montange, M., Fouladi, M., French, P.J., Kros, M., Grajkowska, W. a., Gupta, N., Weiss, W. a., Hauser, P., Jabado, N., Jouvet, A., Jung, S., Kumabe, T., Lach, B., Leonard, J.R., Rubin, J.B., Liau, L.M., Massimi, L., Pollack, I.F., Shin Ra, Y., Van Meir, E.G., Zitterbart, K., Schuller, U., Hill, R.M., Lindsey, J.C., Schwalbe, E.C., Bailey, S., Ellison, D.W., Hawkins, C., Malkin, D., Clifford, S.C., Korshunov, A., Pfister, S., Taylor, M.D., Tabori, U., 2013. Subgroup-Specific Prognostic Implications of TP53 Mutation in Medulloblastoma. J. Clin. Oncol. 31, 2927–2935.

Zitouni, S., Nabais, C., Jana, S.C., Guerrero, A., Bettencourt-Dias, M., 2014. Polo-like kinases: structural variations lead to multiple functions. Nat. Rev. Mol. Cell Biol. 15, 433–52.

Zurawel, R.H., Chiappa, S.A., Allen, C., Raffel, C., 1998. Sporadic medulloblastomas contain oncogenic beta-catenin mutations. Cancer Res. 58, 896–9.

APPENDICES

Appendix A Young adult MB

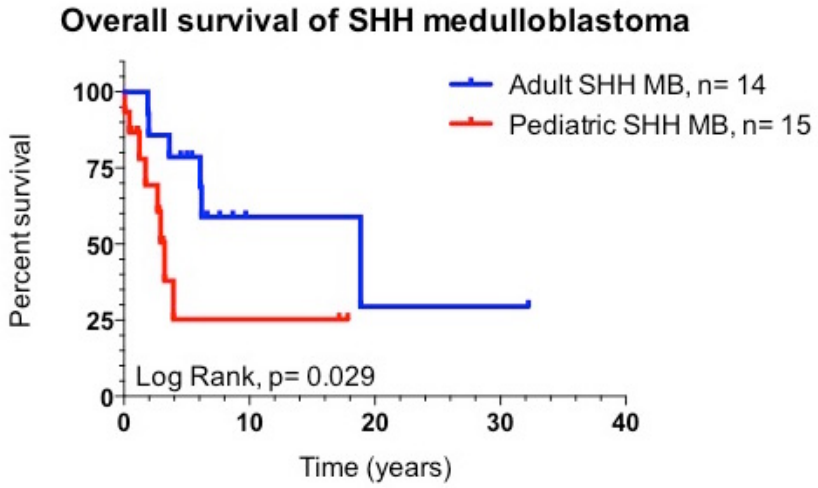

Appendix B Technical Report: Development of a brain tumor xenograft model through using bioluminescent and fluorescent markers for monitoring progression.

It is essential that researchers develop tumor models that reflect native growth conditions of human disease. A flaw of many *in vitro* drug screens is that they do not model how well a drug penetrates tumor tissue, or how cancer cells associate within their microenvironment. This is especially the case for brain tumors, where drug delivery is often obstructed by the BBB Xenograft surgeries, such as a flank injection, are easy to perform, monitor, and have a low impact on animal well-being. In contrast, intracranial xenografts are associated with additional challenges. These include: the sensitive nature of brain tissue, smaller tumor volume, and monitoring tumor growth in live animals. Therefore, our objective is to (1) optimize a surgical technique for intracranial implantation of tumor cells, and (2) establish a non-invasive method to monitor tumor growth in live animals.

B.1 Labeling Daoy cells with Luc2=tdT expression vector.

Daoy MB cells were transfected with pcDNA3.1(+)/Luc2=tdT plasmid for dual label expression of luciferase and tandem tomato (tdT) markers. Cells were transfected using Lipofectamine 2000 (Invitrogen) and then maintained in G418 selective medium containing (Figure B.1i). Daoy Luc2=tdT cells were sorted for high and medium expressers based on tdT fluorescent expression. Cut-offs were determined using the highest 10-20% tdT expressers and compared to negative control cells (Figure B.1ii). Once cells are implanted into mice, the activity of the luciferase enzyme is needed to measure tumor burden. To assess if cells high in the tdT marker also expressed luciferase Daoy Luc2=tdT cells that were previously sorted were plated in serial cell dilutions and treated with the luciferin substrate. Luminescence was measured using the SPECTRAL Ami & Ami X (Spectral Instruments Imaging, LLC) *in vivo* imager and AMIView Version 1.6.0 software. The intensity of luciferase bioluminescence correlated with cell concentration and enriched in populations sorted for high tdT. Daoy Luc2=tdT cells could be detected with great sensitivity (Figure B.1iii). Prior to implantation, Daoy Luc2=tdT cells were resorted for high tdT expressers. These cells retained the luciferase and tdT markers even after weeks of passaging *in vitro*, which suggest retention once used *in vivo* (Figure B.1iv). The Luc2=tdT markers offer a robust method for detection of tumor cells in animal models.

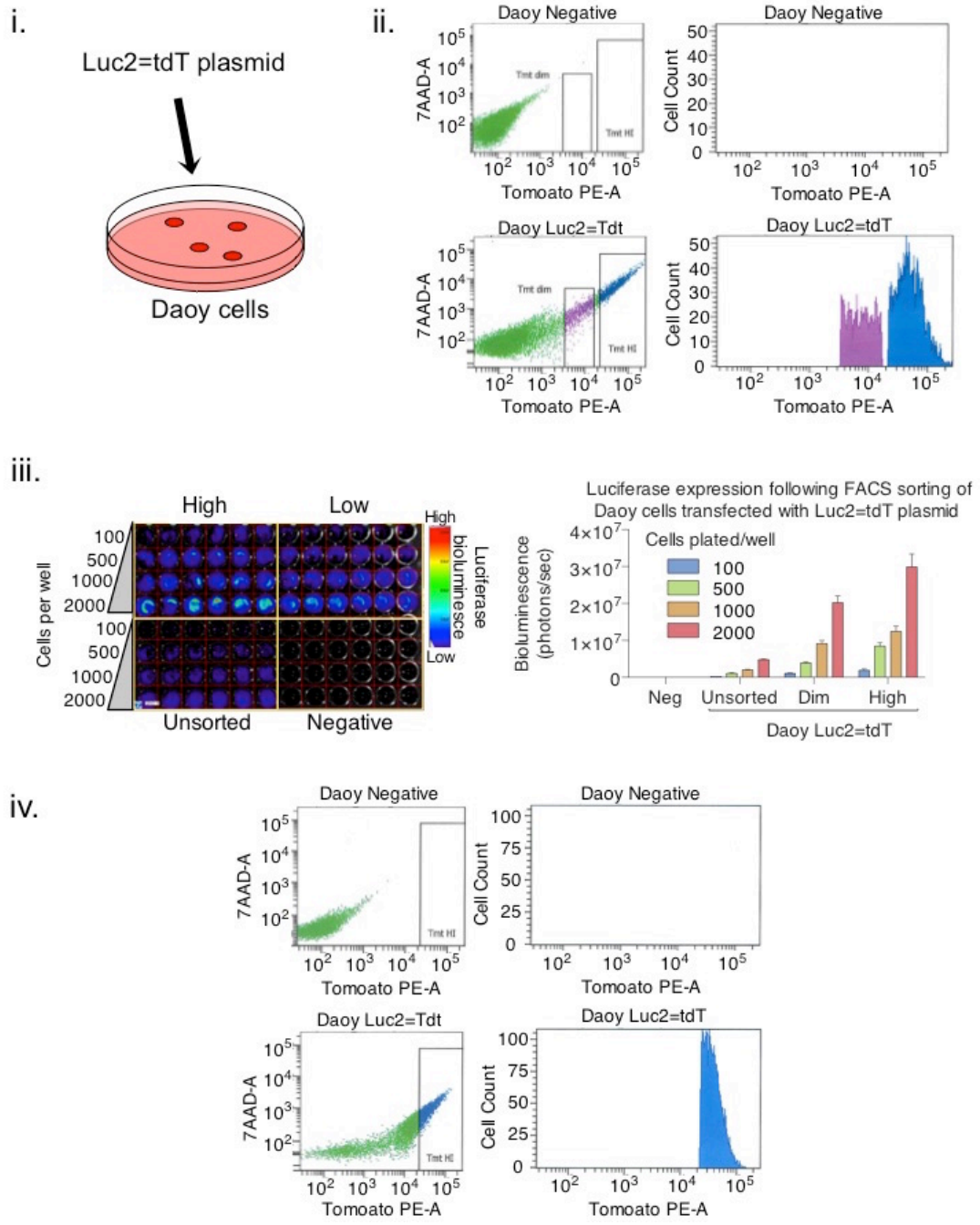

Figure B.1 Expression of Luc2=tdT in Daoy MB cells.

(i) Daoy cells were transfected with pcDNA3.1(+)/Luc2=tdT. (ii) Using expression of the tandem tomato fluorescent marker, Daoy Luc2=tdT cells were sorted using FACS. (iii) Cells sorted for high tomato fluorescence correlated were assessed for luciferase enzyme activity in a 96 well format with serial diluted concentration of cells. (iv) Daoy Luc=tdT cells retained marker expression following passaging in cell culture and are sorted prior to surgical implantation into mice.

B.2 Intracranial implantation of labeled Daoy cells into NOD/SCID mice.

The surgical procedure for injection of Daoy Luc2=tdT cells into mice is depicted in Figure B.2. NOD/SCID immunocompromised mice aged 6-8 weeks were allowed 5-7 days between arriving to the facility before surgery to adjust and reduce stress.

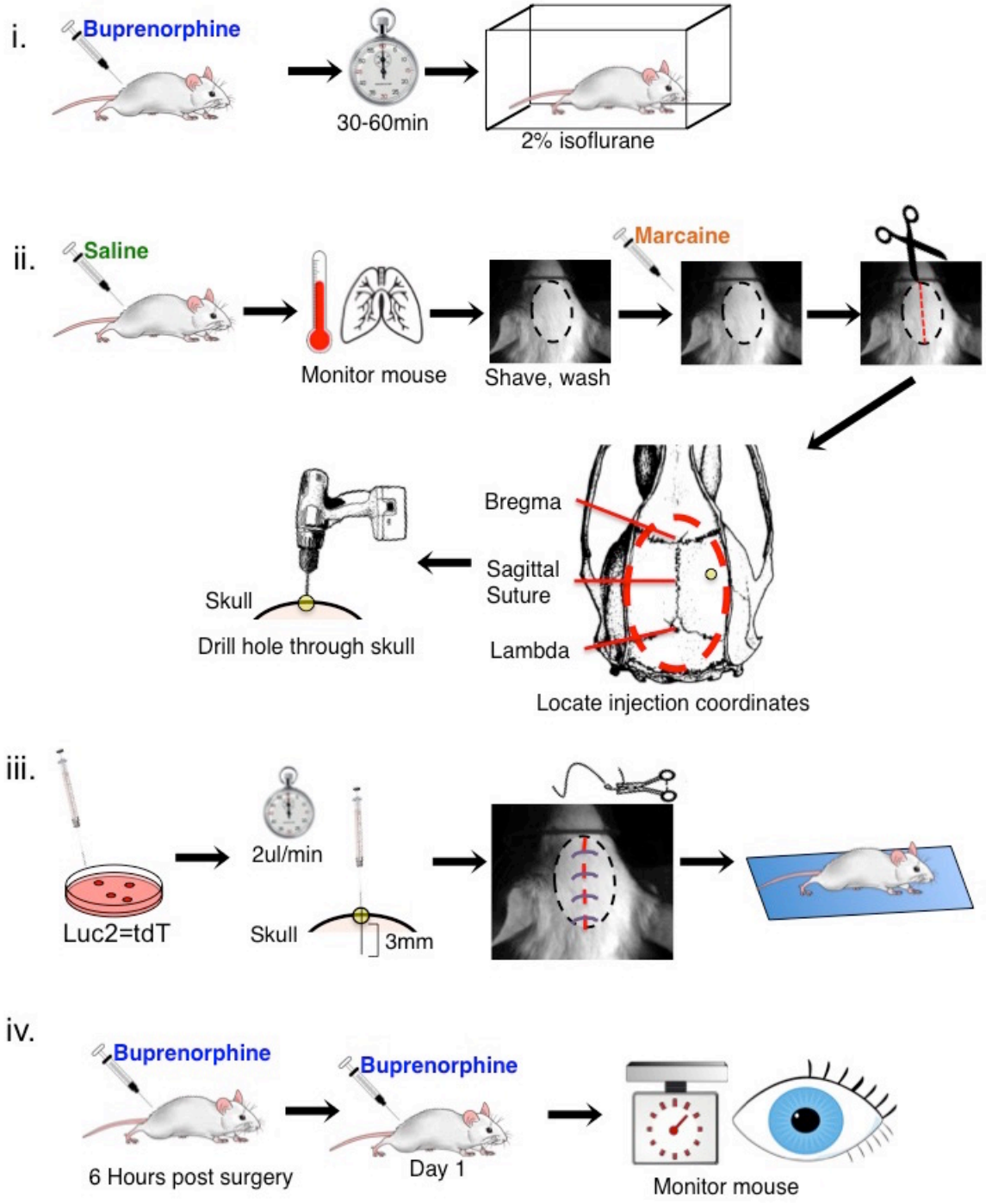

Figure B.2 Graphic of surgical workflow used for intracranial injection of NOD/SCID mice.

Daoy Luc2=tdT cells were expanded and prepared prior to surgery. (i) NOD/SCID mice were pretreated with the analgesic, buprenorphine (0.05mg/kg dose), using subcutaneous injection. After 30 to 60 minutes mice were induced using 2% isoflurane using an induction chamber. Mice were transferred to a nose cone and assessed for anesthetic depth using toe pinch. (ii) Mice were provided with supportive care and injected with subcutaneous saline. Body temperature and respiration rate was monitored and necessary adjustment to isoflurane or heat sources was made accordingly. Fur clippers were used to remove hair from the surgical site. Three round of soap and 70% ethanol were used to clean the shaven site. Marcaine was injected subcutaneously along the surgical site to provide local anesthetic. A 1cm incision was made using sterile scissors and sterile cotton tips were used to expose the skull. *To find the correct coordinates for injection, bregma and lambda were located. A site of 2mm back from bregma and 3mm right of the midline (sagittal suture) was selected. A small hole in the skull was made at these coordinates using a drill without penetrating the brain tissue. (iii) A 10ul volume containing 1X10E6 Daoy Luc2=tdT cells was prepared in a Hamilton syringe. The needle of the syringe was slowly lowered through the burred hole to a depth of 3mm into the brain from the skull. Cells were injected at a rate of 2ul/min. Before removing the syringe, the needle was left for 2-5 minutes to allow dissipation of the injected cell solution. Simple interrupted sutures were used to repair the cut from the incision site and mice were recovered on a heat pad. (iv) Another subcutaneous injection of buprenorphine was provided 6 hours following surgery, and again the following day depending on perceived need for pain relief. Mice were monitored daily for well-being and neurological signs of tumor burden. Changes in weight were also recorded.

*(coordinate image from (ii) was adapted from Paxinos, George, et al. "Bregma, lambda and the interaural midpoint in stereotaxic surgery with rats of different sex, strain and weight." Journal of neuroscience methods 13.2 (1985): 139-143.)

B.3 Optimization of tumor monitoring using Luc2=tdT detection.

The *in vivo* detection of luciferase labeled cells is done by injecting mice with the luciferase substrate, luciferin. Signal intensity depends on a couple factors: (1) presence of luciferase enzyme, (2) tissue distribution of active luciferin substrate, and (3) time post injection (Klerk et al., 2007). We questioned whether the blood-brain barrier might hamper detection of Daoy Luc2=tdT cells in the brain. Therefore, we sought to optimize our imaging protocol. Mice bearing Daoy Luc2=tdT cells were induced with 2% isoflurane and injected with 100ul luciferin. A timer recorded the time elapsed following luciferin injection, and multiple images were recorded using the SPECTRAL Ami & Ami X. (Figure B.3i-ii). The imaging timecourse showed that luciferase detection required an incubation period to allow substrate distribution into the brain. Very little bioluminescence was measured less than 10 minutes following luciferin injection. However, a peak of maximal detection occurred between 15-17.5 minutes (Figure B.3iii). Images acquired 20 minutes or later demonstrated diminished signal, which suggests exhaustion of the luciferase substrate in the tumor tissue. Average bioluminescence was calculated in a timecourse experiment with 6 individual mice and 1 negative imaging control mouse that was measured in duplicate (Figure B.3iv). For subsequent monitoring of Daoy Luc2=tdT NOD/SCID xenograft mice, a time of 17.5 minutes post-injection was selected for optimal and consistent tumor imaging.

Mice were imaged using luciferase bioluminescence once a week and weighed 1-2 times a week. Bioluminescent signal differences of an order of $\log^{10}$ magnitude were considered a significant change in tumor growth (i.e., 10E6 to 10E7). Increases of luciferase bioluminescence over time correlated with a decline in animal well-being, as indicated by body weight (Figure B.4i). Although no neurological signs were evident, this suggests mice might still be experiencing clinical symptoms of a brain tumor (i.e., headache). Mice were sacked, and tissues were fixed using formalin. Although luciferase detection requires tissue viability, the tdT marker can be used to visualize labeled tumor cells in fixed tissues (tdT; excitation: 554nm, emission: 581nm). This is a valuable tool in mapping the location of tumors in order to process brain tissues that are especially small and delicate (Figure B.4ii-iv).

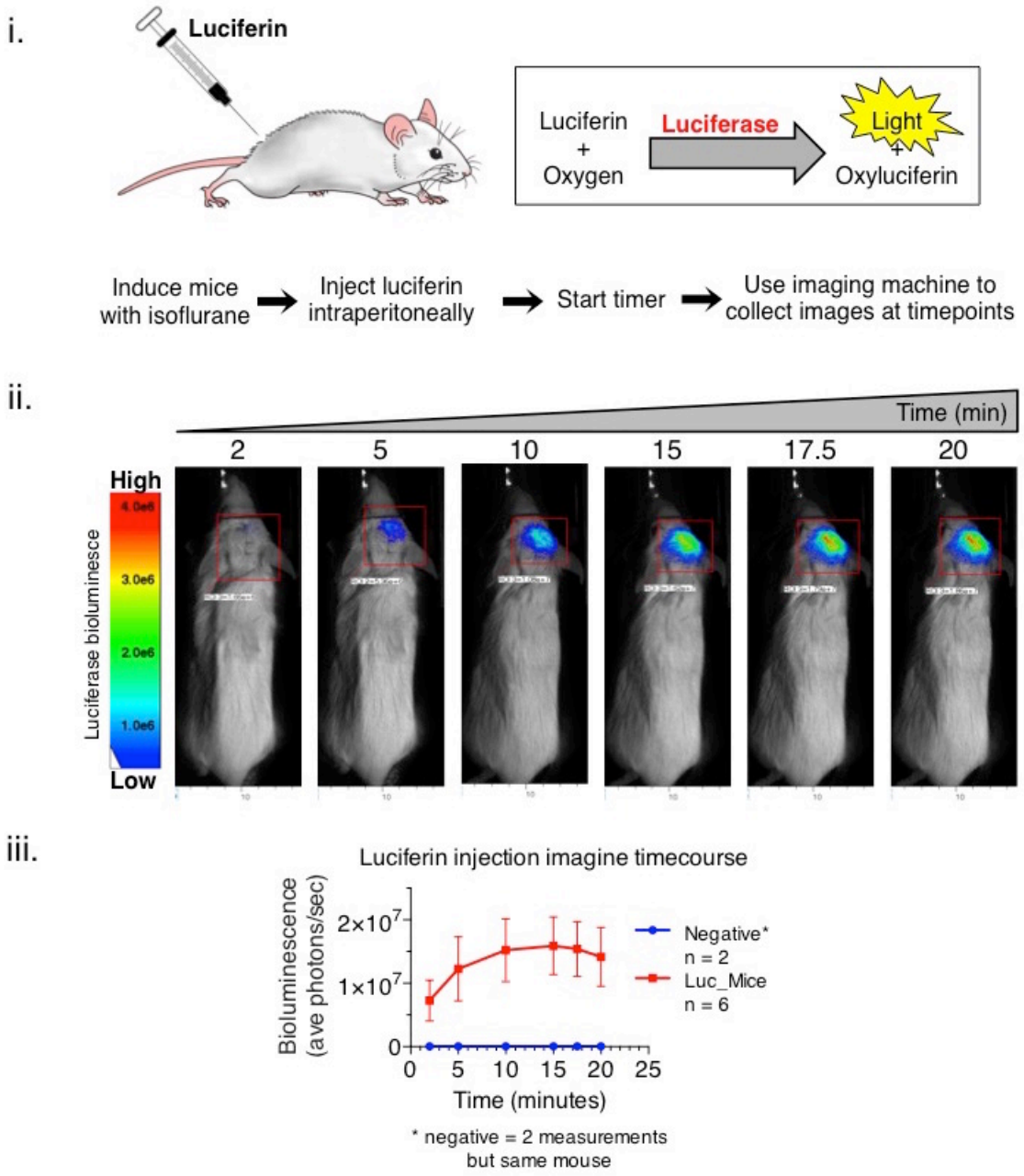

Figure B.3 Optimization of luciferase based tumor detection.

(i) Luciferin substrate is injected intraperitoneally to activate the light producing luciferase reaction. The time between luciferin injection and image acquisition was recorded in order to examine the timeframe required for detection in the brain. (iii) Representative images of a single Daoy Luc2=tdT NOD/SCID mouse injected with luciferin for 2- 20 minutes. Bioluminescence was used to measure luciferase detection (blue, low; red, high). (iii) Luminescence was quantified using imaging software for 6 mice previously injected with Daoy Luc2=tdT cells and compared to a single imagining control mouse.

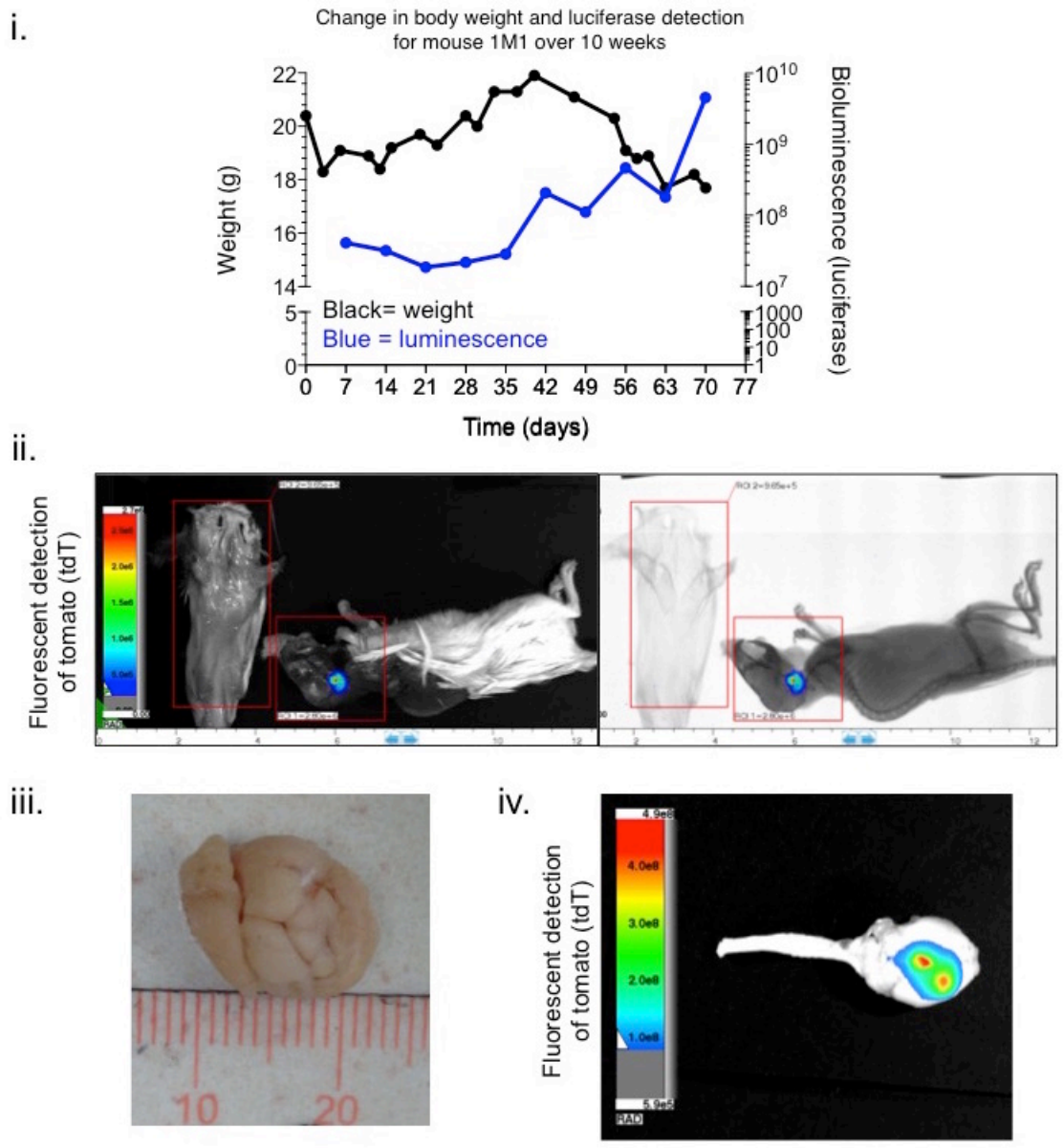

Figure B.4 Development of brain tumor xenograft and use of tdT marker in fixed tissues.

(i) Changes in mouse 1M1 body weight (black) and bioluminescent tumor detection (blue) over 10 weeks following Daoy Luc2=tdt injection. Data displayed is representative of a single mouse for which the greatest number of time points was collected. (ii-iv) Tumor detection using the tdT fluorescent label is used to map the affected neurological regions following sacrifice and tissue fixation. Signal is exclusive to the brain and not epidermal tissue suggesting cell proliferation occurred in the desired location.

B.4 Histological characteristics of xenografts reflect human disease.

Histological processing was used to confirm the tissue morphology of tumor cells. Tumors were removed, fixed using formalin, prepared on slides, and stained with hematoxylin and eosin (H&E). There were clear observable regions of tumor growth along ventricular areas with some intraparenchymal spread (Figure B.5).

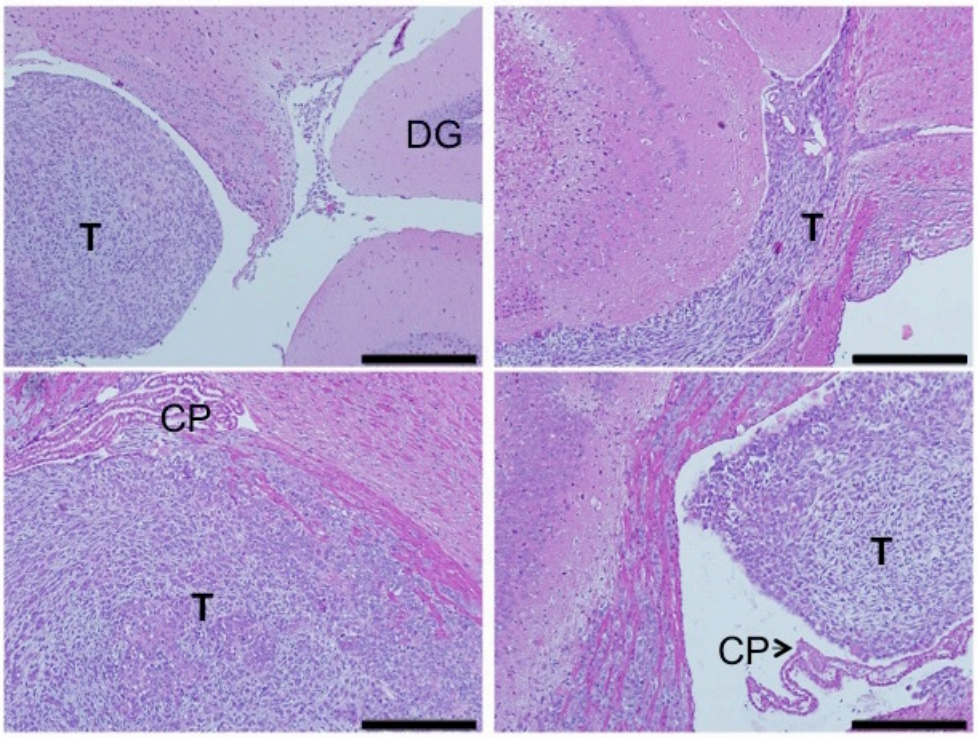

Figure B.5 Histology of Daoy xenograft tumor formation.

Histological profiling of tumor tissue from mouse 1M1 using hematoxylin and eosin (H&E) staining (T, tumor; CP, choroid plexus; DG, dentate gyrus). Scale bars represent 500μm.